NASA Tech Briefs

National
Aeronautics and
Space
Administration

Space-Derived Fishing Nets —

The first fishing net to be manufactured by an American company in over 15 years is an outgrowth of technology originally developed for crew safety nets aboard the Space Shuttle. New fibers and twisting techniques produce a dense, streamlined net that sinks rapidly. *[See the bottom of page A1.]*

Vol. 8, No. 2

Winter 1983

About the NASA Technology Utilization Program

The National Aeronautics and Space Act of 1958, which established NASA and the United States civilian space program, requires that "The Administration shall provide for the widest practicable and appropriate dissemination of information concerning its activities and the results thereof."

To help carry out this objective, NASA's Technology Utilization (TU) Program was established in 1962. Now, as an element of NASA's Technology Utilization and Industry Affairs Division, this program offers a variety of valuable services to help transfer aerospace technology to nonaerospace applications, thus assuring American taxpayers maximum return on their investment in space research; thousands of spinoffs of NASA research have already occurred in virtually every area of our economy.

The TU program has worked for engineers, scientists, technicians, and businessmen; and it can work for you.

NASA Tech Briefs

Tech Briefs is published quarterly and is free to engineers in U.S. industry and to other domestic technology transfer agents. It is both a current-awareness medium and a problem-solving tool. Potential products . . . industrial processes . .. basic and applied research . . . shop and lab techniques . . . computer software . . . new sources of technical data . . . concepts . . . can be found here. The short section on New Product Ideas highlights a few of the potential new products contained in this issue. The remainder of the volume is organized by technical category to help you quickly review new developments in your areas of interest. Finally, a subject index makes each issue a convenient reference file.

Further Information on Innovations

Although some new technology announcements are complete in themselves, most are backed up by Technical Support Packages (TSP's). TSP's are available without charge and may be ordered by simply completing a TSP Request Card found at the back of this volume. Further information on some innovations is available for a nominal fee from other sources, as indicated. In addition, Technology Utilization Officers at NASA Field Centers will often be able to lend necessary guidance and assistance.

Patent Licenses

Patents have been issued to NASA on some of the inventions described, and patent applications have been submitted on others. Each announcement indicates patent status and availability of patent licenses if applicable.

Other Technology Utilization Services

To assist engineers, industrial researchers, business executives, Government officials, and other potential users in applying space technology to their problems, NASA sponsors Industrial Applications Centers. Their services are described on page A7. In addition, an extensive library of computer programs is available through COSMIC, the Technology Utilization Program's outlet for NASA-developed software.

Applications Program

NASA conducts applications engineering projects to help solve public-sector problems in such areas as safety, health, transportation, and environmental protection. Two applications teams, staffed by professionals from a variety of disciplines, assist in this effort by working with Federal agencies and health organizations to identify critical problems amenable to solution by the application of existing NASA technology.

Reader Feedback

We hope you find the information in *NASA Tech Briefs* useful. A reader-feedback card has been included because we want your comments and suggestions on how we can further help you apply NASA innovations and technology to your needs. Please use it, or if you need more space, write to the Manager, Technology Transfer Division, P.O. Box 8757, Baltimore/ Washington International Airport, Maryland 21240.

NASA Tech Briefs

National Aeronautics and Space Administration

WINTER 1983
Volume 8, Number 2

NASA TU Services	A3	Technology Utilization services that can assist you in learning about and applying NASA technology.
New Product Ideas	A9	A summary of selected innovations of value to manufacturers for the development of new products.
Tech Briefs	163	**Electronic Components and Circuits**
	177	**Electronic Systems**
	189	**Physical Sciences**
	203	**Materials**
	219	**Life Sciences**
	223	**Mechanics**
	251	**Machinery**
	269	**Fabrication Technology**
	293	**Mathematics and Information Sciences**
Subject Index	299	Items in this issue are indexed by subject; a cumulative index will be published yearly.

COVERS: The photographs on the front and back covers illustrate developments by NASA and its contractors that have resulted in commercial and nonaerospace spinoffs. You can use the TSP Request Card at the back of this issue to learn more about the Improved Fishing Nets [Circle 183] and the Automated Electrophoresis System [Circle 184].

About This NASA Publication

NASA Tech Briefs, a quarterly publication, is distributed free to qualified U.S. citizens to encourage commercial application of U.S. space technology. For information on publications and services available through the NASA Technology Utilization Program, write to the Manager, Technology Transfer Division, P.O. Box 8757, Baltimore/Washington International Airport, Maryland 21240.

"The Administrator of National Aeronautics and Space Administration has determined that the publication of this periodical is necessary in the transaction of the public business required by law of this Agency. Use of funds for printing this periodical has been approved by the Director of the Office of Management and Budget."

Change of Address

If you wish to have NASA Tech Briefs forwarded to your new address, use the Subscription Card enclosed at the back of this volume of NASA Tech Briefs. Be sure to check the appropriate box indicating change of address, and also fill in your identification number (T number) in the space indicated.

Communications Concerning Editorial Matter

For editorial comments or general communications about NASA Tech Briefs, you may use the Feedback card in the back of NASA Tech Briefs, or write to: The Publications Manager, Technology Utilization Office (LGT-1), NASA Headquarters, Washington, DC 20546. Technical questions concerning specific articles should be directed to the Technology Utilization Officer of the sponsoring NASA Center (addresses listed on page A4).

Expanded Format

To speed the publication of our backlog of Tech Brief items, we have increased our per-issue contents by adding short articles to the end of each subject section of NASA Tech Briefs. Titled "MiniBriefs," these short articles describe NASA innovations and reports in an abbreviated format. Most are backed up by Technical Support Packages (TSP's), which can be obtained by using the TSP Request Card at the back of this issue.

Acknowledgements

NASA Tech Briefs is published quarterly by the National Aeronautics and Space Administration, Technology Transfer Division, Washington, DC: Administrator: **James M. Beggs;** Director, Technology Utilization and Industry Affairs Division: **Ronald J. Philips;** Publications Manager: **Leonard A. Ault.** Prepared for the National Aeronautics and Space Administration by **Logical Technical Services Corp.:** Editor-in-Chief: **Jay Kirschenbaum;** Art Director: **Ernest Gillespie;** Managing Editor: **Jerome Rosen;** Chief Copy Editor: **Oden Browne;** Staff Editors: **James Boyd, Larry Grunberger, Paul Johnson, Jordan Randjelovich, Ted Selinsky, George Watson;** Graphics: **Andrew Abramoske, Ron Krause, Luis Martinez, Huburn Profitt;** Editorial & Production: **Camille McQueen, Richard Johnson, Tony Franchina, Sabrina Gibson, Stephanie Godino, Leslie Iwaskow, Henry Lai, Marion Larson, Linda Lucas, Frank Ponce, Joe Renzler, Melanie Tarka, Elizabeth Texeira, Ernestine Walker.**

NASA TU SERVICES

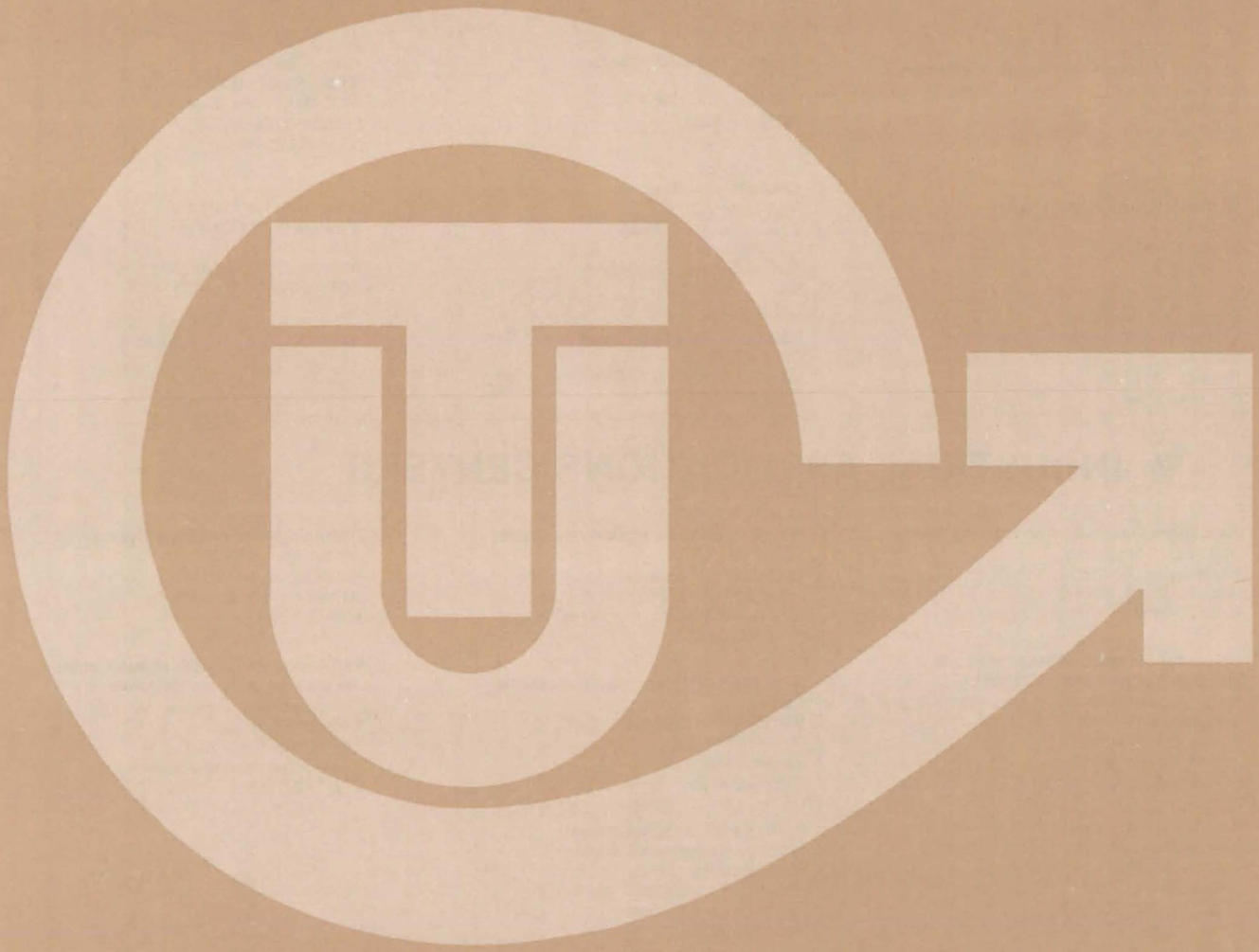

NASA TECHNOLOGY UTILIZATION NETWORK

★ TECHNOLOGY UTILIZATION OFFICERS

Stanley A. Miller
Ames Research Center
Code 240-10
Moffett Field, CA 94035
(415) 965-6471

Stanley A. Miller
Hugh L. Dryden Flight Research Center
Code 240-10
Moffett Field, CA 94035
(415) 965-6471

Donald S. Friedman
Goddard Space Flight Center
Code 702.1
Greenbelt, MD 20771
(301) 344-6242

William Chmylak
Lyndon B. Johnson Space Center
Code AL-32
Houston, TX 77058
(713) 483-3809

U. Reed Barnett
John F. Kennedy Space Center
Code PT-SPD
Kennedy Space Center, FL 32899
(305) 867-3017

John Samos
Langley Research Center
Mail Stop 139A
Hampton, VA 23665
(804) 865-3281

Harrison Allen, Jr.
Lewis Research Center
Mail Code 7-3
21000 Brookpark Road
Cleveland, OH 44135
(216) 433-4000, Ext. 6422

Ismail Akbay
George C. Marshall Space Flight Center
Code AT01
Marshall Space Flight Center, AL 35812
(205) 453-2224

Leonard A. Ault
NASA Headquarters
Code ETD-6
Washington, DC 20546
(202) 453-8424

Aubrey Smith
NASA Resident Office-JPL
4800 Oak Grove Drive
Pasadena, CA 91103
(213) 354-4849

Gilmore H. Trafford
Wallops Flight Center
Code OD
Wallops Island, VA 23337
(804) 824-3411, Ext. 201

● INDUSTRIAL APPLICATIONS CENTERS

Aerospace Research Applications Center
1201 East 38th Street
Indianapolis, IN 46205
John M. Ulrich, director
(317) 264-4644

Computer Software Management and Information Center (COSMIC)
Suite 112, Barrow Hall
University of Georgia
Athens, GA 30602
John A. Gibson, director
(404) 542-3265

Kerr Industrial Applications Center
Southeastern Oklahoma State University
Durant, OK 74701
James Harmon, director
(405) 924-0121, Ext. 413

NASA Industrial Applications Center
701 LIS Building
University of Pittsburgh
Pittsburgh, PA 15260
Paul A. McWilliams, executive director
(412) 624-5211

New England Research Applications Center
Mansfield Professional Park
Storrs, CT 06268
Daniel Wilde, director
(203) 486-4533

North Carolina Science and Technology Research Center
Post Office Box 12235
Research Triangle Park, NC 27709
James E. Vann, director
(919) 549-0671

Technology Applications Center
University of New Mexico
Albuquerque, NM 87131
Stanley Morain, director
(505) 277-3622

NASA Industrial Applications Center
University of Southern California
Denny Research Building
University Park
Los Angeles, CA 90007
Robert Mixer, acting director
(213) 743-6132

■ STATE TECHNOLOGY APPLICATIONS CENTERS

NASA/University of Florida
State Technology Applications Center
500 Weil Hall
University of Florida
Gainesville, FL 32611
J. Ronald Thornton, director

Gainesville:	(904) 392-6760
Boca Raton:	(305) 395-5100, Ext. 2292
Fort Lauderdale:	(305) 776-6645
Jacksonville:	(904) 646-2478
Orlando:	(305) 275-2706
Pensacola:	(904) 476-9500, Ext. 426
Tampa:	(813) 974-2499

NASA/University of Kentucky
State Technology Applications Program
109 Kinkead Hall
University of Kentucky
Lexington, KY 40508
William R. Strong, manager
(606) 258-4632

◆ PATENT COUNSELS

Robert F. Kempf
Asst. Gen. Counsel for patent matters
NASA Headquarters
Code GP-4
400 Maryland Avenue, SW.
Washington, DC 20546
(202) 755-3954

Darrell G. Brekke
Ames Research Center
Mail Code: 200-11A
Moffett Field, CA 94035
(415) 965-5104

Darrell G. Brekke
Hugh L. Dryden Flight Research Center
Mail Code: 201-11A
Moffett Field, CA 94035
(415) 965-5104

John O. Tresansky
Goddard Space Flight Center
Mail Code: 204
Greenbelt, MD 20771
(301) 344-7351

Marvin F. Matthews
Lyndon B. Johnson Space Center
Mail Code: AL-3
Houston, TX 77058
(713) 483-4871

James O. Harrell
John F. Kennedy Space Center
Mail Code: SA-PAT
Kennedy Space Center, FL 32899
(305) 867-2544

Howard J. Osborn
Langley Research Center
Mail Code: 279
Hampton, VA 23665
(804) 827-3725

Norman T. Musial
Lewis Research Center
Mail Code: 500-311
21000 Brookpark Road
Cleveland, OH 44135
(216) 433-4000, Ext. 346

Leon D. Wofford, Jr.
George C. Marshall Space Flight Center
Mail Code: CC01
Marshall Space Flight Center, AL 35812
(205) 453-0020

Paul F. McCaul
NASA Resident Office-JPL
Mail Code: 180-601
4800 Oak Grove Drive
Pasadena, CA 91103
(213) 354-2700

▲ APPLICATION TEAMS

Doris Rouse, director
Research Triangle Institute
Post Office Box 12194
Research Triangle Park, NC 27709
(919) 541-6980

James P. Wilhelm, director
SRI International
333 Ravenswood Avenue
Menlo Park, CA 94026
(415) 326-6200, Ext. 3520

TECHNOLOGY UTILIZATION OFFICERS

Technology transfer experts can help you apply the innovations in NASA Tech Briefs.

The Technology Utilization Officer at each NASA Field Center is an applications engineer who can help you make use of new technology developed at his center. He brings you NASA Tech Briefs and other special publications, sponsors conferences, and arranges for expert assistance in solving technical problems.

Technical assistance, in the form of further information about NASA innovations and technology, is one of the services available from the TUO. Together with NASA scientists and engineers, he can often help you find and implement NASA technology to meet your specific needs.

Technical Support Packages (TSP's) are prepared by the center TUO's. They provide further technical details for articles in NASA Tech Briefs. This additional material can help you evaluate and use NASA technology. You may receive most TSP's free of charge by using the TSP Request Card found at the back of this issue.

Technical questions about articles *in NASA Tech Briefs are answered in the TSP's. When no TSP is available, or you have further questions, contact the Technology Utilization Officer at the center that sponsored the research* [see page A4].

NASA INVENTIONS AVAILABLE FOR LICENSING

Over 3,500 NASA inventions are available for licensing in the United States — both exclusive and nonexclusive.

NASA grants patent licenses, both exclusive and nonexclusive, for the commercial use of U.S. and foreign patents and patent applications owned by NASA. All licenses require royalties and are granted by express written agreements in accordance with the NASA Patent-Licensing Regulations.

Additional information about NASA inventions may be found in the *"NASA Patent Abstract Bibliography"* (PAB), containing abstracts of all NASA inventions, which can be purchased from the National Technical Information Service, Springfield, VA 22161. The PAB is updated semiannually.

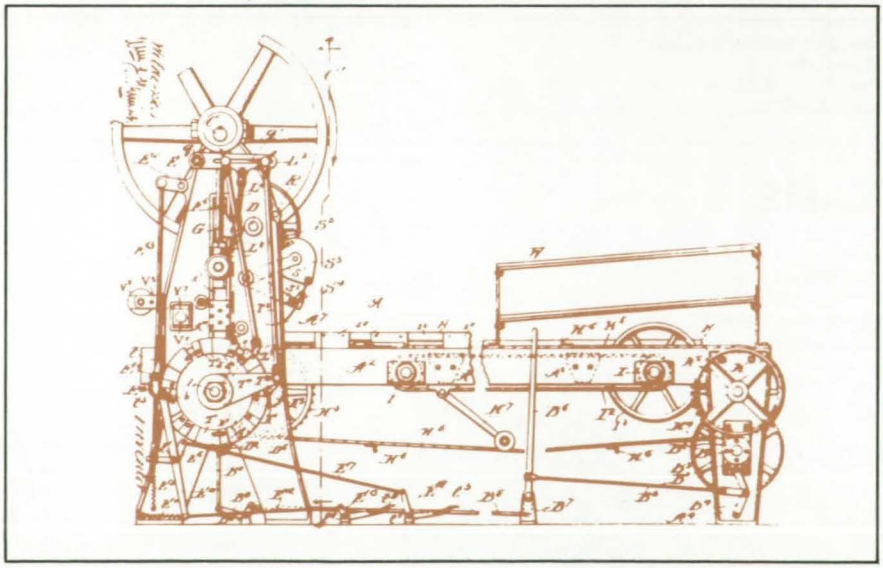

Patent licenses for inventions *described in NASA Tech Briefs are frequently available. Many of the inventions reported in NASA Tech Briefs are patented or are under consideration for a patent at the time they are published. The current patent status is described at the end of the article; if no patent action is contemplated by NASA, there is no statement about patents. If you want to know more about the patent program or are interested in licensing a particular invention, contact the Patent Counsel at the NASA Field Center that sponsored the research* [see page A5]. *Be sure to refer to the NASA reference number at the end of the Tech Brief.*

APPLICATION TEAMS

Technology-matching and problem-solving assistance to public-sector organizations

Application engineering projects are conducted by NASA to help solve public-sector problems in such areas as safety, health, transportation, and environmental protection. Some application teams specialize in biomedical disciplines; others, in engineering and scientific problems. Staffed by professionals from various disciplines, these teams work with other Federal agencies and health organizations to identify critical problems amenable to solution by the application of existing NASA technology.

Public-sector organization *representatives can learn more about application teams by contacting a nearby NASA Field Center Technology Utilization Office* [see page A4].

INDUSTRIAL APPLICATIONS CENTERS

Computerized access to over 10 million documents worldwide

Computerized information retrieval from one of the world's largest banks of technical data is available from NASA's network of Industrial Applications Centers (IAC's). The IAC's give you access to 1,800,000 technical reports in the NASA data base and to more than 10 times that many reports and articles found in nearly 200 other computerized data bases.

The major sources include:

- *750,000 NASA Technical Reports*
- *Selected Water Resources Abstracts*
- *NASA Scientific and Technical Aerospace Reports*
- *Air Pollution Technical Information Center*
- *NASA International Aerospace Abstracts*
- *Chem Abstracts Condensates*
- *Engineering Index*
- *Energy Research Abstracts*
- *NASA Tech Briefs*
- *Government Reports*
- *Announcements*

and many other specialized files on food technology, textile technology, metallurgy, medicine, business, economics, social sciences, and physical science.

The IAC services range from tailored literature searches through expert technical assistance:

- *Retrospective Searches:* Published or unpublished literature is screened, and documents are identified according to your interest profile. IAC engineers tailor results to your specific needs and furnish abstracts considered the most pertinent. Complete reports are available upon request.
- *Current-Awareness Searches:* IAC engineers will help design a program to suit your needs. You will receive selected monthly or quarterly abstracts on new developments in your area of interest.
- *Technical Assistance:* IAC engineers will help you evaluate the results of your literature searches. They can help find answers to your technical problems and put you in touch with scientists and engineers at appropriate NASA Field Centers.

Prospective clients *can obtain more information about these services by contacting the nearest IAC* [see page A4]. *User fees are charged for IAC information services.*

STATE TECHNOLOGY APPLICATIONS CENTERS

Technical information services for industry and state and local government agencies.

Government and private industry in Florida and Kentucky can utilize the services of NASA's State Technology Applications Centers (STAC's). The STAC's differ from the Industrial Applications Centers described on page A7, primarily in that they are integrated into existing state technical assistance programs and serve only the host state, whereas the IAC's serve multistate regions.

Many data bases, including the NASA base and several commercial bases, are available for automatic data retrieval through the STAC's. Other services such as document retrieval and special searches are also provided. (Like the IAC's, the STAC's normally charge a fee for their services.)

To obtain information *about the services offered, write or call the STAC in your state* [*see page A4*].

COSMIC®

An economical source of computer programs developed by NASA and other government agencies

A vast software library is maintained by COSMIC — the Computer Software Management and Information Center. COSMIC gives you access to approximately 1,600 computer programs developed for NASA and the Department of Defense and selected programs for other government agencies. Programs and documentation are available at reasonable cost.

Available programs range from management (PERT scheduling) to information science (retrieval systems) and computer operations (hardware and software). Hundreds of engineering programs perform such tasks as structural analysis, electronic circuit design, chemical analysis, and the design of fluid systems. Others determine building energy requirements and optimize mineral exploration.

COSMIC services go beyond the collection and storage of software packages. Programs are checked for completeness; special announcements and an indexed software catalog are prepared; and programs are reproduced for distribution. Customers are helped to identify their software needs; and COSMIC follows up to determine the successes and problems and to provide updates and error corrections. In some cases, NASA engineers can offer guidance to users in installing or running a program.

Information about programs *described in NASA Tech Briefs articles can be obtained by completing the COSMIC Request Card at the back of this issue. Just circle the letters that correspond to the programs in which you are interested.*

NEW PRODUCT IDEAS

NEW PRODUCT IDEAS are just a few of the many innovations described in this issue of NASA Tech Briefs and having promising commercial applications. Each is discussed further on the referenced page in the appropriate section in this issue. If you are interested in developing a product from these or other NASA innovations, you can receive further technical information by requesting the TSP referenced at the end of the full-length article or by writing the Technology Utilization Office of the sponsoring NASA center (see page A4). NASA's patent-licensing program to encourage commercial development is described on page A6.

IC Fabrication Methods Improve Laser Diodes

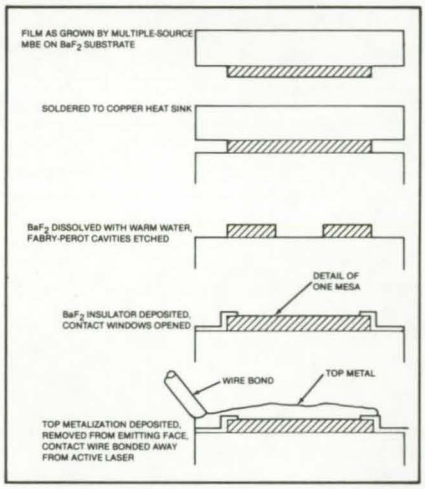

A family of high-performance, tunable diode lasers has been developed for use in passive laser heterodyne spectrometers. Multiple-source molecular-beam epitaxy (MBE) is employed to grow precisely-controlled multilayer structures of (Pb/Sn)Te on BaF_2 substrates. The diodes are fabricated using standard IC processes that include photolithography, selective etching, and vacuum deposition of metals and insulators. Packaging refinements have improved the thermal-cycling characteristics of the diodes and increased their room-temperature shelf life.
(See page 275.)

Two-Layer Glass Thermal-Control Coating

All-glass thermal-control coatings withstand repeated exposure to temperatures as high as 2,000° F (1,095° C) with only minimal degradation of optical properties. The coatings have an outer scattering layer and an inner high-emissivity layer, for a net absorptivity/emissivity ratio less than 0.4. Although originally developed to prevent excessive solar heating of spacecraft, the new coatings may have industrial uses in solar-energy equipment, high-temperature chemical processing, and high-temperature instrumentation.
(See page 209.)

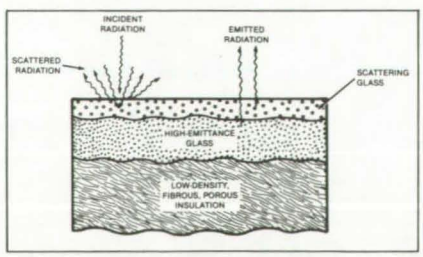

Vise for Crystal Cleavage

A vise manipulates brittle crystals, such as lithium fluoride, and other workpieces so that they are in the proper position for cleavage. The vise jaws are fitted with ball bushings that ride on guide rods. The guide rods support the jaws and maintain their alinement,

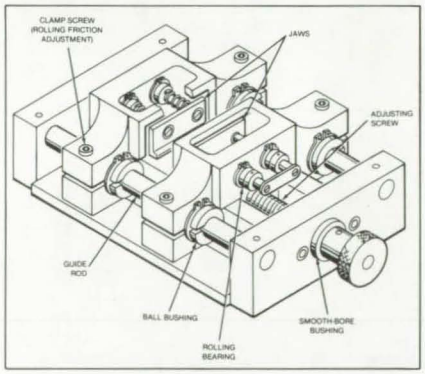

thereby maintaining the crystal or other workpiece in alinement. Both starting friction and sliding friction are reduced by the bushings so that the operator always has a good tactile sense of the forces on the jaws.
(See page 282.)

Automatic Guidance System for Welding Torches

A digital system under development automatically guides a welding torch to produce square-butt, V-groove, and lap-joint weldments within a tracking accuracy of +0.2 millimeter. The guidance system employs a digital television

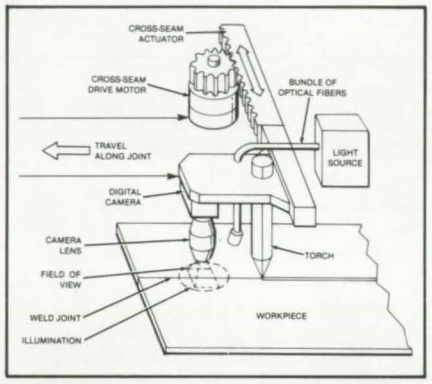

camera and a microprocessor. It compensates for thermal expansion and intense heat at the joint. In addition, the system uses algorithms that minimize the effects of stray light reflection, changes in light level, erroneous signals, momentary loss of signal, and scratches on the workpiece.
(See page 273.)

Liquid-Droplet Radiative Cooler

A large-area, low-mass radiative cooler originally proposed for spacecraft may be applicable to industrial processes requiring noncontacting cooling of process liquids. In the cooler, low-vapor-pressure oil at a temperature of about 300 K would be sprayed as fine

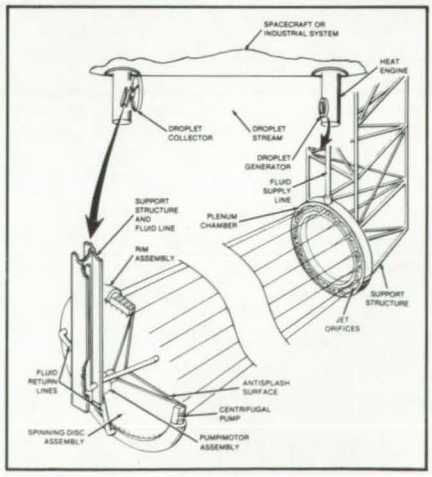

droplets from a spray head toward a collector. The disk-shaped collector would

rotate, its periphery acting as a centrifugal pump to recirculate the oil. During transit from the spray head to the collector, the droplets would cool by radiating to space, thus removing waste heat.
(See page 225.)

Low-Density High-Strength Foamed Materials

Molten bubbles of metal or plastic coalesce into strong, lightweight materials that look like solidified foam. The bubbles are formed in a compartment that receives the molten material and the compressed gas that fills the bubbles.

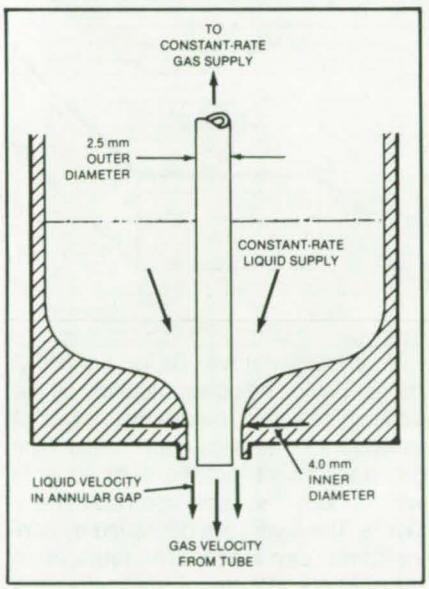

The process can tailor materials for different uses by varying the combinations of gases, gas pressures, and base materials. The materials can be used for construction and can be extruded into molds, sawed, nailed, and generally handled as wood.
(See page 211.)

Miniature Airflow Sensor

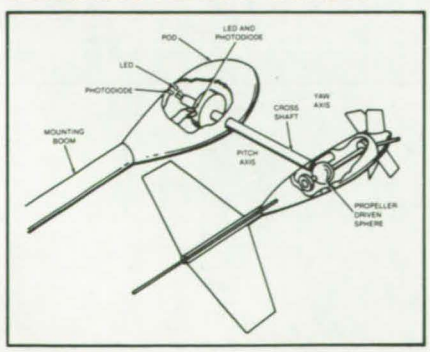

A miniature, tape-mounted flow-angle and velocity sensor measures the local flow ahead of a wing. The sensor, which uses an electro-optic technique, operates as a wind vane that self-alines in the airstream through two independent axes. The vane is attached to the wing surface through a hollow boom that fits on a plate attached to the wing with two-sided, neoprenefoam tape.
(See page 226.)

Integrated Tactile Sensor for Robots

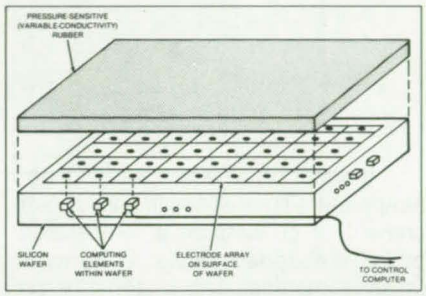

A proposed large-scale integrated (LSI) circuit on a silicon wafer would give robots, parts-handling machines, and remote-control devices a sense of touch. The wafer, placed on the contact surfaces of manipulators, would transduce, compute, and communicate touch information. The exposed surface of the LSI wafer contains an array of electrode pairs covered by a sheet of electrically conducting rubber, the resistivity of which varies with pressure. The electrodes furnish a pressure-dependent signal to computation elements.
(See page 233.)

Reusable Explosive-Release Mechanism

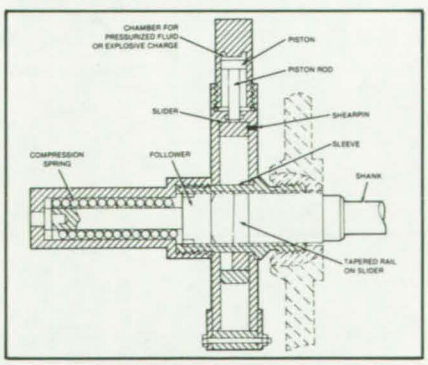

A lightweight release mechanism replaces exploding bolts in applications where reuse is an advantage. The mechanism is activated by the detonation of a small explosive charge or the rush of pressurized gas or other fluid into a small chamber above a piston. Only the charge has to be replaced for the new device to be ready for service. A slider release mechanism bears heavy loads while latched, yet gives a smooth release motion. Potential applications of the device include the emergency release of lifting cables from helicopters, cranes, and hoists.
(See page 261.)

Continuous-Reading Cryogen Level Sensor

Two pressure transducers are used in a system for measuring the amount of cryogenic liquid in a tank. The system provides continuous measurements accurate within 0.03 percent despite variations in liquid density. Vibrating-cylinder pressure sensors are situated outside the tank — at the bottom and at the top.

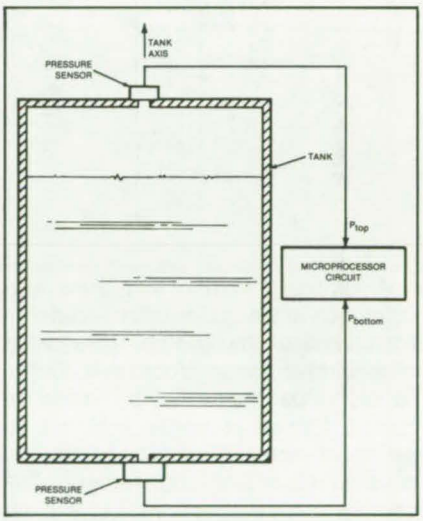

Each sensor communicates with the interior of the tank through a narrow tube. Cryogenic vapor transmits the local liquid pressure to the sensor. A microprocessor uses the pressure difference to compute the mass of cryogenic liquid in the tank.
(See page 234.)

High-Flow Desalination Membranes

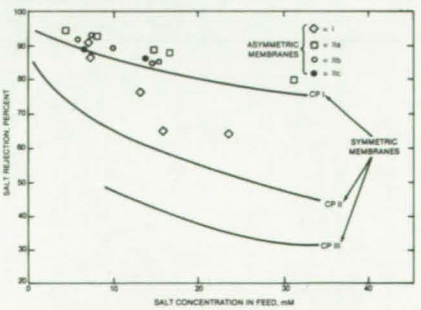

Asymmetric reverse-osmosis desalination membranes prepared by a new
(continued on next page)

method are capable of high waterflow rates and high salt rejection. The preparation uses water as the solvent. The asymmetric structure is achieved without employing a solvent/nonsolvent liquid precipitation system like that used in a previous asymmetric fabrication method. The new membranes can purify or desalinate seawater, brackish water, or industrial or domestic wastewater.
(See page 221.)

Improved Gamma- and X-Ray Pinhole Camera

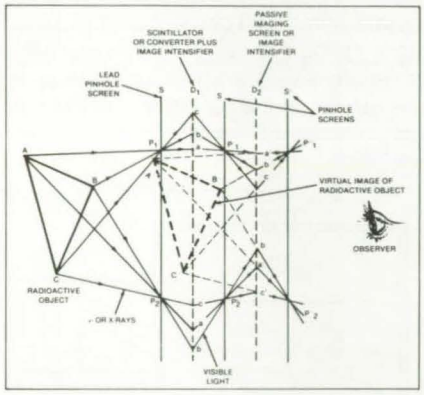

An imaging system that gives low-resolution views of radioactivity distributions has been improved by the addition of electronic image processing. Orthoscopic virtual images of a radioactive object, formed in visible light with a series of screens and pinholes, are coupled to a digitizing camera. The camera output is then sent to a data-processing system that digitally inverts each pinhole image about its pinhole axis. The image data may be then stored, subjected to enhancement or other processing, or converted back to analog form on a television screen or other display. When fully developed, the system will be useful in nuclear medicine or radioisotope imaging, tomography, and the nuclear industry.
(See page 191.)

Temperature-Averaging Thermal Probe

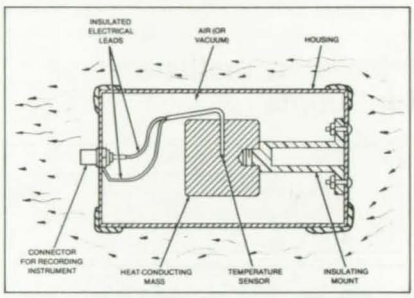

A thermal probe averages long-term temperature fluctuations in a fluid environment. It consists of a temperature probe embedded inside a thermally massive material. The material, is enclosed in a sealed housing to suppress the effects of cyclical and short-term temperature fluctuations. The probe can be used to estimate powerplant heating and cooling loads, to map temperature profiles, and to calibrate more-sensitive temperature probes.
(See page 236.)

High-Capacity Heat Pipe

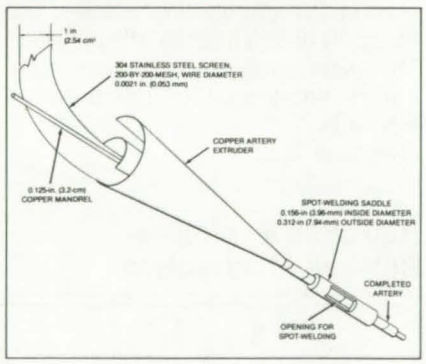

A long heat pipe employs a slender artery-and-wick structure to transport thermal energy at a rate of 2.6 kW at an operating temperature 923 K. Two layers of stainless-steel screen on its inner wall act as a wick to provide circumferential flow of the working fluid. Two arteries, also of stainless steel, provide axial flow. The thin arteries are made with a special extrusion tool.
(See page 231.)

Schottky-Barrier Photocell With Intermediate Metal Layer

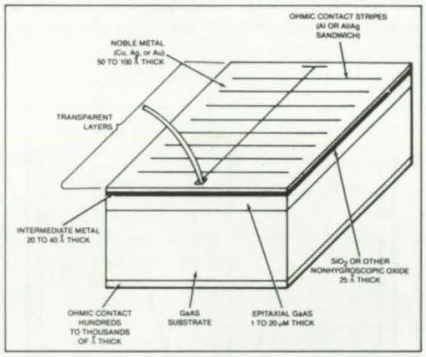

A photosensitive GaAs Schottky-barrier device has been modified by the addition of a thin intermediate layer of refractory or alkaline-earth metal. The thin transparent metallic layer adheres well to both the oxide and noble-metal layers. The layers are deposited by conventional semiconductor fabrication techniques. Photovoltaic cells and photosensors made with the new design will put out higher short-circuit currents and be better able to withstand the rigors of handling and connection to other circuit components.
(See page 169.)

Electronic Components and Circuits

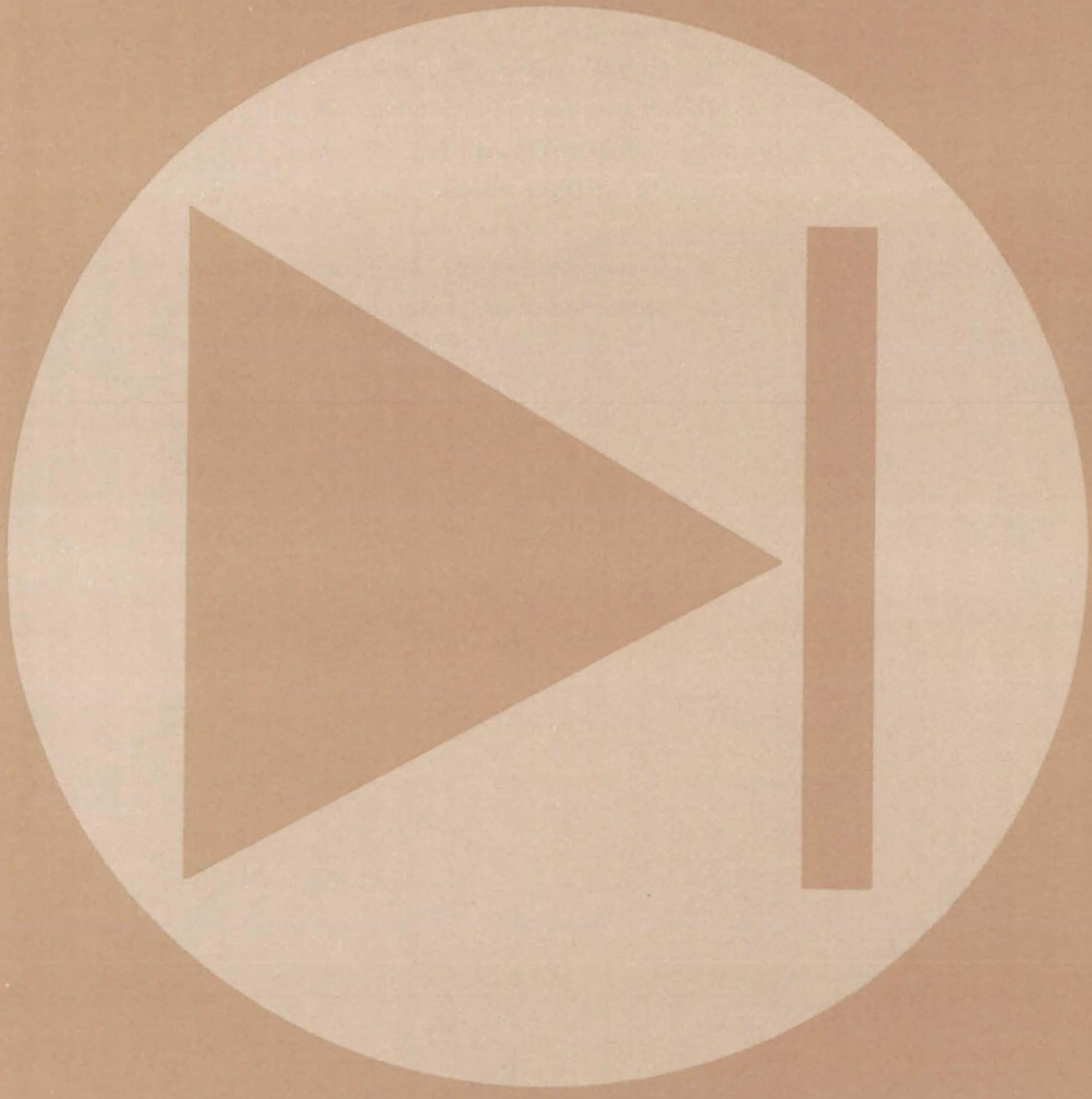

Hardware, Techniques, and Processes

165 Infrared-Responsive Monolithic MOS Circuit
166 Low-Noise Submillimeter-Wave Diode
167 Simplified High-Power Inverter
168 Energy-Saving Inverter
169 Schottky-Barrier Photocell With Intermediate Metal Layer
170 Feedthrough Seal for High-Pressure Vessel
171 Stripline Antenna Beam-Forming Network
171 Finding Open Faults in CMOS Circuits
172 Flip-Flop Digital Modulator

Books and Reports

173 Screening Plastic-Encapsulated Solid-State Devices
174 Radiation-Hardness Data for Semiconductor Devices

MiniBriefs

174

Infrared-Responsive Monolithic MOS Circuit

Lead chalcogenide photoresistors are integrated with FET amplifiers.

Goddard Space Flight Center, Greenbelt, Maryland

A monolithic interconnection technique incorporates infrared-sensitive lead chalcogenide photoresistors into metal-oxide-semiconductor (MOS) integrated circuits. This avoids the use of welded interconnection wires and separate preamplifier circuits. By thus saving space, the technique extends the benefits of high detector-packing density to infrared wavelengths between 1.65 and 2.3 μm, which are not detected by present monolithic extrinsic silicon infrared detectors.

The figure shows the structure of a detector element that includes a voltage divider containing the lead chalcogenide photoresistor and a source-follower circuit as the preamplifier or buffer. The detector element shown has six contact tabs for signal-output and power leads. If the element were to be incorporated in an array, monolithic interconnections would replace the tabs. Arrays with up to 10,000 detector elements are under consideration: These would be much too large to be practical if each photoresistor required a pair of interconnection wires running to its preamplifier.

The device is fabricated on a wafer of n-type, phosphorus-doped, 3- to 5-ohm-cm-resistivity <111> silicon. After fabricating a field-effect transistor (FET) on the wafer and covering it with an SiO_2 insulating layer [leaving two windows for contacting the source (S) and drain (D) of the FET], two metalization layers are deposited on the wafer: first a chromium layer 100 Å thick, then a gold layer 4,000 Å thick. The metalization is then photolithographically etched away except in the regions that form the contact tabs and interconnections between the various circuit elements. The gold is etched with potassium iodide, the chromium with a mixture of glycerin and hydrochloric acid.

Two of the metalization strips form ohmic contacts to the S and D regions of the FET. The chromium-and-gold structure is chemically and electrically compatible with both the FET and with the lead chalcogenide resistor material, thereby avoiding the need for wire interconnections.

The three lead chalcogenide resistors R_D, R_L, and R_S are deposited with a chemical process. Before deposition, a thickness of 30 to 50 angstroms of the exposed SiO_2 layer is etched away by immersion for a few seconds in a solution of three parts water, one part hydrofluoric acid. This forms a fresh SiO_2 surface for nucleation and cleans the metalization, all without damaging the FET already formed. The wafer is then immersed in a deposition solution of base-catalyzed thiourea complex until a first coat of a mirrorlike film of lead sulfide forms on the wafer. The lead sulfide layer is built up in stages by repeated cycles of water rinsing, drying, and deposition.

Positive photoresist is applied to the wafer; a chromium mask defining the pattern of R_D, R_L, and R_S is alined with

(continued on next page)

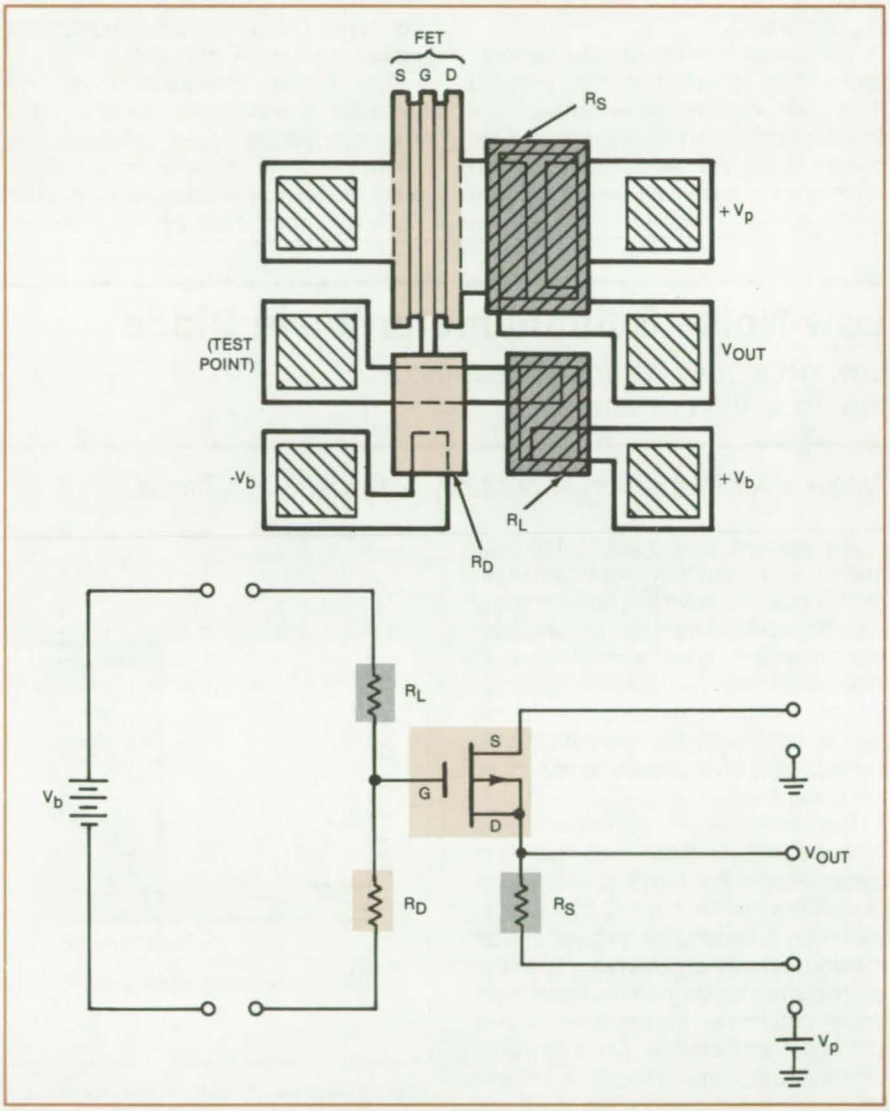

An **Infrared-Sensitive Monolithic Integrated Circuit** (above) combines a voltage divider containing a lead chalcogenide photoresistor with an FET source follower. The circuit is shown schematically below. The source and drain of the FET are p-doped regions in the underlying n-type silicon wafer. All the other structures are formed at or deposited above the original surface plane of the wafer.

the wafer; and the photoresist is exposed through the mask. The pattern is developed and unwanted photoresist removed. Lead sulfide not protected by photoresist is etched away by a brief immersion in fresh, concentrated hydrochloric acid at 25° to 30° C. The wafer is then gently rinsed in water at the same temperature and dried with an inert gas. Acetone is used to remove the remaining photoresist.

The three resistors make ohmic contact with the metalization strips beneath them. The resistors are sensitized to infrared radiation by brief heating and exposure to oxygen. An SiO_2 passivation layer is then deposited over the entire wafer surface, followed by an opaque layer of aluminum. The aluminum is then photolithographically etched away except immediately over resistors R_L and R_S. The remaining aluminum prevents infrared from reaching R_L and R_S, so that only R_D will change when the device is illuminated.

Finally, six windows are etched through the SiO_2 passivation layer to expose the contact areas on the metalization layer: These allow signal-output and power leads to be attached.

The circuit configuration can be modified depending on requirements: The conductivity types (positive- and negative-doping, depletion- or enhancement-mode) may be interchanged in the FET. R_L rather than R_D may be left exposed to act as the photosensitive element; and other lead chalcogenide materials, such as lead selenide or lead telluride, may be used to obtain a different spectral response.

This work was done by Murzban D. Jhabvala, David R. Dargo, and John C. Lyons of **Goddard Space Flight Center.** *For further information, Circle 1 on the TSP Request Card.*

This invention is owned by NASA, and a patent application has been filed. Inquiries concerning nonexclusive or exclusive license for its commercial development should be addressed to the Patent Counsel, Goddard Space Flight Center [see page A5]. Refer to GSC-12782.

Low-Noise Submillimeter-Wave Diode

Low noise may be achieved without the usual high resistance.

NASA's Jet Propulsion Laboratory, Pasadena, California

A proposed mixing diode for millimeter- and submillimeter-wavelength receivers would have low noise and low resistance. Heretofore, the same doping that minimized noise also resulted in high resistance. Low noise is essential for sensitivity in reception, and low resistance (interacting with the junction capacitance) is necessary to maximize the cutoff frequency.

The semiconductor portion of a conventional mixing diode (see figure) is composed of a thin n-type epitaxial layer of gallium arsenide, 500 to 2,500 Å thick, grown on a degenerately-doped n-type substrate of gallium arsenide. The concentration of dopant in the epitaxial layer largely determines the series resistance and noise temperature. For a low concentration (for example, 10^{16} dopant atoms per cubic centimeter), the noise will be low, but the series resistance will be high. For a high concentration (3×10^{17} atoms per cubic centimeter), series resistance will be low, but noise will be high.

In the new diode structure, a barrier of p-type material 200 to 300 Å thick is placed between the metal anode and heavily-doped gallium arsenide. The n-type epitaxial layer is eliminated. The barrier prevents quantum tunneling of electrons between the semiconductor and the metal. Such tunneling would otherwise cause high noise levels in the device. At the same time, the degenerately doped substrate presents a very low series resistance.

The dopant level in the p-type barrier is not critical. It is important, however, that the resulting potential barrier have a flat top if it is to prevent tunneling. The dopant concentration in the part of the substrate beyond the barrier can be reduced if a higher reverse-breakdown voltage is needed.

Doping Profiles of old and new devices are compared. A high-breakdown-voltage option is provided in the new structure.

This work was done by Robert J. Mattauch of the University of Virginia for **NASA's Jet Propulsion Laboratory.** *For further information, Circle 2 on the TSP Request Card.*

Inquiries concerning rights for the commercial use of this invention should be addressed to the Patent Counsel, NASA Resident Office-JPL [see page A5]. Refer to NPO-15935.

Simplified High-Power Inverter

Only one gate-turnoff device commutates all thyristors in the circuit.

NASA's Jet Propulsion Laboratory, Pasadena, California

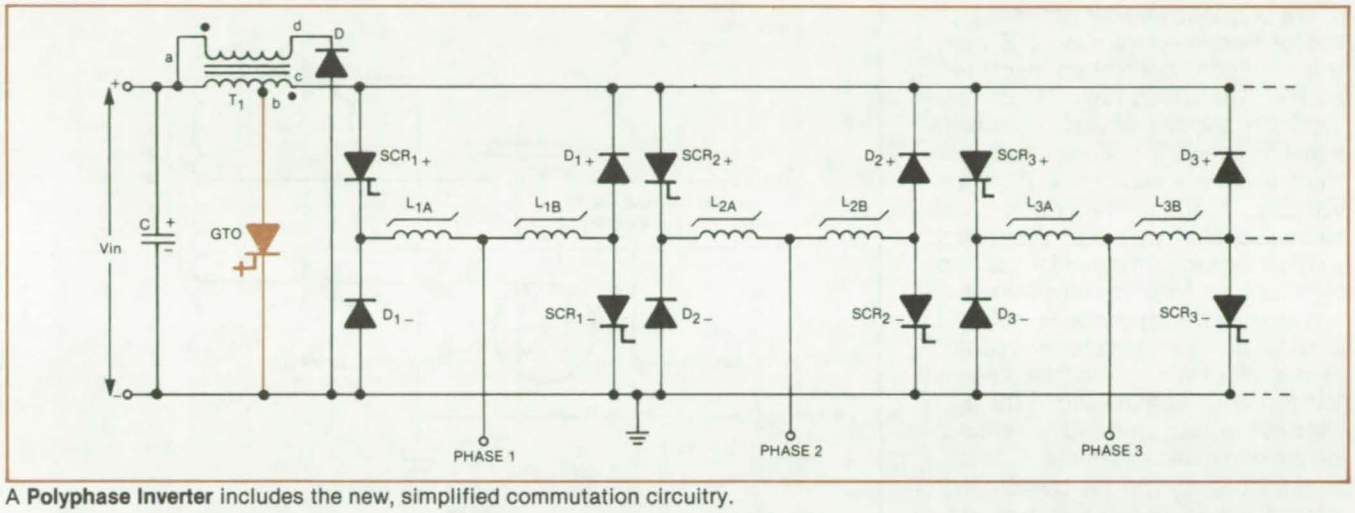

A **Polyphase Inverter** includes the new, simplified commutation circuitry.

A solid-state inverter is simplified by the use of a single gate-turnoff device (GTO) to commutate multiple silicon controlled rectifiers (SCR's). By eliminating conventional commutation circuitry, the GTO reduces cost, size, and weight. GTO commutation is expected to be generally applicable to inverters of greater than 1-kilowatt capacity. Applications include emergency power, load leveling, drives for traction and stationary polyphase motors, and photovoltaic-power conditioning.

The GTO is connected to a tap on an input inductor that feeds an SCR inverting bridge (see figure). Turning on the GTO causes all the SCR's to become back-biased, and the required SCR's can then be turned off.

Only two SCR's per phase need be turned on. Each SCR is turned on in the conventional manner — that is, a positive pulse of the appropriate duration is applied to the gate of the positive-side or negative-side SCR in the affected phase.

The commutation sequence is as follows: Gate drive to the proper SCR is removed (or made negative). The GTO is turned on with a positive current pulse to its gate. This action pulls tap b of transformer T_1 to near-ground level. Autotransformer action of T_1 causes leg c to drop below ground. This in turn causes each of the SCR's to become reverse-biased. The GTO remains conducting for an interval greater than the required SCR turnoff time. After this interval, the GTO is turned off by a negative current pulse applied to its gate.

Small saturating inductors L_{iA} and L_{iB} isolate each SCR from its corresponding antiparallel diode during the commutation interval. They also enable the reverse SCR voltage to exceed the diode forward voltage drop and prevent excessive currents from flowing in the diode and GTO during that time.

Winding ab of transformer T_1 must have enough inductance to limit the current increase through the GTO during the commutation interval. The core must not saturate at peak current. Winding ad and diode D enable energy stored in T_1 during the commutation interval to be returned to the power source when the GTO is turned off.

Upon turnoff of the GTO the rate of voltage rise across the GTO and SCR's must not be allowed to exceed the critical values for spurious self-triggering. Control of the voltage rise is provided by a capacitor/resistor/diode "snubber" between point b and ground or point c and ground.

In industrial applications, it is often desirable that a motor being driven by the inverter provide negative torques for dynamic braking. When the power source is a battery or other bidirectional device, the circuit is adequate as shown in the figure. However, when power is derived from a unidirectional source (a bridge rectifier, for example), it is necessary to divert the reverse current through an external load resistance that can be connected across the input-voltage terminals as needed.

Conventional turn-on and turnoff control algorithms may be used with the new inverter. For example, the GTO may be made conductive during regular intervals. The commutation of any one or more SCR's may be performed during (but only during) any such interval. The frequency of the intervals may be varied in accordance with load voltage and current to minimize losses.

Whenever current through a given SCR exceeds a threshold (for example, a sine-wave reference), gate drive is removed from that SCR. Commutation of that SCR will occur automatically during the next commutation interval. Whenever current in a given phase drops below a second lower threshold, the appropriate SCR is fired (provided that the opposing SCR is not conducting at the moment).

This work was done by Dean B. Edwards and Wally E. Rippel of Caltech for **NASA's Jet Propulsion Laboratory.** *For further information, Circle 3 on the TSP Request Card.*

Inquiries concerning rights for the commercial use of this invention should be addressed to the Patent Counsel, NASA Resident Office-JPL [see page A5]. Refer to NPO-15961.

Energy-Saving Inverter

Commutation by a field-effect transistor allows more efficient operation.

NASA's Jet Propulsion Laboratory, Pasadena, California

In a proposed inverter circuit, a high-voltage field-effect transistor (FET) controls silicon controlled rectifiers (SCR's). The circuit requires only one capacitor and one inductor in its commutation circuit: It is simpler, more efficient, and more economical than conventional inverters. The principle can also be adapted to dc-to-dc converters.

The inverter is intended for such applications as dc-to-dc converters, battery chargers, and polyphase motors. It provides both commutation and control of the time rate of voltage change (dV/dt) during commutation. The FET handles the main switched current during the commutation interval.

At the beginning of the commutation interval, a given SCR is switched off by simultaneously removing the SCR gate drive and applying an appropriate current pulse to the gate/capacitor node (see upper part of figure). The FET is turned on, and both SCR's in an opposed pair are reverse-biased by the autotransformer action of inductor L_1. At the end of the commutation interval, the FET is turned off but in such a gradual way that the dV/dt applied to the SCR does not exceed its breakdown limit. During the commutation interval, gate drive is maintained for the opposing SCR to keep it from turning off.

The FET can also be used with a pair of bipolar transistors (see lower part of figure) to enhance switching speed and to improve ruggedness. The FET is pulsed on when either transistor is turning on or off. The FET reduces switching stress on the bipolar transistors, which are susceptible to second breakdown. Since the FET is faster in switching than a bipolar transistor, switching loss is less. Also, since the bipolars have lower saturation losses and cost than do FET's, power losses and costs are less than in pure-FET circuits.

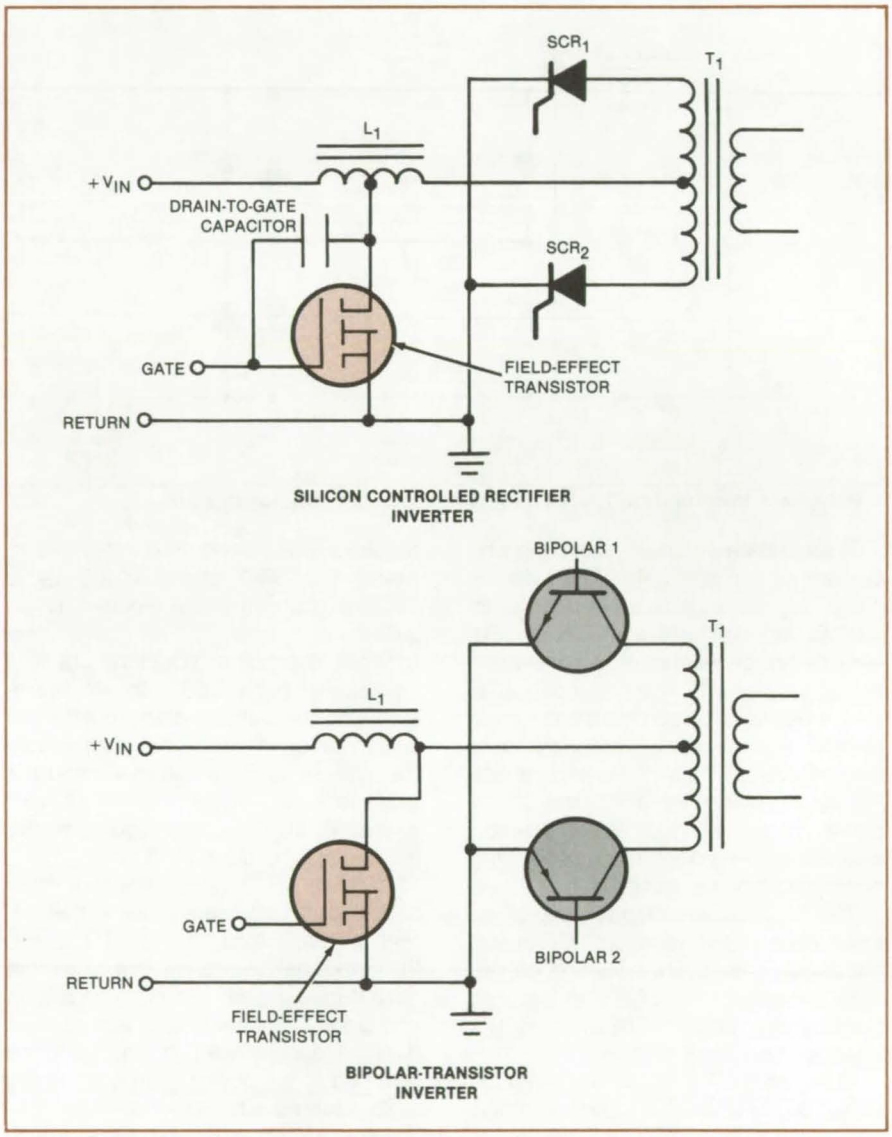

A **Field-Effect Transistor** can commutate either silicon controlled rectifiers or bipolar transistors.

This work was done by Wally E. Rippel and Dean B. Edwards of Caltech for **NASA's Jet Propulsion Laboratory.** *For further information, Circle 4 on the TSP Request Card.*

Inquiries concerning rights for the commercial use of this invention should be addressed to the Patent Counsel, NASA Resident Office-JPL [see page A5]. Refer to NPO-15291.

Schottky-Barrier Photocell With Intermediate Metal Layer

Device output and durability are increased.

Goddard Space Flight Center, Greenbelt, Maryland

The design of a photosensitive GaAs Schottky-barrier device has been modified by the addition of an intermediate layer of refractory or alkaline earth metal. Photovoltaic cells and photosensors made with the new design will put out higher short-circuit currents and be better able to withstand the rigors of handling and connection to other circuit components.

A previous design includes a GaAs substrate with a thin epitaxial layer of semiconducting GaAs, followed by a layer of oxide, followed next by a layer of noble metal thin enough to transmit appreciable light. The noble-metal and epitaxial-GaAs layers form a Schottky barrier. A major disadvantage of the previous design is that none of the noble metals adheres well to the oxide layer. The new design (see Figure 1) is similar to the older version but includes a thin, transparent metallic layer that adheres well to both the oxide and noble-metal layers.

The substrate is highly doped GaAs with a charge-carrier concentration of $\sim 10^{17}$ cm^{-3}. The second GaAs layer is grown by liquid-phase epitaxy to a thickness of 1 to 20 μm, with a charge-carrier density of $\sim 10^{16}$ cm^{-3}. If the substrate is n-type GaAs, the epitaxial layer has n + conductivity. If the substrate is p-type, then a p + epitaxial layer is used. The ohmic contact is applied to the bottom surface by vacuum deposition of a conductive material — for example, Au/Ge eutectic alloy.

An insulating transparent layer of SiO_2 or other nonhygroscopic oxide is applied to a thickness of 25Å by anodic or vacuum deposition or by a proprietary solution method. The intermediate metal layer is vapor-deposited on the oxide to a thickness of 20 to 40Å. A refractory metal, such as Ni or Mo, is used with an n-type substrate; while an alkaline earth metal, such as Mg, is used with a p-type substrate.

Without breaking the vacuum after the intermediate-metal deposition, the layer of noble metal is deposited to a thickness of 50 to 100 Å. Ohmic contact stripes of Al or Al/Ag sandwich are deposited through a mask onto the noble

(continued on next page)

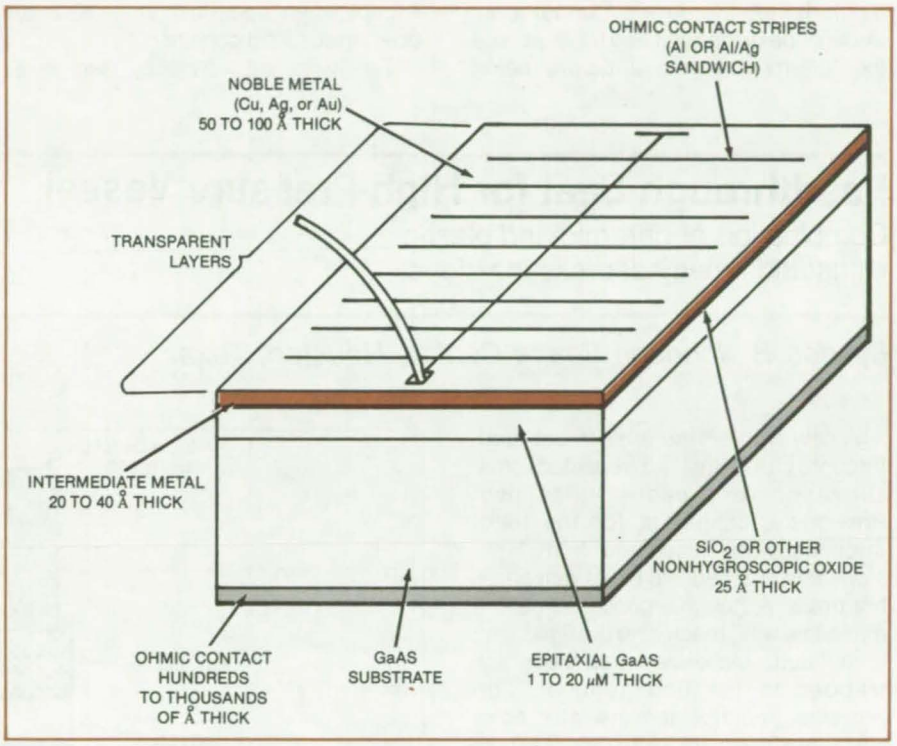

Figure 1. The **GaAS Schottky-Barrier Device** is composed of layers deposited by conventional semiconductor fabrication techniques. This device differs from earlier ones of the same general type in its inclusion of an intermediate metal layer.

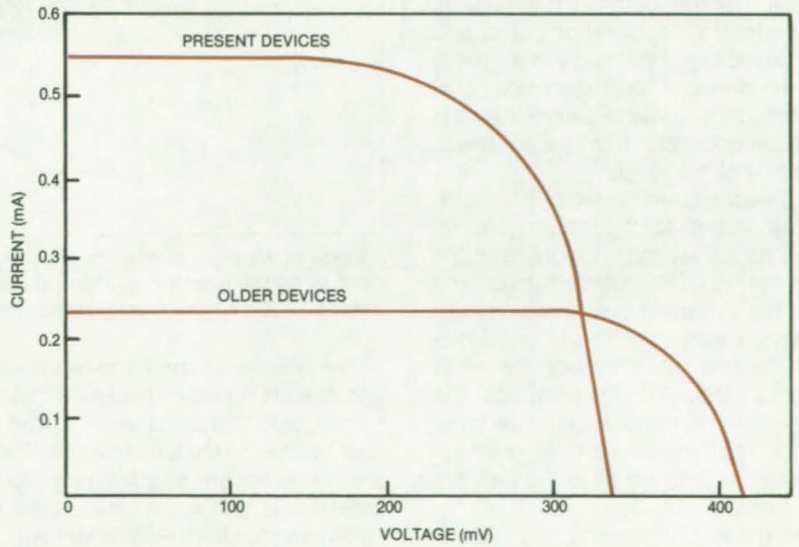

Figure 2. **Output Current Versus Voltage** was measured under identical illumination for representative devices of the present and older types.

metal. A wire lead is connected to the contact structure by thermal-compression bonding or another conventional technique.

The thinness of the intermediate metal layer permits the transmission of sufficient light and minimizes the contribution of additional electrical resistance. Charge carriers traveling perpendicularly to the layers tunnel only through the oxide layer and travel across the intermediate metal before being swept through the highly-conductive noble metal to the contact stripes.

The performances of representative devices are compared in Figure 2. The newer devices are capable of higher short-circuit currents as well as higher currents over most of the voltage range. Thus, the new devices have lower internal voltage drop and higher efficiency except when operating at or near an open-circuit load condition.

This work was done by George E. Alcorn, Charles Z. Leinkram, and Olatunji Okunola of **Goddard Space Flight Center.** *For further information, Circle 5 on the TSP Request Card.*

This invention is owned by NASA, and a patent application has been filed. Inquiries concerning nonexclusive or exclusive license for its commercial development should be addressed to the Patent Counsel, Goddard Space Flight Center [see page A5]. Refer to GSC-12816.

Feedthrough Seal for High-Pressure Vessel

Combination of ceramic and plastic withstands many depressurizations.

Lyndon B. Johnson Space Center, Houston, Texas

A new high-pressure electrical feedthrough can withstand repeated pressurizations and depressurizations. Previously, insulators for the feedthroughs were machined from limestone and crushed into place with an arbor press. Although a good seal can be made this way, machining the limestone is difficult. Moreover, gas becomes trapped in the limestone at high pressure and rips the insulator apart when the pressure is released. Thus, new insulators must be made for every use of the vessel.

The new seal is composed of washers of neoprene, polytetrafluoroethylene, nylon, and high-purity, high-density commercial alumina ceramic (see figure). The parts are machined or cut to size and nested together snugly in a hole in the vessel wall. A steel electrode passing through the washers serves as the electrical connector from the outside to the inside of the vessel.

The washers are seated by pressurizing the vessel to 2 kilobars (2×10^8 N/m^2). As the seating pressure rises, the neoprene, polytetrafluoroethylene, and nylon are deformed in succession to fill the space available. The alumina provides the strength to support the other washers and position the electrode. The steel electrode material must be hardened: If a soft material is used, the electrode will be pinched off as the washers are seated.

The grade of neoprene is critical. It should be fine-grain, high-quality material. Coarse-grain material becomes electronically conductive upon compression, causing an electrical short circuit.

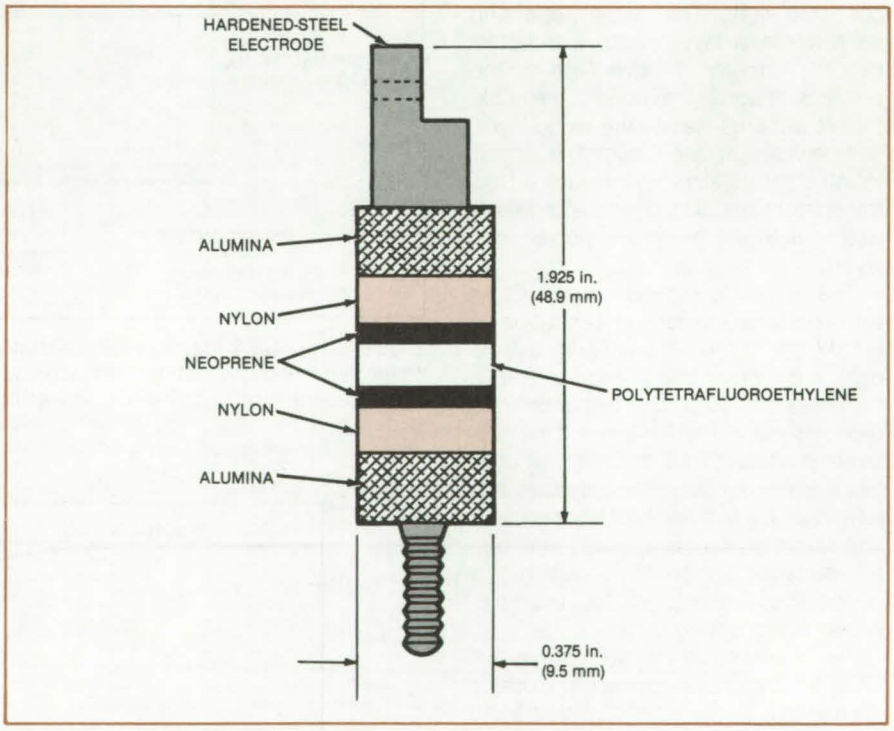

A **Stack of Washers** surrounds a leadthrough electrode. Under pressure, the washers expand to fill the leadthrough hole in the high-pressure vessel. The seal thus formed can withstand 20 or more pressurization/depressurization cycles.

The vessel wall should be well cooled; and its ends should be packed with an insulator, such as silica wool, to reduce heat transfer to the feedthroughs. These provisions ensure that the polytetrafluoroethylene and nylon washers do not soften and fail from excessive heat.

This work was done by Richard J. Williams of **Johnson Space Center** *and Oscar Mullins, Dennis Smith, and Glen Teasley of Lockheed Engineering and Management Services Co., Inc. Further information may be found in NASA TM-8251 [N83-18999/NSP], "Electrically Insulating High-Pressure Seals for Internally Heated Pressure Vessels" [$7]. A copy may be purchased [prepayment required] from the National Technical Information Service, Springfield, Virginia 22161.*

MSC-20625

Stripline Antenna Beam-Forming Network

Many contiguous beams would give even coverage to a large area.

NASA's Jet Propulsion Laboratory, Pasadena, California

A new stripline antenna beam-forming network would include 87 beam ports and 136 feed-element ports and would be contained on only two microstrip boards. Both uplink and downlink strips would be supported on the same boards. Originally proposed for the communications coverage of the continental United States for the Land Mobile Satellite System, the structure should be of interest to antenna designers in other applications.

To illuminate the antenna paraboloid properly and obtain low side-lobe levels, the feeds associated with each beam have spacings of about 2 wavelengths but with apertures of about 6 wavelengths: This geometry requires that each beam share feed elements with adjacent beams.

The feed elements for both the uplink and downlink are connected to the 87 uplink and 87 downlink cables through beam-forming networks on the two microstrip boards. For the downlink, power from each downlink cable is fed to a one-to-seven power divider on the first microstrip board that dispatches the power to the seven feed elements in a hexagonal array corresponding to the downlink beam of that cable. On the second microstrip board (which is mounted in registration with the first board), a seven-to-one power combiner for each feed element receives the power from the seven beams in the hexagonal array on the first board that share that feed element. The uplink cables and feed elements are similarly arrayed.

By using a curved strip-line shape, designers were able to lay out uplink and downlink strip lines side-by-side on each board. The weight of the beam-forming network is minimized by using the same boards for the uplink and downlink and by constructing the network as a lightweight sandwich of etched circuit boards and dielectric honeycomb. The area and mass of the network are estimated at 650 ft^2 (60.4 m^2) and 714 lbm (324 kg), respectively.

This work was done by Paul W. Cramer of Caltech for **NASA's Jet Propulsion Laboratory.** *For further information, Circle 6 on the TSP Request Card.*

Inquiries concerning rights for the commercial use of this invention should be addressed to the Patent Counsel, NASA Resident Office-JPL [see page A5]. Refer to NPO-15743.

Finding Open Faults in CMOS Circuits

Spurious memory requires a series of test inputs.

NASA's Jet Propulsion Laboratory, Pasadena, California

An algorithm specifies a sequence of input test signals and the interpretation of the resulting output signals for identifying stuck-open faults in complementary metal-oxide-semiconductor (CMOS) integrated logic circuits. It can be incorporated in software for online production testing of CMOS circuits.

In CMOS circuits, a stuck-open fault introduces "memory" into the affected circuit element, so that the output depends on past as well as on present inputs. The spurious memory occurs because the output of a CMOS device drives a primarily capacitive load. A stuck-open fault (failure of a pullup or pulldown transistor to connect this capacitance to the "1" or "0" reference potential) causes the capacitance to retain its initial charge and logic state. Thus the test for this type of fault requires the application of a sequence of inputs to see if any spurious memory exists.

The algorithm assumes a combinatorial circuit with n inputs and one output. It specifies the following sequence of operations applied to the inputs:

1. Lower all inputs to logic "0,"
2. Raise all inputs to logic "1,"
3. Lower one input to logic "0" while the others are kept at logic "1," and
4. Repeat steps one through three, each time lowering a different input to logic "0," until all n inputs have been tested.

A portion of the circuit is tested each time steps one through three are applied. If no fault exists, the expected output for that circuit will be observed. If there is a fault, a spurious output will be recorded.

For an example of the testing problem and a testing sequence, consider the CMOS NAND gate of the figure. In normal operation, inputs of $(X_1,X_2) = (1,1)$ turn off the p transistors and turn on the n transistors, resulting in an output of $F = 0$. If a logic "0" is applied to either or both of X_1 or X_2, the corresponding p transistor will conduct while the corresponding n transistor will not, so that F will be pulled up to V_{DD}; that is, to logic "1."

Now suppose that there is an open circuit at the point shown in the source line of the right p transistor. If (0,1) is applied to (X_1,X_2), then the topmost n transistor will not conduct, the left p transistor will not conduct, and the right p transistor wil not conduct due to the fault. This isolates the F node, causing it to retain the previous output state. If the previous input state was (0,0), then the previous output state was $F = 1$. A mere examination of the present inputs and

(continued on next page)

outputs would not reveal anything amiss. If, however, the previous input state were (1,1), then the previous output would have been F = 0, and the present output would still be F = 0, which is erroneous. Thus, the fault in question could be detected by the occurence of the output F = 0 after the input sequence (1,1);(0,1). [The first step (0,0) of the general algorithm could have been included, but would not have made any difference in this case.]

This work was done by Ramamorti Chandramouli of Caltech for **NASA's Jet Propulsion Laboratory.** *For further information, Circle 7 on the TSP Request Card.*
NPO-15838

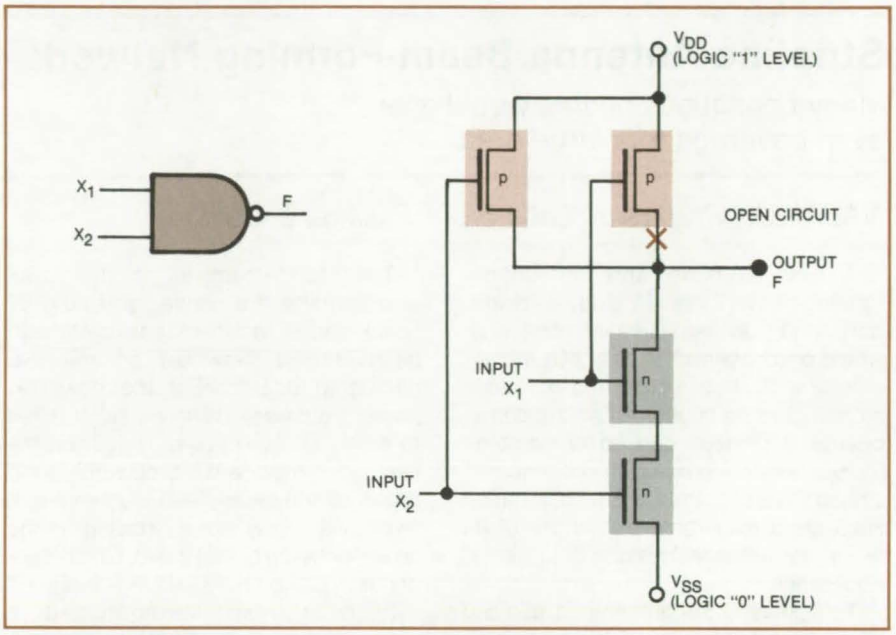

A **CMOS NAND Gate** has an open circuit at the marked point. This fault can be detected by the occurrence of the output F = 0 at the end of the input sequence $(X_1,X_2) = (1,1);(0,1)$.

Flip-Flop Digital Modulator

A clock is switched on and off in response to a data signal.

Lyndon B. Johnson Space Center, Houston, Texas

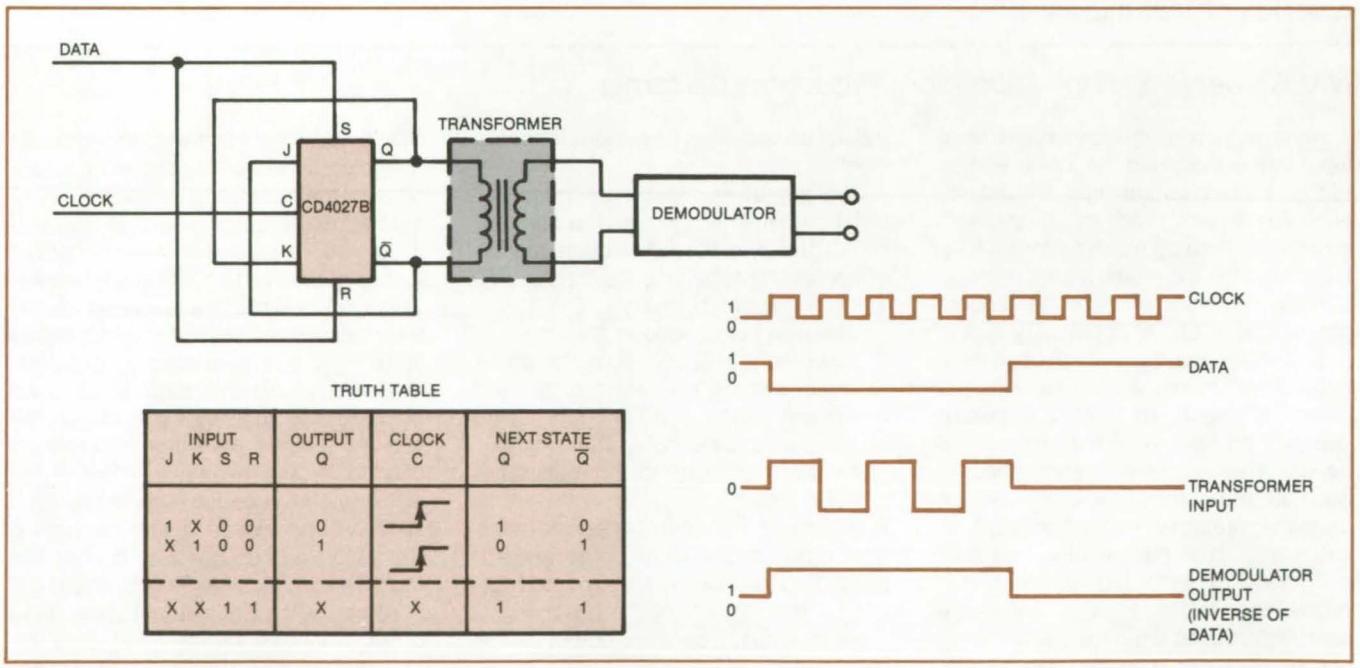

TRUTH TABLE

INPUT J K S R	OUTPUT Q	CLOCK C	NEXT STATE Q	$\overline{Q}$
1 X 0 0	0	⌐	1	0
X 1 0 0	1	⌐	0	1
X X 1 1	X	X	1	1

The **Flip-Flop Modulator** generates a square-wave carrier frequency that is half the clock frequency and turns the carrier on and off. The final demodulator output is the logical inverse of the data input.

A single J-K flip-flop is the heart of a new digital modulator circuit. The circuit modulates a square wave by turning it on and off in response to a data signal.

The circuit is built with a J-K flip-flop for which both outputs remain in the "1" state when the set and reset (S and R) inputs are in the "1" state. The CD4027B flip-flop (or equivalent) has this characteristic. With the data line connected to the R and S inputs as shown in the figure, a logic "1" on the data line raises both the Q and $\overline{Q}$ outputs to logic "1"; and there is zero voltage difference across the transformer primary. In other words, a logic "1" on the data line turns off the transformer output.

When the data line carries a "0" signal, the circuit functions as a normal J-K flip-flop. The application of a "1" to the J input along with a positive-going pulse to the clock input raises the Q output to "1" and lowers the $\overline{Q}$ output to "0." Similarly, a "1" at the K input accompanied by a positive-going clock pulse raises $\overline{Q}$ to "1" and lowers Q to "0." In this case, the logic "1" voltages for the J and K inputs are provided by direct feedback from $\overline{Q}$ and Q, respectively.

When the data line is at "0," the effect of a positive-going clock pulse is thus to reverse the logic state of the output and the polarity of the voltage difference across the transformer primary. Since two clock pulses are required for one complete cycle (two reversals) of the output, the transformer output is a train of pulses at half the clock frequency.

The half-clock frequency serves, in effect, as the carrier frequency. By turning the carrier on with a logic "0" and off with a logic "1," the circuit modulates the carrier with the logical inverse of the data signal.

The data frequency should not exceed one-fourth the clock frequency or else the output would not contain at least one complete cycle for each data "0" pulse. There is also some ambiguity as to which output state will prevail when the data signal goes to zero before the arrival of the next positive-going clock pulse. The uncertainty in the output starting time is one clock period at most. This may be acceptable if the modulating frequency is much less than the carrier frequency. The ambiguity can be resolved by imposing a slight delay in the signal line between R and S or by using a modulating signal that is synchronized to the clock.

This work was done by Robert F. Eno of Rockwell International Corp. for **Johnson Space Center.** *For further information, Circle 8 on the TSP Request Card.*
MSC-20334

Books and Reports

These reports, studies, and handbooks are available from NASA as Technical Support Packages (TSP's) when a Request Card number is cited; otherwise they are available from the National Technical Information Service.

Screening Plastic-Encapsulated Solid-State Devices

Field data and experiments enable reliability assessment.

The suitability of plastic-encapsulated solid-state electronic devices for use in spacecraft is discussed in a pair of reports. Despite the specialized purpose of the reports, engineers may find them useful as guides to the testing or use of plastic-encapsulated semiconductors in severe terrestrial environments.

As described in the first document, field data were compiled to develop selection criteria and tests for components. The literature on the use of plastic-encapsulated semiconductors was searched. Information was solicited on failure rates and reliability from manufacturers who use such parts. Information on anticipated failure rates was also gathered from the manufacturers of these parts.

The conclusion of this preliminary study was that plastic-encapsulated parts are sufficiently reliable to be at least considered for use in low-cost equipment that is to be used at moderate temperature and low humidity. The parts should be bought in small quantities from manufacturer's standard high-volume production lines. Every part should then be screened in the following series of tests:

- Temperature cycling: 30 times, 0° to 100° C;
- Pre-burn-in electrical tests of all device functions and parameters;
- Burn-in for 1 week at 125° C; and
- Post-burn-in electrical tests of all device functions and parameters: Each unit should be tested twice.

The evaluation and refinement of screening tests are described in the second report. The objectives of this phase of the study were as follows:

- To determine the effectiveness and cost of selected screening tests as applied to various integrated circuits and transistors;
- To identify test procedures and performance or design weaknesses of specific component types;
- To determine the effects of operating temperature on overall performance; and
- To obtain experimental screening data on selected devices to augment the field data obtained previously.

The experiments were conducted with low-power bipolar Schottky transistor/transistor-logic (TTL) digital circuits, complementary metal/oxide/semiconductor (CMOS) digital circuits, operational-amplifier linear circuits, and npn transistors. Of each type tested, 1,035 units were encapsulated in plastic and 75 units were hermetically sealed, to be used as a control group. The parts were subjected to electrical-measurement and burn-in screening, and those that survived were given 4,000-hour life tests with intermediate measurements at logarithmic intervals. Failures were analyzed where possible; and some parts underwent special flammability, humidity-cycling, high-pressure-steam, and high-temperature-storage tests.

The experimental results were somewhat unexpected. The findings of the first report are largely contradicted by the accelerated life tests. Operation at 40° C in some cases appears to be more deleterious than operation at higher temperatures; and the usual relationship between time, temperature, and failure rate does not seem to hold. There are serious reliability problems with linear and CMOS circuits, and in the case of CMOS circuits the defects appear to be un-

(continued on next page)

screenable. There are significant differences among parts made by different manufacturers, with the consequence that any use must be accompanied by intensive parts engineering to insure integrity. The conclusion is that plastic-encapsulated semiconductors are probably not cost-effective for the intended spacecraft application.

This work was done by L. F. Buldhaupt of The Boeing Aerospace Co. for **Marshall Space Flight Center.** *Further information may be found in:*

NASA CR-161946 [N82-16343/NSP], "Analysis of Field Usage Failure Rate Data for Plastic Encapsulated Solid State Devices" [$22], and

NASA CR-161947 [N82-16344/NSP], "Development of Design, Qualification, Screening, and Application Requirements for Plastic Encapsulated Solid-State Devices for Space Applications" [$17.50].

Paper copies of these reports may be purchased [prepayment required] from the National Technical Information Service, Springfield, Virginia 22161. The reports are also available on microfiche at no charge. To obtain microfiche copies, Circle 9 on the TSP Request Card.
MFS-25802

Radiation-Hardness Data for Semiconductor Devices

Three-volume report covers devices from integrated circuits to power transistors.

A document presents data on, and analysis of, the radiation hardness of various semiconductor devices. The data specify the total-dose radiation tolerance of the devices.

The radiation data were obtained specifically for a space mission to Jupiter, but are applicable to other ionizing radiation environments. Two radiation sources were employed. A cobalt-60 gamma source was used when bulk radiation damage was expected to be negligible (npn transistors and field-effect transistors) or when a 2.5-MeV electron source could not penetrate the package (power transistors). The electron source was used for pnp transistors and many integrated circuits.

The document offers a useful comparison of the radiation response of devices that might be considered in the design and development of electronic circuits for radiation-hardened systems. It can also assist an engineer in determining quickly the weak links in an existing system and the radiation tolerance of a system as a whole.

Volume 1 of the report covers diodes, bipolar transistors, field-effect transistors, silicon controlled rectifiers, and optical devices (light-emitting diodes, phototransistors, and optical isolators). Volume 2 covers integrated circuits.

In volume 1, the data are graphed for various electrical operating conditions as a function of dose. Standard deviations are tabulated and sample size is stated for each lot to provide a measure of statistical variations. Irradiations of two or more lots are treated as entirely separate tests.

In volume 2, information on some of the integrated circuits is presented in tables. However, for the more-complex large-scale-integration devices, the data are presented in narrative form to give proper emphasis to the radiation-induced changes in the device parameters.

The third volume to this series provides a detailed analysis of much of the data in volumes 1 and 2. It provides comparisons of the radiation sensitivity of devices of a given type but different manufacturer, multiple tests of one date code, multiple tests of a single lot, and sensitivities versus time of packaging (date code).

This work was done by William E. Price, Donald K. Nichols, S. Frederick Brown, Michael K. Gauthier, and Keith E. Martin of Caltech for **NASA's Jet Propulsion Laboratory.** *To obtain a copy of the report, Circle 10 on the TSP Request Card.*
NPO-15787

MiniBriefs describe NASA innovations and reports in an abbreviated format. Readers desiring additional information on these items should request the Technical Support Packages (TSP's), available in most cases, which can be obtained by using the TSP Request Card at the back of this issue.

Optical Testing of Integrated Circuits

Nondestructive test uses digital analysis of weighted photoresponse image.

An optical spot-raster scanner is used to produce a weighted photoresponse image (PI) of an operating CMOS IC. Digital analysis of PI's, which correlates differences in PI's with electrical behavior of the IC, shows promise both as a 100-percent screening method for use in IC manufacture and as a diagnostic tool in IC development.

As the light spot scans the IC, photoinduced currents cause the current drawn by the IC to fluctuate; the current at each pixel in the raster is recorded digitally, forming the PI. A weighted PI is obtained by a "state superposition technique"; namely, cycling the IC very rapidly through a specially selected series of digital states during scanning.

This work was done by J. J. Erickson of Hughes Aircraft Co. for **Marshall Space Flight Center.** *For further information, Circle 74 on the TSP Request Card.*
MFS-25498

Demodulator for AM and SSB-SC Signals

Its dynamic range is better than 60 dB for AM signals.

A demodulator called a "Compatible Linear Demodulator" (CLD) detects either amplitude modulation (AM) or single-sideband suppressed-carrier (SSB-SC) modulation. It is a carrier-recovery homodyne product detector designed for voice communication but easily scaled to other frequencies. The signal-level range over which the CLD

provides linear demodulation of an AM signal is over 60 dB, which is significantly better than that of a diode detector. The demodulating linearity of the CLD exceeds 40 dB. A readily-available integrated circuit intended for quadrature detection of frequency-modulated signals is used in the circuit to perform the functions of limiting and product demodulation.

This work was done by Chase P. Hearn, and Edward S. Bradshaw of **Langley Research Center.** *For further information, Circle 75 on the TSP Request Card.*
LAR-12716

Controlling an Inverter-Driven Three-Phase Motor

A speed control loop applies feedback to the inverter.

A control system for a three-phase permanent-magnet motor driven by a line-commutated inverter uses signals that are generated by integrating the back emf of each phase of the motor. A full-wave rectifier provides feedback signals to gain-compensation circuits, which are then applied to integrator circuits. The output of the integrators control the firing angles for all three phases of the inverter. A high-pass filter network eliminates low-frequency components from the control loop while maintaining a desired power factor.

This work was done by Carlisle Dolland of Airesearch Manufacturing Co. for **Marshall Space Flight Center.** *For further information, Circle 76 on the TSP Request Card.*

This invention has been patented by NASA [U.S. Patent No. 4,401,934]. Inquiries concerning nonexclusive or exclusive license for its commercial development should be addressed to the Patent Counsel, Marshall Space Flight Center [see page A5]. Refer to MFS-25215.

Shielding Electric Connectors From Lightning

A grounding shell is made from steel tubing.

A metallic shield for plastic-body electrical power connectors, with provision for attaching the cable shielding, prevents lightning-induced overvoltages from damaging sensitive electronic equipment. The shell is fabricated from a plated, cylindrical section of steel tubing or a pipe. It is attached to the plastic housing by four screws. An L-shaped flange on the shell is for attachment of a ground wire.

This work was done by Wallace B. Pierce and Walter G. Collins of Caltech for **NASA's Jet Propulsion Laboratory.** *For further information, Circle 77 on the TSP Request Card.*
NPO-15688

Remotely-Operated Traffic Control Light

A strobe light is activated on command from a hand-held transmitter.

A traffic warning light for school crossings, construction zones, and other hazardous areas is activated by remote control using an apparatus developed at Ames Research Center. The warning light can be operated by a crossing guard, who would not have to enter the intersection until traffic had actually come to a halt.

The apparatus consists of a small radio transmitter, which would be held by the crossing guard, and a pole-mounted strobe light with attached power supply and radio receiver, which would be placed in the intersection. Current drain would be only about 300 mA, so it would not be necessary to recharge the battery very often.

This work was done by Jerry S. Reedy of **Ames Research Center.** *For further information, Circle 78 on the TSP Request Card.*
ARC-11406

Servo Lead Compensation

Lead compensation in a servosystem can be adjusted continuously.

A circuit for continuously varying the lead compensation in a servosystem is operative even when the integrating amplifier goes into saturation. Previous lead-compensation circuits either become inoperative when the integrator saturates or are not continuously adjustable.

The circuit incorporates an operational amplifier wired as a voltage follower. The operational amplifier is placed in the summing-resistor portion of the integrator circuit. Its function is to allow a continuous change in the value of the integrator coupling capacitor.

This work was done by E. C. Buchanan of Rockwell International Corp. for **Marshall Space Flight Center.** *For further information, Circle 79 on the TSP Request Card.*
MFS-19614

Digital Control of Analog Detector

Computer-controlled digital-to-analog converter sets reference level of uncompensated analog comparator.

The reference level required to set the switching point of an analog comparator at a desired level can be determined and set by a computer-controlled circuit. The comparator reference input is driven by a digital-to-analog converter (DAC) controlled by the computer. The comparator output is connected to the computer as a digital input signal. A calibration signal equal to the desired switching level is applied to the comparator signal input. The computer steps the DAC input through its range to find the value that toggles the comparator output. Separate correction of DAC and comparator offset errors is not required.

This work was done by J. P. Brown of Rockwell International Corp. for **Marshall Space Flight Center.** *For further information, Circle 80 on the TSP Request Card.*
MFS-19608

Miniature Temperature-Control Circuit

It operates on any power-supply voltage from 6 to 28 volts.

A miniature thermostat circuit controls an electric heating element so as to maintain a constant temperature in an oven or other thermal environment. The circuit contains a comparator IC, a Darlington power transistor, a linearized thermistor temperature sensor, and resistors and capacitors. It operates on any power-supply voltage from 6 to 28 volts and can be made small enough to be installed within the temperature stabilized enclosure it controls. A pro-

(continued on next page)

totype circuit was fabricated on a printed-circuit board 2 in. (5.1 cm) square.

This work was done by Richard H. Couch of **Langley Research Center.** *For further information, Circle 81 on the TSP Request Card.*
LAR-12900

Power-Measurement Errors Due to Instrument Lag

Short-risetime pulses contain frequency components above the flat-response region of typical instrumentation amplifiers.

Errors in measuring the power output of electric-vehicle controllers with transistor or SCR pulse-width control were analyzed using classical frequency-analysis techniques. The results are presented in a report that is now available.

The power measured using an instrumentation amplifier with frequency response assumed to be flat to 50 kHz was less than actual power output by as much as 7.6 percent. This is for a typical 2-kHz-controller. The largest errors occur for the narrow pulses used at low speeds. Maximum power dissipation occurs during the switching transitions, so accurate measurements are required particularly in these intervals.

This work was done by Dean P. Athans of Caltech for **NASA's Jet Propulsion Laboratory.** *For further information, Circle 82 on the TSP Request Card.*
NPO-15029

Multiple-Band-Gap Solar-Cell Concept

Energy-conversion efficiency would be increased.

Proposed multiple-band-gap photovoltaic structures may convert a greater portion of insolation to electricity than do present solar cells. Since different band gaps absorb light from different spectral bands, the multiple band gaps would utilize the incident spectrum more completely.

According to the concept, layers of solar cells would be made of different materials having different band gaps. The layers would be stacked optically in series. Dichroic mirrors between the layers would apportion the radiation so that each layer receives the wavelengths to which it is most responsive. The layers may be electrically isolated from each other but are preferably connected in series. Preliminary designs have been worked out for two- and three-junction structures in various gallium-based semiconductors.

This work was done by Arthur A. Nussberger of Rockwell International Corp. for **Marshall Space Flight Center.** *For further information, Circle 83 on the TSP Request Card.*
MFS-25724

Continuity/Isolation Checker

A buzzer indicates very high or very low resistance between probes.

An instrument checks for either continuity or isolation between two points in an electrical circuit. A buzzer sounds when the resistance between the continuity probe and circuit ground is less than 100 ohms, or if the resistance to the isolation probe exceeds 100 megohms. The resistance comparisons are performed by two CMOS comparators, the outputs of which are ANDed into the audio transducer. The inputs are protected from electrostatic discharge by resistors and clamping diodes.

The instrument is useful for a technician making a series of rapid checks on circuit integrity. The upper and lower resistance limits are easily modified by replacing the appropriate resistors.

This work was done by James O. Lonborg for **NASA's Jet Propulsion Laboratory.** *For further information, Circle 84 on the TSP Request Card.*
NPO-15632

High-Common-Mode-Rejection Differential Amplifier

The circuit features inexpensive components.

A high-common-mode-rejection differential amplifier amplifies low-level signals in the presence of high-frequency noise. The amplifier can be used in power systems that require current monitoring on the high side of a high-voltage powerline. The circuit comprises inexpensive standard resistors, transistors, and operational amplifiers.

The amplifier, which is accurate to 1 percent, functions with an applied common-mode voltage of up to 500 V and a corresponding full-scale differential voltage of up to 0.2 V. The amplifier output is 5 V at the full-scale differential voltage, corresponding to a differential voltage gain of 25. The amplifier responds within 5 μs to a step change in the input voltage.

This work was done by Fred E. Lukens of **Marshall Space Flight Center.** *For further information, Circle 85 on the TSP Request Card.*

Inquiries concerning rights for the commercial use of this invention should be addressed to the Patent Counsel, Marshall Space Flight Center [see page A5]. *Refer to MFS-25868.*

Paint-Thickness Checker

An eddy-current flaw detector with a cathode-ray tube (CRT) can be used to compare layer thicknesses of conductive paint on metallic substrates.

The layer thicknesses of a zinc-rich anticorrosion paint on various stainless-steel fittings, plates, and tubing were determined using an NDT6 eddy-current system, or equivalent, and a Nortec SP-100 100-kHz, or equivalent, probe. In eddy-current testing, each metal or alloy gives a slightly different impedance curve. The amplitude of the endpoint of the curve decreases as the probe is raised off the surface. Measurement of paint-film thickness was based on a procedure using shims of known thickness to correlate spot position on the CRT screen with film thickness.

This work was done by C. W. Nelson of Beech Aircarft Corp. for **Kennedy Space Center.** *For further information, Circle 124 on the TSP Request Card.*

Inquiries concerning rights for the commercial use of this invention should be addressed to the Patent Counsel, Kennedy Space Center [see page A5]. *Refer to KSC-11270.*

Electronic Systems

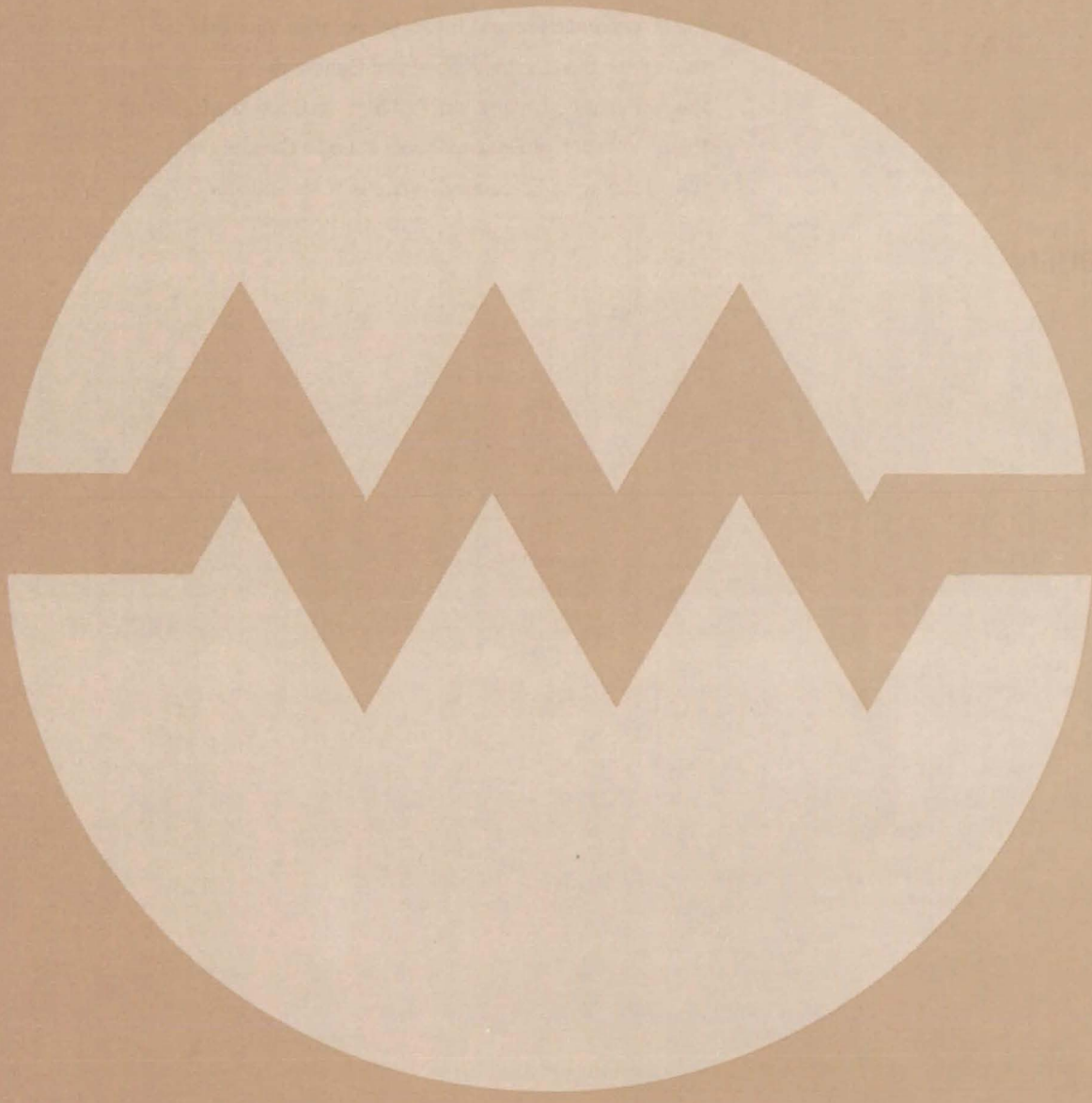

Hardware, Techniques, and Processes

179 Self-Checking Memory Interface

180 Sideband-Aided Receiver Arrays

181 Detecting Deformations in Phased-Array Antennas

182 Automatic Phasing for Active Antenna Elements

183 Interstitial Digital-Image-Point Generator

184 Unmanned Instrument Platform for Undersea Exploration

185 Detection of Floating Inputs in Logic Circuits

186 Displaying Force and Torque of a Manipulator

MiniBriefs

187

Self-Checking Memory Interface

A VLSI chip implements morphic Boolean algebra.

NASA's Jet Propulsion Laboratory, Pasadena, California

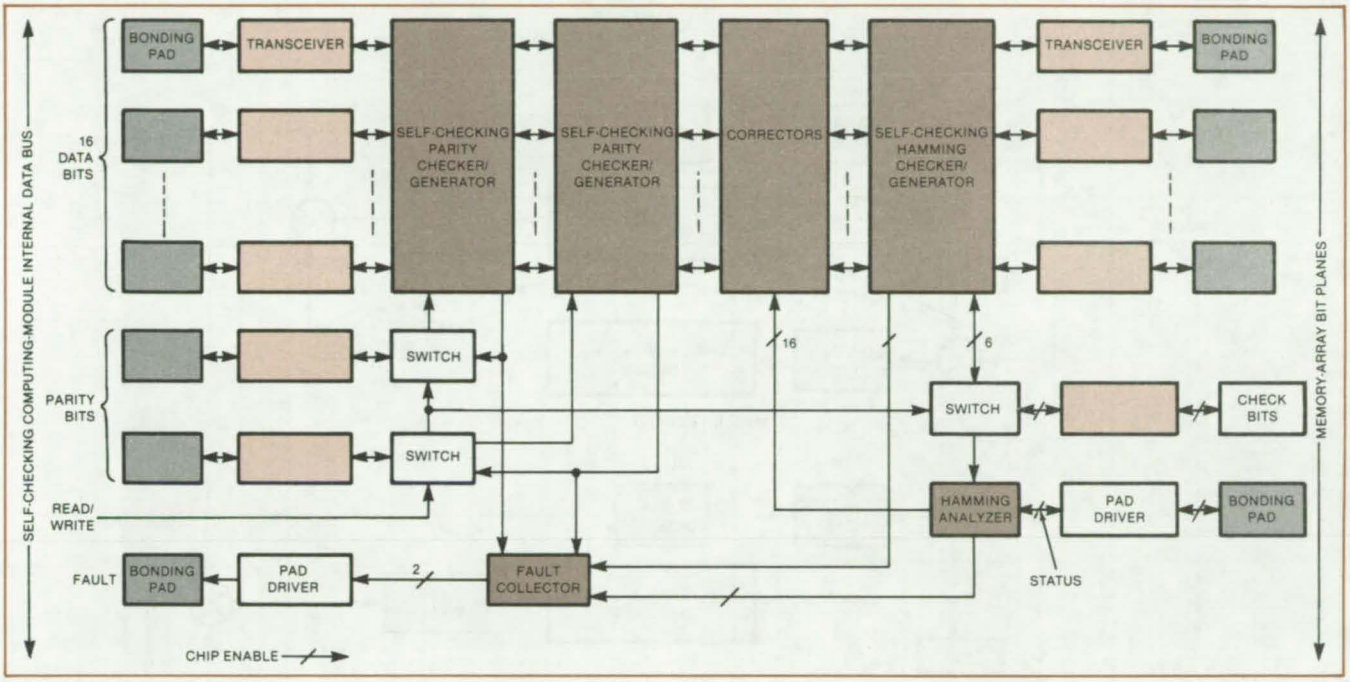

The **Memory-Interface Chip** encodes 16-bit words with a Hamming code for single-error correction or double-error detection. The chip also detects faults within itself.

A memory-interface integrated circuit not only detects errors in data from other circuits but also detects errors within itself. Designed for VLSI (very-large-scale integration), the chip will be used in fault-tolerant computers under development by NASA.

The memory-interface chip (see figure) connects a memory array to the address, data, and control buses of a "self-checking" computing module. The combination of memory, self-checking computer module, and interface forms a "memory module" for a fault-tolerant computer.

The interface does the following:

- Encodes 16-bit words destined for storage with an additional 6 bits to form a Hamming single-error-correcting/double-error-detecting code;
- Provides single-error correction and double-error detection on data read from memory;
- Detects data-bus faults inside the self-checking computing module; and
- Detects faults within itself, concurrently with normal operation.

The self-checking attributes are derived from two circuits: a morphic parity checker and a morphic AND operator. The parity checker is used both in the parity checker/generator and in the Hamming checker/generator. It produces a morphic 1 output for correctly coded inputs and no internal faults. A tree of such AND circuits is used in the fault collector, which receives morphic parity and syndrome signals generated on the chip along with two morphic externally generated signals: chip enable and read/write. The fault-collector readout is a series of master fault indications.

The circuit has been breadboarded, with small-scale and medium-scale integration chips. It is now being developed as a single chip employing complementary metal-oxide/semiconductor (CMOS) technology. The CMOS chip will cope with parasitic flip-flop faults, which are peculiar to CMOS structures. Toward this end, special discharge transistors are included in the circuit to prevent the charge buildup in parasitic capacitances that causes the parasitic flip-flop effect.

This work was done by Michael W. Sievers and David A. Rennels of Caltech for **NASA's Jet Propulsion Laboratory.** *For further information, Circle 11 on the TSP Request Card.*
NPO-15889

Sideband-Aided Receiver Arrays

"Slave" receivers obtain modulation information from a "master" receiver.

NASA's Jet Propulsion Laboratory, Pasadena, California

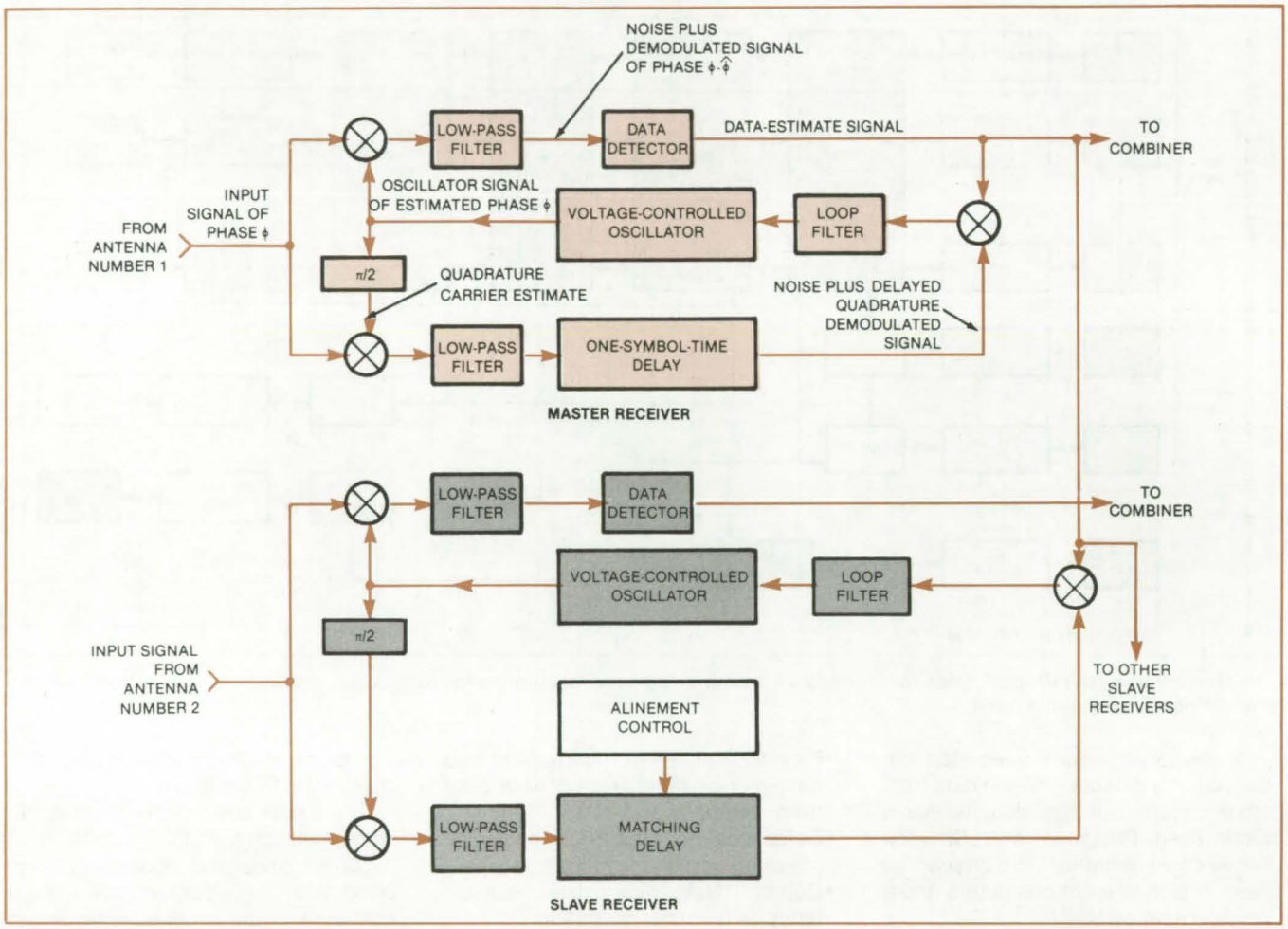

The **Sideband-Aided Receiving Array Mechanization** is illustrated in this block diagram.

Sideband-aided receiver arrays (SARA's) offer a way of extracting greater energy per bit in radio data signals. Developed for the reception of telemetry from vehicles in deep space, the SARA concept is applicable to commercial data-signal reception whenever two or more antennas are combined through diversity reception to improve reliability, to increase effective antenna area, or to allow increased coverage time of a moving transmitter. Computer simulations predict that SARA's will increase the apparent bit power over that attainable in other systems.

The SARA concept offers improved performance particularly at high modulation indices. A SARA system is operated as a "master/slave" system. Either a conventional tracking loop or a suppressed-carrier tracking loop may be used in the master channel to demodulate the carrier. A suppressed-carrier loop will yield better performance in most cases.

The master channel is associated with the largest antenna in the array, in which the signal-to-noise ratio is largest. The slave receivers contain conventional tracking loops that are aided by the subcarrier and data estimates derived in the master channel (see figure). These are relatively low-frequency, low-bandwidth signals that can be transmitted digitally to the slave receivers over existing microwave radio links.

Each slave receiver includes circuits for the proper alinement of its modulation with the modulation estimate it receives from the master receiver. This "aiding" allows the slave receivers to track the sideband power (rather than the carrier power) with losses that are lower than they would be in a system with separate suppressed-carrier loops in each slave receiver. The demodulated baseband signals from the master and all slaves are combined in a baseband combiner.

Two effects account for the superior performance afforded by a SARA system:

- It can operate in a suppressed-carrier environment. For example, while the modulation index of one alternative non-suppressed-carrier scheme for a Uranus mission is 76°, a SARA system

can operate at an index of 90°. This results in an increase of 6 percent in the apparent data power.

- SARA signals exhibit lower radio loss than that of other systems. The sideband aiding in both the master receiver and the slave receivers greatly increases the receiver-loop signal-to-noise ratios over those of conventional phase-locked loops. A greater signal-to-noise ratio results in smaller phase jitter and better tracking.

A further advantage of the SARA concept is that it can be effected with only small modifications to existing hardware. In NASA's deep-space receiving network, for example, a slave receiver can be an existing receiver with a mixer added for sideband aiding. An existing receiver can be used for the master receiver if modulation estimates are taken from the subcarrier-demodulation assembly and the symbol-synchronizer assembly. The modulation can be sent to the slave receivers over existing microwave links, which can be alined with the modulations in the slave receivers by reprogramed real-time combiners.

This work was done by Stanley A. Butman, Leslie J. Deutsch, and Robin A. Winkelstein of Caltech for **NASA's Jet Propulsion Laboratory.** *For further information, Circle 12 on the TSP Request Card.*
NPO-15873

Detecting Deformations in Phased-Array Antennas

Deflections would be measured by shifts in Doppler spectra and echo profiles.

NASA's Jet Propulsion Laboratory, Pasadena, California

A proposed Doppler technique would detect deformations of a large phased-array radar antenna. By monitoring the antenna Doppler spectrum and echo signals the technique would enable continuous examination of the antenna stability and would provide the information for correcting deformations.

In the new method, the antenna array is electrically divided into several subarrays as shown in the figure. The Doppler spectrum of each subarray is obtained, using a pulse repetition frequency consistent with the expected width of the Doppler spectrum of that subarray. The received signal is spectrum-analyzed in the along track dimension. The spectrum exhibits a pattern that corresponds to the radiation pattern of that subarray. If there is an angular deformation of one subarray relative to another, the observed Doppler spectra for the two subarrays will be shifted relative to each other.

Although the accuracy of the measurements of these shifts has not been directly evaluated, data from spaceborne synthetic-aperture-radar observations indicate that a deformation of 1 percent of the wavelength from one end of the subarray to the other is detectable. This sensitivity is sufficient for most applications of the phased array.

Once the pointing errors of the subarrays have been determined, phase adjustments can be programed into the various transmit/receive units. The deformations of the array in the across-track dimension can be measured and corrected by similar techniques, using the echo profiles received from each subarray. The profiles will be shifted relative to each other if deformation is present.

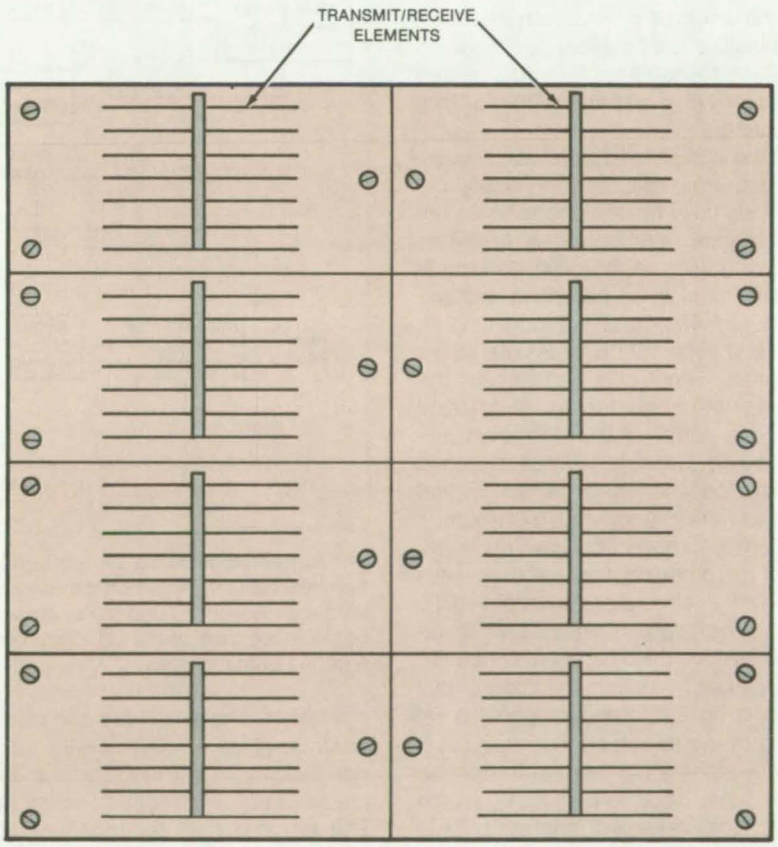

The **Phased-Array Antenna** is electrically split into subarrays, the individual phases of which can be measured when the antenna is illuminated by a quasi-point source (a single echo).

This work was done by Fuk-Kwok Li and Dan N. Held of Caltech for **NASA's Jet Propulsion Laboratory.** *For further information, Circle 13 on the TSP Request Card.*
NPO-15390

Automatic Phasing for Active Antenna Elements

Beam focus would be maintained despite structural deformations.

NASA's Jet Propulsion Laboratory, Pasadena, California

Phase changes at microwave antenna elements due to component drift and structural deformations would be compensated by a proposed feedback system. The system would enable the antenna to maintain a desired fixed gain pattern automatically. The principal use would be in focusing large phased arrays for radar or point-to-point communications.

The phasing system would ordinarily be used with a nominally planar array of active antenna elements, shown in simplified form as a linear array in the figure. The normal operation of the antenna would be interrupted periodically for calibration intervals during which the phase measurements would be performed and compensating factors calculated.

During a calibration interval the central feed transmits a continuous, coherent signal to the feed ports of the active antenna elements. At first, the phase shifter in each active element is set at the ideal value, assuming no structure deformation and component drift. Then, in a series of discrete time steps, the phase controller advances the phase of each element by a different rate. For a portion of the calibration period, a microwave short-circuit switch is turned on between the phase shifter and the amplifiers in each active element.

When the short-circuit switch is off, part of the outgoing signal energy leaks through the circulator, is amplified by the receiving preamplifier, and is returned through the directional coupler to the phase shifter. When the short-circuit switch is on, the outgoing signal is reflected at the switch so that the active-element electronics beyond the phase shifter have no effect. In both switch modes, the reflected energy passes back through the feed system to the central feed and from there to the synchronous receiver.

The distinct phase-shift rate of each element imposes a distinct frequency modulation on the signal returned to the receiver from that element. In the receiver, the demodulated signals are sampled at time steps synchronous with those of the phase shifts, and the samples are fed to the Fourier-transform processor. The amplitude and phase of each complex Fourier coefficient T_{mn} correspond directly to the amplitude and phase of an element (m,n) of the array. The process may be repeated at different carrier frequencies to resolve the multiple-2π ambiguity in the phase determination.

Since the signal passes through the antenna system twice (transmission plus reflection), the Fourier coefficient corresponding to a single pass would be $T_{mn}^{1/2}$. Consequently, the system applies an amplitude-and-phase correction factor $T_{mn}^{-1/2}$ to each array element during the subsequent normal-operation interval. A calibration and correction for a single pass through the receiving path alone can be done in a similar manner (but excluding the square-root calculation) by using an external antenna to transmit a pilot carrier for reflection from a stationary remote object.

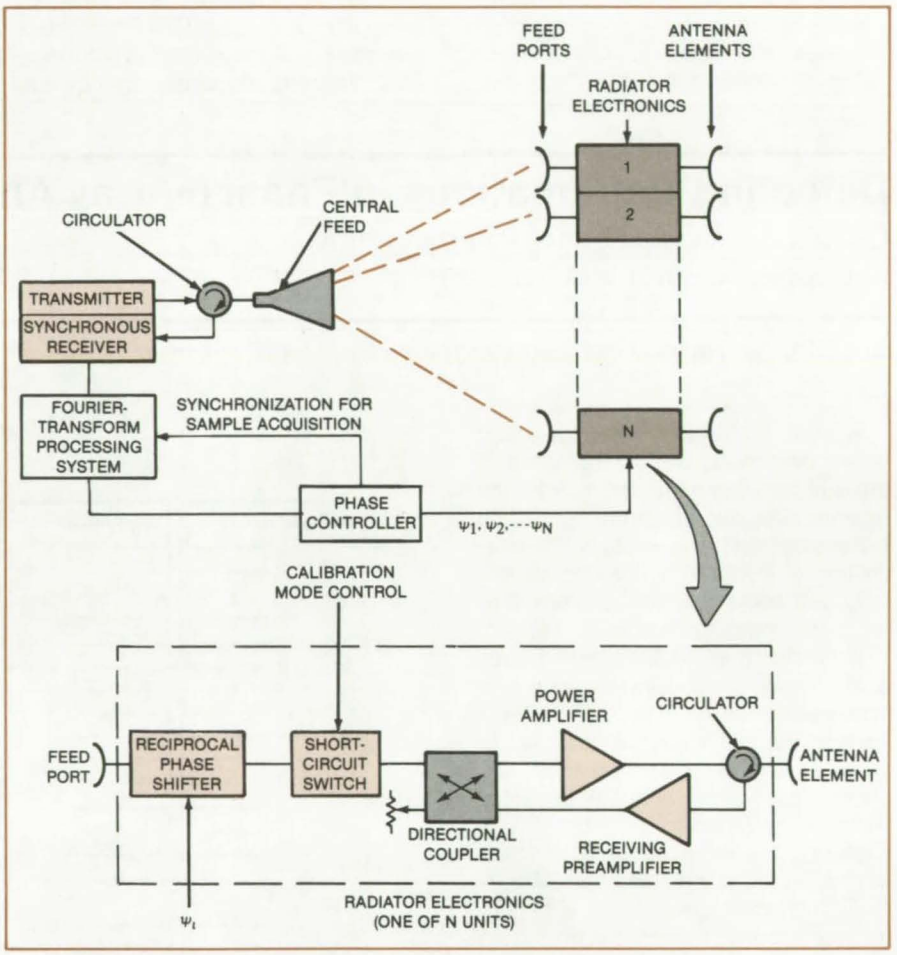

The **Automatic Phasing System** periodically interrupts the antenna operation for calibration intervals during which it measures the phase and amplitude response at each active antenna element. Using these measurements, the system adjusts the phase shift (and possibly the gain) of the active elements during the operating intervals to give the desired antenna-gain pattern.

This work was done by Chialin Wu of Caltech for **NASA's Jet Propulsion Laboratory.** *For further information, Circle 14 on the TSP Request Card.*

Inquiries concerning rights for the commercial use of this invention should be addressed to the Patent Counsel, NASA Resident Office-JPL [see page A5]. Refer to NPO-15920.

Interstitial Digital-Image-Point Generator

A digital filter interpolates values in a two-dimensional array.

Marshall Space Flight Center, Alabama

The apparent resolution of digital imagery (for example: visible, radar, or infrared) is increased by calculating estimated values of the intensity at coordinate points between the original intensity-data points. A proposed calculator (see figure) would implement an algorithm that generates such interstitial points using a four-by-four array of convolute integer coefficients. These coefficients are multiplied by the intensities at the 16 original image points nearest each interstice to obtain a weighted average intensity at each interstice. [See also "Digital Filters for Two-Dimensional Data" (MFS-25790) on page 481 of *NASA Tech Briefs*, Vol. 7, No. 4 (Summer 1983).]

The method is equivalent to fitting a surface to the image data by a regression calculation. Since the data and the coefficients are integers, only integer multiplications are required, making the calculation faster than if floating-point multiplications were required. The calculation is further simplified and speeded by taking advantage of the symmetry of the coefficients about the center and diagonals of the array: Only three independent coefficients are needed for the four-by-four array, and the number of multiplications is therefore reduced by first adding the intensities that are to be multiplied by the same coefficient.

After completing one pass over the entire original data array with the interstitial-point generator, an interstitial point will have been calculated at the center of each square of 16 adjacent data points (except along the perimeter of the array). In the interior of the array the number of points per unit area is doubled: Half of the points are the original data; and half, the newly-calculated interstitial points. The apparent resolution will have increased by a factor of $\sqrt{2}$.

By processing the resulting array a second time with the coordinate axes rotated by 45°, the number of points can be doubled again, producing an array with four times as many columns and rows per unit distance as the original array. The apparent resolution is thus

(continued on next page)

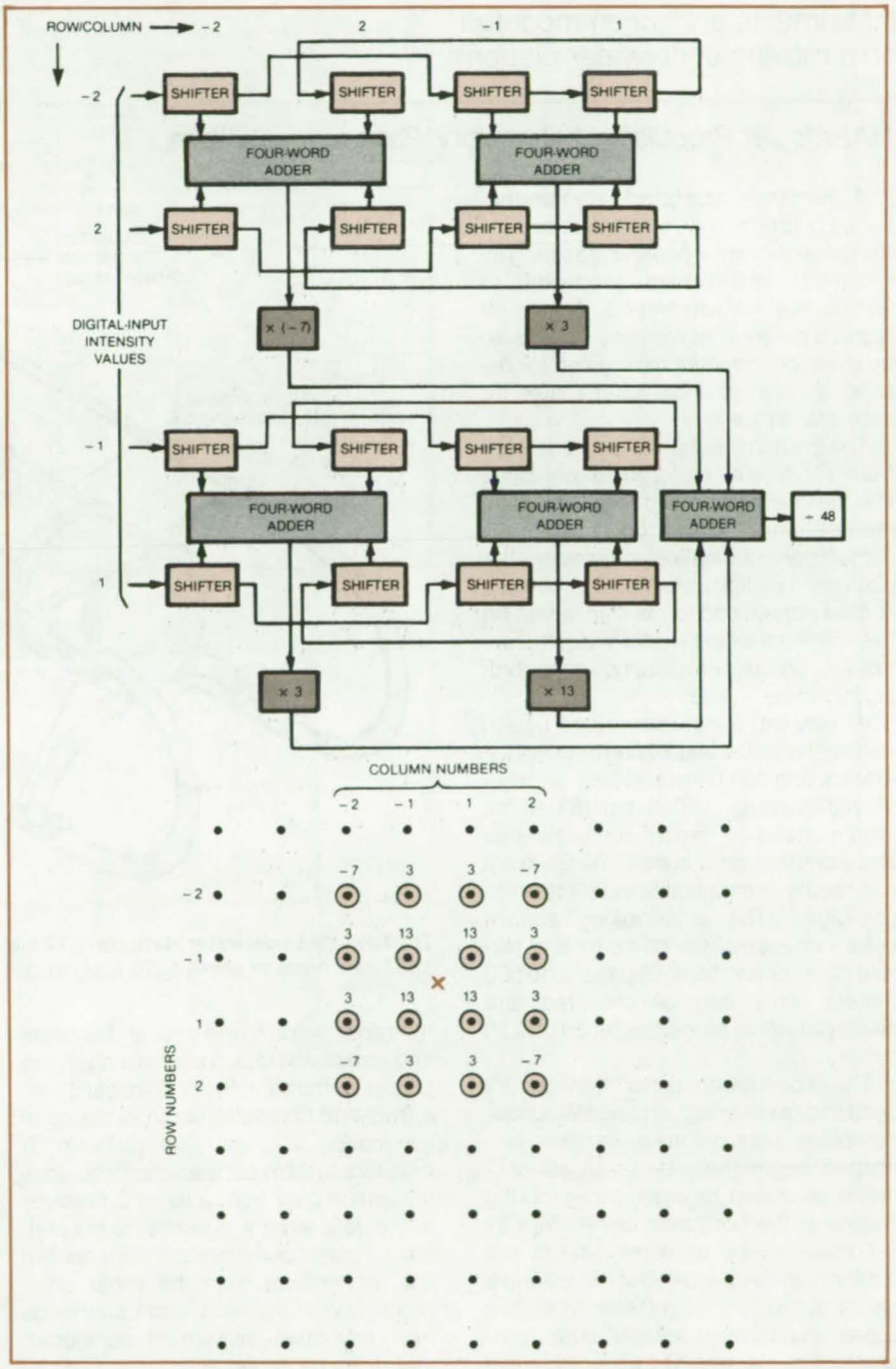

The **Interstitial-Point Generator** estimates the value of the data at the point in the center of each four-by-four subarray. In calculating a value for the point indicated, the data values at the circled points are weighted by the integer values -7, 3, or 13 as shown. To achieve high speed, the calculator is implemented in the hardware shown below. After each calculation, the data of the three leftmost columns are shifted one column to the right, and the data from the next column to the left are read in. Thus, the generator progresses to the left across the array.

twice as large as in the original array. This does not mean that finer detail is present in the final array than in the original one. Rather, the original data are represented more smoothly using smaller picture elements so that the continuous image structure will be less obscured by the steplike structure of the data.

This work was done by Thomas R. Edwards of **Marshall Space Flight Center.** *For further information, Circle 15 on the TSP Request Card.*
MFS-25871

Unmanned Instrument Platform for Undersea Exploration

Instruments are accommodated on a moving underwater platform.

NASA's Jet Propulsion Laboratory, Pasadena, California

A remotely operated, unmanned, towed platform serves as a test-bed for the development of ocean-measuring instruments and sonars at depths to 20,000 feet (6 kilometers). An instrumented platform of this type could also be used for undersea mining and for detailed surveys of underwater routes for cables and pipelines.

The platform is towed and operated from a ship by an armored coaxial cable that carries power and two-way communications. Based on spacecraft digital communication concepts, the platform data link transmits 250,000 bits of data per second to the ship. A van on the ship houses the platform depth control data processing, display, and recording facilities.

At present, the platform (see figure) carries the digital and analog circuitry for side-looking sonar in a steel hull capable of withstanding 10,000 psi (69 MPa). With modular equipment compartments and common data buses, the platform can readily accept additional electronics packages. The side-looking sonars create images of the contours and texture of the ocean floor. Objects up to 500 meters away can be detected and displayed with a range resolution of 0.75 meter.

The side-looking sonar transducers send and receive acoustic signals, under computer control, in a narrow, fan-shaped beam that starts out about 1 meter wide and diverges three-fourths degree in the horizontal plane. With its 500-meter range on either side of the platform, the side-looking sonar covers a swath of seafloor 1 kilometer wide. The sonar computer controls such parameters as transmitter frequency, pulse shape, pulse amplitude, receiver gain, and time-varying gain.

A computer subsystem on the platform controls the instruments, collects and organizes data from the instruments for transmission to the ship, and accepts and routes shipboard commands to the proper instrument. In the shipboard van, a front-end computer controls the communication link with the platform. It monitors system performance and adds navigation data from a loran C receiver to the data stream. It sends, to the platform, control commands from a control unit, commands from the sonar computer (also in the van), and commands from any other instrument computers that might be added.

The side-looking sonar computer performs slant-range corrections, zoom processing, color coding of the data, and the calculation of histograms. The results are displayed on a color monitor and on a gray-scale hard-copy recorder.

Since the image data are in digital form and are processed digitally, other useful data can be appended to images. For example, such information as position, course, speed, and elapsed time aids in the preparation of mosaic composite pictures of the seafloor. These mosaics provide coverage comparable to wide-area aerial photographs.

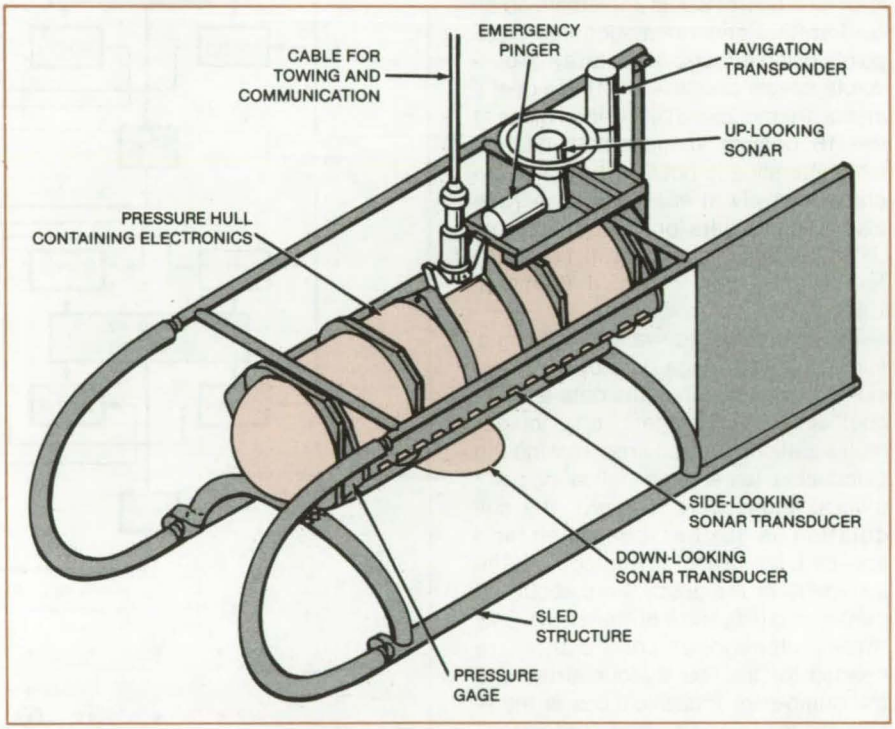

The **Towable Underwater Platform** is 3.2 meters long, 1.2 meters wide, and 1.4 meters high and has a mass of about 1,250 kilograms.

This work was done by Garrett Paine, George R. Hansen, R. William Gulizia, and Peter Paluzzi of Caltech for **NASA's Jet Propulsion Laboratory.** *For further information, Circle 16 on the TSP Request Card.*
NPO-15878

Eliminating "Hotspots" in Digital Image Processing

Signals from defective picture elements are rejected.

NASA's Jet Propulsion Laboratory, Pasadena, California

The image-processing program for use with a charge-coupled device (CCD) or other mosaic imager can now be augmented with an algorithm that compensates for a common type of electronic defect. Such an algorithm has been used in a star-tracking telescope to prevent the false interpretation of "hotspots" (picture elements of unusually high dark current) as stars. Since even the best CCD's usually have at least a dozen hotspots apiece, this method of defect compensation should be of interest in automatic navigation systems, robotics, image enhancement, image analysis, and digital television.

In the star-tracking application the lens is deliberately defocused by a small amount so that the light from one star falls on as many as nine picture elements without the risk of being lost in the interstices. The luminous flux density is reduced by the defocusing to such an extent that the hotspot dark currents often exceed the currents excited by stars. In a typical system that tracks the ten or so brightest stars, a hotspot can be mistaken for one of the stars (see figure).

To compensate, the telescope computer memory is equipped with a "spot table" that lists the locations of the hotspots. The table is derived by scanning the CCD elements with the telescope shutter closed. This scan is done before putting the telescope into service and is repeated at intervals during service to update the table. When the telescope operates in the acquisition mode, the image-processing algorithm rejects any star indication that comes from a known hotspot. In the tracking mode, a true star image that encroaches on a known hotspot is rejected and another star image substituted for tracking. When a previously-rejected star image emerges from a known hotspot, tracking of that image is resumed.

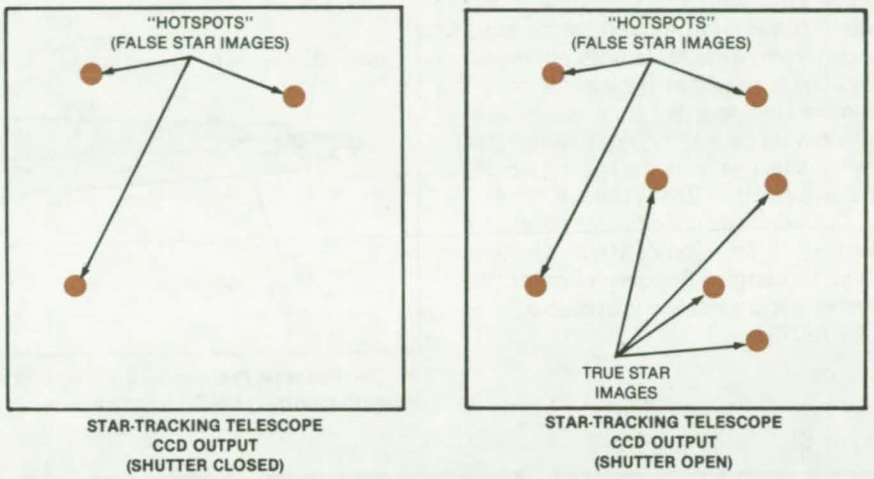

"Hotspots" (picture elements with high dark current) are identified by scanning the CCD without illumination (left). This allows the image-processing system to eliminate false star indications (right).

This work was done by Phil M. Salomon of Caltech for **NASA's Jet Propulsion Laboratory.** *For further information, Circle 17 on the TSP Request Card.*

NPO-15684

Detection of Floating Inputs in Logic Circuits

Modified oscilloscope probe applies a momentary pullup voltage.

Langley Research Center, Hampton, Virginia

A simple modification to an oscilloscope probe allows easy detection of floating inputs or tristate outputs in digital-IC's. Floating inputs, especially in high-impedance CMOS logic, can cause insidious problems that are difficult to troubleshoot. A floating CMOS input looks like a positive-logic low on an oscilloscope, because the probe impedance is low enough to "pull" down the floating node. Commercially-available logic probes can detect floating inputs, but for some applications it may be preferable to have a full oscilloscope display, rather than just the LED readout of typical logic probes.

The probe is modified with a subminiature momentary pushbutton switch and a resistor connected to the spring-loaded probe tip (see figure). The only permanent change in the probe is a 0.020-in. (0.5-mm) hole in the tip. This hole accepts a contact pin held in place by the spring tension of the tip.

A 1/4-W resistor, 5 to 6 kΩ for CMOS logic circuits, is soldered between the contact pin and one side of the switch. The switch is mounted in a screw of a standard cable clamp that encircles the probe housing. The other side of the switch is connected to a short lead terminated by an alligator clip or other con-

(continued on next page)

venient termination. The modified tip is inserted into the probe housing.

During the tests, the alligator clip is clamped to the circuit supply voltage; the circuit nodes are probed with the tip. When a node is suspected of being in a floating or tristate condition, the push-button switch is pressed to apply a momentary pullup voltage, and the scope is observed to determine if the trace moves from ground to the logic supply level. If the trace does not move, the node is grounded. If the trace "tries" to move, the node is held at a logic low by a driving gate and is not floating. The switch thus uncovers the floating inputs; it draws less than 2 mA of circuit current.

This work was done by Bob Cash and Michael G. Thornton of Martin Marietta Corp. for **Langley Research Center.** *No further documentation is available.*
LAR-13073

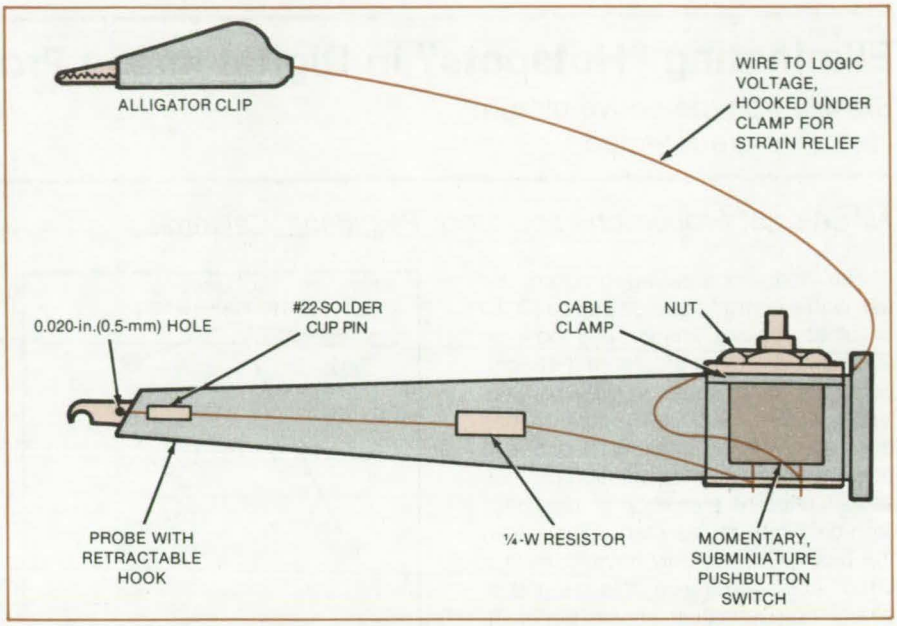

An **Oscilloscope Probe** is easily modified with a 1/4-W resistor and a switch for detecting floating inputs in CMOS logic circuits.

Displaying Force and Torque of a Manipulator

Video graphics display shows force and torque values in easy-to-comprehend form.

NASA's Jet Propulsion Laboratory, Pasadena, California

A video system displays the values of forces and torques exerted by the end effector of a manipulator. Both magnitude and direction are displayed. The system allows an operator to control the manipulator and avoid damage to objects being handled. It is especially helpful when the operator's view of the end effector is obscured.

The operator can change coordinate axes, scales, labels, colors, and other aspects of the display by voice command or via a keyboard. The system records end-effector signals, raw or processed, in digital or analog form.

The display screen (see figure) shows forces and torques for the x, y, and z directions as horizontal bars. The length of each bar is proportional to magnitude: The scale appears at the bottom of the bar chart. The bars elongate to the left or right, depending on whether the values are negative or positive. Usually the axes and polarities are defined by the spatial reference frame of the end effector. However, the operator can command the system to use any other preset reference, such as the workspace geometry or the operator's position.

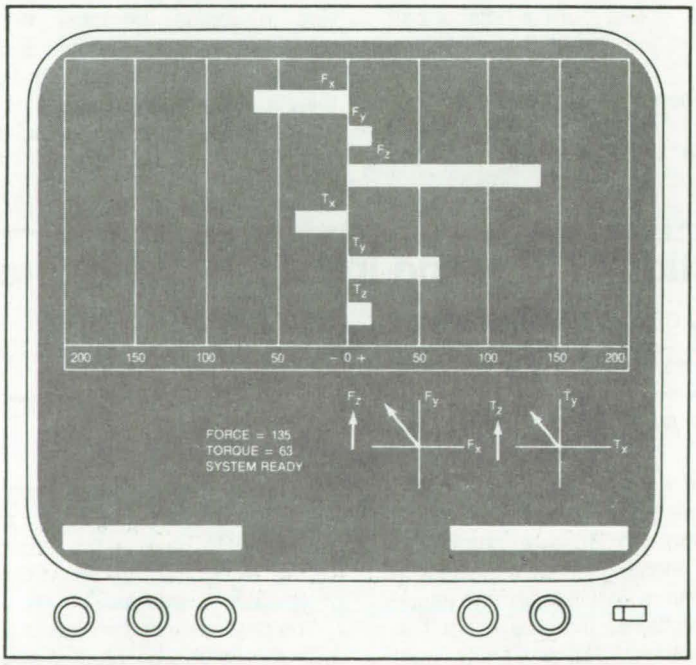

Display Combines Bar Charts, Vector Diagrams, and Numerical Values to inform an operator of the forces and torques exerted by the end effector of a manipulator. Simply by speaking a command, the operator can have the numerical values displayed alongside the corresponding bars. Here, forces are in pounds, and torques are in pound-feet: The operator can command a display in metric units, however.

The magnitudes of the resultant forces and torques are displayed numerically under the bar graph, with identifying labels. Also below the bar graph are pictorial displays of the projections of the force and torque vectors on the x-y plane. Vertical lines immediately to the left of the force and torque vectors indicate the magnitude of the z-axis components of vectors.

Two bars at the bottom of the screen indicate the degree of closure of the claws on the end effector. As the claws close, the bars elongate toward one another, touching just as the claws meet.

On voice or keyboard command, an eight-channel strip-chart recorder traces the force and torque components and claw position or the raw measurements from the eight strain-gage sensors in the end effector. Digital sensor data may also be sent digitally to a minicomputer and displayed on a cathode-ray-tube terminal.

This work was done by Antal K. Bejczy, Ronald S. Dotson, and Howard C. Primus of Caltech for **NASA's Jet Propulsion Laboratory.** *For further information, Circle 18 on the TSP Request Card.*
NPO-15942

MiniBriefs describe NASA innovations and reports in an abbreviated format. Readers desiring additional information on these items should request the Technical Support Packages (TSP's), available in most cases, which can be obtained by using the TSP Request Card at the back of this issue.

Digital-Image Enhancement

The intensity of resolution of each digitized video input is 256 discrete levels.

A programable system enhances digitally monocular and stereographic images at video rates. It provides both automatic and interactive enhancement modes based on histogram modification and intensity-mapping techniques.

The system is capable of simultaneously processing two video sources with a resolution of 2^Q pixels per scan line with Q being an integer in the range $5 \leq Q \leq 10$. The system operates in real time in the sense that its throughput delay is well below the standard television refresh rate or 30 frames/s.

This work was done by R. E. Woods and R. C. Gonzalez of the University of Tennessee for **Marshall Space Flight Center.** *For further information, Circle 86 on the TSP Request Card.*
MFS-25679

Instrumentation and Control for Fossil-Energy Processes

A working document fosters development of instrumentation and control technology.

The instrumentation and control requirements for fossil-energy processes are discussed in a working document. Advanced conversion processes for fossil fuels have created an urgent need for plant equipment beyond the present state of the art. The document is published to foster the advancement of instrumentation and control technology by making equipment suppliers and others aware of specifications, needs, and potential markets.

Technical requirements for critical instruments and controls are presented on the basis of information supplied by process designers and operators. The document will be revised and disseminated from time to time.

This work was done by Alexander Mark, Jr., of Caltech for **NASA's Jet Propulsion Laboratory.** *For further information, Circle 87 on the TSP Request Card.*
NPO-15581

Status Panel for Video Cassette Recorders

Panel simultaneously monitors 30 video cassette recorders on a remote panel.

A central array of light-emitting diodes displays the status of 30 video cassette recorders (VCR's) monitoring integrated testing of the Space Shuttle. The remote status panel is linked to the VCR's by one 37-conductor cable. Transistor/transistor logic chips in the interface circuit allow the LED array to function without drawing power from the VCR control circuits.

Supervisors can tell at a glance whether all the VCR's are recording properly, and a technician can be dispatched to identify and correct problems. This panel could be applied to other installations having large numbers of VCR's.

This work was done by Gerald L. Talley, Jr., and Daniel R. Herbison of Information Systems Directorate for **Kennedy Space Center.** *For further information, Circle 88 on the TSP Request Card.*

Inquiries concerning rights for the commercial use of this invention should be addressed to the Patent Counsel, Kennedy Space Center [see page A5]. *Refer to KSC-11254.*

Central Control of Local Oscillator Frequencies

Microprocessor-based unit monitors and corrects multiple frequencies.

A central unit automatically controls the frequencies of a group of independent crystal-controlled low-power oscillators. The unit is well-suited for regulating local oscillators in multiple-channel transmitters.

The unit checks its own frequency against an accurate frequency reference, such as station WWV, and corrects its own timing circuit as necessary. For each local oscillator, a processor in the control unit compares the duration of an interval (defined by a fixed number of machine cycles) with the pulse count from the local oscillator during that interval. The deficiency or excess of pulses corresponds to a correction stored in memory. The control unit shifts the frequency of the local oscillator as necessary.

This work was done by Steven F. Smith of the University of Tennessee for **Goddard Space Flight Center.** *For further information, Circle 89 on the TSP Request Card.*

This invention is owned by NASA, and a patent application has been filed. Inquiries concerning nonexclusive or exclusive license for its commercial development should be addressed to the Patent Counsel, Goddard Space Flight Center [see page A5]. *Refer to GSC-12804.*

Deallocating Defective Space on Winchester Disks

Data integrity is maintained in a two-operating-system, partitioned-disk environment.

A method is given for locating and deallocating defective sectors or tracks in a Winchester-disk system that is partitioned into two regions, one for each of two operating systems (OS). The first is a real-time (on-line) OS, the second a diagnostic (off-line) OS.

Disk formatting for the first OS is by sectors; for the second, by tracks. The program that tests the disk surfaces for defects and creates a table listing bad sectors operates under either OS. Application load programs that execute under either OS will utilize the bad sector information to ensure that no application programs are stored on defective areas of the disk.

This work was done by W. King, Jr., of IBM Corp. for **Kennedy Space Center.** *For further information, Circle 90 on the TSP Request Card.*
KSC-11287

Display for Mining-Machine Operators

Unit gathers data and presents it in easy-to-understand form.

An electronic display unit provides the operator of a longwall shearer with the information needed to control the machine. The unit samples sensors on the shearer. Using the sensor signals, it executes mathematical calculations, performs decisionmaking routines, and displays results to the operator. The unit also logs data for later analysis.

The unit is lightweight, portable, and explosion-proof. It is unaffected by the usual mining conditions involving water, dust, debris, and large rock failures.

Software in the unit activates indicator lights so that if the shearer drum is out of tolerance on the low side, a green light appears. If the drum is out of tolerance on the high side, a red light appears. If the drum is within tolerance, a yellow light is activated.

This work was done by Peter Paulson of Adjunct Technologies, Inc., for **Marshall Space Flight Center.** *For further information, Circle 91 on the TSP Request Card.*
MFS-25955

Determining the Nonlinearity of Microwave Receivers

A noise-adding radiometer is built into the receiving circuit.

The nonlinearity of a microwave receiver is measured and automatically corrected for by a noise-adding radiometer built into the microwave receiving circuit. The radiometer includes a noise-adding diode, which is turned on and off by a computer-controlled processor. The system turns the diode on and off with the receiver connected alternately to the antenna and to an ambient termination. The degree of nonlinearity is indicated by the difference in the noise temperature increases produced by the diode for the two configurations — antenna input and ambient-termination input. A corrected system noise temperature is then computed.

This work was done by Charles T. Stelzried and John E. Ohlson of Caltech for **NASA's Jet Propulsion Laboratory.** *For further information, Circle 92 on the TSP Request Card.*
NPO-15355

Estimating Effects of Flicker Noise in Clock Signals

Two mathematical estimation techniques are given.

Two techniques mathematically estimate the effects of flicker noise in pulse trains used as clock signals. Flicker noise cannot be treated as Gaussian noise because in each instance it is spread among several clock pulses. As a consequence, the noise is correlated among all observations with hopelessly-complicated correlation coefficients.

In one technique, a sequence of numbers is generated to simulate the flicker noise, which is then treated as though it were a systematic error that can be removed in computing the cross-correlation function. In the other technique, a clock fluctuation is expressed as a sum of uncorrelated triangular-pulse trains, the statistics of which can be analyzed. When tested with experimental radio-interferometric geodesic data, the two techniques showed good agreement.

This work was done by Sien-Chong Wu of Caltech for **NASA's Jet Propulsion Laboratory.** *For further information, Circle 93 on the TSP Request Card.*
NPO-15525

Hardware Fault Simulator Generates Test Vectors for Complex IC's

It is faster and more cost effective than software simulation.

A final report describes a technique that uses a fault simulator implemented entirely in hardware to generate and optimize test vectors for a microprocessor. The hardware fault simulator approach reduces test time, while maintaining high reliability in detecting faults.

The development and optimization of test vectors was done with the fault simulator plugged directly into the test head. The fault simulator automatically injected over 1,000 faults in the sequential and combinatorial circuits of the microprocessor. Detection of single stuck faults was 99.7 percent, using 14,000 vectors.

This work was done by Constantin C. Timoc, Lawrence M. Hess, and Frank R. Stott of Caltech for **NASA's Jet Propulsion Laboratory.** *To obtain a copy of the report, Circle 94 on the TSP Request Card.*
NPO-15362

Physical Sciences

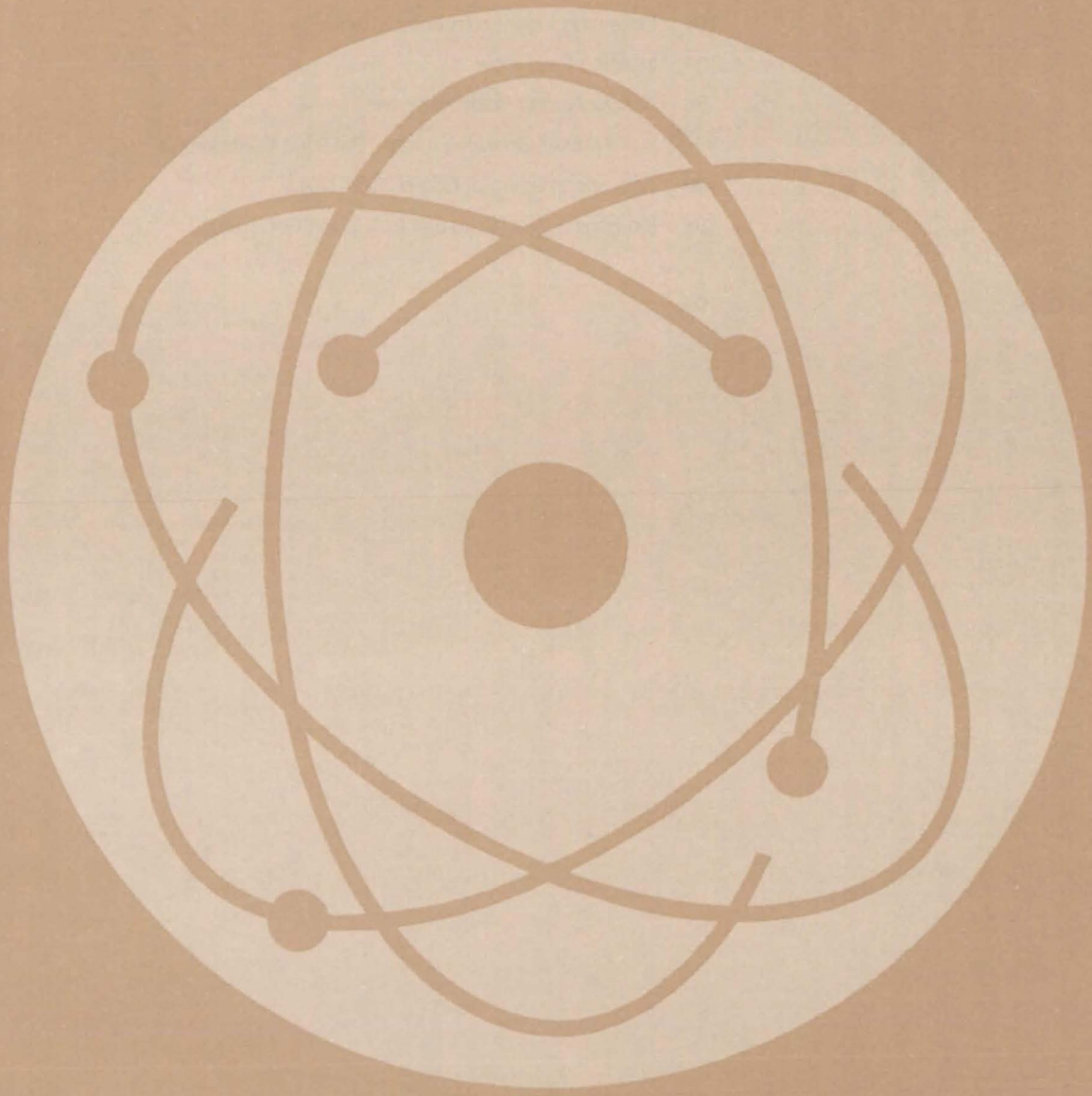

Hardware, Techniques, and Processes

191 Improved Gamma- and X-Ray Pinhole Camera

192 Ion Accelerator Merges Several Beams

193 Neutron Probe of Building-Wall Composition

194 Collecting Light From Point Images

195 Imaging Fluid Flow

196 Airflow Assists Solar Receiver

197 Sun Tracker Operates a Year Between Calibrations

198 Acoustic Imaging of Combustion Noise

199 Ion Engine With Solid-Electrolyte Ion Generator

MiniBriefs

199

Improved Gamma- and X-Ray Pinhole Camera

Electronic additions increase image quality.

Goddard Space Flight Center, Greenbelt, Maryland

An imaging system that gives low-resolution three-dimensional views of radioactivity distributions has been improved by the addition of electronic image processing. When fully developed, the system will be useful in nuclear medicine or radioisotope imaging, tomography, and the nuclear industry.

The basic optical principle of the system without electronic image processing is described in "Viewer Makes Radioactivity 'Visible' " (GSC-12640), *NASA Tech Briefs*, Vol. 7, No. 3 (Spring 1983), p. 271. In essence, an orthoscopic virtual image $A''B''C''$ in visible light is formed from radioactive object ABC with an arrangement of multiple-pinhole screens, a scintillator screen or other X-ray-to-visible converter, and passive optical-imaging screens or image intensifiers (see Figure 1). The many imaging-screen views seen by the observer through the pinholes of screen S'' have the same parallax as would multiple views of the object seen through the same pinholes. Consequently, the observer has the perception of depth and the ability to see part way around corners by moving laterally, as if viewing a true three-dimensional object through screen S''.

(continued on next page)

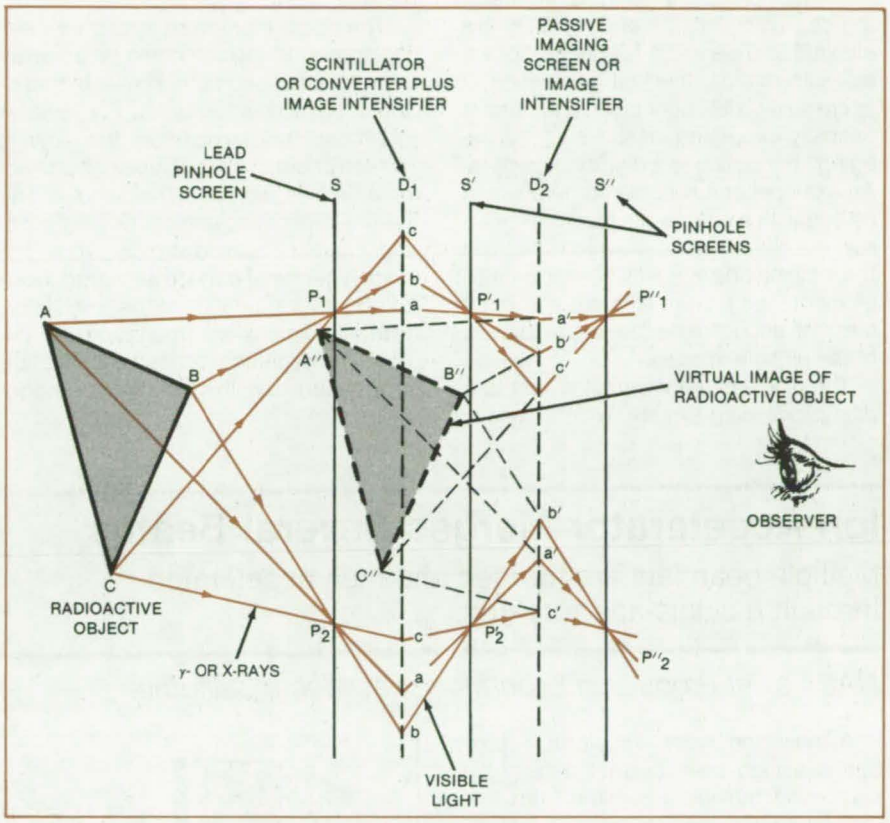

Figure 1. An **Orthoscopic Virtual Image** of a radioactive object is formed in visible light with a series of screens and pinholes.

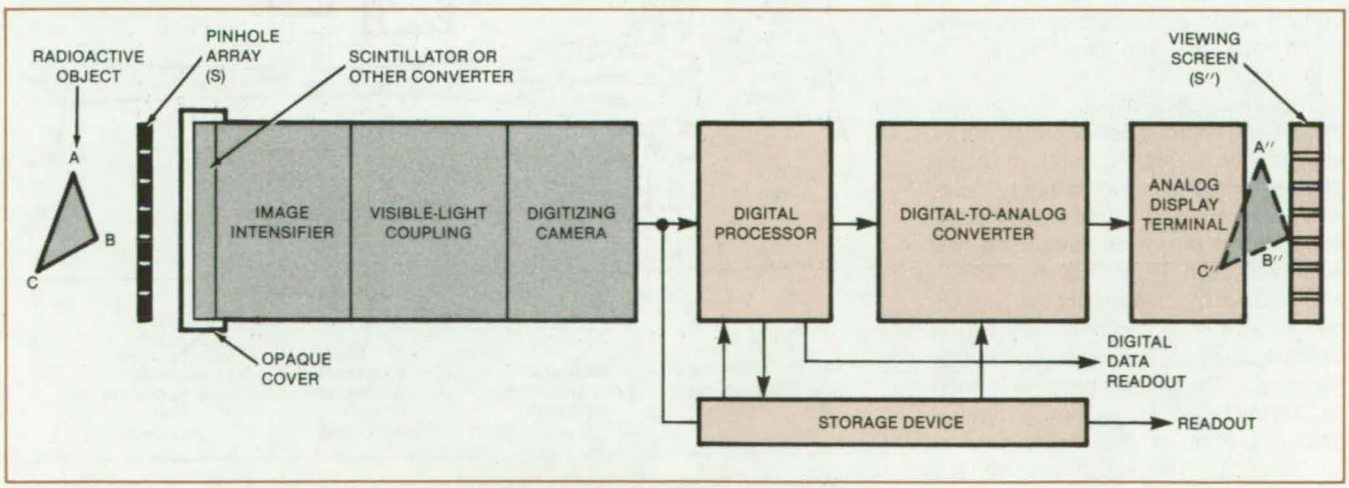

Figure 2. **Digital Image-Processing Equipment** electronically performs the functions of S' and D_2, thus improving the resolution and adding the capability for image storage and further processing.

The quality of the final image seen by the observer is limited by the competing needs of image intensity (requires large pinholes) and geometric resolution (requires small pinholes). Furthermore, diffraction limits the resolution at pinhole sizes comparable to visible-light-wavelengths. The resolution is further limited by screens D_1 and D_2.

In the improved system (see Figure 2), the degrading effects of S' and D_2 are eliminated. To avoid a further loss of image information, the first generation of intensified visible-light pinhole images is optically projected or coupled by imaging fiber optics to a digitizing camera. An example of a suitable camera would be one with a charge-coupled-device array, the digital output of which specifies the location and intensity of each picture element. The picture-element size must be small enough for adequate resolution of the pinhole images.

The digital camera output is sent to a data-processing system, which digitally inverts each pinhole image about its pinhole axis: The digital system thus performs the geometric inversion formerly done by S' and D_2 but without the loss of resolution. The image data may then be stored, subjected to digital image enhancement or other processing, or converted back to analog form on a television screen or other display device.

The display is viewed through a viewing screen S'', which could be an array of pinholes of geometry similar to that of the first pinhole array, S. For greater brightness and resolution, the viewing screen could consist of a planar array of small lenses in place of the pinholes. The lateral alinement, pinhole or lens spacing, and optical distance from the display terminal may be similar to those of screen S in relation to the scintillator, with all dimensions multiplied by the overall magnification or minification introduced by the electronic-image-processing and optical-coupling portions of the system. If desired, an exaggerated sensation of depth can be obtained by disproportionately increasing the distance from the display terminal to the viewing screen.

In addition to analog 3-D viewing, the digitized information from the detector can be used to produce quantitative tomograms of the object. Image digitization also allows the visualization of X-ray and gamma-ray objects of very low intensity through long integration times.

This work was done by Lo I. Yin of **Goddard Space Flight Center.** *For further information, Circle 19 on the TSP Request Card.*

This invention is owned by NASA, and a patent application has been filed. Inquiries concerning nonexclusive or exclusive license for its commercial development should be addressed to the Patent Counsel, Goddard Space Flight Center [see page A5]. *Refer to GSC-12851.*

Ion Accelerator Merges Several Beams

Multiple beamlets are merged and then accelerated through a single-aperture grid.

NASA's Jet Propulsion Laboratory, Pasadena, California

A new ion-beam accelerator produces a high peak current density by combining multiple beamlets from the ion source into one high-intensity beam. This peak is over 25 times as high as that produced from the same plasma source with electrodes in a single-beam Pierce configuration. Ion-extraction efficiency, beam intensity, and focusing are all improved.

The new ion-beam-accelerator system should improve performance of ion-implantation systems used in some processes for making integrated circuits and solar cells and in passivating metal surfaces for corrosion resistance and wear protection. The new system should also improve the performance of neutral-beam injectors for thermonuclear-fusion devices, such as Tokomaks and mirror machines. (The neutral beam is formed by passing the ion beam through neutral gas. A portion of the beam ions is neutralized by charge exchange with the gas atoms.)

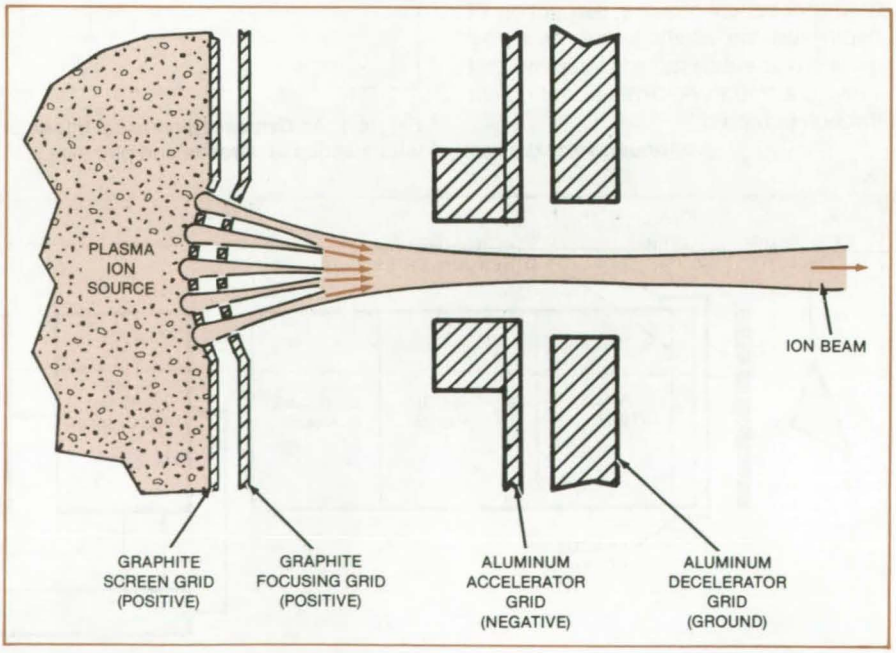

An **Intense Ion Beam** is formed by merging multiple ion beamlets into one concentrated beam. The beamlet holes in the graphite screen and focusing grids are arranged in a hexagonal pattern. The merged beam passes through a single hole in each of the aluminum accelerator and decelerator grids.

The accelerator is divided into two sections: an ion-extraction section consisting of a thin dome-shaped graphite screen and focusing grids (see figure) and an accelerating and focusing section consisting of a single-hole aluminum accelerator and decelerator (ground) grids. The screen and focusing grids control the density of the ion current extracted from the plasma, and they prefocus the ion beamlets. A hexagonal array of holes is drilled in each of these grids. The holes in the two grids line up so that the axes of all the pairs of holes aim toward a common line of focus.

Ion-extraction efficiency is maximized by making the screen grid as thin as possible to reduce ion-recombination losses on the screen. The grids are made of graphite for dimensional stability at high temperatures and to resist ion-sputter damage. The screen- and focusing-grid potentials are adjusted to maximize beam current at a given plasma density.

The accelerator grid is placed far enough downstream that the combined electrostatic and geometrical focusing effects have merged the beamlets into a single intense beam when they reach the accelerator. The merging effect is a function of the screen- and focusing-grid radii of curvature and of the distance between the focusing and accelerator grids. The optimum values of these variables depend on the ion-energy and beam-current density desired.

This work was done by Graeme Aston of Caltech for **NASA's Jet Propulsion Laboratory.** *For further information, Circle 20 on the TSP Request Card.*

Inquiries concerning rights for the commercial use of this invention should be addressed to the Patent Counsel, NASA Resident Office-JPL [see page A5]. Refer to NPO-15547.

Neutron Probe of Building-Wall Composition

Walls of historic buildings are charted by neutron radiography.

Goddard Space Flight Center, Greenbelt, Maryland

Neutron radiography aids the preservation and restoration of historic buildings by producing a map showing the presence of contaminants and chemical changes in a wall. The map indicates the nature and extent of changes in the building materials so that the proper treatment can be applied.

A neutron source such as californium-252 is positioned on the rear wall surface, opposite a gamma-ray detector on the front wall surface (see figure). The detector is part of a gamma-ray spectrometer.

Low-energy (thermal) neutrons passing through the wall tend to be captured by nuclei, yielding gamma rays. Each chemical element in the wall produces a characteristic gamma-ray spectrum by which it can be identified.

Any movement of the neutron source is accompanied by corresponding movement of the detector so that they are constantly facing each other on opposite sides of the wall. A gamma-ray source next to the neutron source and a collimated auxiliary detector next to the spectrometer detector ensure alinement; when the intensity of the gamma-ray spectral line between the auxiliary source and detector is at its peak, the primary source and detector are in their proper positions relative to each other.

The spectrometer system computes the ratio of the intensity of the spectral lines of the constituent elements to the

(continued on next page)

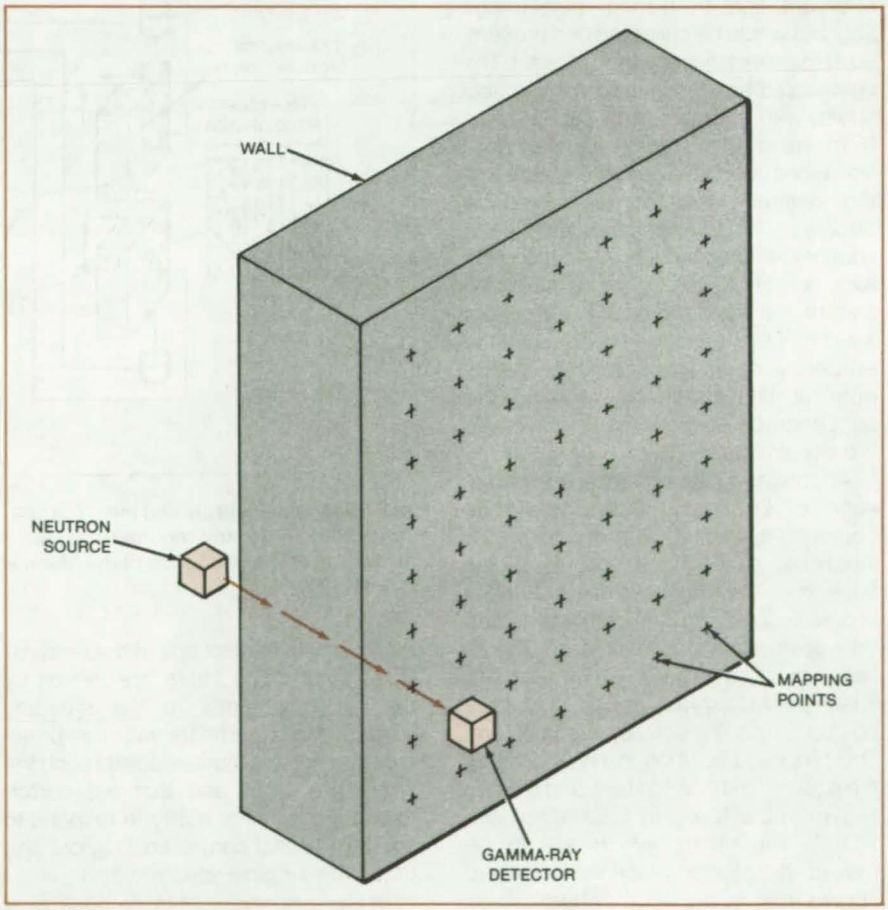

A **Neutron Source and Gamma-Ray Detector** alined with each other yield a map of the composition of a wall. The points are spaced for minimal overlap based on the mean free path of gamma rays emitted from the wall materials.

intensity of the predominant element (silicon in the case of a brick wall). The ratio for the hydrogen line, for example, indicates the concentration of water in the wall, and the ratio for the chlorine line indicates the salt concentration.

In typical wall materials the mean free path of gamma rays from hydrogen and chlorine is about 8 inches (20 cm). Thus, walls up to about 16 inches (40 cm) can be mapped by two scans — one with the source on the inside and the detector on the outside and one with the positions reversed. The scanning can be done by positioning the source and detector at points spaced 16 inches apart horizontally and vertically to give a comprehensive view of the wall interior.

For metal testing, the neutron source and gamma-ray detector can be positioned at opposite sides of a ladle, flowing metal, or moving slab or ribbon. The composition of the metal can then be monitored continuously by the ratios of the measured intensities of the spectral lines. In steel, for example, the ratios of iron to carbon, iron to nickel, and iron to chromium would be measured.

This work was done by Jacob I. Trombka of **Goddard Space Flight Center** *and Larry G. Evans of Computer Sciences Corp. For further information, Circle 21 on the TSP Request Card.*

This invention is owned by NASA, and a patent application has been filed. Inquiries concerning nonexclusive or exclusive license for its commercial development should be addressed to the Patent Counsel, Goddard Space Flight Center [see page A5]. *Refer to GSC-12808.*

Collecting Light From Point Images

Light from sources at varying positions is brought to a fixed opening.

NASA's Jet Propulsion Laboratory, Pasadena, California

In a proposed spectrograph-feed instrument, light from many point-image sources would be collected and presented at the spectroscope entrance slit. The light would be transmitted over optical fibers, with the fiber from each source terminating at a fixed designated position along the slit. Thus, the spectra of the several point sources would be displayed simultaneously, with each source identified by its position along the axis perpendicular to the wavelength axis of the spectrogram. The concept was originally developed to enhance the efficiency of spectrographs on astronomical telescopes by allowing the spectrograph to view many objects in the sky simultaneously.

According to the concept, one end of each of 20 optical fibers would be computer-controlled to move to preset locations in the focal plane of the telescope. The major technical difficulty is precisely moving the fibers and setting their positions in a confined area: The 20 fibers must be moved within a square 3 inches (7.6 cm) on a side, and their positions must be correct within 20 μm. The proposed solution involves dividing the square field into 10 strips and placing two movable fibers in each strip (see figure). The fibers, which are to be moved by stepping-motor-driven lead screws, may be placed anywhere in their strip provided that each fiber does not pass the other fiber occupying the strip.

To test the concept, a prototype consisting of a single strip with two fibers was constructed and tested on the 200 inch (5m) Hale telescope at the Palomar Observatory. The fibers are moved by manual commands to the stepping motors. Measurements with the prototype showed that light losses through the fibers are small and that the performance (in terms of ability to respond to low light levels) comes up to about half that of the original spectrograph.

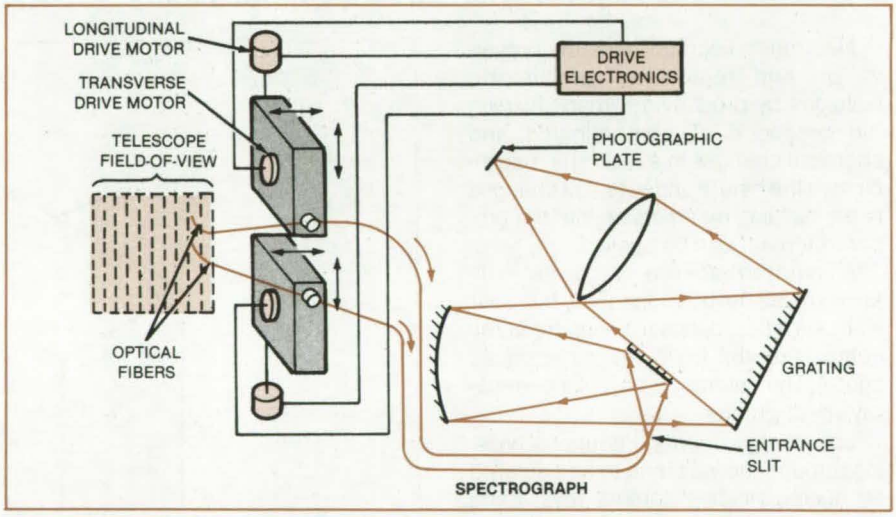

In a Telescope Field divided into 10 strips, 10 pairs of optical fibers are moved laterally and longitudinally to any required position in their assigned strips. Only one fiber pair is shown here. The fixed ends of the fibers are arrayed in a line at the spectrograph entrance slit.

In the prototype, both motions of a fiber — longitudinal and lateral — are driven through lead screws by 90° permanent-magnet stepping motors. The lead-screw pitch is 52 to the inch (about 20.5 to the centimeter). This pitch, combined with the 6-to-1 gear ratio on the motors, gives the requisite 20-μm increment per step. Permanent-magnet motors were chosen because they hold their position when power is off. Fibers hold their position from one night to the next even when the telescope is subjected to attitude tests during the day.

Glass rather than plastic was chosen as the fiber-core material because glass carries light more efficiently in the 0.3- to 0.7-μm wavelength range used by the spectrograph. The fiber-core diameter is 250 μm: This value accommodates the 100- to 200-μm diameter of star images

at the telescope focal plane. The fiber is protected by a polymer jacket that provides strain relief, cushioning, and protection against abrasion.

The concept is not limited to astronomical spectrography. The principle of movable optical fibers can be adapted to such applications as microscopy, measurements by television camera, photographic analysis, thermal analysis, and surveying.

This work was done by Willis C. Goss, Eldred F. Tubbs, and Judith G. Cohen of Caltech for **NASA's Jet Propulsion Laboratory.** *For further information, Circle 22 on the TSP Request Card.*
NPO-15887

Imaging Fluid Flow

Four beam splitters are used.

Marshall Space Flight Center, Alabama

An electro-optical system allows simultaneous viewing of schlieren, shadowgraph, and interferometric images of a volume of fluid under test.

In the system shown in the figure, a spatially-filtered and collimated laser beam passes through cube beam splitter 1. The reflected portion of this beam is incident on a mirror that has micrometer adjustment knobs; the mirror reflects the light to cube beam splitter 2. The transmissive portion of light from beam splitter 1 passes through the test area and falls on beam splitter 3. The reflected portion of light from beam splitter 3 goes to beam splitter 2 where the two beams that were separated at beam splitter 1 are brought back together. The two beams interfere with one another, giving a Mach-Zehnder interferometric image of the test area.

The transmissive portion of light from beam splitter 3, after passing through a focusing lens, is incident on beam splitter 4. The reflected portion of this beam is focused to a point where a knife edge is placed to block the undeviated portion of the light coming from the test area. The deviated light from the test area passes around the knife edge, expands, and is incident on a screen, giving a schlieren image of the test area. The transmissive portion of light from cube beam splitter 4 is incident on another mirror that directs the beam onto a screen, producing a shadowgraph image of the test area.

This work was done by William K. Witherow of **Marshall Space Center.** *No further documentation is available.*

Inquiries concerning rights for the commercial use of this invention should be addressed to the Patent Counsel, Marshall Space Flight Center [see page A5]. Refer to MFS-25897.

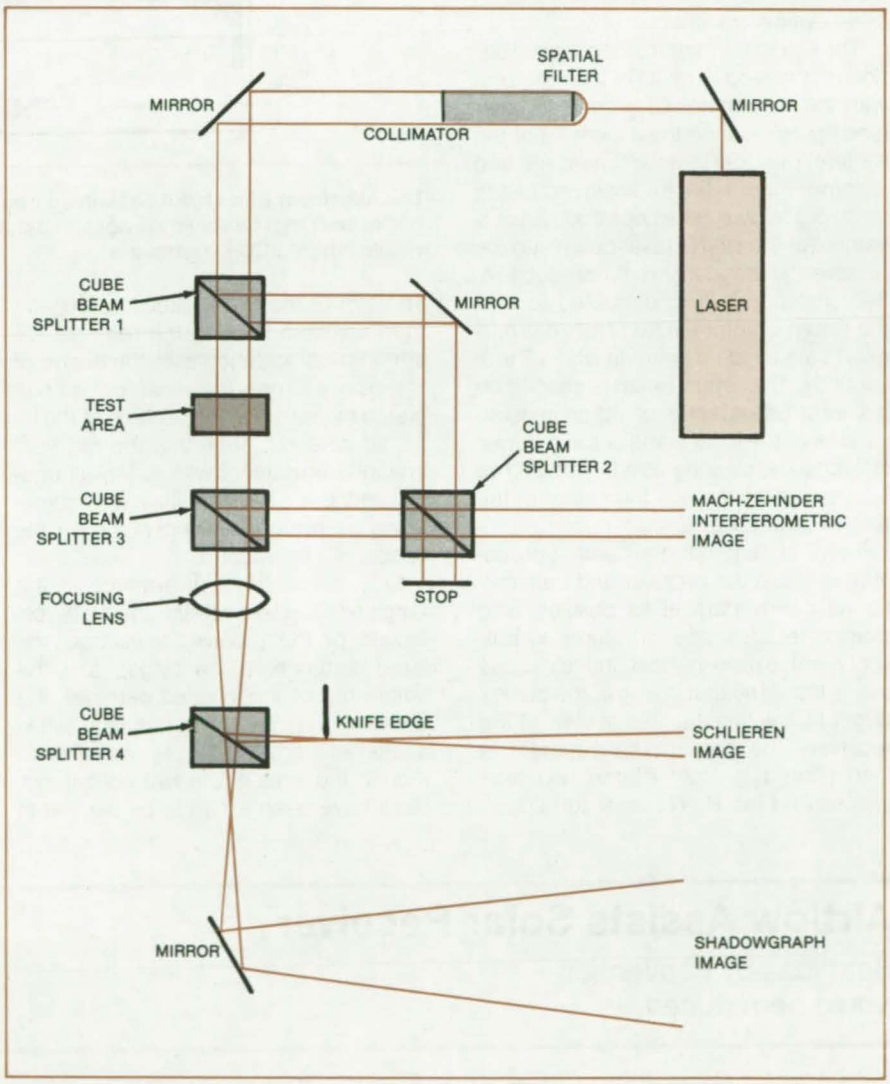

In this **Imaging System** designed for use in fluid-flow research, the cube beam splitters can be replaced by plate-type beam splitters or pellicle beam splitters.

Visual Alinement Technique for Infrared LIDAR

A red He/Ne laser beam indicates aim direction.

NASA's Jet Propulsion Laboratory, Pasadena, California

A method for alining the optics of an infrared light-detection and ranging (LIDAR) system is accurate for target distances of several kilometers. A visible He/Ne laser beam is substituted for the invisible CO_2 beam during the alinement. The new method could also be used to aline adjacent telescopes in other optical systems.

The key to the new method is the addition of a low-power He/Ne laser coaxial with the transmitter CO_2 infrared laser (see figure). During the alinement of the system, the CO_2 laser is turned off, and a corner-cube reflector is placed just in front of the two telescopes to divert a sample of the He/Ne laser beam into the receiver telescope. The corner-cube reflector is precisely constructed so that the return beam reflected from it is parallel to the incident beam to within 2 arcseconds. The return beam is imaged on the infrared detector or other imaging surface at the focal plane of the receiver telescope, appearing as a tiny bright red spot superimposed on the image of the distant target scene.

The first step in the alinement procedure is to set the receiver and transmitter as nearly parallel as possible and clamp the telescope structures to prevent relative motion. Next, the telescope pair is aimed so that image of the distant target falls within the field of view of the receiver. The corner-cube reflector is then placed in front of the two telescopes and the He/Ne laser turned on.

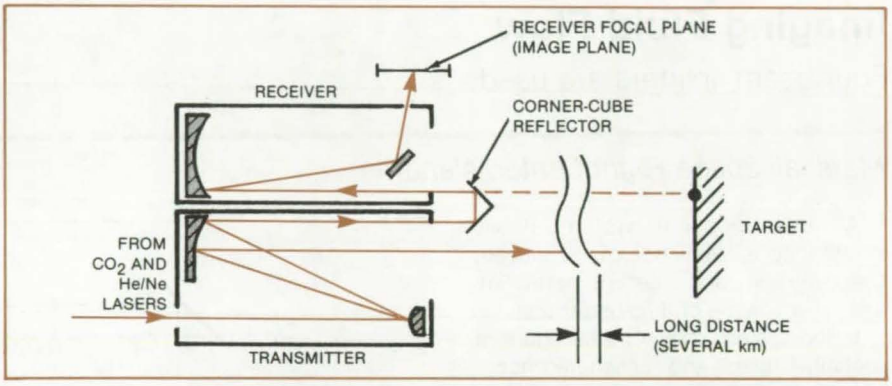

The **Alinement of a LIDAR System** can be accomplished visually by using a low-power He/Ne laser that has been previously adjusted so that its visible beam is parallel to the invisible infrared CO_2 laser beam.

The aim of the transmitter telescope is then adjusted to bring the red spot image into coincidence with the image of the distant target. The alinement is completed by adjusting the position of the infrared detector, such that the red spot image is coincident with it. (An alternative sequence of these steps may sometimes be preferable, depending on the optical configuration.)

Due to the slight divergence of the outgoing CO_2 laser beam, the finite resolution of the receiver telescope, the large distance to the target, and the finite area of the infrared detector, the detector will "see" the radiation backscattered from the target region even though the axes of the two optical systems have been alined to be parallel to each other rather than to converge to one point on the distant target. That is, the effective diameter of both the transmitter beam at the target and the target region sensed by the receiver are large compared to the distance between the axes of the two telescopes.

The adequacy of the alinement procedure was demonstrated experimentally: A return beam of adequate strength was detected from a reflecting target at distances up to 2 km from the instruments.

This work was done by Robert T. Menzies and Uri P. Oppenheim of Caltech for **NASA's Jet Propulsion Laboratory.** *For further information, Circle 23 on the TSP Request Card.*
NPO-15826

Airflow Assists Solar Receiver

Heat loss by convection would be reduced.

NASA's Jet Propulsion Laboratory, Pasadena, California

A proposed receiver for a hot-air solar energy-concentration system would operate with an inwardly directed airflow and an "air door" across the aperture to minimize the loss of heat by convection. The unit could be constructed from inexpensive materials, using ordinary sheet-metal fabrication techniques.

The receiver components are generally conical in shape (see figure); but some variation is possible, as the design is not particularly critical. The radiation-absorbing and heat-exchange medium is a mass of stainless-steel wool retained by a screen. The amount of steel wool required depends on the size of the steel filaments, the packing density, the expected airflow rate, and the re-

quirement that the pack be opaque. The diffuser cone might be made from single- or multiple-layer perforated metal sheet, metal screen, ceramic, or other porous material. The diffuser design depends on the concentrator accuracy, concentrator radiation cone angle, airflow rate, and reradiation from the heat exchanger.

Exhaust air from the heat engine or other heat-utilization system first enters cavity A where it cools the outer shell, thus recovering some of its heat for utilization and reducing heat loss from the outer shell to the atmosphere. The air then passes through the diffuser into cavity B, cooling the diffuser, the aperture edge, and the front surface of the insulating shell. The flow into cavity B constitutes the "air door" across the aperture, preventing the entrance and exit of convection currents and preventing the formation of parasitic convection currents within the receiver. Since the aperture is not otherwise blocked, the internal pressure of the air-circulation system automatically adjusts to changes in ambient pressure. From cavity B the air flows through the heat exchanger where it is heated by contact with and radiation from the steel wool. The hot air then flows to the heat-utilization system.

Closed-cycle versions have also been envisioned, including those using working fluids other than air. The diffuser cone would be changed to a dual-shell configuration to serve as a boiling section for the fluid. The heat exchanger and the diffuser would both have to be closed and sealed to contain the fluid. A closed-cycle version could be designed in the same nonstressed, nonrigidly constrained style as in the open-cycle versions, except for the additional restrictions imposed by the containment of the fluid at the expected temperature and pressure, with regard for its chemical reactivity and other safety concerns.

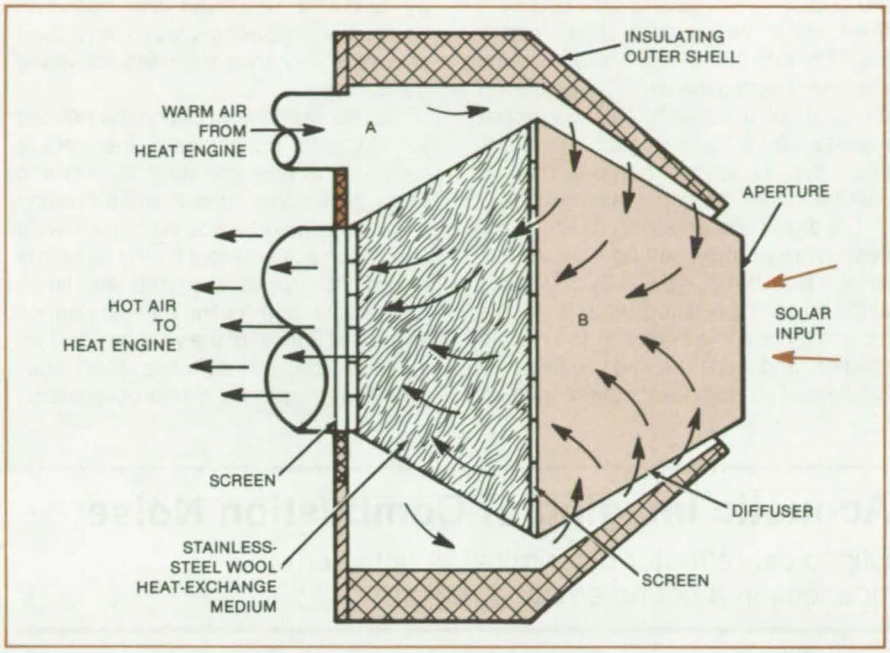

The Simplified Solar Receiver concept involves an inwardly directed flow of cooling air and an "air door" to reduce heat loss by convection. The receiver can be constructed from inexpensive materials.

This work was done by William R. Revere and Eugene A. Laumann of Caltech for **NASA's Jet Propulsion Laboratory.** *For further information, Circle 24 on the TSP Request Card.*
NPO-15784

Sun Tracker Operates a Year Between Calibrations

Modified tracker compensates for seasonal variations in solar declination.

NASA's Jet Propulsion Laboratory, Pasadena, California

A low-cost modification of a Sun tracker automatically compensates for the equation of time (the change of apparent solar time or time of Sunrise and Sunset) and for seasonal variations in the declination of the Sun. The modified tracker can operate unattended for a year before it needs corrections. It can be used for industrial solar-energy monitoring and in remote meteorological stations.

The basic solar tracker is a relatively-inexpensive commercial model that ordinarily requires daily adjustment. A Scotch-yoke drive mechanism was added to the tracker to supply declination motion. The Scotch yoke (see figure) provides a sinusoidal output motion, which approximates the Sun's yearly declination within 2°. The Scotch yoke is a simple mechanical device and is not Sun seeking; it is therefore inexpensive and reliable — even on overcast days.

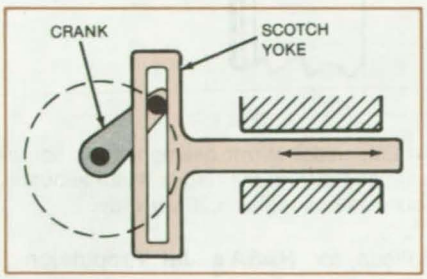

The Output of the Scotch Yoke drive mechanism is adjusted through proper sizing of the crank, yoke, and other components and through choice of gear ratios to approximate the seasonal north-and-south motion of the Sun.

The solar period is approximated in the tracker by a 360-day cycle — a period that is less costly to provide than the true 365-day cycle. The 365-day year has prime factors of 5 and 73; therefore a gear-train drive would have to have these tooth ratios between the input and

(continued on next page)

the output. A 5:1 ratio is provided by a five-tooth indexing drive that rotates one-fifth turn each night and remains stationary during the day. This gear is on the shaft of a single-thread worm that meshes with a 72-tooth gear — a stock gear that is less expensive than a custom-made 73-tooth gear would be.

The drive mechanism is adjusted for a best average fit by setting it so that its motion lags that of the Sun by 2 1/4 days at the beginning solstice, leads the Sun's motion by one-fourth day at the middle solstice, and leads the end solstice by 2 3/4 days. The equinox timing is thus off by about a day, and the complete declination-follower cycle is 5 days short of a year — hence the need for yearly adjustment.

So that sliprings would not be needed for electrical connections, the tracker reverses its direction after Sunset and turns back toward the Sunrise position at a higher speed, since in the summer a shorter time is available for the nighttime return. The tracker start and stop times are set manually for the earliest Sunrise and latest Sunset of the year by positioning cams on limit switches. Daily start time is provided by a microprocessor. The microprocessor tallies the days and on certain days stored in its memory updates the starting time. The number of updates and the size of the update increments depend on the pointing accuracy required. The updating can be done daily or — if a 4° tracking error is acceptable — not at all.

This work was done by C. Martin Berdahl of Caltech for **NASA's Jet Propulsion Laboratory.** *For further information, Circle 25 on the TSP Request Card.*
NPO-15810

Acoustic Imaging of Combustion Noise

Ellipsoidal reflector discriminates between locations in a sound-emitting region.

NASA's Jet Propulsion Laboratory, Pasadena, California

An ellipsoidal acoustic mirror is used to measure the sound emitted at discrete points in burning turbulent jets. The highly directional characteristics of the reflector can be utilized in a variety of monitoring or control systems involving flames or other reacting flows — in furnace combustion control, for example. It is currently used by NASA for research on jet flames and produces a clearly identifiable and measurable variation of the acoustic spectral intensities along the length of a flame.

The reflector concentrates energy originating at its far focus into a microphone at its near focus (see figure). Thus, when the reflector is positioned with its far focus in the jet flame, the microphone receives sound predominantly from a small region around that point in the flame. The reflector can be scanned along the flame so that it measures the acoustic spatial and spectral distributions.

The size of the region that contributes appreciably to the sound level at the microphone decreases with frequency increase. The resolution is determined by the diffraction pattern at the image plane. For example, a mirror with focal length/diameter ratio of 0.75 has a half-power central acoustic-image width of 56 cm at 0.5 kHz and 1.25 cm at 20 kHz.

This work was done by Kumar N. R. Ramohalli and Panchalam K. Seshan of Caltech for **NASA's Jet Propulsion Laboratory.** *For further information, Circle 26 on the TSP Request Card.*
NPO-15698

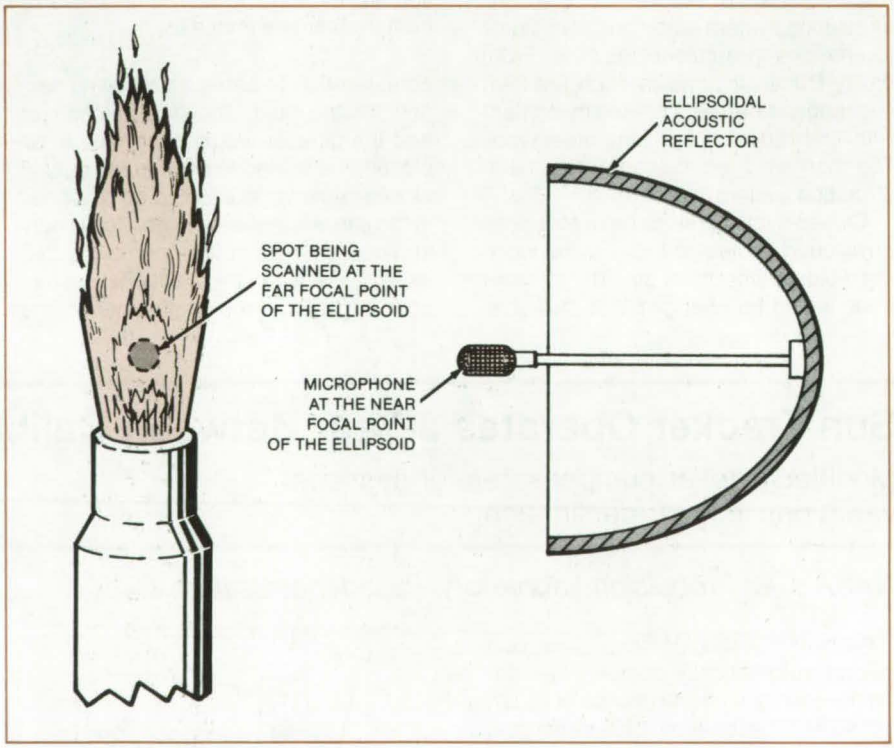

An **Ellipsoidal Mirror** deemphasizes sources close to the target source and excludes sources far from the target. At an acoustic frequency of 20 kHz, the mirror can resolve sound from a region 1.25 cm wide.

Ion Engine With Solid-Electrolyte Ion Generator

The working fluid would be utilized efficiently.

NASA's Jet Propulsion Laboratory, Pasadena, California

Fuel-cell technology may provide a new way to generate a beam of ions for implantation in semiconductors or other applications. Using a solid-state ion generator that operates on the same ion-conduction principle as that of fuel cells, a large flux of ions would be produced. In comparison with other contact-ionization generators, the proposed apparatus should waste little working fluid.

One version of the new ion engine is shown in the figure. A suitable working fluid and solid electrolyte might be sodium and β_2 alumina, respectively.

The working fluid and solid electrolyte are heated to about 1,000 K, at which temperature the vapor pressure forces the ions of the working fluid through the solid electrolyte to the outer surface. Because the solid electrolyte passes only ions but not neutral atoms of the working fluid, the neutral working-fluid atoms remain contained in the solid-electrolyte vessel until ionized.

Once the ions reach the outside of the solid electrolyte, they are accelerated by the electrodes downstream of the ion generator. The system should convert all working-fluid atoms to accelerated ions, the efficiency of conversion being 100 percent.

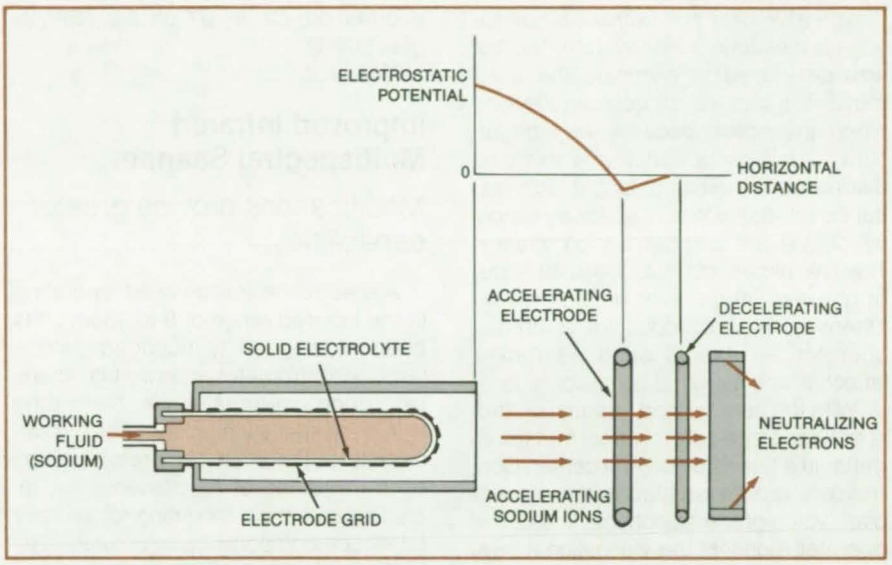

Working-Fluid Positive Ions (but not neutral atoms) are conducted through the solid electrolyte to the outside, then accelerated in the external electric field. While in the solid-electrolyte material, the ions do not recombine with electrons: They are therefore transported to the surface with high ionization efficiency.

This work was done by Robert Richter of Caltech for **NASA's Jet Propulsion Laboratory.** *For further information, Circle 27 on the TSP Request Card.*
NPO-15809

MiniBriefs describe NASA innovations and reports in an abbreviated format. Readers desiring additional information on these items should request the Technical Support Packages (TSP's), available in most cases, which can be obtained by using the TSP Request Card at the back of this issue.

Air-Conditioning for Electric Vehicles

The evaporative cooling uses solar heat and motor waste heat.

A combination of an ammonia-absorption refrigerator, roof-mounted solar collectors, and a 200° C service electric-vehicle motor provides an evaporative space-heating/space-cooling system for electric-powered and hybrid fuel/electric vehicles. The refrigerator can use either bromide salts in water or ammonia/water as the working fluid.

The evaporative cooling system requires less power than mechanical compressor-type air-conditioning. The recirculating liquid can also cool the vehicle motor. As a result, the motor can be operated at higher load levels, as would be required in climbing a hill, for example.

This work was done by Zenon Popinski of Caltech for **NASA's Jet Propulsion Laboratory.** *For further information, Circle 95 on the TSP Request Card.*

This invention has been patented by NASA (U.S. Patent No. 4,307,575). Inquiries concerning nonexclusive or exclusive license for its commercial development should be addressed to the Patent Counsel, NASA Resident Office-JPL [see page A5]. Refer to NPO-15183.

Controlling TV-Camera f-Stop Remotely

Iris is controlled manually without lens modifications.

The lens opening of a television camera can be controlled manually from a remote location by a simple and inexpensive data link, without modifications to the camera lens system. The link was developed to eliminate the automatic lens cap, which covered the lens when the scene became very bright. Now, a human operator can exercise discretion in viewing bright scenes, but can close the lens if necessary simply by closing the camera iris completely. The link allows closeup views of wide-brightness-range events that would otherwise be hazardous for a human operator — events such as rocket launches and many industrial operations.

With the new method, manual control is provided by a control panel and transmitter in a television control center. Control data are transmitted to the camera over voice-grade telephone lines. The operator monitors the video signal level while actuating an iris control switch to open or close the iris by means of a relay in the camera.

This work was done by Gerald L. Talley, Jr., Daniel R. Herbison, and Glenn F. Routh of **Kennedy Space Center.** *For further information, Circle 96 on the TSP Request Card.*

Inquiries concerning rights for the commercial use of this invention should be addressed to the Patent Counsel, Kennedy Space Center [see page A5]. Refer to KSC-11269.

High-Resolution X-Ray Telescope

Secondary mirror doubles the image resolution.

An X-ray telescope for mapping celestial X-ray sources from locations in space uses a secondary mirror to magnify the images formed by the primary mirror. The secondary mirror with its hyperboloid/hyperboloid surface is located at the focal plane of the primary mirror.

The secondary mirror magnifies the image formed by the primary mirror by a factor of 6. The resulting images have a spatial resolution twice that obtained in a single-mirror telescope of the same optical length. Higher image resolution is particularly significant when the image recording is electronic rather than optical, because electronic recording has higher resolution. The spatial resolution of the image now matches the resolution of the detector.

This work was done by John M. Davis and Richard C. Chase of American Science & Engineering, Inc. and James H. Underwood of Caltech, for **NASA's Jet Propulsion Laboratory.** *For further information, Circle 97 on the TSP Request Card.*
NPO-15971

Improved Infrared Multispectral Scanner

Modifications provide greater capabilities.

A spectrometer scan head, operating in the infrared range of 8 to 13 μm, has been redesigned to accommodate a larger spectrometer and two blackbody reference sources while remaining within the space limitations of its aircraft mounting. The scan head retains many of the features of its predecessor, including an optical mounting for primary telescope components, structural rigidity to maintain optical stability, and temperature compensation to maintain optical focus over a wide range of operating temperatures.

This work was done by Charles G. Stanich and Frederick G. Osterwisch of Daedalus Enterprises, Inc., for **NASA's Jet Propulsion Laboratory.** *For further information, Circle 98 on the TSP Request Card.*
NPO-16143

Lensless Image Scanner

Pictures are produced by Fourier transformation of fringe patterns.

A proposed image scanner uses moving and stationary parallel slits to produce pictures of visible, infrared, X-ray, microwave, or acoustic sources. No lenses or mirrors are required. A single detector views all parts of the image simultaneously, rather than as a raster, making relatively-short exposure times possible.

The detector views a source through two sets of parallel slits. The spacing between the sets is varied and the resulting Moire fringe patterns are recorded. A computer produces a picture of the source by Fourier transforming and plotting the recorded signals. Potential applications of the system include medical X-ray imaging.

This work was done by Rudolf A. Schindler of Caltech for **NASA's Jet Propulsion Laboratory.** *For further information, Circle 99 on the TSP Request Card.*
NPO-16004

Optical Measurement of Particle Size and Velocity

Diffraction grating simulates Doppler interference in proposed low-cost anemometer.

Dual-beam laser-Doppler anemometers can simultaneously determine the velocity and size distribution of particles in a flowing fluid. In a preliminary study, a single laser beam passing through a Ronchi ruling projected fringe patterns onto a rotating disk. Either sandpaper or glass beads were attached to the disk to provide known particle size distributions. The reflected light was focused onto a photomultiplier tube and the velocity signal amplitude was determined via an oscilloscope.

A known particle size distribution is sufficient to determine the velocity, but the converse is not true. However, inclusion of a second independent measurement may make the projected fringe technique a practical low-cost alternative to laser-Doppler anemometry.

This work was done by James Lee Smith of **Marshall Space Flight Center.** *For further information, Circle 100 on the TSP Request Card.*
MFS-27036

Improved Hollow Cathode

It can be rapidly started and kept in an idling state.

An improved hollow cathode for neutral-beam injector ion sources is rapidly started by the dielectric breakdown of an ignitor plug located at one end of an open-ended tube. The arc discharge initiated by the breakdown heats the cathode to electron-emitting temperatures in about 1 to 2 seconds.

The compact size and moderate power level of this new cathode make it a suitable replacement for filament cathodes. It can be used in low-current ion implantation, ion milling, ion sputtering, and ion bombardment for surface treatment. Also, the cathode can be kept in a low power-on (idling) condition, by maintaining only a cathode/keeper discharge.

This work was done by Graeme Aston of Caltech for **NASA's Jet Propulsion Laboratory.** *For further information, Circle 101 on the TSP Request Card.*

Inquiries concerning rights for the commercial use of this invention should be addressed to the Patent Counsel, NASA Resident Office-JPL [see page A5]. Refer to NPO-15560.

Catalog of Spectral Lines

Submillimeter, millimeter, and microwave spectral lines are catalogued for selected molecules.

A report available on request describes a computer-accessible catalog of calculated and experimental spectral lines in the frequency range between zero and 300 GHz for selected molecules, including chlorine oxide, bromine oxide, nitric oxide, phosphine, and oxygen. The catalog, which is intended to serve as a reference guide in the identification and analysis of observed spectral lines, should interest atmospheric scientists, radio astronomers, and chemists. The catalog is constructed using theoretical least-squares fits and predictions based on spectral lines, mostly obtained from the literature.

This work was done by Robert L. Poynter and Herbert M. Pickett of Caltech for **NASA's Jet Propulsion Laboratory.** *To obtain a copy of the report, Circle 102 on the TSP Request Card.*
NPO-15181

Laser-Beam Separator

Four prisms are used to separate laser wavelengths.

A train of prisms and an optical stop separate the fundamental beam of a laser from second and higher order harmonics of the beam that are produced in certain crystals and by stimulated Raman scattering in gases and liquids. Such harmonics are generated from nonlinear processes occurring within the media and exit colinearly with the fundamental beam.

The optical train contains four prisms: the first for intercepting the beam and separating the fundamental beam from its harmonics by dispersion, the second for directing these harmonics to the optical stop, and the remaining two for steering the fundamental beam back onto its original path.

This work was done by Iain Stuart McDermid of Caltech for **NASA's Jet Propulsion Laboratory.** *For further information, Circle 103 on the TSP Request Card.*
NPO-15723

Measuring Delay in Lasers

The resolution of the instrumentation is about 5 picoseconds.

A technique measures the delay; i.e., response time of a modulated diode laser, as a function of temperature by comparing the excitation signal to the laser output signal with a vector voltmeter. The diode is contained in a temperature-regulated chamber. The voltmeter uses phase-locked coherent sampling at a rate that preserves the phase relationship, waveshape, and amplitude of the original laser signal. Vector addition of the reference and the output signals produces a signal that is representative of the delay. A delay is exhibited as a phase difference between the reference and the output vectors. The instrument is sensitive to changes in delay as small as 5 picoseconds.

This work was done by Larry A. Bergman and Sverre T. Eng of Caltech for **NASA's Jet Propulsion Laboratory.** *For further information, Circle 104 on the TSP Request Card.*
NPO-15242

Laser Diode Schlieren Photography

Laser diodes are used in Schlieren flow analysis.

Laser diodes may be preferable to conventional lasers or incandescent lamps for Schlieren flow analysis because they are smaller, more rugged, less costly, and have lower power requirements. In a prototype system at Langley Research Center, infrared light from a laser diode is collimated and directed at helium flowing over a model. The beam is then focused on a high-pass filter and the transmitted light recorded on infrared film. The filter is a photographic plate exposed by the diode beam without the model in place. The apparatus is alined visually with a phosphor screen that fluoresces in the presence of infrared light.

This work was done by John M. Franke and Alpheus W. Burner, Jr., of **Langley Research Center.** *No further documentation is available.*
LAR-12897

Improved Heat-Engine Solar-Energy System

A buffer loop and overcapacity heat exchanger is used.

A heat engine solar-energy system is improved by installing an overcapacity heat exchanger and a buffer loop between the engine fluid and the solar-heated fluid. The buffer-loop fluid is always in the liquid state. The previous design was inefficient because of its long flow path, which permitted conversion of the engine fluid to a vapor or gas. As a result of the improvement, the engine heat exchanger has low and nearly-constant flow resistance.

This work was done by David C. Miller of Caltech for **NASA's Jet Propulsion Laboratory.** *For further information, Circle 105 on the TSP Request Card.*
NPO-15762

Predicting Solar Deficits

Deviations from long-term averages are determined.

A statistical method uses available long-term solar irradiance data at selected sites in the United States to predict probable deviations from long-term monthly averages. The technique should be useful in sizing solar collectors and backup storage systems to cover solar deficits.

Statistically probable deviations are developed by computer analysis of available data for 10 years of hourly irradiance for each of the sites. Because irradiance deviations vary with time of year, the statistics are analyzed separately for six consecutive 60-day periods.

This work was done by Ronald G. Ross, Jr., and Charles C. Gonzalez of Caltech for **NASA's Jet Propulsion Laboratory.** *For further information, Circle 106 on the TSP Request Card.*
NPO-15667

Modeling of Solar Concentrators

Computer modeling helps optimize performance before building scale models.

An algorithm has been developed for predicting the power output, uniformity of intensity, and operating temperature of concentrator-enhanced photovoltaic

(continued on next page)

solar-cell arrays. Optimum values for parameters such as reflector geometry can be found prior to constructing scale models for testing.

A ray-trace routine determines the intensity of the solar radiation arriving at each cell. An iterative calculation determines the steady-state operating temperature. A solution is found that is consistent both with steady-state energy flow and the known relationship between cell temperature and efficiency. After the power output of each cell is determined, the output of the entire array is predicted by combining the individual cell outputs using the single-diode solar-cell model.

This work was done by Donald E. Rockey of Caltech for **NASA's Jet Propulsion Laboratory.** *For further information, Circle 107 on the TSP Request Card.*
NPO-15034

Saltless Solar Ponds

Honeycomb cover improves heat storage.

Several problems associated with heat storage in solar ponds are eliminated by a transparent insulating cover at the surface of the pond. The cover would make unnecessary the salt gradient that suppresses natural convection within the pond to promote thermal storage.

The transparent cover consists of air-filled plastic cells arranged in a honeycomb configuration. In addition to suppressing natural convection, the cover enhances transmission of solar energy into the fluid, reduces conductive heat losses, and retards reradiation of infrared energy to the atmosphere.

This work was done by Edward I. H. Lin of Caltech for **NASA's Jet Propulsion Laboratory.** *For further information, Circle 108 on the TSP Request Card.*

Inquiries concerning rights for the commercial use of this invention should be addressed to the Patent Counsel, NASA Resident Office-JPL *[see page A5].* *Refer to NPO-15808*

Parabolic Solar Collectors

Tutorial document reviews technology for nonspecialists.

A paper presents a tutorial overview of point-focusing parabolic reflectors for solar-energy collectors. The optical and thermal characteristics of such collectors are discussed in detail. Data representing typical collector efficiencies are presented, and the importance of balancing collector cost with concentrator quality is argued through the development of a figure-of-merit for the collector. The impact of receiver performance is assessed, and the general observation is made that temperatures much in excess 1,500° to 2,000° F (815° to 1,095° C) can actually result in decreased performance.

Various types of two-axis-tracking collectors are described, as are two forms of fixed-mirror collectors with articulating receivers. The present Department of Energy program to develop these devices is briefly discussed. Finally, present and projected costs of these collectors are considered. Price information is presented for a commercial unit.

This work was done by Vincent C. Truscello of Caltech for **NASA's Jet Propulsion Laboratory.** *For further information, Circle 125 on the TSP Request Card.*
NPO-15674

High-Temperature Helical-Tube Solar Receiver

A gas is heated in a thin-walled sintered silicon nitride tube.

A solar-thermal receiver is proposed for use with a circular parabolic concentrator to supply about 58 kW thermal power to a Brayton engine or an industrial process. The solar radiation would be focused into the open end of a cylindrical ceramic thermal inertial sleeve 8 in. (20 cm) in diameter that reradiates the energy to a helical heat-exchanger tube surrounding the sleeve. Air flowing through the tube [0.11 kg/s at a pressure of 3.2 atmospheres (3.24×10^5 N/m^2)] would be heated from 1,750° to 2,500° F (954° to 1,371° C). Rigidized fiber insulation would support the heat exchanger. The helical tube could be produced from sintered silicon nitride.

This work was done by C. S. Robertson, Jr., and L. R. McCreight of General Electric Co. for **NASA's Jet Propulsion Laboratory.** *For further information, Circle 126 on the TSP Request Card.*
NPO-15768

Concentrator-Enhanced Solar Array

Deployable reflectors increase power-to-mass ratio of GaAs solar panel by 42 percent.

A proposed deployable solar array for satellites uses slanted low-mass planar mirrors as walls of a trough to triple the light falling on GaAs solar cells forming the bottom of the trough. The power-to-mass ratio of the new design is 42 percent higher than that of a planar array of the same power output.

Before deployment, both the solar array and the 1/3-mil (0.008-mm) polyimide mirrors are stored on rollers attached to one of two folded support booms. The booms unfold and form two flat-bottomed V's, which then spread apart, unrolling the mirrors and solar arrays to form the trough.

This work was done by Brian J. Morse of Hughes Aircraft Co. for **NASA's Jet Propulsion Laboratory.** *For further information, Circle 127 on the TSP Request Card.*
NPO-15628

Efficiency of Reflection Gratings

Dichromated gelatin plates are evaluated as optical elements for phase-volume holography.

A report describing experiments on dichromated gelatin reflection gratings is available on request. Dichromated gelatin reflection gratings were prepared and their efficiencies measured by established methods. The experimental results agree with theory in showing a sharp drop in diffraction efficiency with angular deviation from Bragg's angle. The curve is flattened by increasing the index of modulation, accomplished through control of dichromate content and energy of exposure. Efficiencies greater than 90 percent are possible, but the field of view is restricted to around 10°.

This work was done by Chungte W. Chen and James C. Wyant of the University of Arizona for **NASA's Jet Propulsion Laboratory.** *For further information, Circle 128 on the TSP Request Card.*
NPO-15852

Materials

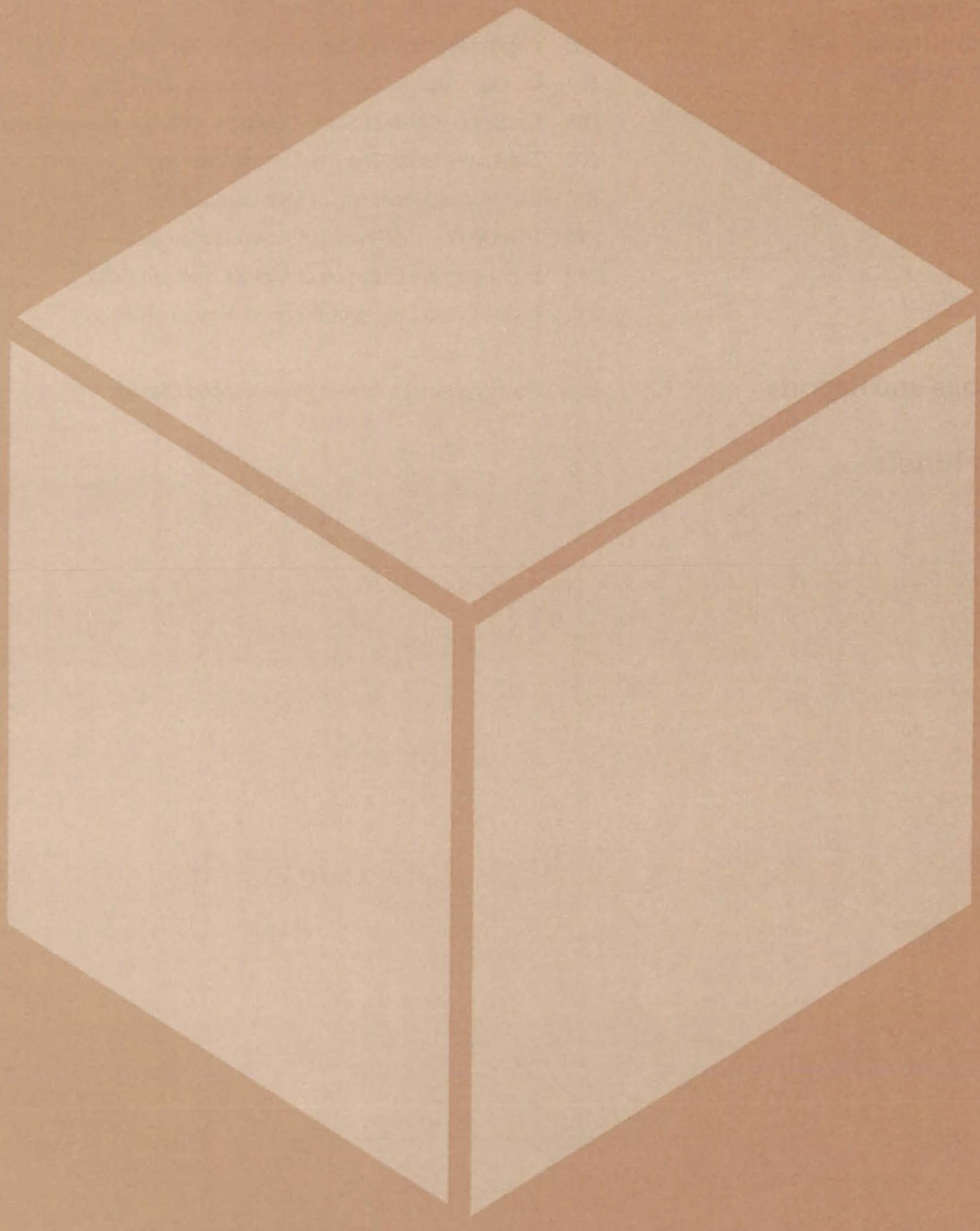

Hardware, Techniques, and Processes

205 Recovering Zinc From Discarded Tires
206 Packed Alumina Absorbs Hypergolic Vapors
207 Containerless Solidification of Amorphous Metals
208 Oxidation-Resistant Slurry Coating for Carbon-Based Materials
209 Two-Layer Glass Thermal-Control Coating
210 Continuous Monitoring of Melt Composition
211 Low-Density High-Strength Foamed Materials
212 Estimating the Lifetimes of Nickel/Cadmium Cells
213 In Situ Cross-Linking of Polyvinyl Alcohol Films

Books and Reports

214 Containerless Processing of Advanced Glasses

MiniBriefs

215

Recovering Zinc From Discarded Tires

Zinc sulfate monohydrate would be sold at a profit.

NASA's Jet Propulsion Laboratory, Pasadena, California

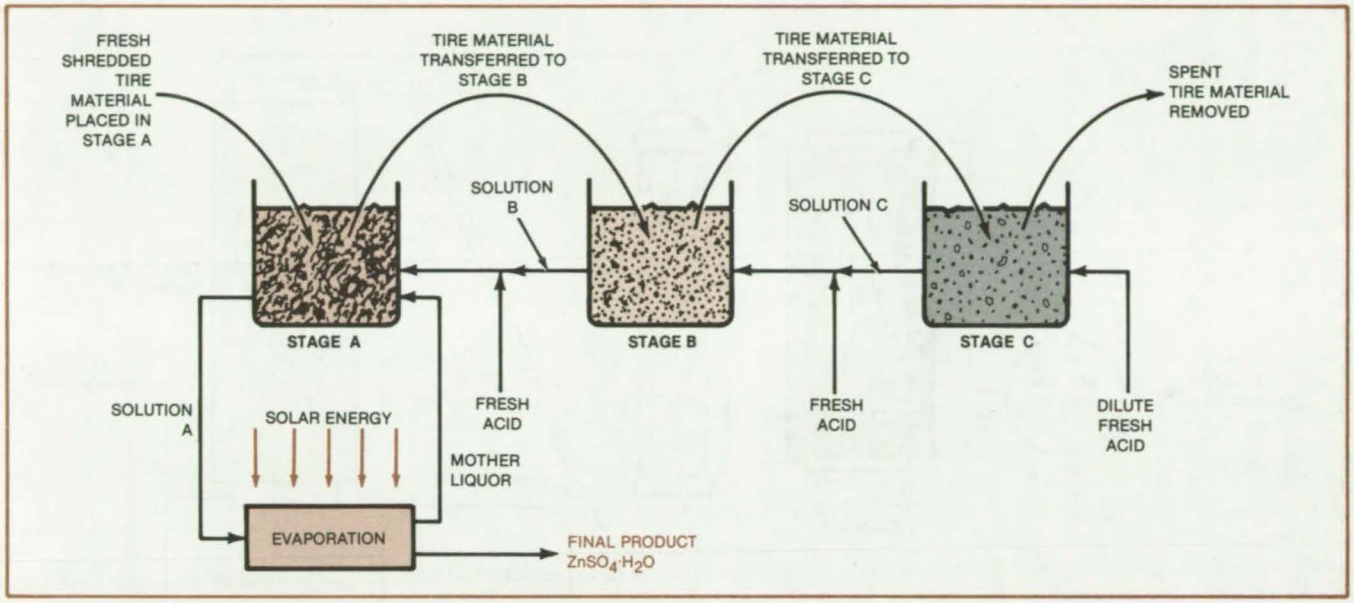

Shredded Tire Material Is Steeped in three sulfuric acid baths to extract the zinc. The final product, $ZnSO_4 \cdot H_2O$, is removed by evaporating part of solution A until the product crystallizes out.

A countercurrent batch chemical process has been suggested for the extraction of zinc from discarded tires. The zinc (incorporated as zinc oxide in tire treads) would be recovered as $ZnSO_4 \cdot H_2O$, which can be sold as a fertilizer or for general use.

A strong acid is required to break up the ZnS that forms in the tire by the reaction of colloidal ZnO with sulfur. In the proposed recovery process, sulfuric acid would be used in three different concentrations (see figure). First, the tires would be shredded and the resulting material placed in solution A (the most concentrated). After steeping in solution A, the material would be steeped in solution B (of intermediate concentration) and then in solution C (the most dilute).

At each stage the acid content must exceed the zinc content anticipated at the end of steeping in order to have a chemical driving force for the extraction. The chemical cost is dictated by the amount of excess. When the solution of the last stage (solution C) is as dilute as practicable, a minimum of acid and zinc will be irretrievably discarded with the rubber: This maximizes zinc recovery and minimizes the cost of makeup acid.

When the rubber is transferred to the next, more dilute solution, it carries some of the more concentrated acid and zinc extract with it, thus enriching the solution of the next stage. To prevent the gradual enrichment of solution C, some of this solution is transferred at intervals to stage B while fresh dilute acid is added. Similarly, the enrichment of solution B is prevented by transferring some of it to stage A, while a portion of solution C is transferred in along with some fresh acid.

Some of solution A is removed for final product extraction and replaced by the portion of solution transferred from stage B plus some fresh acid. The removed portion of solution A is concentrated by solar-assisted evaporation. The evaporation continues until $ZnSO_4 \cdot H_2O$ crystallizes out, leaving excess acid and some zinc extract in the mother liquor. The zinc sulfate is removed and sold, while the mother liquor is diluted and recycled to solution A with fresh acid. Such a crystallization process is now used in the manufacture of zinc sulfate.

Depending on the grade of $ZnSO_4 \cdot H_2O$, the product could be sold for 50¢ to 75¢ per lb ($1.10 to $1.65 per kg), 1980 prices. The cost of recovery has been estimated at 5.7¢ to 7.7¢ per lb (12.6¢ to 17.0¢ per kg) of Zn. This estimate is, however, based on the assumption that some other end use will pay for most or all of the cost of shredding the tires. The cost of shredding would otherwise make the recovery of zinc uneconomical. Suitable uses for the extracted shredded tires would include incorporation in asphalt topping for road surfaces and pyrolysis to produce motor fuel and coke.

This work was done by Eugene R. du Fresne of Caltech for **NASA's Jet Propulsion Laboratory.** *For further information, Circle 28 on the TSP Request Card.*
NPO-16046

Packed Alumina Absorbs Hypergolic Vapors

Activated alumina particles act as filters.

John F. Kennedy Space Center, Florida

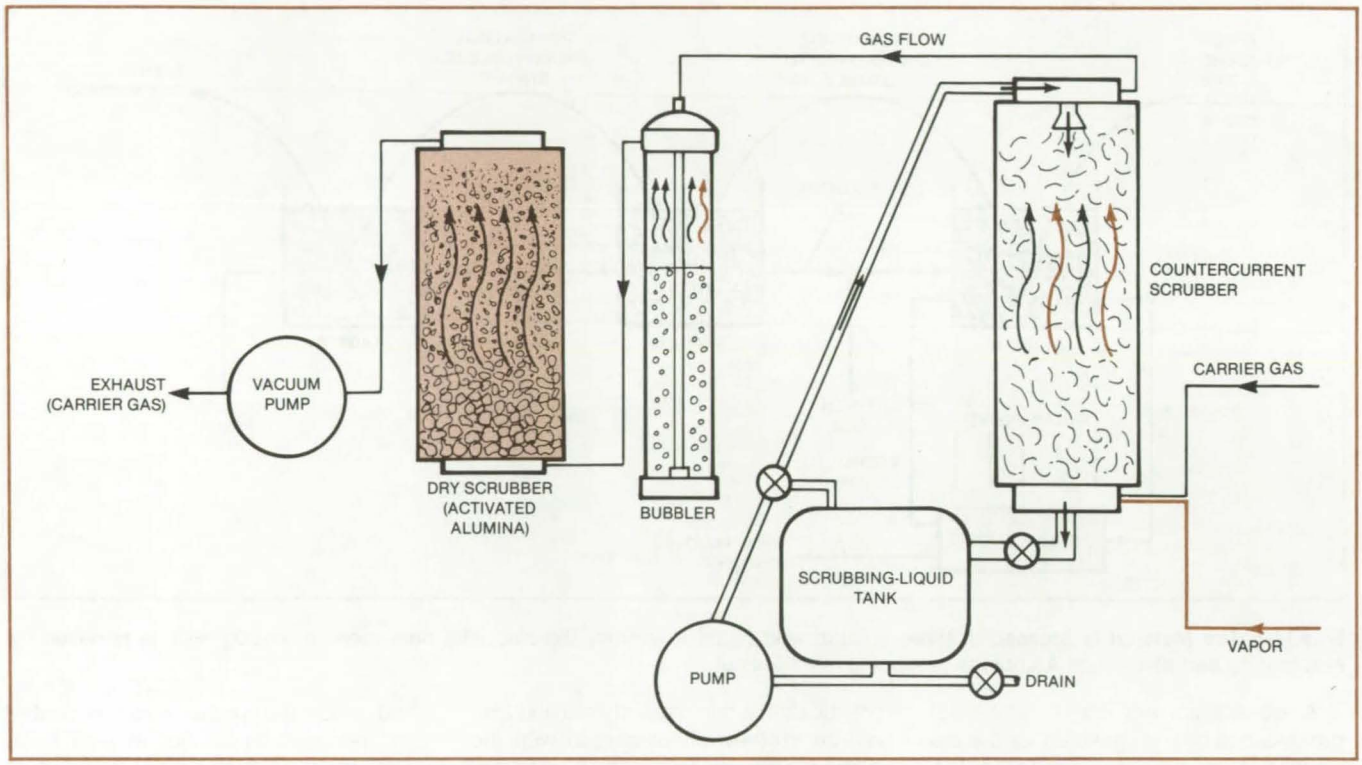

An Effective Removal System for N_2H_4 and N_2O_4 vapors consists of a scrubber, a bubbler, and an activated alumina bed in series. The bed eliminates most of the vapors remaining after the wet treatments.

Beds of activated alumina have been found effective as filters to remove hypergolic vapors from gas streams. The beds absorb such substances as nitrogen oxides and hydrazines. They may also absorb acetylene, ethylene, hydrogen sulfide, benzene, butadiene, butene, styrene, toluene, and xylene.

Purification by activated alumina particles offers many advantages. The bed has no moving parts, such as pumps, blowers, and mixers, and is therefore reliable and energy-conservative. Activated alumina is inexpensive, nontoxic, and easy to handle. The bed can be readily adapted to any size, from small portable units for use where little vapor release is expected to large stationary units for extensive transfer operations.

The alumina-bed method was developed to eliminate poisonous vapor discharges that occur when hypergolic fuels and oxidizers for the Space Shuttle are transferred. Air laden with the vapors is passed through conventional countercurrent wet scrubbers and bubblers, but some of the harmful materials remain. A packed bed of activated alumina was found to remove most of the remaining vapors (see figure).

The fuel (for example, hydrazine, N_2H_4) and the oxidizer (dinitrogen tetroxide, N_2O_4) must be treated differently. Activated alumina can be used as delivered to absorb oxidizer vapor. However, the activated alumina is first soaked in sulfuric acid before it is used to treat fuel vapor, which requires an acidic medium.

Laboratory tests were performed with a clear acrylic tower, 22 inches (56 cm) high and 3.5 inches (8.9 cm) in diameter, containing 9.6 pounds (4.4 kg) of activated alumina. The alumina particles ranged in size from 0.5 inch (13 mm) at the bottom to a coarse powder at the top. Helium bearing the fuel or oxidizer vapors flowed through the tower at a rate of 5.4 liters per minute.

In the tests, the average efficiency of fuel removal was 72 percent for inlet concentrations from 1 to 100 ppm. Oxidizer-removal efficiency was 45 percent for inlet concentrations ranging from 3 to 1,194 ppm.

The absorption capacity of the bed for N_2O_4 oxidizer is at least 0.0007 lb per pound (0.7 g per kilogram) of bed material. The oxidizer-absorption bed can be regenerated in place by washing with a dilute sodium hydroxide solution.

The ability of the bed to absorb fuel decreases gradually rather than sharply as in oxidizer absorption. The fuel-absorption bed can be rejuvenated by washing with sodium hypochlorite solution. The hydrochloric acid thus generated restores the acidity needed for fuel absorption.

This work was done by John J. Thomas and David M. Mauro of Florida Institute of Technology for **Kennedy Space Center.** *For further information, Circle 29 on the TSP Request Card.*

Inquiries concerning rights for the commercial use of this invention should be addressed to the Patent Counsel, Kennedy Space Center [see page A5]. *Refer to KSC-11278.*

Containerless Solidification of Amorphous Metals

A proposed method could produce large amorphous alloys.

NASA's Jet Propulsion Laboratory, Pasadena, California

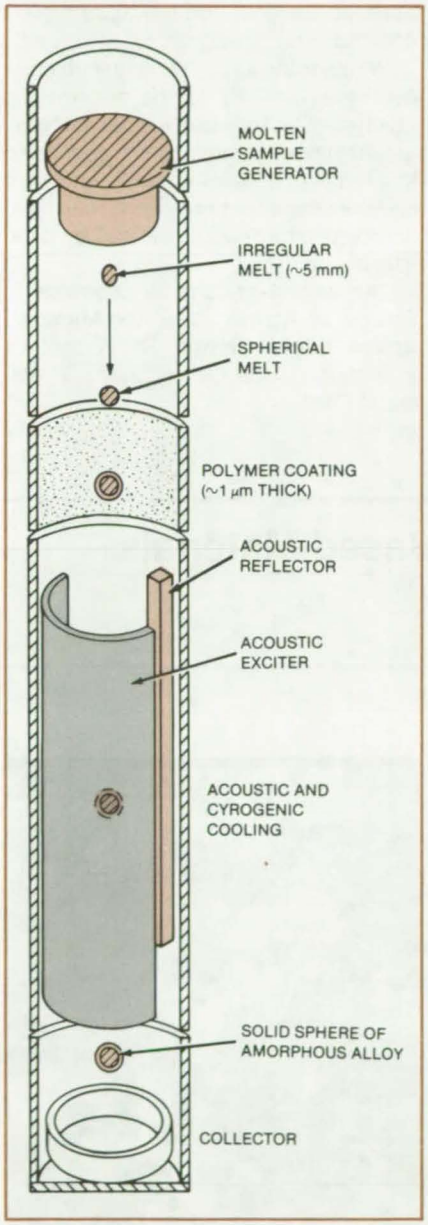

Spheres of Amorphous Metal Alloys are formed and collected after molten samples are coated and cooled in a drop tube. The coated spheres are cooled acoustically and cryogenically.

In a proposed containerless method of producing amorphous metals, spheres of the molten metal fall through a drop tube, are coated with a polymer, and then the composite is cooled both cryogenically and by an acoustically-excited jetstream before being collected at the bottom of the drop tube. The containerless melting and the polymer coating minimize nucleation at the surface of the melt. Amorphous specimens 5 mm in diameter or larger are possible.

The method for producing amorphous alloys is shown in the figure. The sample of ultrapure alloy leaves the generator and assumes a spherical shape before being coated by plasma deposition. Since most polymer coatings vaporize above 400° C, the method currently would be limited to amorphous alloys that melt at low temperatures.

The coated sphere then enters the acoustic cooling region to solidify and form an amorphous alloy. The primary coolant is helium gas at the temperature of liquid nitrogen. Additional cooling is provided by a focused acoustic field that creates jetstreams in the atmosphere surrounding the falling molten drop. [The concept of cooling with acoustically induced jetstreams is described in the article "Producing Metallic Glasses With Acoustic Levitation" (NPO-15658) on page 472 of Vol. 7, No. 4 of *NASA Tech Briefs*.] To accommodate drop-tube geometries, the acoustic-levitation cooling section is a half cylinder with a reflector strip at a focal line.

This work was done by Mark C. Lee and William L. Johnson of Caltech for **NASA's Jet Propulsion Laboratory.** *For further information, Circle 30 on the TSP Request Card.*
NPO-15776

Positioning Vise for Crystal Cleavage

A vise manipulates brittle crystals, such as lithium fluoride, so that they are in the proper position for cleavage. The vise allows crystals as thin as 2 millimeters or less to be positioned so that they can be cleaved without breakage. Previously, the crystal had to be carefully measured, clamped in a jig, and painstakingly centered under a cleaving blade by an operator. In the new vise, the jaws are fitted with ball bushings that ride on guide rods. The guide rods support the jaws and maintain the crystal or other workpiece in an alinement. The bushings reduce both starting friction and sliding friction so that the operator always has a good tactile sense of the forces on the jaws.
(See page 282.)

Fabrication of Multi-Ply Birefringent Fibrous Composite Laminates

A fabrication method produces unidirectional, multi-ply, transparent birefrigent fibrous composite laminates for use in macromechanical stress analysis anisotropic photoelasticity. The new laminates are glass-fiber-reinforced plastics for which the matrix and fibers have the same index of refraction. Such transparent fibrous composites can be made to simulate anisotropy of opaque fibrous composites, such as boron/epoxy, graphite/epoxy, and others. Before this development, the material for anisotropic photoelastic studies had not been readily available. Existing fabrication techniques produced materials with limitations in mechanical and optical properties.
(See page 284.)

Charring, Nonmelting Epoxy Foams

The addition of some vanadium compounds prevents melting.

Marshall Space Flight Center, Alabama

For safety, a structural plastic foam should turn into a rigid char when it burns, without melting. The addition of small amounts of vanadium compounds to some epoxy resins has been found to promote such char formation.

Normally, when epoxy foams are exposed to high heat fluxes or flames, they melt before they char. Chopped fibers of asbestos can be added to foams to increase their melt resistance. Fiber additives, however, increase the weight of a foam. Alternatively, high-temperature-curing resins can be used. However, these resins must be cured in an oven, and the maximum size of a foam part is limited by the size of the available oven.

Cured epoxy foam samples were treated with methylene chloride solutions of vanadium acetylacetonate, vanadyl acetylacetonate, and vanadium trisacetylacetonate. In each case, about 2 percent by weight of the vanadium compound was added to the foam sample. When solvent was removed from the blocks of foam, much of the additive bled back to the top surface. The first two additives did not change the response of the foam to a propane torch: The foam melted. However, the latter two additives inhibited melting, and the foam merely charred under the torch.

Whether the action of vanadium compounds is specific to the epoxy resin used in the test or whether specific types of vanadium compounds are applicable to a range of epoxies is not yet known. It is known that the change from melting to nonmelting behavior is caused by catalytic action.

This work was done by Chadwick B. Delano of Acurex Corp. for **Marshall Space Flight Center.** *For further information, Circle 31 on the TSP Request Card.*
MFS-25911

Oxidation-Resistant Slurry Coating for Carbon-Based Materials

New process uses a paint sprayer and vacuum furnace to produce a silicon carbide outer layer.

Lewis Research Center, Cleveland, Ohio

Carbon-based materials, such as graphite or carbon/carbon composites, are very lightweight, possess excellent mechanical properties at high temperatures [2,200° to 3,300° F (1,200° to 1,800° C)], and are resistant to thermal shock. However, above about 900° F (480° C), these materials oxidize rapidly unless they are coated with oxidation-resistant materials. Most commercially available coatings are based on chemical-vapor deposition (CVD) processes, which require specialized equipment to produce a silicon carbide (SiC) outer layer.

The process described here also produces an oxidation-resistant SiC outer layer; but it may be produced more easily, using only a paint sprayer and a conventional vacuum furnace. Fine nickel and silicon powders are blended in proper proportions, mixed with nitrocellulose lacquer, and sprayed on the graphite parts to be coated. The coatings are air-dried and vacuum-fused at

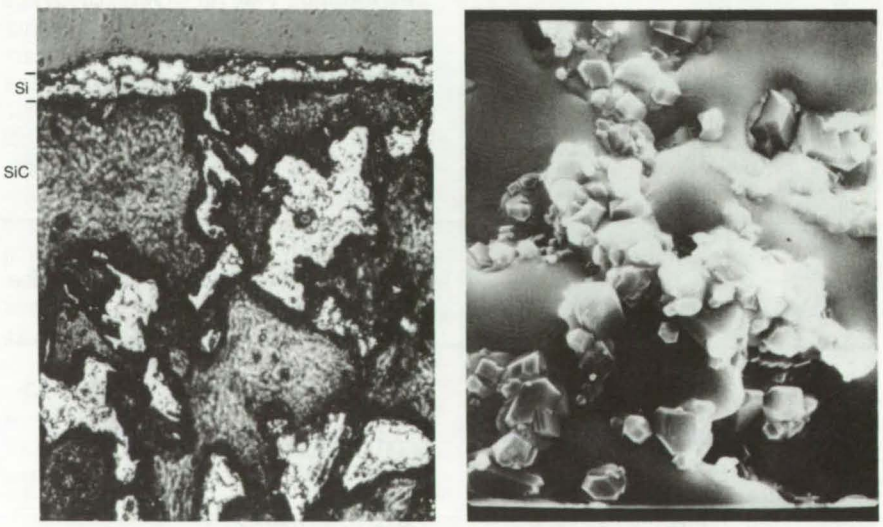

The **Microstructure of a Fused Nickel and Silicon Slurry Coating** on a graphite substrate is shown here. In the cross section (magnified 500×) of a silicon and silicon carbide reaction zone (a), a top layer of silicon adheres to the silicon carbide layer. In (b), crystals are prominent on the melted top surface (magnified 3,000×) of a slurry coating.

temperatures near 2,400° F (1,300° C). The resultant coatings wet the graphite, penetrate any open porosity, and produce a SiC reaction zone. A top surface of silicon (see figure), which has a metallic luster may also exist. Upon exposure to air at high temperature, the Si + SiC coating protects the graphite part from catastrophic oxidation by forming an impervious slow-growing silicon dioxide (SiO_2) surface scale.

Preliminary 2,200° F cyclic oxidation tests showed that the coatings themselves are very oxidation resistant and protected the graphite for about 5 to 10 hours. Uncoated graphite by comparison was totally consumed by oxidation after only 5 hours at 2,200° F. However, localized coating infiltration of the excessive porosity in the graphite resulted in premature oxidation of the substrate. Use of less-porous carbon/carbon composite substrates will produce more protective coatings.

It is expected that these materials and coatings could find application in areas where short exposures to high-temperature oxidative gases are experienced. The fused-slurry process offers some flexibility over conventional CVD processing in terms of coating composition and localized application. The process may be especially useful in coating repair.

This work was done by James L. Smialek of **Lewis Research Center.** *For further information, Circle 32 on the TSP Request Card.*

Inquiries concerning rights for the commercial use of this invention should be addressed to the Patent Counsel, Lewis Research Center [see page A5]. *Refer to LEW-13951.*

Two-Layer Glass Thermal-Control Coating

Optical properties endure at high temperatures.

Ames Research Center, Moffett Field, California

New all-glass thermal-control coatings withstand repeated exposure to temperatures as high as 2,000° F (1,093° C) with only minimal degradation of optical properties. In contrast, older formulations contain organic binders that degrade above 500° to 600° F (260° to 316° C). The coating helps to prevent excessive solar heating of spacecraft or other objects at moderate operating temperatures, typically room temperature to 150° F (66° C). It also radiates heat away during convective heating at typical spacecraft reentry temperatures around 1,200° F (649° C). The new coating may have industrial uses in solar-energy equipment, some high-temperature chemical processing systems, laboratory equipment, and high-temperature instrumentation.

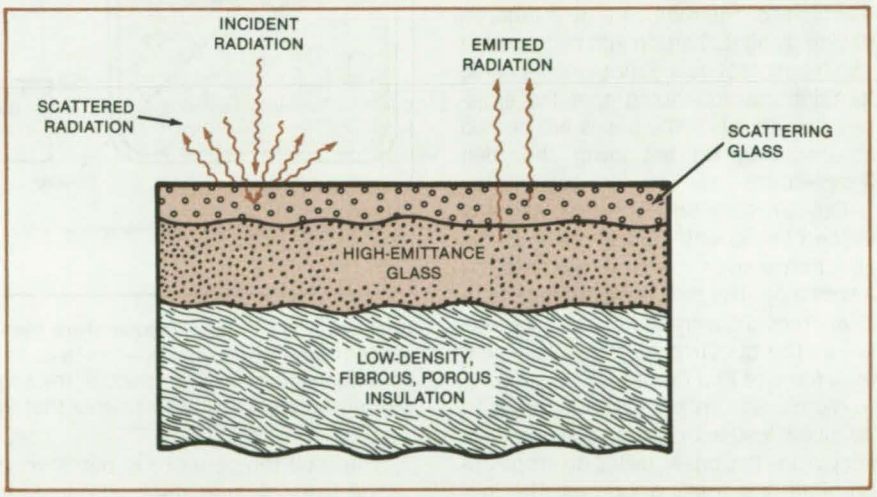

The Glass Thermal-Control Coating has an outer scattering layer and an inner high-emissivity layer. The absorptivity/emissivity ratio is less than 0.4. The coating can withstand repeated exposure to temperatures in excess of 2,000° F (1,093° C).

As shown in the figure, the coating is applied in two layers to a tile of low-density, fibrous, porous insulation. The inner layer, 0.3 to 0.45 mm thick, has high emissivity for cooling the surface by radiation. It is a frit made from a reactive borosilicate glass, an emittance agent such as silicon tetraboride, and a flux glass.

The outer layer is 0.013 to 0.13 mm thick, depending on optical requirements. It must scatter incoming solar radiation but be as transparent as possible to the predominantly-longer-wavelength thermal radiation emitted by the inner layer. It is a sintered high-silica glass containing particles of 1- to 4-mm size. The particles scatter radiation at wavelengths of 0.35 to 2.3 μm while permitting longer wavelengths to pass. The high silica content also gives this layer a low thermal-expansion coefficient that helps to minimize the generation of residual thermal stresses during fabrication.

The coating layers are prepared as water/alcohol slurries and sprayed in turn onto the fibrous insulating tile. After drying for a few hours at or slightly above room temperature, the coated tile is glazed in a furnace for 1 to 2 hours at 1,092° to 1,231° C. Because of the particular combination of thermal-expansion coefficients of the layers, the residual thermal stress is minimized by inserting the tile when the furnace is at the glazing temperature and rapidly removing the tile at the end of the glazing period.

Coatings of the new type have a ratio of absorptivity to emissivity of ≤ 0.4 at room temperature and a total hemispheric emissivity of 0.8 or greater at

(continued on next page)

1,200° F (649° C). Even after 100 cycles of heating to 2,300° F (1,260° C), one such coating still had an emissivity of 0.88, only sightly less than the original value of 0.92.

This work was done by David A. Stewart and Howard E. Goldstein of **Ames Research Center** *and Daniel B. Leiser of Stanford University. For further information, Circle 33 on the TSP Request Card.*

This invention has been patented by NASA (U.S. Patent No. 4,381,333). Inquiries concerning nonexclusive or exclusive license for its commercial development should be addressed to the Patent Counsel, Ames Research Center [see page A5]. Refer to ARC-11164.

Continuous Monitoring of Melt Composition

Compositions of glasses and alloys may be analyzed and corrected in real time.

NASA's Jet Propulsion Laboratory, Pasadena, California

A proposed spectrometer would determine the composition of molten materials. The instrument could be used to monitor molten glasses and metals to control manufacturing processes.

According to the concept (see figure), a plasma is created at the surface of the melt by a high-power laser beam or an electric arc. The melt surface is cleared of slag by a jet of argon and hydrogen, a combination of gases that inhibits oxide formation (which would alter the emissivity of the melt). The gases are heated so that they do not lower the melt temperature.

Optical radiation from the plasma is carried to the entry slit of an emission spectrometer or spectrophotometer by a light pipe. The pipe is made of a clear, heat-compatible material, such as sapphire. The spectrometer is outside the melt furnace in a protective housing.

Atomic absorption spectroscopy can be used instead of emission spectroscopy. In this case, radiation from appropriate line-emitting sources is led into the furnace, traverses the gas or plasma generated from the melt, and is conducted to a spectrograph by the light pipe.

The spectra produced by the emission or absorption instrument are processed by a computer. The computer sends instructions to an operator or automatic controller for modification of the melt as necessary.

The radiation delivered by the pipe to the spectrometer is a combination of the blackbody thermal radiation of the melt and the line-emission spectrum of the excited plasma that characterizes the composition of the melt. Both components are needed for useful results. The blackbody radiation is always present; the line spectrum is present only when the plasma is excited by a pulse generator.

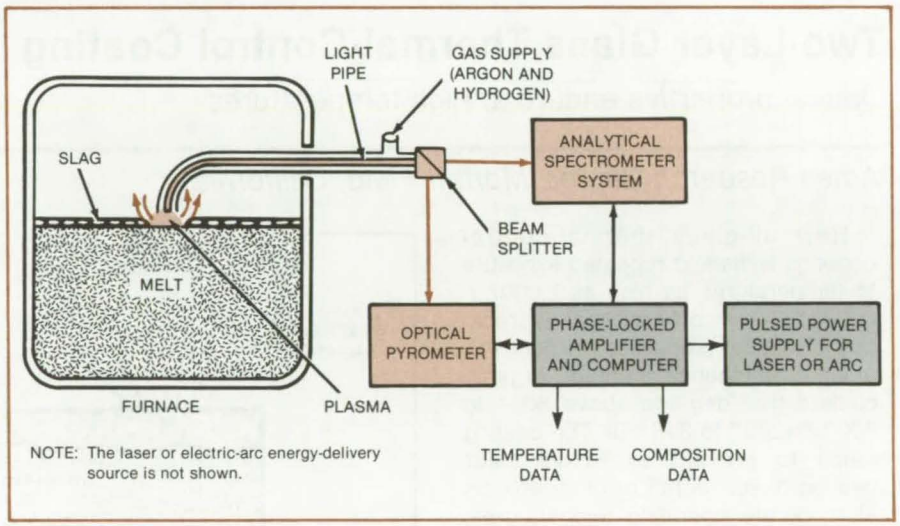

Spectral Analysis and Temperature Measurement are performed simultaneously on a molten material in a container, such as an open-hearth furnace, a crucible, or the tank of a continuous furnace. The speed of the analysis makes it possible to quickly measure the concentration of volatile elements that might be depleted by prolonged heating.

The melt temperature is determined at the same time as the melt contents. The spectrometer has a line of light sensors at its exit slit. When the plasma is unexcited, the image on the line of picture elements is that of a blackbody, the temperature of which is derived from the ratio of the signal strength at 2 wavelengths. The blackbody spectrum and the temperature calculated therefrom are stored in the computer memory.

When the plasma is energized, the additional energy impinging on the picture elements is attributable to the line emission from the components of the melt in the plasma. The plasma is excited in a pulsed mode phase-locked to the sensor for time sharing background and emission spectra. The computer subtracts the previously-stored blackbody data from the total plasma spectral data to obtain the emission spectrum.

The computer converts the radiant flux at several wavelengths, as detected by the picture elements, into an analysis of the melt. Since the spectrum for the desired melt is stored in memory, the computer can calculate the additions necessary to bring the melt composition within specifications.

The melt temperature could also be determined independently by an optical pyrometer viewing the melt. The pyrometer sends a temperature signal to the computer. The computer corrects the signal for emissivity and generates a control signal for raising, maintaining, or lowering the melt temperature as necessary.

This work was done by Robert E. Frazer and Thomas W. Andrews of Caltech for **NASA's Jet Propulsion Laboratory.** *For further information, Circle 34 on the TSP Request Card.*
NPO-15896

Low-Density High-Strength Foamed Materials

Strong, lightweight materials are made from bubbles of metal or plastic.

NASA's Jet Propulsion Laboratory, Pasadena, California

Molten bubbles of metal or plastic coalesce into strong, lightweight materials that look like solidified foam. The materials can be used for construction and can be extruded into molds, sawed, nailed, and generally handled as wood.

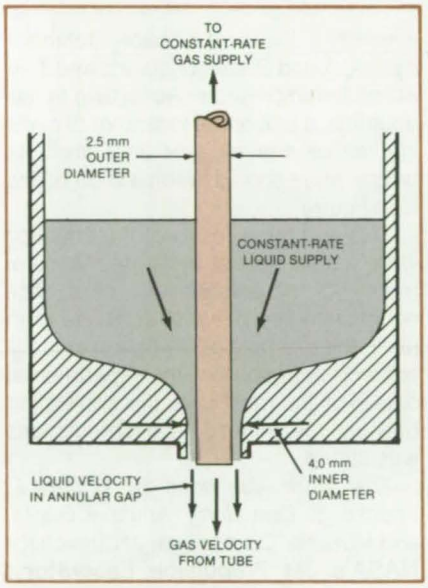

Figure 1. The **Inner Tube** of the bubble generator nozzle feeds the gas at the desired pressure. To form a 7-mm bubble, for example, from molten tin, the gas velocity is between 1.5 and 4.0 m/s, and the tin flows at 1.0 m/s through the annular gap.

The bubbles are formed in a compartment that receives the molten material and the compressed gas that fills the bubbles. The compartment has a matrix of nozzles. The matrix can be almost any dimension, and the nozzles are sized for the desired material density or bubble size. After leaving the nozzles, the bubbles fall into an acoustic chamber, where they coalesce. They then drop through a funnel and are cast into the desired shape by extrusion or molding.

The outer shell of each nozzle (see Figure 1) is a container, which holds the liquefied material, with a 4-mm opening at the bottom. A tube 2.5 mm in diameter, which feeds the gas for the bubbles, passes through the container along its axis and extends through the opening. The amount that the tube protrudes out of the container depends on the viscosity of the liquefied material and the velocity of the gas from the tube.

Metallic bubbles are kept in a semi-molten state while they are extruded or molded inside an oven. For plastics, such as epoxies and polymers, no oven is needed, and the coalescing is assisted by chemical interaction or electrostatic attraction.

The foamed materials have very high strength-to-weight ratios and have uniform elastic moduli throughout because of the uniformity of the spheres produced by precision nozzles. The density of the material is controlled by the bubble size, which can range between 0.5 mm and 1 cm in diameter and can be controlled within 1 percent. The bubbles can be formed with an internal gas pressure of over 2,000 psi (13.8×10^6 N/m^2); any compatible gas can be used. The high internal pressure further increases the strength-to-weight ratio.

The process can tailor materials for different end uses by varying the combinations of gases, gas pressures, and base materials. For example, an aluminum base material with carbon dioxide gas bubbles could be molded for fabrication into flame-resistant fuel tanks. The density can be controlled so that castings can be made for such products as aluminum engine blocks, instrument frames, and packaging spacers. Figure 2 lists the base materials, bubble sizes, and gases that can be used in combination for different applications.

This work was done by Taylor Wang, Dan Elleman, and James M. Kendall, Jr., of Caltech for **NASA's Jet Propulsion Laboratory.** *For further information, Circle 35 on the TSP Request Card.*

Inquiries concerning rights for the commercial use of this invention should be addressed to the Patent Counsel, NASA Resident Office-JPL [see page A5]. Refer to NPO-15411.

BASE MATERIAL	SHELL SIZE	GAS	GAS PRESSURE	PROPERTIES	APPLICATIONS
Aluminum	0.5 cm	Air	Atmospheric	Strong, Lightweight, Weatherproof	2 by 4's and Similar Construction Modules and Beams
	1.0 mm	Air	1,000 psi (6.9×10^6 N/m^2)	Dense, Lightweight	Engine Blocks and Castings
	1.0 cm	Carbon Dioxide	2,000 psi (13.8×10^6 N/m^2)	Flame-Resistant	Fuel Tanks and Baffles
	1.0 cm	Air	1,000 psi	Strong, Lightweight	Aircraft Structures and Wings
	0.5 mm to 1.0 cm	Inert Gases	Atmospheric to 2,000 psi	Containment for Gases and Aerosols	Storage for Gases and Aerosols
Epoxy	1.0 cm	Air	Atmospheric	Lightweight	Packing Materials and Moldings
Polyethylene	1.0 cm	Air or Carbon Dioxide	Atmospheric	Flexible, Buoyant, High Tensile Strength	Flame-Resistant Electrical Insulation and Packing Material
Tin	0.5 to 1.0 cm	Exotic Gases (Deuterium-Tritium)	To 2,000 psi	Lightweight	Storage Medium

Figure 2. The **Properties and Applications** of some combinations of base materials, gases, and bubble sizes are listed. All the foamed materials are lightweight and strong, with a density that depends on the bubble size.

Estimating the Lifetimes of Nickel/Cadmium Cells

The equation is based on a model of flaw growth.

NASA's Jet Propulsion Laboratory, Pasadena, California

An equation has been developed for estimating the life expectancy of sealed nickel/cadmium electrochemical cells. The equation relates the depth of charge and discharge, temperature, charge and discharge rates, and the number of cycles to failure.

The equation is based on a model in which it is assumed that a cell fails by the growth of preexisting flaws. Flaws are described by three important quantities: total number of flaws, the distribution of flaw sizes, and the rate of flaw growth. When the flaw reaches a critical size, failure occurs.

The flaw concept has had a long and successful history in the formulation of failure models. For example, it has been invoked to explain why the strength of metal is so much less than that calculated for a perfect specimen. The measured tensile strength of a metal is 100 to 1,000 times less than theory predicts. It is therefore assumed that there are always flaws in specimens that weaken them. The flaw concept, in addition to providing a ready explanation for reduced lifetime, predicts two important characteristics: statistical variability of lifetime data and the dependence of lifetime on the volume of a sample.

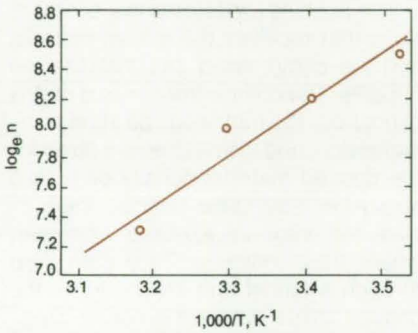

Measured (Dots) and Predicted (Line) logarithms of cell life for a particular test series are plotted as a function of the reciprocal of the absolute temperature.

The model provides insight into the nature of flaw growth in electrochemical cells. It shows that the calculated value of activation energy is appropriate for a diffusive or transport process of growth but is too low for a chemical reaction. It also shows that the change of flaw size is almost exclusively a function of the number of charge/discharge cycles and not of cycle time.

The equation can be written in its full complexity with all variables and constants or in a simplified form. As an example of the simplified form, the effect of temperature on a particular type of cell (assuming all other conditions to be held constant) is expressed by

$$n = Ae^{-B/T}$$

where n = the most probable lifetime in cycles, A and B are constants, and T = absolute temperature. According to this equation, a plot of the logarithm of cycle life versus the reciprocal of absolute temperature should fall on a straight line (see figure).

This and other forms of the equation were tested against cycle-life measurements of nickel/cadmium cells. The equations were put in straight-line form (as in the example of the figure) to facilitate comparisons with experimental data. For the most part, the correlation between measured data and predictions was strong.

This work was done by Robert F. Fedors, Su-Don Hong, Amitava Gupta, and Muzaffer Cizmecioglu of Caltech for **NASA's Jet Propulsion Laboratory.** *For further information, Circle 36 on the TSP Request Card.*
NPO-15145

Fire-Resistant TFE Extrusions

A new wetting agent improves product quality while it reduces flammability.

Marshall Space Flight Center, Alabama

The fire resistance of extruded tetrafluoroethylene (TFE) polymers can be improved by the substitution of a chlorinated hydrocarbon as the wetting agent. TFE-insulated wire and cable and TFE tubing, tape, and forms can benefit by the substitution.

In the conventional manufacturing process, an aliphatic petroleum hydrocarbon (naphtha) is routinely used to wet the TFE resin powder when it is formed into billets for ram extrusion. After extrusion, the polymer is heated to a temperature of 200° to 575° F (93° to 302° C) to evaporate the wetting agent. However, sometimes evaporation is incomplete: Entrapped fluids and gases then form pinholes in the insulation to escape or, worse, remain as flammable contamination. The finished product may then ignite at a low temperature and may support flames by releasing the entrapped gas or volatile liquid.

Replacement of the naphtha with perchloroethylene yields a polymer that extrudes well and generates fewer pinholes. More important, since perchloroethylene is not flammable, the product is less susceptible to fire during manufacturing and in service.

This work was done by Alvin T. Sheppard of Martin Marietta Corp. for **Marshall Space Flight Center.** *No further documentation is available.*
MFS-25917

In Situ Cross-Linking of Polyvinyl Alcohol Films

Three methods can create hydrophilic films, without using undesirable organic solvents.

Lewis Research Center, Cleveland, Ohio

The coulombic and energy efficiency, cycle life, and power output of secondary alkaline batteries are dependent upon effective low-resistance battery separators. One of the most common separators in use today is regenerated cellulose film, which is well suited for use in nickel/zinc-type cells. These films, however, rapidly deteriorate in the oxidative environment of silver/zinc-type cells.

Research was conducted to provide low-cost, easily-fabricable, highly-ion-conductive battery separators. This work resulted in the development of techniques for the in situ cross-linking of polyvinyl alcohol films.

Films or impregnated matrices can be readily made from an aqueous polyvinyl alcohol solution. Controlled-thickness films are made by casting precise quantities of the aqueous polymer solution on a smooth surface, allowing the water to evaporate, and then removing the film. Composite separators can be formed in a similar fashion by impregnating a cloth matrix with a polyvinyl alcohol solution and drying the composite.

At that point, the un-cross-linked or linear-polymer material is still soluble in water, and in this form the films or composites can be easily fabricated into various articles by cementing with a concentrated polyvinyl alcohol solution and drying. To convert the water-soluble polymer to a water-insoluble material requires cross-linking of the polyvinyl alcohol. This enables this material to be used in aqueous systems without dissolving. The advantage of in situ cross-linking is that it facilitates fabrication with the linear polymer. Cross-linking of the fabricated article is done as the final step.

Three methods of cross-linking were investigated: The first method involves treating a polyvinyl alcohol film containing a water-soluble dialdehyde cross-linker with an aqueous acid solution that catalyzes acetalization cross-linking. The main advantage of this cross-linking method is that the degree of cross-linking can be regulated by the amount of dialdehyde incorporated into the film. Cross-linking increases with dialdehyde content. More cross-linking results in greater hardness of the film and higher resistivity; thus, a compromise must be reached in the amount of dialdehyde used so that a tough insoluble film of good ionic conductivity results.

The second cross-linking method involves treating the fabricated polyvinyl alcohol with a periodic acid (acidified aqueous potassium periodate). Polyvinyl alcohol is composed of 1,3 diol units pendant to the carbon chain backbone; however, the commercial material contains minor amounts of 1,2 diol units. The extent of cross-linking is determined by the proportion of 1,2 diol units in the original polyvinyl alcohol. This cross-linking technique is designed to provide greater oxidation resistance to the cross-linked films because oxidation-prone 1,2 diol units are essentially used up. Although the periodic-acid-treated films have excellent mechanical properties, their resistivities are higher than films treated by the other two methods. Area resistivity in 45-percent aqueous KOH for a film thickness of 180 μm is about 1.0 ohm-cm^2.

The third cross-linking method utilizes ionizing radiation. The fabricated films were swelled in moist air and exposed to ionizing radiation, such as 2-MeV electrons from a linear accelerator or Dynamitron (or equivalent) accelerator at a beam flux of 10^{-6} A/cm^2 for about 5 minutes. The radical formed from the irradiated water, namely hydrogen atoms, abstracts hydrogen atoms on the alpha carbon of the polymer, which form linear polymer radicals. The radical sites recombine to form a cross-linked polymer structure. Radiative cross-linking may also be used to cross-link other linear polymers, such as polyacrylic acid, polyacrylamide, and polyvinyl pyrolidone.

Radiolytic cross-linking produces the least amount of cross-linking of the three methods; but this method is the most versatile. The radiolytic cross-linking can be used to cross-link polymer blends to form copolymers. One such cross-linked copolymer, comprising a 1-to-1 ratio of polyvinyl alcohol and polyacrylic acid, shows promise as an ion-exchange membrane. Thin membranes of this type have been shown to be effective in removing metal cations, such as silver, copper, and cobalt, from dilute solution.

An important feature of the in situ cross-linking method is that insoluble thin hydrophilic membranes can be made from aqueous systems, and the use of undesirable organic solvents is not required.

This work was done by Warren H. Philipp, Li-Chen Shu, and Charles E. May of **Lewis Research Center.** *Further information may be found in NASA TP-1407 [N79-21128/NSP], "Three Methods for In Situ Cross-Linking of Polyvinyl Alcohol Films for Application as Ion-Conducting Membranes in Potassium Hydroxide Electrolyte" [$7]. A copy may be purchased [prepayment required] from the National Technical Information Service, Springfield, Virginia 22161.*

This invention has been patented by NASA [U.S. Patent Nos. 4,262,067; 4,218,280; and 4,272,470]. Inquiries concerning nonexclusive or exclusive license for its commercial development should be addressed to the Patent Counsel, Lewis Research Center [see page A5]. Refer to LEW-13135.

Binder for Carbon-Fiber Coating

An insoluble, even coating is formed by soaking in polyacrylic acid.

NASA's Jet Propulsion Laboratory, Pasadena, California

Thin, even coatings of divalent metal ions on carbon fibers are applied with the help of a common ingredient of floor wax. The metallic ion coatings serve as catalysts for the gasification of the fibers in composite structural materials that are destructively heated, as in accidental fires. An even catalytic coating is necessary for even gasification, or else small, electrically-conductive fiber fragments will be released and pose an electrical short-circuit hazard.

Calcium acetate has been used as a coating, but it tends to clump together on the fibers. In the new coating the calcium ions are polymerically bound in place instead of simply precipitated from solution.

The carbon fiber material is prepared by soaking in a solution of 20 percent polyacrylic acid in water. The material is then blotted and dried at 120° C for at least 2 hours. The dried material is reacted with a boiling aqueous solution of calcium acetate (or any other suitable aqueous solution with a combination of divalent metal ions). The treated material is removed from the boiling solution, blotted, dried at 120° C, washed with distilled water, and dried again.

The metal ions cross-link the chains of the acrylate polymer, forming an insoluble metal catalytic coating on the fiber. The last wash in distilled water removes any calcium that is not strongly bonded. The average weight gain of the fibers due to the formation of the calcium polyacrylate coating is about 6 percent.

This work was done by Warren L. Dowler, Kumar N. Ramohalli, Shiao-Ping S. Yen, William A. Mueller, and Jan Harper of Caltech for **NASA's Jet Propulsion Laboratory.** *For further information, Circle 37 on the TSP Request Card.*

This invention has been patented by NASA (U.S. Patent No. 4,351,878). Inquiries concerning nonexclusive or exclusive license for its commercial development should be addressed to the Patent Counsel, NASA Resident Office-JPL [see page A5]. Refer to NPO-14988.

Dye Indicators for Acidic or Basic Surface Contamination

Secondary contamination due to cleaning processes is detected.

Marshall Space Flight Center, Alabama

The application of a pH-sensitive dye solution can serve as a test for acidic or basic contamination of a critical bonding surface. The detection of such contamination is important where the incomplete removal of cleaning- or activating-solution residue might result in eventual failure of a bond or coating on the surface.

In the case that gave rise to the technique, an aqueous solution of 0.1 percent Direct Red No. 28 was found to be capable of indicating acid activating solutions down to 10 parts per million on hardware and tooling. The dye did not cause detectable contamination of the surface.

The technique may be feasible with other pH-sensitive dyes. For example, thymosulfonphthalein in alcohol may serve as an acid/base indicator.

This work was done by A. W. Lakin and F. T. Schuler of Rockwell International Corp. for **Marshall Space Flight Center.** *No further documentation is available.*
MFS-19387

Books and Reports

These reports, studies, and handbooks are available from NASA as Technical Support Packages (TSP's) when a Request Card number is cited; otherwise they are available from the National Technical Information Service.

Containerless Processing of Advanced Glasses

New compositions with remarkable properties are possible.

A report describes an investigation of containerless processing of glass, conducted in preparation for gravity-free processing experiments on board the Space Shuttle. A total of 105 candidate glass materials were screened. In particular, a mixture of oxides of niobium, titanium, and calcium ($Nb_2O_5/TiO_2/CaO$) was found to be rich in new containerless glass compositions. A large number of oxide proportions were studied, and a ternary phase diagram of glass formation was developed as a result.

In the screening experiments, which were conducted in a vertical wind tunnel,

compacted powder formulations were melted by a high-power carbon dioxide laser. Supported by a silica sting rotating about a vertical axis, the composition was further supported by the wind-tunnel air currents while molten.

Containerless processing often produces previously unknown glasses having desirable properties: The elimination of contact with solids removes most of the nucleation sites that precipitate undesirable crystallization of the supercooled melt, thereby facilitating glass formation. The technique may therefore offer advantages for terrestrial use as well as in space — for example, with the aid of acoustic levitation to prevent molten glasses from contacting their surroundings.

Hardware for containerless processing was also evaluated. In particular, experimental and commercial acoustic levitators were examined for their applicability to space experiments.

Procedures for the experiments were established. Methods for handling and analyzing samples were developed. These procedures and methods are not limited to a particular experiment; instead, they can be modified easily for future flight experiments.

The report concludes that broad new families of glasses may become a reality through space processing. Values of refractive indices, dispersions, absorptions, and other optical properties previously unattainable may be exploited in optical components, such as lenses, filters, and windows. Indeed, the frequent occurrence of new glasses in the $Nb_2O_5/TiO_2/CaO$ system suggests that new and unique glasses may also be found by containerless processing of other systems — the halide and the chalcogenide systems, for example.

This work was done by R. A. Happe and K. S. Kim of Rockwell International Corp. for **Marshall Space Flight Center.** *To obtain a copy of the report, "Containerless Preparation of Advanced Optical Glasses — Final Report," Circle 38 on the TSP Request Card.*
MFS-27002

MiniBriefs describe NASA innovations and reports in an abbreviated format. Readers desiring additional information on these items should request the Technical Support Packages (TSP's), available in most cases, which can be obtained by using the TSP Request Card at the back of this issue.

Destroying Toxic Wastes

Poisonous materials are converted to useful fuels.

Toxic pesticides and halogenated hydrocarbons are converted to fuels and harmless waste by catalyzed combustion. The toxic materials are partially oxidized with air. This forms gases such as hydrogen sulfide, phosphine, hydrogen chloride, and ammonia; these gases are subsequently reacted with each other or oxygen, or both, and scrubbed in a conventional manner to clean hydrogen and carbon monoxide. These product gases can be used directly as fuel or can be catalytically converted to methanol.

In operation, the toxic waste is first chopped up, in the case of solids, and either vaporized or sprayed (liquid), together with a limited amount of air, into a catalyst bed. The catalyst bed allows rapid heat transfer throughout the bed and provides excellent reaction control with no carbon formation at temperatures approaching 2,200° F (1,200° C). Subsequently, the hydrogen- and carbon monoxide-rich gas is scrubbed of all heteroatomic gaseous species.

This work was done by Gerald E. Voecks of Caltech for **NASA's Jet Propulsion Laboratory.** *For further information, Circle 109 on the TSP Request Card.*
NPO-15655

Hollow Spheres of Metallic Glass

Controlled cooling yields uniform hollow spheres of metallic glass.

Uniform hollow spheres of gold/lead/antimony glass are formed by blowing bubbles of the molten metal into a helium-filled drop tube. The bubbles fall first through a high-temperature zone, where their shape is stabilized. The next two zones are cryogenic, quenching the spheres before nucleation can set in. The spheres are 1.5 millimeters in diameter, with a wall thickness of 15 microns. They may be useful in fusion target applications.

This work was done by Mark C. Lee of Caltech for **NASA's Jet Propulsion Laboratory.** *For further information, Circle 110 on the TSP Request Card.*
NPO-15991

Plasma-Sprayed Copper Tie-In for Nickel Plating

Foam insulation is nickel-plated with one less step.

A process for nickel-plating foam insulation has been simplified. Changing a tie-in layer from plasma-sprayed nickel to plasma-sprayed copper eliminates an intermediate copper electroplating step previously required before the final nickel electroplating step. In the revised process, the physically-cleaned insulation surface is coated with silver lacquer, then plasma-sprayed with copper, solvent-cleaned, swabbed with an activating solution containing Oxyvate 397 and 398, or their equivalents, rinsed, and electroplated with nickel. The plating-current density is 10 A/ft^2 (108 A/m^2) for the first 2 hours and 20 A/ft^2 (215 A/m^2) thereafter. The previous copper-plating step prevented damage to the lacquer during the nickel-plating step.

This work was done by John W. Lombard and Joseph E. O'Tousa of Rockwell International Corp. for **Marshall Space Flight Center.** *For further information, Circle 111 on the TSP Request Card.*

Inquiries concerning rights for the commercial use of this invention should be addressed to the Patent Counsel, Marshall Space Flight Center [see page A5]. *Refer to MFS-19481*

Making $Si_XN_YC_Z$ Fibers by Pyrolysis

Report presents experimental results.

A report presents the results of experiments in making Si_3N_4/SiC fibers by the controlled pyrolysis of organosilicon

(continued on next page)

polymeric fibers. This investigation is part of a continuing effort to produce fibers strong enough to replace graphite in fiber/polymer composites. Unlike graphite, the material must be electrically resistive enough not to disrupt delicate electronic circuits when a stray fiber falls on two contacts.

Experimental Si_3N_4/SiC fibers exhibited resistivities of 10^{10} to 10^{12} that of graphite fibers — sufficient to prevent most spurious signals, arcing, and shorting. However, the experimental fibers are much weaker than graphite and some commercial SiC fibers, and are therefore not strong enough for use in composites.

This work was done by R. A. Markle, I. Sekercioglu, D. L. Hill, Roger R. Willis, and R. G. Sinclair of Battelle Columbus Laboratories for **Marshall Space Flight Center.** *To obtain a copy of the report, Circle 112 on the TSP Request Card.*

Title to this invention has been waived under the provisions of the National Aeronautics and Space Act (42 U.S.C. 2457(f)), to the Battelle Columbus Laboratories, 505 King Ave. , Columbus, OH 43201.
MFS-25621

Etchants for Some Corrosion-Resistant Metals

Surface material is removed without intergranular attack.

Solutions that etch some corrosion-resistant metals are described in a test report. The etchants selected are those that remove at least 0.4 mil (0.01 mm) of surface material per hour from nickel alloys, austenitic stainless steel, and annealed titanium alloys, without intergranular attack.

All the recipes include HNO_3, and each includes one or more of the following in various proportions: H_2O, HCl, HF, $NiCl_2$, $FeCl_3$, CrO_3, H_3PO_4, H_2O_2, and a silica thickening agent. The solutions are applied by brushing (with or without the thickening agent) or the metal is immersed in the solution. The solution, the application method, the temperature, and the etching time are determined according to the metal, the part configuration, and other specific factors.

This work was done by J. R. Simmons of Martin Marietta Aerospace for **Marshall Space Flight Center.** *Further information may be found in NASA CR-161431 [N80-25414/NSP], "Study of Etchants for Corrosion-Resistant Metals, Space Shuttle External Tank" [$8.50]. A paper copy may be purchased [prepayment required] from the National Technical Information Service, Springfield, Virginia 22161. A copy is also available on microfiche at no charge. To obtain a microfiche copy, Circle 113 on the TSP Request Card.*
MFS-25467

Hot Microfissuring in Nickel Alloy

Correct process design may reduce cracking.

Experiments in the intergranular cracking of a nickel alloy near the solidus temperature are discussed in a contractor report. The purpose of this and similar investigations is to eventually develop a schedule (for example, temperature and/or strain versus time) for welding, casting, forging, or other processing of the alloy without causing microfissuring. An interim goal is to draw the boundaries of microfissuring regions on plots of plastic strain versus temperature.

In these experiments, the temperature range for low-strain incipient cracking was determined from hot ductility tests. The incipient-crack data for a specific process must be considered carefully since each process leads to different mechanical properties in the heat-affected zone.

This work was done by Raymond G. Thompson of the University of Alabama and A. C. Nunes of **Marshall Space Flight Center.** *Further information may be found in NASA CR-161878 [N82-10194/NSP], "Further Study of Near Solidus Intergranular Cracking in Inconel 718" [$8.50]. A paper copy may be purchased [prepayment required] from the National Technical Information Service, Springfield, Virginia 22161. A copy is also available on microfiche at no charge. To obtain a microfiche copy, Circle 114 on the TSP Request Card.*
MFS-25763

Additional Heat Treatment for Silica-Fiber Insulation

Heat treatment prevents cracking during sintering.

Presintering heat treatment has been found to prevent cracking in silica-fiber billets used to make thermally-insulating tiles. Such preprocessing heat treatment is well known in the ceramic and metalworking industries.

The cracking occurs in some production lots that undergo excessive shrinkage during the sintering. Sintering imparts the desired thermal and mechanical properties to the finished billets. Preheating mixed lots of billets at 1,000° F (540° C) produces less thermal shock than does rapid heating to the sintering temperature and allows more gradual initial shrinkage, thereby preventing cracking.

This work was done by E. Maduk, I. Carpenter, and E. Gzowski of Lockheed Missiles & Space Co., Inc., for **Johnson Space Center.** *No further documentation is available.*
MSC-20600

Catalytic Coal Liquefaction With Iron Sulfate

Recoverable catalyst promises high conversion yields.

Iron sulfate is a cheap, readily recoverable catalyst for the conversion of coal into liquid fuel oil. Catalysts such as cobalt, molybdenum, nickel, and tungsten sulfides, in contrast, are not easily recoverable and substantially increase the cost of the liquefaction process.

Very high conversion yields were demonstrated with the iron sulfate, which was used in solution with water or solvent to impregnate the coal. At 1,000° F (540° C) and 3,000 psi (20.7×10^6 N/m^2), 70 percent of the coal was converted to liquid and gas in a fluidized-bed reactor, yielding 45 percent as distillate oil. Even higher yields were obtained at 900° F (480° C) and 2,000 psi (13.8×10^6 N/m^2) in a stirred tank reactor where 90 percent of the coal was converted with 70 percent liquid yield.

This work was done by Shaik A. Qader of Caltech for **NASA's Jet Propulsion Laboratory.** *For further information, Circle 115 on the TSP Request Card.*
NPO-15727

Sampling of Silicon Powder for Impurity Analysis

An electron beam forms dense pellets of powdered silicon for Zeeman analysis.

A new sampling method focuses an electron beam on submicron silicon powder. The molten droplets quickly solidify into pellets of 2 to 10 milligrams, a

size convenient for Zeeman atomic-absorption analysis. Each pellet reflects the composition of only a small region of the powder. The distribution of metallic impurities may thus be determined, as well as the overall concentration. The process enhances quality control in production of low-cost silicon powder for the semiconductor industry.

This work was done by Kazuo A. Yamakawa and Oliver R. McCullough of Caltech for **NASA's Jet Propulsion Laboratory.** *For further information, Circle 116 on the TSP Request Card.*
NPO-15840

Silane Pyrolysis With Silicon-Seed Aerosol

Large silicon particles result from controlled pyrolysis of silane.

A mixture of 1 percent silane in nitrogen is pyrolyzed at 300° to 400° C to generate an aerosol of silicon seed particles. The cooled aerosol is mixed with silane and passed through a second furnace at 900° C. The resulting silicon particles are at least 4 microns in size, and are readily collected as a powder. The submicron particles resulting from bulk pyrolysis are much more difficult to collect, and their larger surface-to-mass ratio makes them more prone to contamination.

This work was done by Richard C. Flagan and Mohammed Khairul Alam of Caltech for **NASA's Jet Propulsion Laboratory.** *For further information, Circle 117 on the TSP Request Card.*

Inquiries concerning rights for the commercial use of this invention should be addressed to the Patent Counsel, NASA Resident Office-JPL [see page A5]. Refer to NPO-16054.

Automated Magnetic-Susceptibility Analysis

Alternating current susceptibility of small samples is determined as function of temperature.

A microprocessor-controlled susceptometer measures the cryogenic temperature dependence of the ac magnetic susceptibility of small cylindrical samples (0.1 to 5 mm in diameter). The cryostat sample chamber, heating rod, and temperature sensor are made of single crystal sapphire. The high thermal conductivity of the sapphire allows rapid equilibration and a short turnaround time between samples.

A microcomputer controls the temperature in a range of 1.5 to 77 K while collecting and analyzing the susceptibility data. The superconductive transition temperature is approached rapidly and then determined with high precision. The sample ac or dc resistivity may be monitored, and the fine structure in the susceptibility data can give qualitative information on the number and volume percentage of macroscopic superconducting inclusions.

This work was done by Thomas J. Rathz of **Marshall Space Flight Center.** *For further information, Circle 118 on the TSP Request Card.*

Inquiries concerning rights for the commercial use of this invention should be addressed to the Patent Counsel, Marshall Space Flight Center [see page A5]. Refer to MFS-25935.

Removing Sulfur Dioxide From Flue Gases

The process uses a regenerable molten salt supported on porous pellets.

In situ removal of SO_2 in flue gases and fluidized-coal combustors, with no waste product, is possible using NaO/LiO as a regenerable supported molten sorbent. Under the new method, SO_2 in the presence of O_2 is rapidly absorbed in the melt, forming sulfates; the sulfates are then reduced and desorbed as elemental sulfur and carbonyl sulfide. After removal of the elemental sulfur, the carbonyl sulfide is recycled to the reduction stage. For removal of SO_2 from coal combustion, the coal is burned in a fluidized bed of the sorbent.

This work was done by George R. Gavalas and Maria F. Stephanopoulos of Caltech for **NASA's Jet Propulsion Laboratory.** *For further information, Circle 119 on the TSP Request Card.*
NPO-15758

X-Ray-Diffraction Analysis of Nb/Ge Alloys

Evidence of a temperature-stable superconducting phase is obtained.

An investigation of a series of niobium/germanium alloys produced by supercooling is discussed in a report. The material studied was stoichiometric Nb_3Ge and has a high superconducting transition temperature.

The supercooling process uses a free-fall drop tower with a cryogenic splat cooler connected to its bottom. Supercooling by 500° C is required, and the optimum sample size is on the order of 0.1 mm in thickness.

This work was done by Jack H. Davis and K. W. House of the University of Alabama for **Marshall Space Flight Center.** *For further information, Circle 120 on the TSP Request Card.*
MFS-27038

Conductive Plasma-Sprayed Coatings

Thin, electrically-conductive plasma coatings have good emittance and adhesion.

Coatings originally designed for spacecraft plume shields may be useful on turbine blades and other metal surfaces exposed to high temperatures. The normal emittance of oxidized titanium foil used as plume shields at high temperature can be significantly increased by plasma coating with specific ceramic materials. Iron titanate powder was plasma sprayed onto titanium foil to a thickness of 25 microns, which resulted in surface electrical resistivity of 1.5×10^4 ohms/square. The ability of the coating to emit radiant energy was excellent (normal emittance of 0.82). The coating showed no signs of peeling when tested with adhesive tape and 180° flexing. Thermal cycling from 538° C to −195° C did not alter these properties.

A plasma coating of silicon carbide over anodized titanium produced a lower surface electrical resistivity of 1.0×10^3 ohms/square and a lower normal emittance (0.62), but was similar in other respects to the iron titanate coating.

This work was done by Victor F. Hribar of Caltech for **NASA's Jet Propulsion Laboratory.** *For further information, Circle 121 on the TSP Request Card.*
NPO-15927

High-Temperature, Low-Gravity Casting Furnace

Up to six different samples can be processed.

An experimental melting and casting furnace has been designed to perform metallurgical studies in low gravity . The

furnace is held on a rotatable support in a canister, which also contains six crucible holders and a movable quenching cup.

During processing, the furnace is lowered over the crucibles one at a time and maintained at the prescribed temperature. At the end of the heating period, the furnace is raised, moved to the next crucible, and lowered for the start of the next experiment. The quenching cup is then lowered over the hot crucible and nitrogen gas is blown around the holder to solidify the sample.

This work was done by Harry M. King, Joe R. Short, Robert E. Shurney, Thomas F. Morris, Richard A. Parr, Mary H. Johnston, and David D. Webb of **Marshall Space Flight Center.** *For further information, Circle 122 on the TSP Request Card.*

Inquiries concerning rights for the commercial use of this invention should be addressed to the Patent Counsel, Marshall Space Flight Center [see page A5]. Refer to MFS-25605.

Furnace for Rapid Heating and Cooling

Compressed solid reactant provides the heat; liquid carbon dioxide provides the cold.

A furnace rapidly heats and quenches materials, controllably and reliably. Developed for processing foamed metals, the furnace can heat a specimen to above 1,200° C and then cool it to below 900° C in just a few minutes.

Several segments of exothermic material are stacked so that when ignited they produce the requisite temperature profile. A specimen container is held in the core of annular segments. The segments ignited simultaneously heat the specimen.

The specimen is cooled by liquid carbon dioxide introduced into the furnace chamber. The carbon dioxide gasifies and flows over the exothermic heating material and the sample container, rapidly reducing the temperature.

This work was done by Richard M. Poorman of **Marshall Space Flight Center.** *For further information, Circle 123 on the TSP Request Card.*

This is the invention of a NASA employee, and a patent application has been filed. Inquiries concerning license for its commercial development may be addressed to the inventor, Mr. Richard M. Poorman, at Marshall Space Flight Center [see page A5]. Refer to MFS-25707.

Life Sciences

Hardware, Techniques, and Processes

221 High-Flow Asymmetric Reverse-Osmosis Membranes

222 Solvent Extraction of Furfural From Biomass

MiniBriefs 222

High-Flow Asymmetric Reverse-Osmosis Membranes

A water-soluble polymer membrane is insolubilized by a transition-metal salt.

Ames Research Center, Moffett Field, California

Asymmetric reverse-osmosis desalination membranes prepared by a new method are capable of high waterflow rates and high salt rejection. In addition to improved performance, the new membranes differ from older types in that they do not have to be stored in water. The new membranes can be used to purify or desalinate seawater, brackish water, or industrial or domestic wastewater.

A reverse-osmosis desalination membrane works better when it has an asymmetric structure than when it has a symmetric structure. A thin layer of lower permeability material is joined with a thicker layer of high-permeability material. The two layers may be chemically identical or chemically distinct. They may differ in density, compactness, or other respects.

Older membrane types were made of water-insoluble polymers — most commonly, cellulose acetate. The new membranes are preferably made from poly(vinyl alcohol), which is more resistant to acids, bases, alcohols, and phenols that may be found in corrosive or contaminated streams.

The new membrane-preparation method uses water as the solvent. The asymmetric structure is achieved without employing a solvent/nonsolvent liquid precipitation system like that used in a previous asymmetric membrane-production method.

The new fabrication method has three essential steps to which modifications can be made. In the first step, a thin layer of a water-soluble polymer is cast from a water-based solution. Layers from about 5 to 50 μm thick perform best: Thinner membranes are difficult to handle, and thicker ones unduly restrict waterflow. On a laboratory scale, the casting can be done with a manual doctor blade. On a commercial scale, an automated continuous-casting machine could be employed.

In the second step, the cast polymer layer is rapidly and partially dehydrated by drying in air while it is still in place on the casting surface. This partial drying does not cause insolubilization. However, it is believed to impart the desired asymmetric structure to the film. (Longer dehydration periods give denser, more restrictive membranes.) Times of 20 to 500 seconds at temperatures from 15° to 50° C and relative humidity between 25 and 75 percent give best results. The resulting water-soluble asymmetric membrane is removed from the casting surface.

In the third step, the membrane is insolubilized by immersion for 10 to 400 hours in a preferably saturated aqueous solution of salt of a polyvalent transition metal; for example, copper sulfate. The metal ion should be selected for low toxicity if the membranes are to be used to produce drinking water. The solution should be concentrated so that the insolubilitization will take place before the membrane has a chance to dissolve. The metal ions are believed to cause cross-linking of the polymer and to form complexes with it.

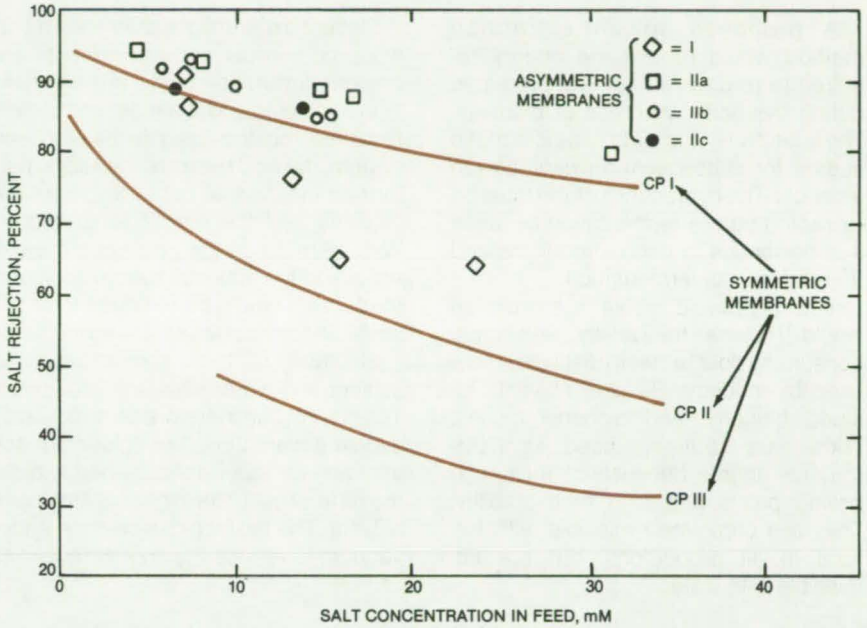

The **Desalination Performances** of four variations of the asymmetric metal-ion complexed membranes (I, IIa, IIb, and IIc) and three variations of symmetric membranes (CP I, CP II, and CP III) were compared at an applied pressure of 1,000 psi (6.9 MN/m^2) at 30° to 40° C. The salt rejection of asymmetric membranes IIa, IIb, and IIc was slightly superior to that of the best symmetric membrane, heat-treated membrane CP I. The water flux through each of the asymmetric membranes was superior to that through any of the symmetric membranes.

The asymmetric physical structure of the new membranes was verified by examining one of them with a scanning electron microscope. At a magnification of 5,000, the underside appeared porous, the top surface nonporous. The salt rejection occurs at the nonporous surface without impeding waterflow as much as the more-uniformly-dense symmetric membranes do. The figure shows salt-rejection rates for asymmetric membranes of the new type and for comparable membranes that were made symmetric by direct cross-linking treatments without intermediate drying.

This work was done by Moshe C. Katz and Theodore J. Wydeven of **Ames Research Center.** *For further information, Circle 39 on the TSP Request Card.*

Inquiries concerning rights for the commercial use of this invention should be addressed to the Patent Counsel, Ames Research Center [see page A5]. *Refer to ARC-11359.*

Solvent Extraction of Furfural From Biomass

Energy and material consumption would be reduced.

NASA's Jet Propulsion Laboratory, Pasadena, California

A proposed solvent-extraction method would reduce the energy required to remove the furfural produced during the acid hydrolysis of biomass. The objective of the hydrolysis is to make sugars for subsequent fermentation to alcohols. The byproduct furfural must be extracted before fermentation because it is poisonous to micro-organisms and thereby inhibits fermentation.

The proposed solvent extraction would replace the costly and time-consuming double steam distillation now used by industry. Suitable solvents include biphenyl and diphenyl oxides: These are routinely used as heat-transfer agents because of their high boiling points and high heat stability. They are completely miscible with furfural in all proportions, but are immiscible with water.

Recent experiments have shown that when both water and the solvents are present, furfural dissolves preferentially in the solvents and is almost completely removed from the water. In the proposed system, the acid hydrolysis would be performed in a vessel containing both the solvents and the reacting ingredients. With intimate contact between the solvents and the aqueous hydrolysis liquor, the furfural would be removed from the liquor almost as fast as it is formed.

Because of their immiscibility, the solvent and water separate into layers. The solvent can therefore be removed by simple decantation. The solution of solvent and furfural is then flashed to distill the furfural out of the higher-boiling-point solvent. The flashing can be done under vacuum to reduce the energy required.

The process has some other advantages: It prevents the acid decomposition of the furfural at the hydrolysis-reaction temperature. Less material will have to be handled because less acid and less neutralization will be required. A further energy saving could be achieved by obtaining heat for the vacuum distillation from a solar concentrator, using the solvent in its traditional role as a heat-exchange fluid to carry the process heat for its own distillation.

This work was done by Marshall F. Humphrey of Caltech for **NASA's Jet Propulsion Laboratory.** *For further information, Circle 40 on the TSP Request Card.*
NPO-15987

MiniBriefs describe NASA innovations and reports in an abbreviated format. Readers desiring additional information on these items should request the Technical Support Packages (TSP's), available in most cases, which can be obtained by using the TSP Request Card at the back of this issue.

Speculation on Ultrasonic Disintegration of Arterial Deposits

An ultrasonic probe might be able to clear arteries.

A small ultrasonic probe, in conjunction with an aspirator, has been proposed to break up and remove atherosclerotic plaque from the insides of arteries. The probe would have to be compact enough to enter arteries yet powerful enough to dislodge and clear the deposits. It would have to disintegrate the plaque without damaging the intima, because the damaged areas could serve as substrates for further plaque aggregation. The loose plaque would have to be aspirated to prevent development of a potentially fatal embolism. The problem of acoustic impedance mismatch would also have to be overcome, so that sufficient acoustic power may be transferred.

This work was done by Johnny M. Clemons and Dale M. Kornfeld of **Marshall Space Flight Center.** *For further information, Circle 41 on the TSP Request Card.*
MFS-25161

Yeasts With Increased Glycogen Levels

They could be used as single-cell food for humans.

A chemical/biological process produces single-cell food from waste carbon dioxide and hydrogen. The two gases are sources of chemical feedstock to produce methanol, which is then fed to mutants of the yeast *Hansenula polymorpha*. In turn, these mutant yeast strains produce and store consumable carbohydrates, such as glycogen, without altering their protein content.

The process could be used in a reactor for producing single-cell food. Strains of the mutants are being sought that have a glycogen content that approaches the desirable ratio of human food; that is, 70 percent carbohydrate, 20 percent protein, and 10 percent fat.

This work was done by Minoo N. Dastoor, Gene R. Petersen, Wayne W. Schubert, and Barry O. Stokes of Caltech for **NASA's Jet Propulsion Laboratory.** *For further information, Circle 42 on the TSP Request Card.*
NPO-15571

Mechanics

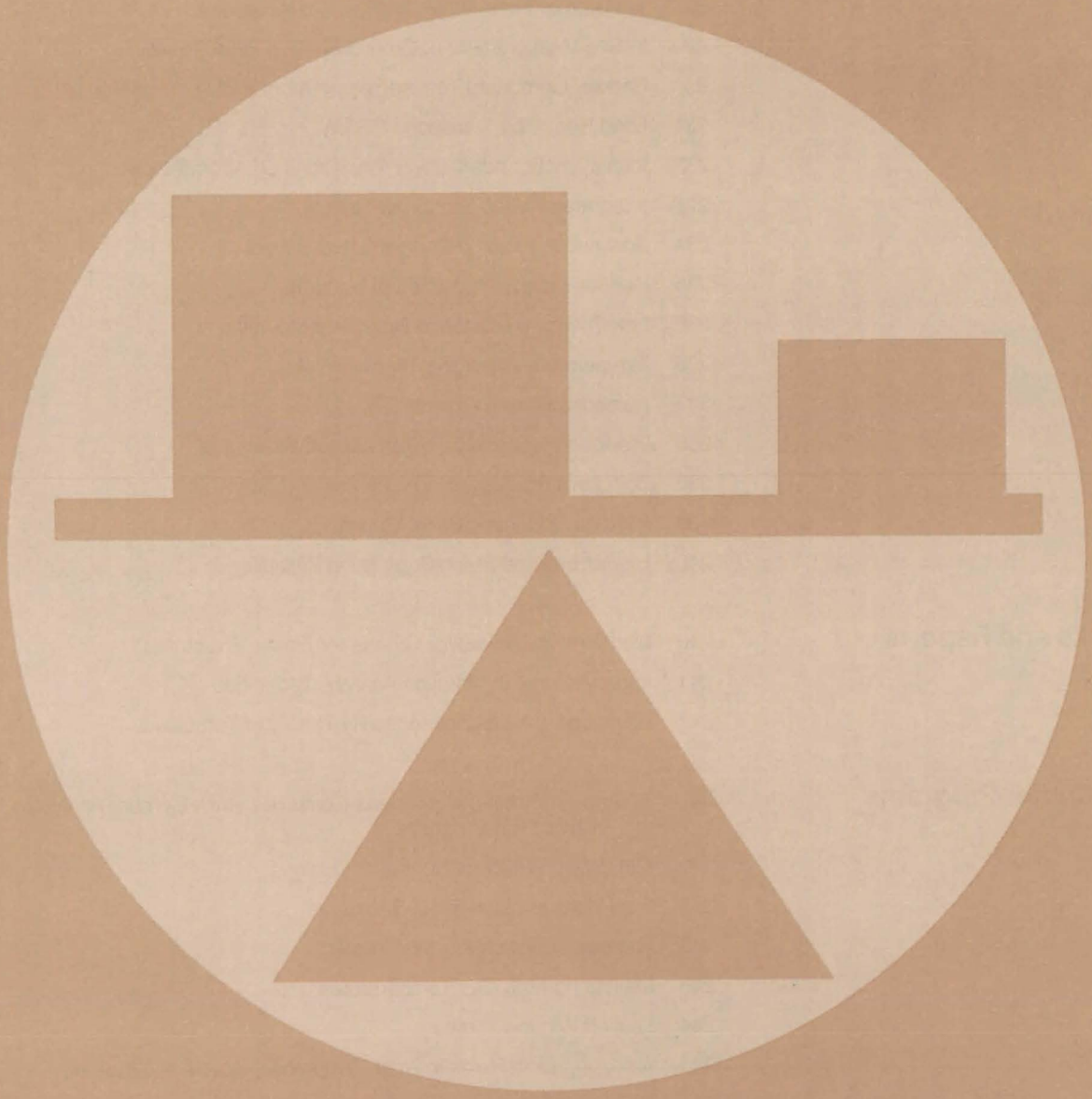

Hardware, Techniques, and Processes

225 Liquid-Droplet Radiative Cooler
226 Miniature Airflow Sensor
227 Automated Mercury Dilatometer
228 Waterproof Floor Makes Utility Lines Accessible
229 In Situ Measurement of Ground-Surface Flow Resistivity
231 Radially-Graduated Turbine-Temperature Profile
231 Long Heat Pipe Transports 2.6 kW
232 Identifying Boundary-Layer Transitions on Aircraft Skin
233 Integrated Tactile Sensor for Robots
234 Continuous-Reading Cryogen Level Sensor
235 General-Purpose Icosahedral Structure
236 Low-Thermal-Resistance Baseplate Mounting
236 Temperature-Averaging Thermal Probe
237 Autocovariance Computer
238 Predicting Noise in Complex Aircraft Structures
238 Cooldown Strategy for Cryogenic Wind Tunnels
239 Internally Mounting Strain Gages
240 Heater Ensures Strain-Gage Bond Reliability

Books and Reports

240 Mathematical Instability Criteria for Elastic Structures
241 Improvements in Vibration-Analysis Technique
241 Advances in Multivalued-Velocity Theory of Turbulence

Computer Programs

242 System for Structural Synthesis Combines Finite-Element Analysis and Optimization Programs
242 Minimizing Weight of Structural Designs
243 Free-Vibration Analysis of Structures
243 Thermal Radiation Analyzer System
243 Measuring High Gas Temperatures
244 Launch-Window Program
244 Analyzing Flow Fields in Axial-Compressor Rotors and Stators
244 General Maneuver Program
245 The Mission Radius and Maneuverability Characteristics of Fighter Aircraft
245 Elliptical Orbit Performance Computer Program
245 Takeoff and Landing of Transport Aircraft

MiniBriefs

246

Liquid-Droplet Radiative Cooler

A fine spray acts as a large-area, low-mass radiator.

Marshall Space Flight Center, Alabama

A large-area, low-mass radiative cooler originally proposed for spacecraft may be applicable to industrial processes requiring noncontacting cooling of process fluids. In the original proposal, low-vapor-pressure oil at a temperature of about 300 K would be sprayed as fine droplets from a spray head toward a collector (see figure). The disk-shaped collector would rotate, its periphery acting as a centrifugal pump to recirculate the oil. During transit from the spray head to the collector, the droplets would cool by radiating to space, thus removing waste heat from the spacecraft.

Calculations show that a droplet radiator with a 1.37-m-diameter head spraying a cylindrical droplet beam to a collector 137 m away could radiate about 100 kW. Droplets were assumed to be about 0.004 inch (0.1 mm) in diameter, about twice the diameter of the spray jets. A total of 10^5 jet orifices of 48-μm diameter spaced 0.5 mm apart would be placed in a band around the spray head. (Jet orifices of similar size and spacing etched from silicon wafers are used in ink-jet printers.) The mass of the entire system, including the generator and the collector with motor, was estimated to be about 77 kg.

The desired properties for the liquid are as follows:

- Vapor pressure less than 10^{-8} torr (10^{-6} N/m^2) at the spray-head temperature to minimize evaporation loss;
- Viscosity less than 10 centistokes (10^{-5} m^2/s) at the spray-head temperature to assure reliable droplet formation;
- High emissivity and low mass density to maximize the power radiated per unit mass;
- High specific heat: the maximum power that can be radiated is proportional to specific heat squared;
- High surface tension for reliable droplet formation;
- High thermal conductivity to facilitate heat transfer; and
- Chemical stability under thermal cycling and under exposure to ultraviolet and particle radiation.

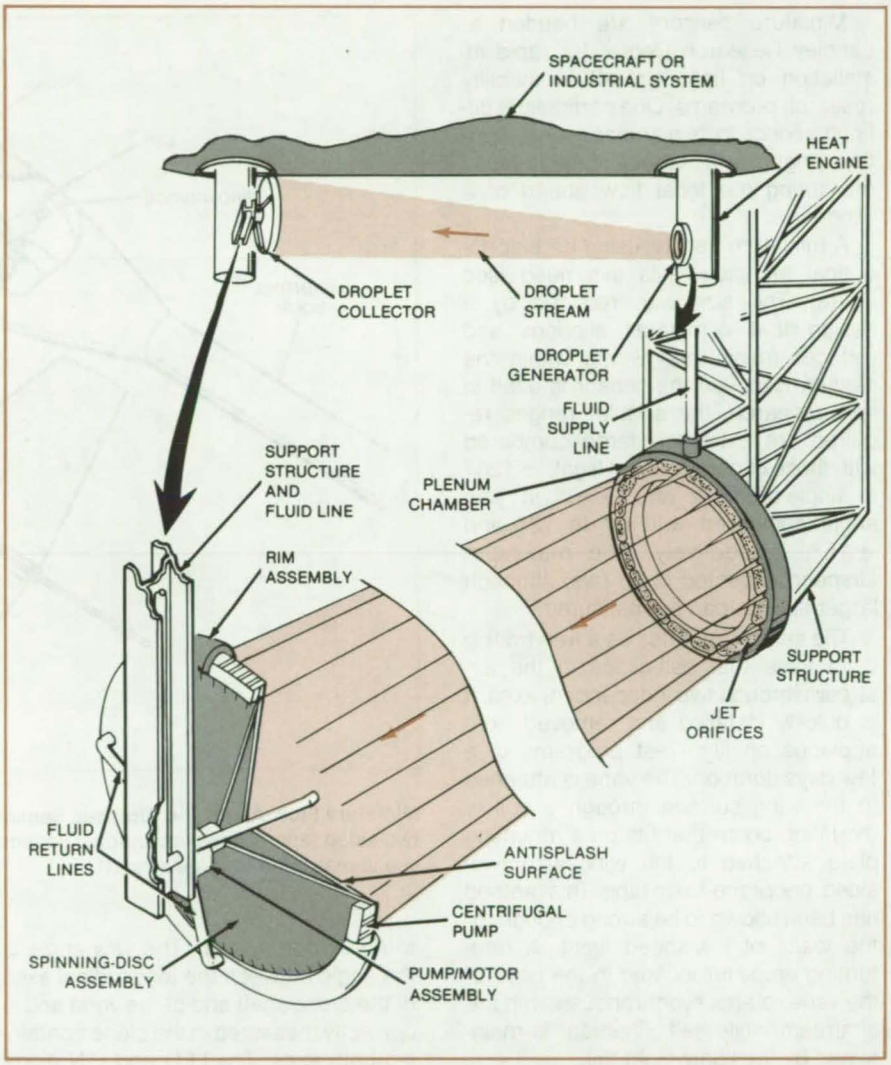

Droplet-Stream Radiators could be used to radiate away waste heat.

Several silicone and fluorinated oils that meet the vapor-pressure requirements are available. (These oils were originally developed for use in diffusion vacuum pumps, as electrical coolants and insulators, or as high-vacuum lubricants.) As supplied, each of these oils has a relatively high viscosity of 40 to 200 centistokes (4×10^{-5} to 2×10^{-4} m^2/s) at temperatures low enough to keep the vapor pressure low enough. The vapor pressure of these oils tends to decrease with use, however; and future tests may show that they can be used at higher temperatures and lower viscosities than are indicated in the manufacturers' published data.

Extensive development would be required to produce a practical system for terrestrial use. The effects of gravity and atmosphere would have to be evaluated. If the viscosity problems can be solved, further work would be warranted to characterize the candidate fluids.

This work was done by Karl K. Knapp of Astro Research Corp. for **Marshall Space Flight Center.** *For further information, Circle 43 on the TSP Request Card.*

MFS-25890

Miniature Airflow Sensor

Accurate, tape-mounted sensor uses electro-optics.

Langley Research Center, Hampton, Virginia

Miniature sensors are needed at Langley Research Center for rapid installation on light aircraft in stability research programs. One particularly difficult sensor to miniaturize has been a flow-angle and velocity sensor for measuring the local flow ahead of a wing.

A miniature sensor using an electro-optical technique fills this need (see figure). The size was reduced by a design that eliminates sliprings and reduces (minimizes) wiring within the sensor. Because the sensor is used in spin research, the angular ranges required are extremely large compared with those of conventional flight: ±120° in angle-of-attack and ±40° in yaw angle compared with 0° to 12° and ±15°, respectively. The maximum airspeed expected is 70 m/s, although larger speeds can be measured.

The sensor operates as a free-trailing wind vane that self-alines in the airstream through two independent axes. It is quickly installed and removed from airplanes on flight-test programs of a few days duration. The vane is attached to the wing surface through a hollow mounting boom that fits on a mounting plate attached to the wing with two-sided, neoprene-foam tape. This method has been shown to be strong enough for the loads of low-speed flight. A free-turning propeller located in the nose of the vane rotates synchronously with the airstream while self-alinement is maintained by the lightweight tail.

Angle-of-attack is the angular position of the cross-shaft relative to the axis of the fixed boom mounted on the wing surface. A target disk attached to the cross-shaft has a reflective strip on the rim that reflects light from a light-emitting diode (LED) to a PIN diode. The amount of light received is a function of the angle-of-attack. The sensor is calibrated by measuring the analog voltage output with precisely set angles.

Both yaw angle and airspeed are derived from the second LED/reflector/PIN-diode system. The yaw angle is the angle between the longitudinal axes of the cross-shaft and of the vane and is correctly measured in the plane containing both axes. The LED and PIN diode are mounted adjacent to each other in the pod and emit and receive light through the fiber-optic bundle that runs through the cross-shaft to the vane. Light reaching the vane reflects off a coded pattern on the propeller-driven sphere, producing an intelligible waveform that contains both the airspeed and yaw-angle information.

The accuracy of the sensor was evaluated and found to meet the requirements of the Langley aerodynamicists. The airspeed was calibrated and found repeatable and linear over the flight range to within ±1 m/s. The dynamic response of the airspeed measuring system, a first-order system, is much faster than the expected gust- or flow-angle changes.

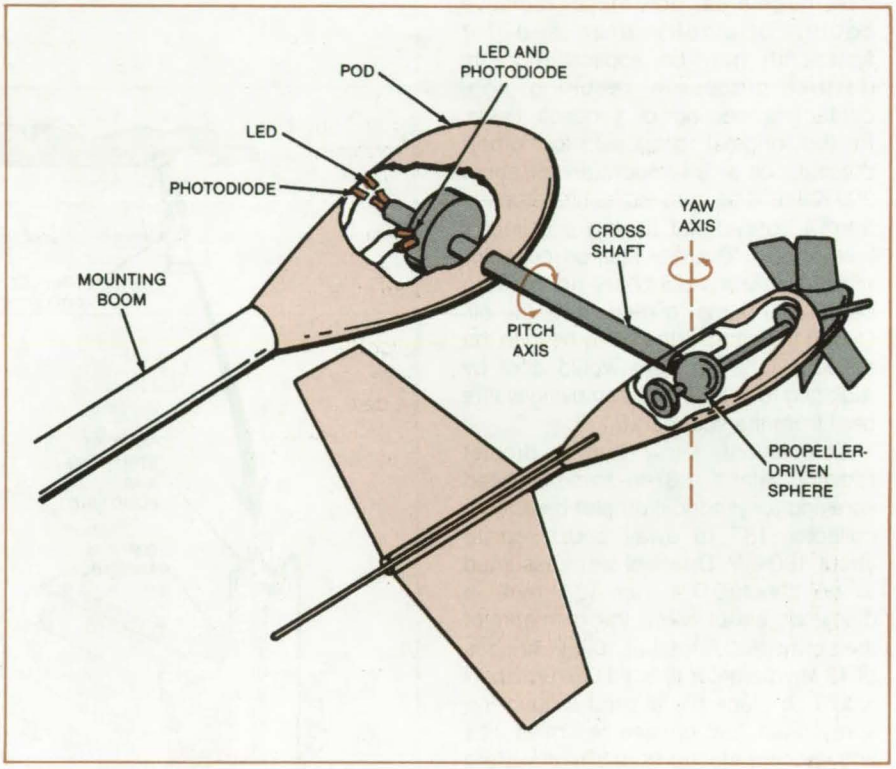

Miniature Flow-Angle and Airspeed Sensor is quickly mounted on light aircraft wing with two-sided tape. Since conventional sensors are bulkier and more complex to install, their use is restricted to large aircraft.

This work was done by David D. Kershner of **Langley Research Center.** *For further information, Circle 44 on the TSP Request Card.*

This invention is owned by NASA, and a patent application has been filed. Inquiries concerning nonexclusive or exclusive license for its commercial development should be addressed to the Patent Counsel, Langley Research Center *[see page A5].* *Refer to LAR-13065.*

Automated Mercury Dilatometer

Volume changes are recorded on a strip chart.

NASA's Jet Propulsion Laboratory, Pasadena, California

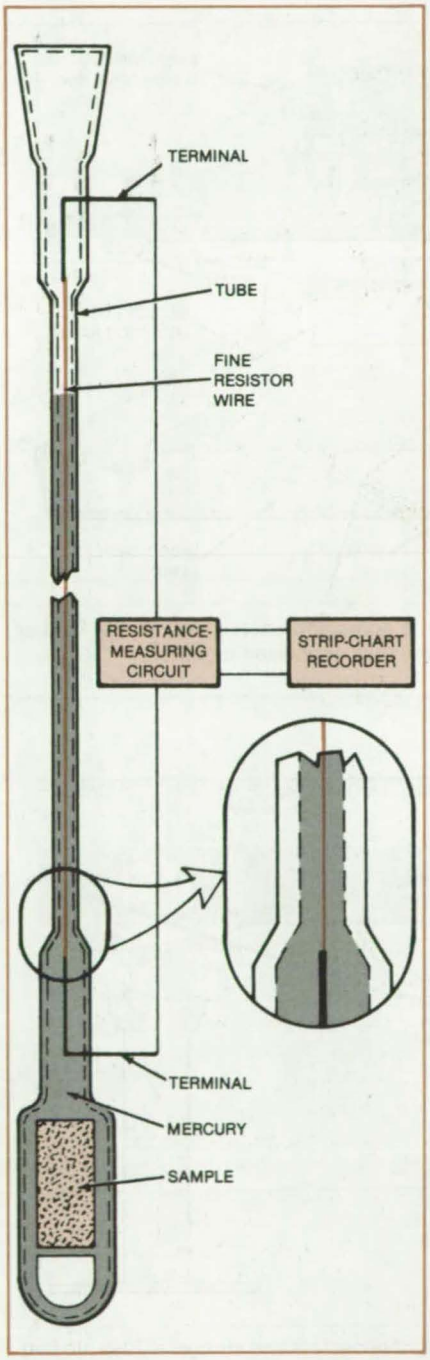

A **Mercury Dilatometer Is Modified** by the addition of a resistance wire to the mercury column. The height of the column is then read indirectly by measuring the resistance between the terminals.

The task of reading and recording the indications of a mercury dilatometer, usually a manual operation, is simplified by an automatic system in which the volume change of the sample under test is converted into an electrical signal. The signal is suitable for strip-chart recording or other processing.

The original configuration is preserved; that is, mercury is in contact with the sample, and the change in sample volume causes a change in the height of mercury in a column that has been calibrated in terms of volume. The inside diameter of the column is typically 0.025 in. (0.635 mm). The dilatometer is modified by the insertion of an Ni/Cr/Fe resistance wire in the center of the column, with platinum leads to the terminals on the outside. The wire is only 0.001 in. (0.025 mm) in diameter, so that it has only a small effect on the volume sensitivity (multiplies it by 1.0016).

The resistance between the terminals is measured with a Wheatstone bridge or other instrument. The instrument output drives a strip-chart recorder. As the mercury rises in the column, it effectively short-circuits part of the wire, causing a decrease in the resistance between the terminals. Calibration points are obtained by measuring the resistance or observing the strip-chart indication at known column heights or sample volumes. Thus, the strip chart can be read directly in terms of sample volume versus time.

This work was done by Su-Don Hong and Virgil H. Culler of Caltech for **NASA's Jet Propulsion Laboratory.** *For further information, Circle 45 on the TSP Request Card.*
NPO-14884

Imaging Fluid Flow

An electro-optical system allows simultaneous viewing of schlieren, shadowgraph, and interferometric images of a volume of fluid under test. Light from a collimated laser beam passes through the sample fluid. The system uses a series of beam splitters and mirrors to break apart and recombine the light to form the images.
(See page 195.)

Low-Vibration Oscillating Compressor

An oscillating compressor has two mutually opposed ferromagnetic pistons. An electromagnet generates a magnetic flux that causes a magnetic attraction between the pistons. The piston motions have substantially equal and opposite momenta. Since the net momentum is close to zero, there is very little vibration.
(See page 253.)

Double-Poppet Valve

A new valve backs itself up by simultaneously activating two poppet/seat combinations. Each poppet seals against one of the two conical surfaces that are part of the valve body. If one of the poppets fails, the other continues to seal against fluid flow. The valve is useful for handling dangerous fluids.
(See page 263.)

Acoustic Imaging of Combustion Noise

An ellipsoidal acoustic mirror measures the sound emitted at discrete points in burning turbulent jets. The reflector concentrates at its near focus energy originating at its far focus. It can be used in furnaces and in control of systems involving flames or reacting flows.
(See page 198.)

Waterproof Raised Floor Makes Utility Lines Accessible

Floor system can be penetrated and resealed without destroying waterproofing or appearance.

Ames Research Center, Moffett Field, California

A floor for laboratories, hospitals, and factories is waterproof yet allows access to subfloor utilities. This elevated access floor system has been designed for installations where a multitude of diverse utility systems must be routed under and up through the floor and where a separation of potentially-conflicting utility services is required (i.e., water and electrical power).

These subfloor utility services may include hot, cold, and distilled water; hydraulic, chemical, or nutrient fluids; natural gas, oxygen, nitrogen, and compressed air; drainage for sewage, acids, and condensate; heating, ventilating, and air-conditioning; electrical power, electrical or pneumatic control systems, computer data links, telephone, intercom, and fire detection and suppression. The actual lines may include cables and conduits, pipes and ducts, and channels and raceways having a variety of physical dimensions, mounting conditions, and connection requirements.

With this new system, the floor is covered by a continuous sheet of heat-resealable vinyl. The floor system can be cut open when changes are made in utility lines and ducts. After the modifications have been completed, the floor covering is resealed to protect the subfloor utilities once again from spills and leaks.

The sheet-vinyl covering is laid on tiles (see Figure 1). Each tile contains a rectangular (or otherwise-shaped) recess that accommodates a similarly shaped frame cemented to the underside of the floor covering. The covering is thus prevented from sliding horizontally. The covering is bonded to the upper frames but not to the lower tiles. In fact, a thin coating of light oil on the tile surface prevents adhesion. This provision ensures that the covering can be readily lifted away from the tiles.

The tiles are supported by an off-the-shelf square grid of stringers and pedestals, of the type commonly used for computer access floors (see Figure 2). The utility lines run in the space below the pedestals, with "wet" lines in dedicated troughs or channels to contain any subfloor leaks or spills. A square grid is painted on the top surface of the sheet-vinyl covering, corresponding to the network of stringers below (see Figure 3).

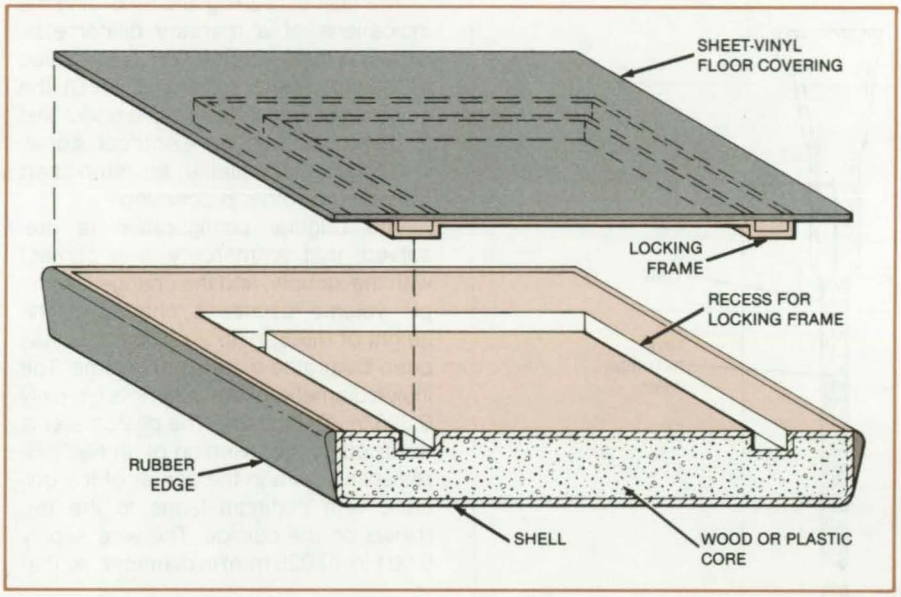

Figure 1. **Subflooring Tiles** have wood or plastic cores and sheet-metal shells. Rubber edges on the tiles allow them to fit snugly where they are butted together.

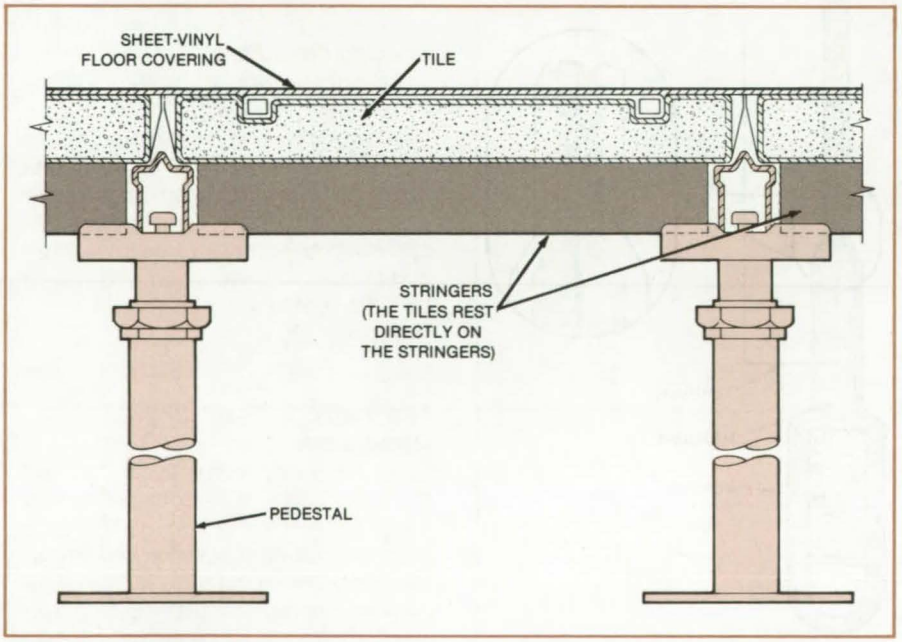

Figure 2. The **Support Grid** consists of a network of pedestals and stringers. Tiles are laid flat on the stringers. The vinyl sheet is laid on the tiles with rectangular frames under the sheet engaging recesses in the tiles. The height of the pedestals is adjustable.

When the floor must be penetrated to give access to the subcavity, the vinyl covering is cut around one or more tiles as indicated by the painted grid. The cut

section of vinyl, with its locking frames, is lifted away from the tiles; and then the tiles are lifted away from the stringers and pedestals. Permanent openings in the floor system are cut directly through the center of the locking frames and floor tiles in the removed sections. Sealable collars are inserted through these openings in the floor system and cemented in place to prevent drainage into the subcavity.

After the subfloor rearrangements or repairs are finished, the tiles and sheet vinyl are replaced, with the locking frames registering exactly into their original positions. The cut edges of the polyvinyl chloride covering are then resealed using commercially-available plastic heat-welding techniques. As the color of the painted grid is selected to match the heat-welded vinyl, the resulting surface is nearly indistinguishable from the original surface.

This work was done by Marc M. Cohen of **Ames Research Center.** *No further documentation is available.*

Inquiries concerning rights for the commercial use of this invention should be addressed to the Patent Counsel, Ames Research Center [see page A5]. Refer to ARC-11363.

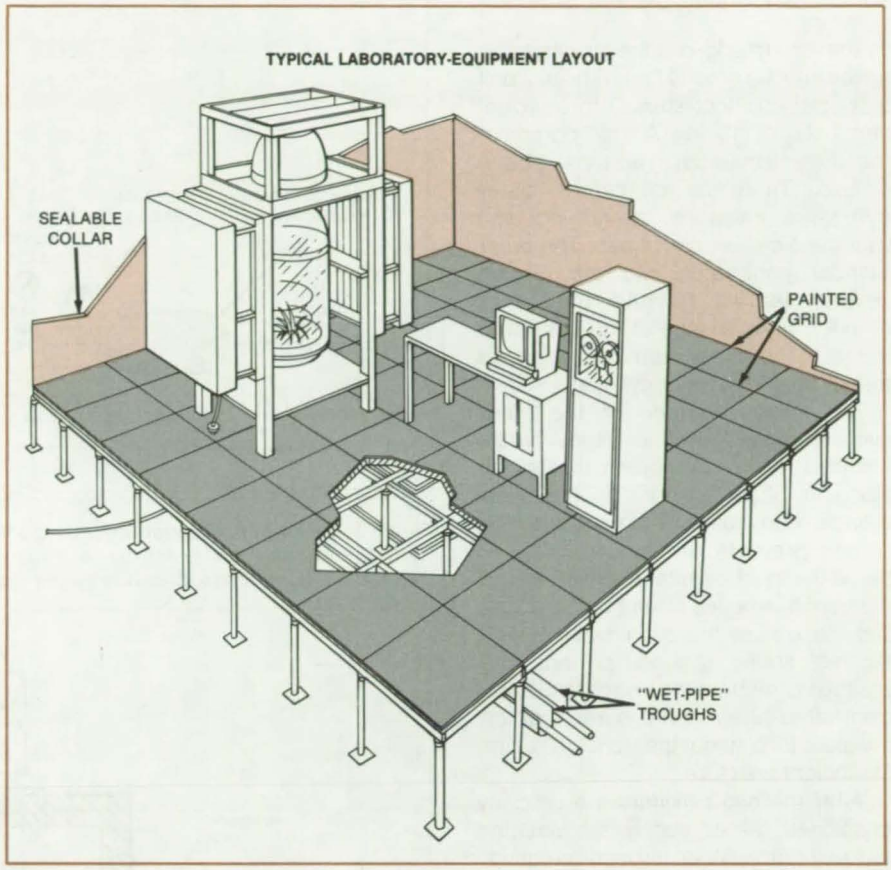

Figure 3. A **Sealable Collar** abuts the tiles around an edge or opening to prevent spillage into the cavity below the floor.

In Situ Measurement of Ground-Surface Flow Resistivity

The flow resistivity of the Earth's ground surface is measured onsite.

Langley Research Center, Hampton, Virginia

A new instrument allows in situ measurement of flow resistivity on the Earth's ground surface. Flow resistivity is the ratio of the pressure gradient across a test specimen to the volume of air flowing through the specimen per unit time. Because flow resistivity is an important parameter appearing in acoustical models of the Earth's ground surface, it is desirable to accompany measurements of acoustic ground impedance with measurements of flow resistivity.

Conventional instruments for measuring the flow resistivity are intrusive. They require that a test specimen be removed from the bulk material for testing. In the case of the Earth's surface, removal of a specimen from the ground causes immediate and irreversible changes, such as the loss of moisture and other volatiles, changes in texture and organic content, and partial or total destruction of the root system of surface vegetation. The in situ instrument is nonintrusive and permits measurement of the ground surface in its unaltered condition.

The basic components of the instrument are shown in Figure 1. Initially, the compressed-air reservoir is pressurized with air through the quick-connect input and shutoff valve. During the flow resistivity measurement, the air flows through a pressure regulator, a needle valve, flowmeters, flexible hose, and into the specimen holder. The flowmeters, which may be of the rotameter type, measure the volume velocity of the airflow. Pressure gage 3, which may be a dial gage with a Bourdon tube, measures the pressure at the inlet of the specimen holder and thus at the upper surface of the specimen. The rotameters and dial gage do not require electricity for operation and are especially convenient for use in the field.

The specimen holder, shown in detail in Figure 2, is the major component of the in situ instrument. It consists of two concentric cylinders, an inner cylinder and an outer cylinder, both made of a sturdy material such as stainless steel. The specimen of ground under test is contained within the inner cylinder. The purpose of this arrangement is to make the air pressure at the upper surface A-A of the specimen equal to the pressure measured on the pressure gage and the pressure at the lower surface B-B ap-

(continued on next page)

proximately equal to the ambient pressure.

The sharp-edged inner cylinder is driven into the ground first with the aid of a special cap (not shown) to a typical depth of 6 in. (15 cm). A small portion of the inner cylinder remains above ground. Then the concentric outer cylinder is driven into the ground, also with the aid of a special cap. The outer cylinder penetrates into the ground several inches beyond the inner cylinder. A knife edge at the bottom of the outer cylinder forms an annular trench about the inner cylinder.

The interior surface of the outer cylinder consists of a rigid, firmly-fastened cylindrical screen that slides along the inner cylinder as the outer cylinder is driven into the ground. The screen prevents the ground material below the inner cylinder from falling into the trench. A series of vent holes, drilled into the wall of the outer cylinder and located above ground, permits the passage of air from the trench to the ambient atmosphere and ensures that the pressure throughout the trench remains at ambient pressure.

After the two cylinders are properly positioned, the air supply is connected to the inner cylinder through the quick-connector fitting. A uniform flow is established in the ground specimen between planes A-A and B-B. The pressure at B-B, because of the proximity of this plane to the trench, is approximately equal to the ambient pressure. After the flow passes plane B-B, it turns radially toward the trench and passes upward through the trench and through the vent-holes. The flow through the specimen holder is indicated by arrows.

The flow resistivity R is determined from the equation

$$R = (P - R_h U)SC/UH$$

where P is the pressure as read on the pressure gage, R_h is the flow resistance of the flexible hose, S is the cross-sectional area of the ground specimen, U is the volume velocity of the airflow as measured on the flowmeters, H is the specimen depth, which is equal to the distance between planes A-A and B-B, and C is a correction factor to account for the pressure drop between plane B-B and the trench. ($C = 1 - 0.324a/H$ where a is the internal radius of the inner cylinder.)

This work was done by Allan J. Zuckerwar of **Langley Research Center.** *For further information, Circle 46 on the TSP Request Card.*

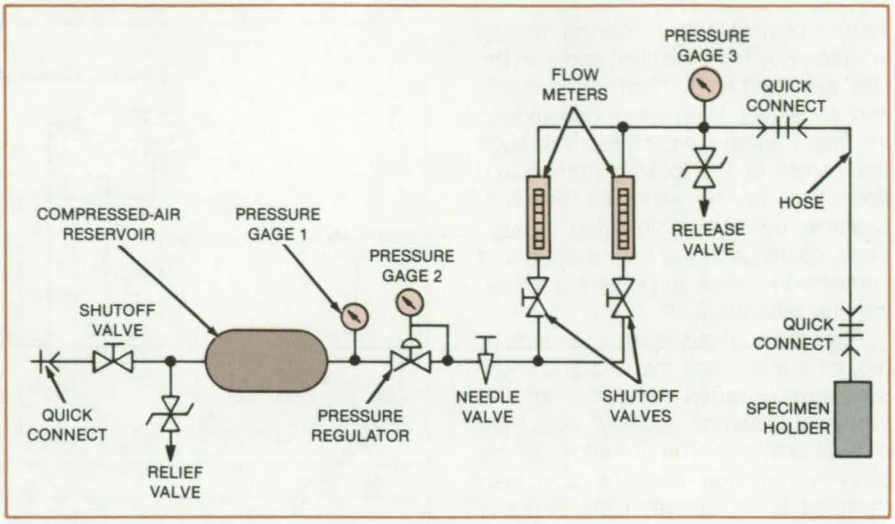

Figure 1. A **Nonintrusive Instrument** includes a specimen holder that is inserted into the Earth's surface. Flow resistivity is measured by monitoring compressed air passing through the flowmeters; pressure gages record the pressure at the ground surface.

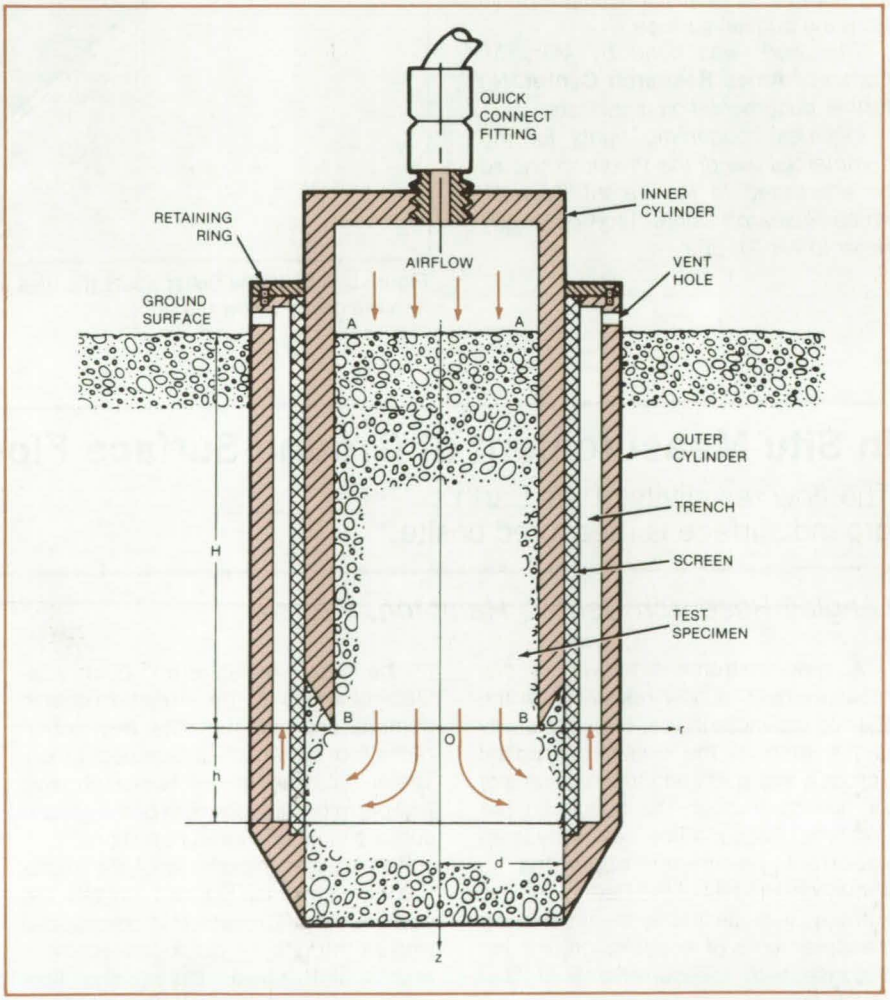

Figure 2. This **Specimen Holder** with its knife-edged inner and outer cylinders is easily driven into the ground. An air-stream, used in measuring flow resistivity of the ground, enters through the quick-connect fitting and exits through a screen and venthole.

This invention is owned by NASA, and a patent application has been filed. Inquiries concerning nonexclusive or exclusive license for its commercial development should be addressed to the Patent Counsel, Langley Research Center [see page A5]. Refer to LAR-13053.

Radially-Graduated Turbine-Temperature Profile

The flame temperature is lower at the blade roots, where stress is highest.

Marshall Space Flight Center, Alabama

A proposed scheme to change the temperature distribution in a gas-turbine flame so that it increases radially instead of remaining spatially uniform may offer important advantages. A radially increasing temperature (see figure) should allow a higher mean gas temperature, greater power output, higher rotational speed, and a longer life for the blades. The principle is suitable for an axial-flow gas turbine that is directly in line with a cylindrical combustor. Included in this category are many rocket, aircraft, stationary, and shipboard turbines.

The requisite temperature distribution can be provided by a fuel injector composed of multiple elements arranged in concentric rings. The fuel/air ratio and flame temperature would be high at the outer elements and would decrease gradually toward the center. Thus, a blade is subjected to the least temperature at the blade root (where the mechanical stress is greatest) and the greatest temperature at the blade tip (where the mechanical stress is least).

Since the ability to withstand high stress is degraded by high temperature and the ability to withstand high temperature is degraded by high stress, the graded temperature profile enables the inner portions of the turbine blades to remain further within the envelope of maximum allowable operating stress and temperature. The result should be greater blade endurance or the ability to operate at higher power or both.

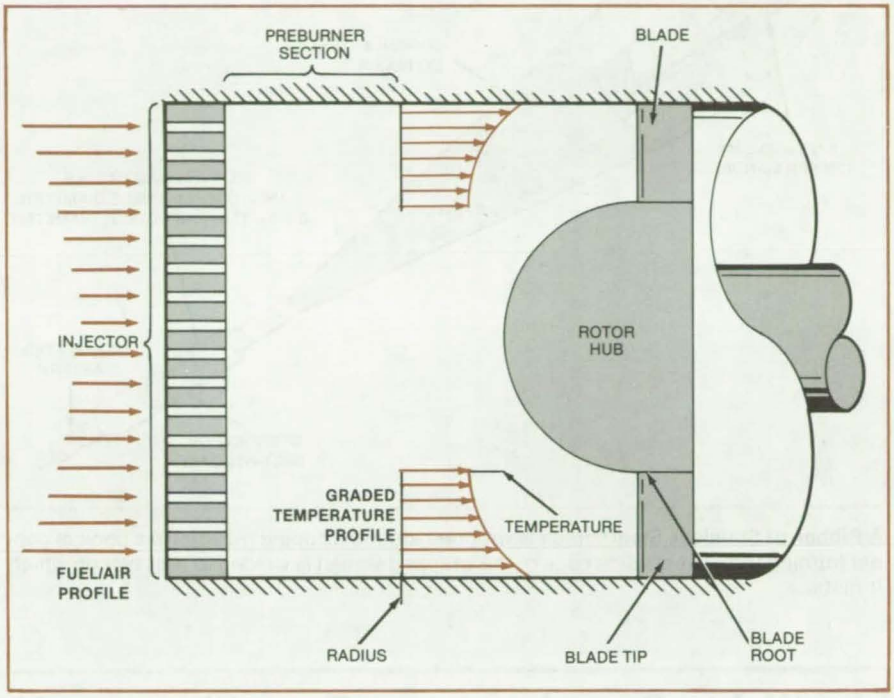

Instead of Burning Fuel Uniformly, the new fuel injector burns more fuel at the perimeter of a turbine and less toward the center. The temperature at the blade roots is thereby made lower than at the blade tips.

This work was done by William R. Wagner, Fred P. Nitz, and Maynard L. Strangeland of Rockwell International Corp. for **Marshall Space Flight Center.** *No further documentation is available.*

MFS-19831

Long Heat Pipe Transports 2.6 kW

A high-capacity heat pipe employs a slender artery-and-wick structure.

NASA's Jet Propulsion Laboratory, Pasadena, California

A long heat pipe transports thermal energy at a rate of 2,600 watts at an operating temperature of 923 K. The pipe is 14.5 ft (4.42 m) long and 0.79 inch (2 cm) in diameter. It employs two layers of 200-mesh stainless-steel screen on its inner wall as a wick to provide circumferential flow of the working fluid. Two arteries, also of 200-mesh stainless steel, provide axial flow. The arteries are 0.125 inch (3.2 mm) in inside diameter and 0.156 inch (4 mm) in outside diameter. The arteries are located between the two layers of wall wick.

The long, thin arteries are made with a special forming process. An extrusion tool (see figure) is used. A 1-inch by 15-foot (2.54-cm by 4.57-m) strip of the stainless-steel screen is fed into the large end of the conical extruder and formed into a loosely wound tube. The tube is then rolled tightly and fed to a spot-welding saddle where its seam is joined. The resulting artery is sealed at one end by twisting it into a tight strand and covering it with a stainless-steel sheath, 0.150 inch (3.81 mm) in outside diameter. The end of the sheath is welded shut.

(continued on next page)

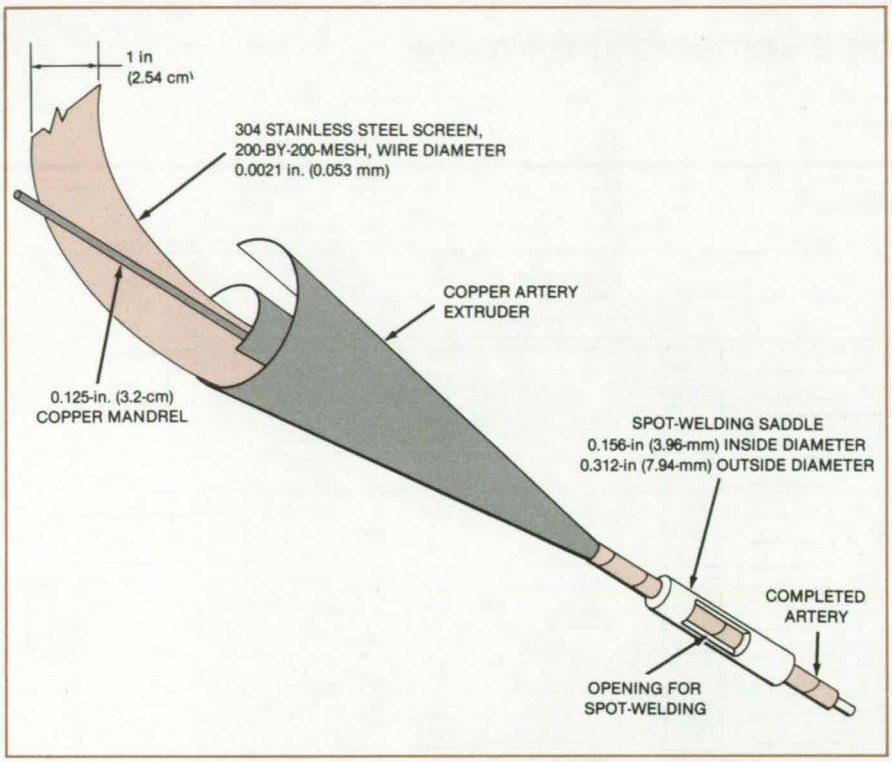

A **Ribbon of Stainless Steel** screen is wrapped around a copper mandrel in a conical copper forming tool. The outside edge of the wrapped screen is welded to the layer on which it rests.

A mandrel with two longitudinal grooves is required for the assembly of the wall-wick layers and arteries. First, a layer of screen is wrapped around the mandrel (this becomes the inner wall-wick layer). The arteries are then forced against the screen over the grooves, thus forcing part of the inner wall-wick layer into the grooves and causing that layer to follow the mandrel contour. A second layer of screen is wrapped around the first layer, covering the arteries.

The assembly of layers is inserted in the pipe, and the mandrel is pulled out. Perforated stainless-steel clips are inserted to hold the wick in place. A cap is welded to one end of the pipe. The pipe is outgassed by evacuating it to 10^{-5} torr (1.3×10^{-3} N/m^2) or less for 24 hours at 400° C. The evacuated pipe is partly filled with the sodium working fluid by distillation of the sodium into the pipe.

This work was done by Donald M. Ernst, Ernest H. Dubble, and Richard L. Copenhaver of Thermacore, Inc., for **NASA's Jet Propulsion Laboratory.** *For further information, Circle 47 on the TSP Request Card.*
NPO-16017

Identifying Boundary-Layer Transitions on Aircraft Skin

Airflow characteristics are determined from coating patterns on the aircraft skin.

Langley Research Center, Hampton, Virginia

Sublimating chemicals offer an accurate, low-cost way of indicating laminar-to-turbulent flow transitions on the surfaces of aircraft. The aerodynamic surfaces are coated with a thin film of such volatile chemical solids as naphthalene, diphenyl, acenaphthene, or fluorene. The film sublimes rapidly because of high local shear stress and heat transfer in the boundary layer. The coating appears white in the regions where the chemical has remained on the surface, indicating laminar flow; the regions where the chemical has disappeared indicate turbulent flow.

The chemical patterns can be used to identify the locations of leading-edge stagnation and of flow separation. Stagnation is observed where sublimation is first complete on the leading edge. With sparsely-distributed roughness elements near the leading edge, stagnation can be located between the apexes of the transition wedges that "point" toward each other. Separation can be observed where chemicals remain on the surface due to greatly-reduced heat transfer in those regions. Good control of coating thickness is essential to the accurate observation of these phenomena.

The chemicals used differ in their rate of sublimation, naphthalene being the fastest to sublime and fluorene being the slowest. Fluorene has an advantage of being fluorescent under UV light. The chemicals are selected depending on ambient temperature at the test altitude, with colder temperatures requiring faster sublimating chemicals. Acenaphthene, for example, is useful for subsonic and transonic flight testing at ambient temperatures between 0° and 40° C. Typical sublimation time at these temperatures, using average coating thickness, is 120 and 5 minutes, respectively.

The chemical cost to treat a moderate-size airplane with 100 ft^2 (9.3 m^2) of wing area is about $10 (1982 dollars). Suitable solvents for these chemicals include 1,1,1-trichloroethane (TCE), acetone, or Freon TF.

Because the chemical coating is white, the surface to be sprayed should be dark. A light-colored surface shows the transitions but is difficult to photograph. The surface should not be allowed to heat up in Sunlight because the heat can cause sublimation before the takeoff. Early morning or late afternoon test periods with low Sun angles are best.

The chemical is applied with a spray gun that has a flat fan nozzle with minimum orifice and needle sizes, the orifice diameter being between 0.030 and 0.040 in. (0.76 and 1.02 mm). The gun is operated at about 25 psi (173 kN/m^2) air pressure or 5 psi (34 kN/m^2) fluid pres-

sure if a pressure feed sprayer is used. For proper dry spraying, the spray nozzle should be held between 15 to 20 in. (38 to 50 cm) from the surface, indicated by a powdery appearance of the chemical coating.

Before the coated aircraft takes off, it should be brushed with a large, soft-bristle brush or wiped with cheesecloth to loosen any particles that may have adhered to the coating. This prevents turbulent wedges, which if too numerous, can obliterate the free transition location. Extra-thick coatings are useful in extending the sublimation time of the more volatile chemicals in experiments at high altitudes.

The spraying solution is prepared by dissolving one part of the chemical solute by volume in eight parts of solvent. A convenient way to measure these amounts is to mix 100 ml of chemical in 1 qt (0.95 l) of solvent. The solution is sprayed when the solute is completely dissolved. A standard application rate is 1 qt per 20 to 30 ft^2 (0.95 l per 2 to 3 m^2) of surface area. With acenaphthene, such a coating thickness has a sufficiently long reaction time to permit ample time to run the flight test without creating confusing chemical patterns. The resulting data are readily observed and recorded on the ground.

During the test flight, the indicated test speed and altitude should be held as long as practical. If the burned fuel lightens the airplane by more than about 10 percent during the test, a speed schedule should be worked out to keep the airplane lift coefficient constant.

A very small, thick piece of masking tape located within 6 in. (15 cm) of the wing leading edge can serve as a boundary-layer trip, a "calibrated" indication of the rate of chemical-transition pattern development. This trip should be visible to the pilot. When the chemical pattern appears mature, the pilot can bring the aircraft down as near to the indicated test speed as is safe. Typically, pattern development times are greater than 10 minutes, allowing ample time for normal approaches and landings.

This work was done by Bruce J. Holmes, Cynthia C. Croom, and Warren C. Kelliher of **Langley Research Center** *and Clifford J. Obara of Kentron International, Inc. For further information, Circle 48 on the TSP Request Card.*
LAR-13089

Integrated Tactile Sensor for Robots

A silicon wafer would transduce, compute, and communicate touch information.

NASA's Jet Propulsion Laboratory, Pasadena, California

A proposed large-scale integrated (LSI) circuit would give robots, parts-handling machines, and remote-control devices a sense of touch. The LSI circuits, placed on the contact surfaces of manipulators, would combine the functions of transduction, computing, and communicating.

The entire surface of an LSI wafer would be used as an array of tactile sensors with sensing material connected directly to computation elements in the wafer. These elements would process and reduce the raw sensory data and send the resulting signals to a control computer. By combining functions, the concept reduces the signal bandwidth, the number of connecting wires, weight, and power consumption while permitting high tactile resolution.

A key feature of the concept is that computation at the site of transduction permits useful information to be extracted from the raw tactile image and selectively communicated to a central controller. For example, manipulator grasping force, touch pattern, contact area, and slippage can be extracted readily. The transmitted signals then resemble words and phrases of a high-level language instead of ones and zeros of raw data.

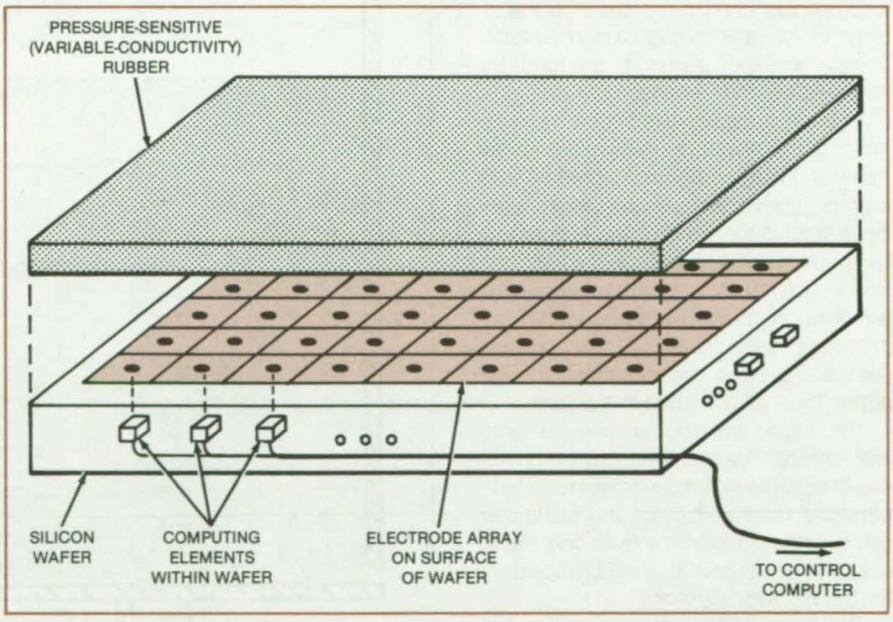

Beneath a Layer, the resistivity of which changes with pressure, electrodes furnish a pressure-dependent signal to computation elements. The electrodes and computation elements are contained in a silicon integrated-circuit wafer.

The exposed surface of the LSI wafer contains an array of pairs of electrodes covered by a sheet of electrically conductive rubber (see figure). When the rubber sheet is deformed by touch, its resistivity varies locally. Thus, current passing through the sheet between a pair of electrodes indicates the local contact pressure.

Associated with each electrode pair is a computation element consisting of an

(continued on next page)

analog comparator, a data register, and an accumulator. Each element reads the local conductivity data from its electrode pair and performs simple calculations. In addition, each element communicates directly with its nearest neighbors and indirectly with others. All elements in the array execute the same sequence of instructions simultaneously, as directed by a controller that is also in the LSI wafer. Together the elements form a tactile-pattern parallel processor.

The processor could store one or more of a variety of algorithms useful in image processing and pattern recognition. A distributed shift register allows all outputs from the wafer to be communicated over a conveniently compact channel — a single wire.

Since a silicon LSI wafer is used intact instead of being sliced into many individual chips, defective chips cannot be discarded. Therefore it is necessary that redundant computation elements be provided for each tactile electrode pair and that a selection circuit be included in the wafer for choosing good elements.

This work was done by Marc H. Raibert and Raymond Eskenazi of Caltech for **NASA's Jet Propulsion Laboratory.** *For further information, Circle 49 on the TSP Request Card.*

Inquiries concerning rights for the commercial use of this invention should be addressed to the Patent Counsel, NASA Resident Office-JPL [see page A5]. Refer to NPO-15094.

Continuous-Reading Cryogen Level Sensor

Tank contents are indicated accurately despite variations in liquid density.

Marshall Space Flight Center, Alabama

Two pressure transducers are used in a system for measuring the amount of cryogenic liquid in a tank. The system provides continuous measurements accurate within 0.03 percent.

Vibrating-cylinder pressure transducers are situated outside the tank — at the bottom and at the top (see figure). Each sensor communicates with the interior of the tank through a narrow tube. Cryogenic vapor transmits the local liquid pressure to the sensor.

In each pressure transducer, a magnetic coil vibrates a thin-walled metal cylinder. Another electromagnet senses the vibration of the cylinder, the frequency of which depends on the pressure and temperature of the vapor in the cylinder. From the pressure measurements, temperature measurements within the pressure sensors, and tank cross-sectional area, a microprocessor computes the mass of liquid in the tank.

The same transducer can be used with different gases. The frequency-versus-pressure and frequency-versus-temperature relationship for the particular gas is programed into a read-only memory chip, which provides calibration data for the microprocessor.

The new system allows continuous sensing, not just at the discrete heights at which level sensors are located. Moreover, the new method is unaffected by localized variations in composition and density as are capacitance-sensing schemes.

This work was done by Frank E. Barone, E. C. Fox and S. W. Macumber of Martin Marietta Corp. for **Marshall Space Flight Center.** *For further information, Circle 50 on the TSP Request Card.*

MFS-25873

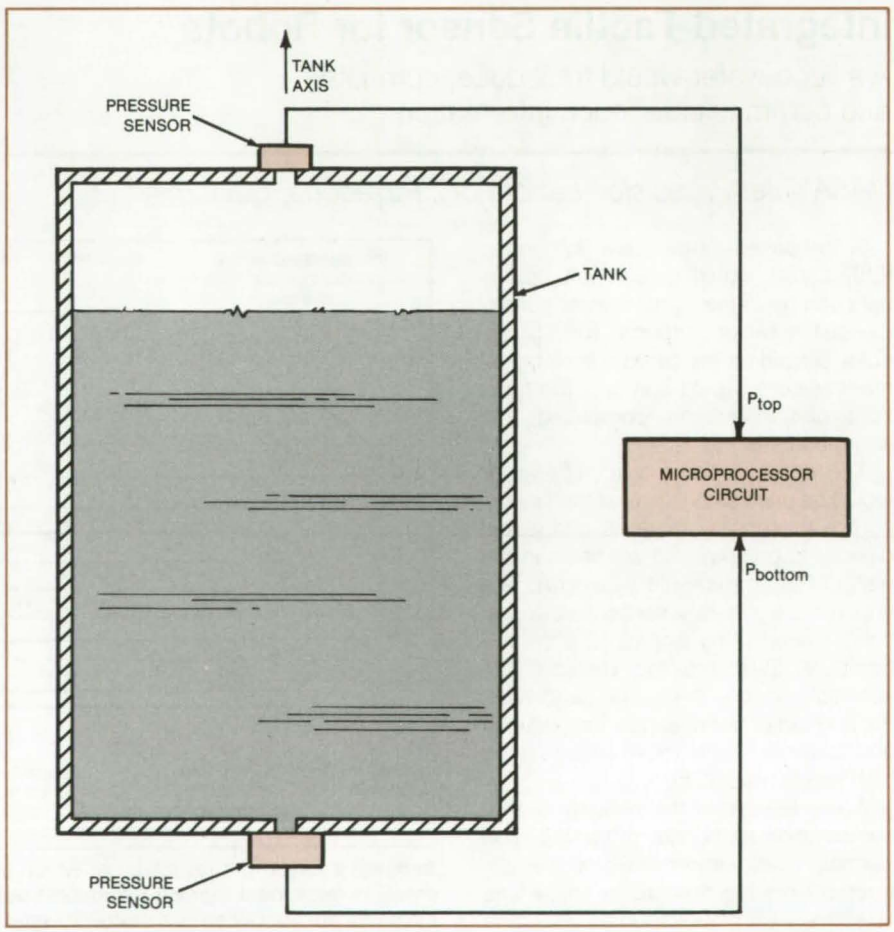

Sensors Determine Pressure in the liquid and vapor in the tank. A microprocessor uses the pressure difference to compute the mass of cryogenic liquid in the tank.

General-Purpose Icosahedral Structure

A versatile modular structure is based on triangular panel units.

Goddard Space Flight Center, Greenbelt, Maryland

A scheme originally proposed for assembling structures in space is based on a geodesic sphere approximated by a regular icosahedron. The structure is rigid and lightweight. It allows access to all subsystems and equipment from the outside, and its components can be carried by the Space Shuttle. A comparable terrestrial structure could be assembled from components carried in a truck or ship.

The "sphere" shown in the figure is composed of 20 panels, all equilateral triangles 12 feet (3.66 m) on a side. When assembled, the panels form an approximately spherical structure 23 feet (7 m) in diameter.

Each panel is secured at its apexes to a five-sided adapter with a single bolt. The adapter allows limited moments and thus differs from a true geodesic member, which acts only in tension and compression.

Electrical cables are routed along the edges of the panels. For example, power cables from the panels containing solar-cell arrays can be run along the panel edges to the power panel containing batteries and regulators. Similarly, cables can be run from the command and data panels to the experiment and propulsion panels.

Any panel can be removed from the sphere and replaced. The structure will not collapse because it has redundant load paths.

The panel and structure size can be increased by combining panels to make a larger triangular panel. Four 12-foot panels can be combined as a triangle 24 feet (7.3 m) on a side. Nine panels can be combined as a triangle 36 feet (11 m) on a side.

The structures can be combined with pressurized vessels for human occupants. A wide variety of configurations, incorporating multiple spheres and pressurized vessels, is possible. In addition a large sphere can totally enclose one or more pressure vessels. A strengthened version may be useful on Earth for rapidly-erectable temporary shelters, industrial structures, or playground equipment.

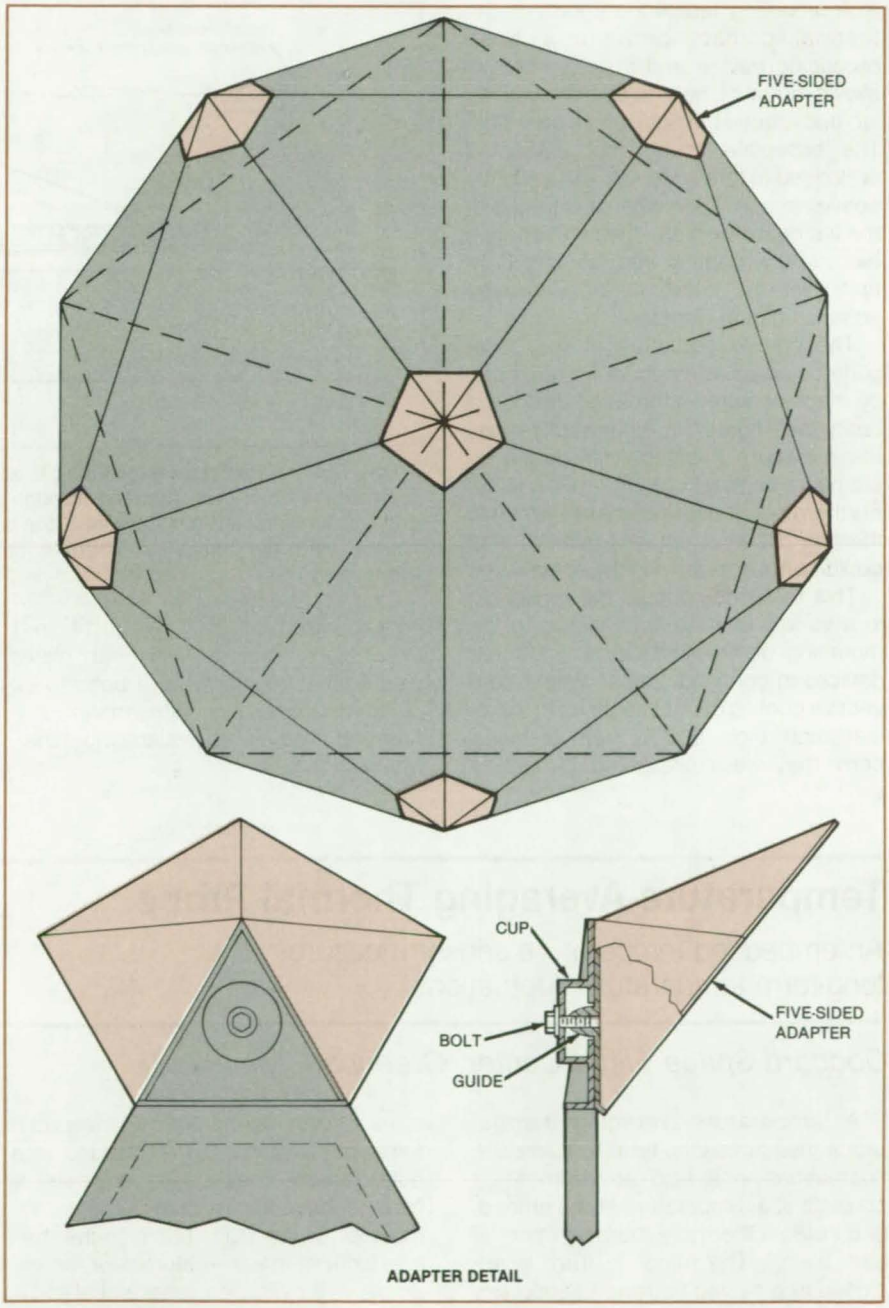

A **Regular Icosahedron** is constructed from triangular panels. The five panels that meet at each corner are all rigidly attached to a five-sided adapter.

This work was done by Jack Evans of **Goddard Space Flight Center.** *For further information, Circle 51 on the TSP Request Card.*

This invention is owned by NASA, and a patent application has been filed. Inquiries concerning nonexclusive or exclusive license for its commercial development should be addressed to the Patent Counsel, Goddard Space Flight Center [see page A5]. Refer to GSC-12854.

Low-Thermal-Resistance Baseplate Mounting

A convex baseplate flattens into large-area contact when bolted down.

Marshall Space Flight Center, Alabama

A mounting technique improves the thermal contact between a heat-producing device and a heat sink, yet allows mounting bolts to be conveniently located around the edge of the heat sink. The baseplate of the hot device is preloaded to force it to assume a slightly convex shape. Then when it is bolted to the flat heat-sink plate, the two surfaces flex slightly, coming into intimate contact over the entire surface, thereby enhancing heat transfer.

The convex curvature of the baseplate could be introduced, for example, by machine screws threaded through a beam (see figure). In other applications the curvature might be introduced by stamping or machining the plate itself. Furthermore, it does not matter which of the two plates is convex: indeed, they could both be made slightly convex.

This technique should be applicable in a variety of situations, including the mounting of heat-producing electronic devices in confined spaces where convective cooling cannot be used. In the initial application, 600 W from a power converter, were dissipated through a contact area of 220 $in.^2$ (0.14 m^2). Previous mountings with flat plates would have required more bolts to be distributed over the entire mating surfaces to produce equivalently low thermal resistance.

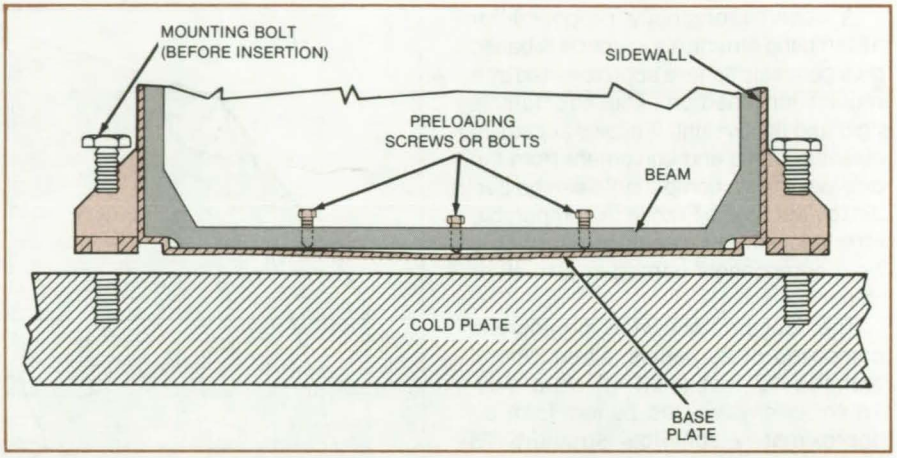

A **Low-Thermal-Resistance Mounting** is achieved by preloading the baseplate to a slight convexity with screws threaded through the beam. As the mounting bolts around the edge of the baseplate are tightened, the baseplate and the cold plate contact first in the center, with the region of intimate contact spreading outward as the bolts are tightened.

This work was done by William T. Perreault of Martin Marietta Corp. for **Marshall Space Flight Center.** *No further documentation is available.*
MFS-25908

Temperature-Averaging Thermal Probe

An embedded temperature sensor measures long-term temperature fluctuations.

Goddard Space Flight Center, Greenbelt, Maryland

A temperature-averaging thermal probe measures long-term temperature fluctuations in a fluid environment. It consists of a temperature probe embedded inside a thermally massive material (see figure). The mass, in turn, is enclosed in a sealed housing to suppress the effects of cyclical and short-term fluctuations in temperature. The probe measurements can be used to estimate powerplant heating and cooling loads, to map temperature profiles, and to calibrate more-sensitive temperature probes.

As shown in the figure, the probe temperature sensor is embedded in a hole in the solid heat-conducting mass; a heat-conducting material fills the remainder of the hole. The high-thermal-conductivity mass — aluminum, for example — is cylindrical or spherical and is mounted on a thermally insulating material that holds it away from the thin housing walls. The housing too is constructed of a thermally conductive material. Prototypes of the probe have a box-shaped housing.

The total surface of the housing is made large enough to maximize the heat flow rate in and out of it. However, the housing surface is not so large as to create a thermal mass of fill gas that is significant compared to the solid thermal mass.

The temperature of the housing is about equal to the instantaneous temperature of the fluid surrounding the housing, while the temperature of the enclosed mass lags behind the temperature of the fluid. The separation of the housing and mass creates a limiting thermal resistance that, together with the mass, determines the thermal time constant — that is, the period of time for

temperature averaging — of the probe independently of the velocity of the fluid contacting the exterior of the housing. The value of the probe time constant can be tailored to different applications by increasing or decreasing the thermal mass; for example, by replacing a mass with one of either smaller or greater thermal conductivity.

The housing can contain either a gas filling or a vacuum. A vacuum would have a longer time constant than a gas filling and would transfer heat by radiation rather than convection.

This work was done by Lou F. Kalil and Victor Reinhardt of **Goddard Space Flight Center.** *For further information, Circle 52 on the TSP Request Card.*

This invention is owned by NASA, and a patent application has been filed. Inquiries concerning nonexclusive or exclusive license for its commercial development should be addressed to the Patent Counsel, Goddard Space Flight Center [see page A5]. Refer to GSC-12795.

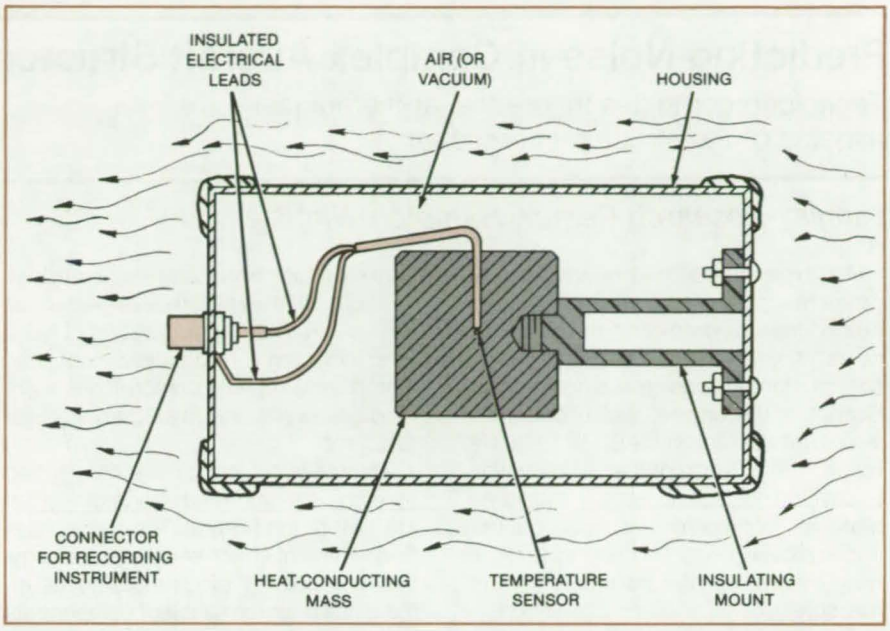

The **Heat-Conducting Mass Is Enclosed** in a sealed housing to shield the thermal mass so that the rate of heat transfer to it is not affected by the circulation of the outside fluid environment. The heat-conducting mass and surrounding mass of air, or vacuum, trapped inside the housing shield the temperature sensor from the effects of short-term and cyclical environmental temperature fluctuations.

Autocovariance Computer

Hardware implementation is fast enough for real-time flow-field diagnostics.

Langley Research Center, Hampton, Virginia

A laser-velocimeter covariance processor calculates the autocovariance and cross-covariance functions for a turbulent flow field, based on Poisson-sampled measurements in time from a laser velocimeter. The unit processes a block of data up to 4,096 data points in length and returns a 512-point covariance function with 48-bit resolution along with a 512-point covariance-function-normalizing histogram of the interarrival times. The processor interfaces with and is controlled by a minicomputer. A typical 4,096-point computation takes approximately 1.5 seconds; i.e., to receive the computer data, to compute the covariance function, and to return the results to the computer.

Classically, correlation functions and turbulence power spectra are determined by direct correlation techniques, Fourier-transform techniques, or both, using uniformly sampled data. In laser velocimeter applications, however, the sampling process is random. Since the measured particles arrive according to Poisson's distribution, classical approaches become inapplicable. A modified direct correlation approach, however, may be used in which the random interarrival times (the time between successive velocity measurements) are used to determine the appropriate delay time interval into which the cross-product is to be summed.

The hardware implementation of the software algorithm processes the correlation function from data obtained by a laser velocimeter. The unit allows the computation of both autocorrelation and cross-correlation functions and performs a correlation computation approximately 200 times faster than does a 16-bit minicomputer while maintaining equal accuracy. This increase in speed is obtained by using high-speed digital circuitry and parallel processing techniques.

This hardware implementation of the correlation technique to a laser velocimeter flow-field diagnostic system is fast enough for online production applications. The unit allows not only online computation of velocity component autocorrelations but determines cross-correlation functions between components, velocity magnitude, and flow angles.

This work was done by James F. Meyers of **Langley Research Center** *and Timothy E. Hepner of the U.S. Army Aviation Research and Development Command. For further information, Circle 53 on the TSP Request Card.*

This invention is owned by NASA, and a patent application has been filed. Inquiries concerning nonexclusive or exclusive license for its commercial development should be addressed to the Patent Counsel, Langley Research Center [see page A5]. Refer to LAR-12968.

Predicting Noise in Complex Aircraft Structures

Technique combines theoretical and empirical aspects of the structural components.

Langley Research Center, Hampton, Virginia

An experimental and analytical program has produced test and analysis procedures for predicting the extent of noise generated in aircraft. The major source of interior noise in single-engine aircraft is the engine, which produces structural vibration in the 60- to 1,600-Hz range. The purpose of the program was to develop ways of screening candidate materials considered for noise control and to establish test procedures for verifying the choice of a particular control measure.

The program focused on a laboratory-based test procedure to simulate engine-induced structurally transmitted noise, to test a range of noise isolators for relative performance and for basic data for analytical model correlation, and to develop an analytical model for isolator design. The test procedure for simulating engine-induced noise involved direct excitation of a rigid engine with an electrodynamic shaker. Candidate noise-control measures were then evaluated from transfer-function data obtained as interior-sound pressure-level response for a given force input. A series of isolators, including a rigid baseline set, was tested; and relative comparisons were made between the measured transfer functions.

An analytical model was developed by empirical characterization of the aircraft aft of the firewall. The model uses finite-element structural analysis and dynamic modeling procedures to determine noise performance of components forward of the firewall. Coupling procedures are used to combine contributions to noise from the various components.

Analytical modeling of the simulated engine, vibration isolators, and engine mount structure was combined with an empirical model of the fuselage to develop a more-realistic noise-transmission model of the test aircraft. A comparison of the predicted structure-borne noise transmission with the laboratory measurements showed that the frequency dependence of the isolator material plays a major role in the noise transmission. Isolator stiffness is a dominant parameter, while the isolator damping characteristic is much less significant.

Results from the tested aircraft show that moderate changes to the engine mount structure do not significantly affect the noise transmission. The developed modeling procedures seem adequate for the evaluation of the relative performance of candidate noise isolators.

This work was done by James F. Unruh and Dennis C. Scheidt of Southwest Research Institute for **Langley Research Center**. *Further information may be found in NASA CR-3427 [N81-25766/NSP], "Engine Isolation for Structural-Borne Interior Noise Reduction in a General Aviation Aircraft" [$16]. A copy may be purchased [prepayment required] from the National Technical Information Service, Springfield, Virginia 22161.*

LAR-13032

Cooldown Strategy for Cryogenic Wind Tunnels

Research reveals ways to reduce both time and LN_2 energy consumption during cooldown.

Langley Research Center, Hampton, Virginia

Criteria substantiated by experimental and real-time simulation data ensure optimal utilization of liquid nitrogen (LN_2) injected for cooling the 0.3-m transonic cryogenic tunnel (TCT) at NASA's Langley Research Center. The results and trends observed during the study can be extrapolated to reduce time required and energy expended in cooling other similarly-constructed cryogenic wind tunnels.

The research included simulated cooldowns using procedures normally employed by each of several TCT operators, simulated cooldowns at constant mach number, simulated cooldowns at various constant fan speeds, and simulated cooldowns at constant metal-to-gas temperature differences. The effects of high and low LN_2 flow rates on cooling time and LN_2 consumption were also investigated. Normal cooldowns, used to show the wide variations in both time and LN_2 consumption that can occur, were made completely open-loop (temperature, pressure, and fan speed), while all other simulated cooldowns used automatic closed-loop pressure-feedback control.

The study showed that open-loop cooldown techniques are a dominant factor in determining the total LN_2 consumption when the cooldown of a cryogenic wind tunnel is manually controlled. In general, relatively low fan speeds (900 to 1,200 rpm) or mach numbers (0.20 to 0.35) during the cooldown are much more time- and energy-efficient when the tunnel is cooled from the ambient to cryogenic temperatures (300 to 100 K). Results showed that much less LN_2 is used if the fan speed or mach number is low during cooldown.

Moderate rates of LN_2 injection (1.2 to 1.8 kg/s), which allow efficient use of both the sensible and latent heats of the injected LN_2, preclude excessive LN_2 consumption during the cooldown. Because of reduced operator attention required as well as decreased LN_2 consumption, it is recommended that the cooldowns at constant fan speed of 1,200 rpm and an LN_2 injection rate of about 1.5 kg/s should be used routinely

for the Langley TCT. This will ensure a fairly low metal-to-gas temperature difference throughout the cooldown while simultaneously allowing the cooldown to proceed at an acceptable rate. Cooldown at higher pressures at mach numbers above about 0.30 is not advocated, because LN_2 consumption and cooldown time drastically increase with lower metal-to-gas temperature difference. Finally, because of the additional LN_2 penalty to be paid for high tunnel pressure buildup, it is better to use existing higher pressures (if possible) when commencing cooldown.

This work was done by Jerry J. Thibodeaux of **Langley Research Center.** *Further information may be found in NASA TM-84527 [N83-10082/NSP], "Sensitivity Analysis of Cool-Down Strategies for a Transonic Cryogenic Tunnel" [$8.50]. A copy may be purchased [prepayment required] from the National Technical Information Service, Springfield, Virginia 22161.*
LAR-13012

Internally Mounting Strain Gages

An inflated tube evenly distributes pressure against the gage.

Goddard Space Flight Center, Greenbelt, Maryland

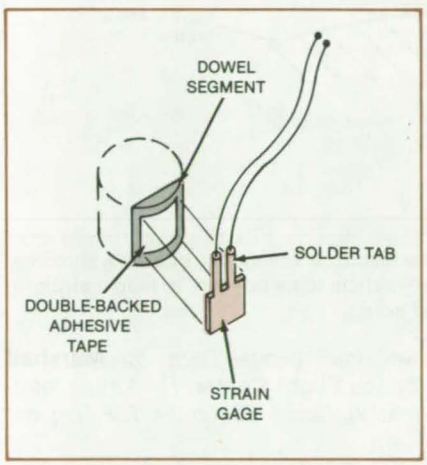

Figure 1. The **Strain Gage Is Attached** to a segment taken from a large cylindrical object. The segment is wider and longer than the gage and conforms to the shape of the bolt hole. A piece of tape with adhesive layers on both sides holds the foil gage against the surface of the segment.

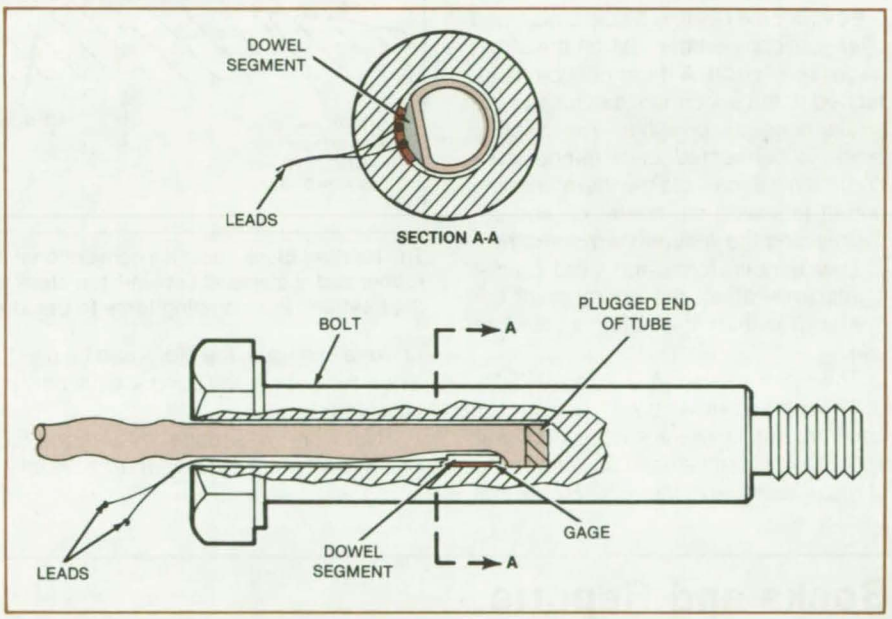

Figure 2. The **Tube, Segment, and Strain Gage** are inserted into the hole in the bolt until the gage adjoins the adhesive-coated area to be gaged. The close correspondence between the curvature of the segment and the curvature of the interior of the hole assures that upon inflation of the tube the full surface of the strain gage will be firmly compressed against the adhesive on the area to be gaged.

A technique for mounting strain gages inside a bolt or cylinder simultaneously inserts the gage, an attached dowel segment, and a length of expandable tubing. The expandable tubing holds the gage in place while an adhesive cures, assuring even distribution of pressure on the gage and area to be gaged.

The gage is attached to a segment of solid material, such as a dowel segment (see Figure 1). A pair of insulated electrical leads is soldered to the gage. A reference mark placed on the leads indicates the depth of the gage in the hole.

Once the leads are connected and the gage attached to the segment, the gage is alined with and held against a length of expansible material, such as surgical hose with an outer diameter slightly less than the hole diameter. The hose is sealed at one end.

After the hole is cleaned, an adhesive is applied to the surface where the gage is to be attached, to the gage, and to both of the leads up to their reference marks. The gage, segment, leads, and tube are then inserted into the hole until the reference marks on the leads are even with the top of the bolthead (see Figure 2).

When the tubing is inflated, it expands and forces the gage against the area to be gaged. The tube remains inflated until the adhesive cures. After the permanent bond forms, the pressure on the tube is released, and the end of the tube protruding from the bolt is sliced off flush against the bolthead.

This work was done by Jay R. Jett, Jr., of Northrop Services, Inc., for **Goddard Space Flight Center.** *For further information, Circle 54 on the TSP Request Card.*

This invention is owned by NASA, and a patent application has been filed. Inquiries concerning nonexclusive or exclusive license for its commercial development should be addressed to the Patent Counsel, Goddard Space Flight Center [see page A5]. Refer to GSC-12824.

Heater Ensures Strain-Gage Bond Reliability

Adhesive cure temperature is controlled by an embedded heater.

Marshall Space Flight Center, Alabama

An aluminum block with an embedded heating element provides concentrated and controllable heat for curing strain-gage adhesives. The device replaces heat lamps and hot-air guns: It provides higher temperatures, allows shorter curing times, and ensures a more reliable bond.

In a NASA application, the small aluminum block incorporates an 80-watt electric heater. After the strain-gage adhesive has been applied to the test specimen, the heating block is clamped over a silicone-rubber pad on the strain gage (see figure). A thermocouple is attached to the specimen, as close to the strain gage as possible. The heating block is connected to a temperature controller, which uses the thermocouple output to switch the heater on and off, maintaining the required temperature.

Low temperatures and wind do not significantly affect the operation of the heater. It is therefore suited to outdoor use.

The block measures 1.75 by 0.75 by 0.5 inches (4.4 by 1.9 by 1.3 centimeters). Unlike a suction-cup heat applicator, it can be used on specimens of radius less than 3 inches (7.6 cm); and unlike a heat gun, the block can be used when the path to the bond area is partly obstructed.

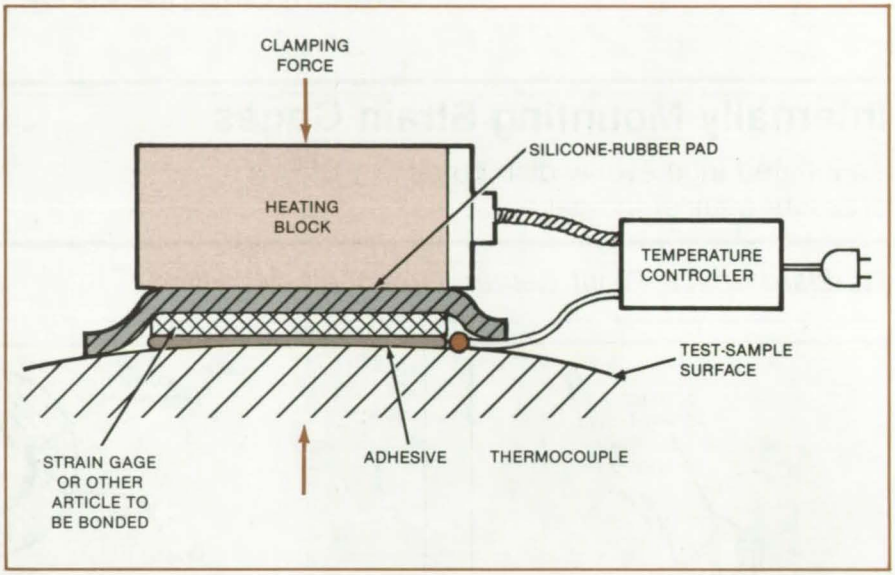

The **Heating Block** houses a conventional tubular electrical-resistance heater. A silicone-rubber pad is clamped between the block and the article to be bonded, to help distribute the heat and the clamping force to the affected area.

This work was done by Jeffrey K. Brown and Mark L. Davenport of Rockwell International Corp. for **Marshall Space Flight Center.** *For further information, Circle 55 on the TSP Request Card.*

MFS-19859

Books and Reports

These reports, studies, and handbooks are available from NASA as Technical Support Packages (TSP's) when a Request Card number is cited; otherwise they are available from the National Technical Information Service.

Mathematical Instability Criteria for Elastic Structures

The vanishing of hyperbolic terms has physical significance.

A theoretical paper discusses the physical significance of the vanishing of hyperbolic coefficients in equations of elastodynamics. As is often the case when partial differential equations fail or change type for certain values of the system parameters, the properties of the mathematical solutions also change fundamentally. In the case of equations describing elastic structures, mathematical instabilities that occur at such critical points correspond to the onset of such physical phenomena as growing oscillations, buckling, or wrinkling.

The paper presents a generalized approach to structural elastodynamics as part of a continuing effort to develop mathematical stability criteria for structures and to simulate postinstability behavior of elastics in general. The equations of motion of elastics are presented in a generalized form. Local accelerations are expressed in terms of externally-applied force densities and spatial derivatives of the potential energy of strains. There is postulated an infinitesimal initial disturbance for which the equations of motion can be linearized during an infinitesimal time.

The equations of motion are put in the form of matrices, the eigenvalues of which are the squares of characteristic roots of the equations of motion. The appearance of negative eigenvalues (and, consequently, of imaginary roots) leads to a violation of the continuous dependence between initial and transient disturbances during an arbitrarily short time and within an arbitrarily selected volume. Examples of physical phenomena with such mathematical behavior include a string or film that is not under tension or which one attempts to compress along its length or surface.

The failure of a hyperbolic form is illustrated by the example of an ideally flexible pipe (or hose) under tension, in

which flows an ideal inviscid fluid. If the end of the hose or pipe is not under tension or otherwise held, then the failure of hyperbolicity predicts that the flow of fluid out the end will cause an instability. In fact, the free end of a hose is known to whip around when a fluid flows out of it.

This work was done by Michail Zak of Caltech for **NASA's Jet Propulsion Laboratory.** *To obtain a copy of the paper, "On the Failure of Hyperbolicity in Elasticity," Circle 56 on the TSP Request Card.*
NPO-15090

Improvements in Vibration-Analysis Technique

A shortcut reduces computation time.

Two reports present further details of the vibration-analysis technique described in "Vibration Analysis Reduces Computer Time" (MFS-25711), page 176, *NASA Tech Briefs,* Vol. 7, No. 2 (Winter 1982). Intended for use in designing spacecraft where the same booster is to be flown with any of a number of interchangeable payloads, the technique is also applicable to large stationary structures, land vehicles, airplanes, ships, or wherever vibration analysis must be done repeatedly after each of many design changes.

The technique is a scheme for the accurate and efficient numerical integration of the coupled equations of motion of a vehicle and its payload(s). It involves no initial approximations or assumptions and is more exact than normal-mode methods that include such assumptions.

The full coupled equations of motion are derived, then transformed to eliminate superfluous terms relating to the vehicle/payload interface degrees-of-freedom. The interface-load-transformation method can just as well be applied to several payloads as to one payload, since the approach and the form of the equations remain the same. The result is a set of reduced equations in matrix form that permits more efficient use of computer time than would the full coupled-system matrices.

A shortcut integration technique called the "base-drive" technique gives a fast solution when the feedback from the payloads to the vehicle is neglected. The equations of motion of the vehicle are first solved, neglecting completely the payload terms. The vehicle solution provides the forcing function for the payload equations.

The payload solution includes terms that represent the feedback from the payload to the vehicle. If the feedback terms are small, they are neglected in the vehicle equations, and the solutions are accepted. When the feedback terms exceed preset values, it is necessary to resort to the full coupled equations. An appropriate computer program would minimize computing time by switching to the base-drive technique whenever it is permissible according to the smallness criterion. Further research is required to answer the question of what constitutes "small" feedback terms.

This work was done by Remi C. Engels of Martin Marietta Corp. for **Marshall Space Flight Center.** *To obtain copies of the reports "An Integration Scheme To Determine the Dynamic Response of a Launch Vehicle With Several Payloads" and "A Short-Cut Version of an Integration Scheme To Obtain the Response and Loads of a Coupled Booster/Payload(s) System," Circle 57 on the TSP Request Card.*
MFS-25919 and MFS-25920

Advances in Multivalued-Velocity Theory of Turbulence

Oscillatory behavior is found in some fluid systems.

Further developments have been reported in the modeling of fluid turbulence as a superposition of a number of interpenetrating velocity fields. (This model was previously discussed in "Multivalued-Velocity-Field Model of Turbulence," (NPO-15748) on page 432 of *NASA Tech Briefs,* Vol. 7, No. 4.) The multivalued-velocity model may have practical implications in the design of aircraft, turbines, nozzles, pumps, and other systems that involve turbulent flow.

As described in the earlier article, the multivalued-velocity field is mathematically represented as a vector that depends not only upon space and time but also upon a multivaluedness parameter, ξ. In cases in which the multivalued-velocity field tends to exhibit instabilities like those of classical single-valued-velocity fields, it may be necessary to introduce a second degree of multivaluedness. In that case, ξ becomes $\xi^{(1)}$ and the further complication of the field at $\xi^{(1)}$ is expressed as a function of $\xi^{(2)}$. The multivalued-velocity field is conveniently decomposed into a center-of-inertia component v_C, which is analogous to the classical single-valued velocity, plus the multivalued pulsational component $v_r(\xi)$.

The equations of fluid motion are treated by a variational method, using the principle of virtual work. An arbitrary tensor having the dimensionality of stress is introduced as a Lagrange multiplier. The solution of the variational equations leads to a stress-tensorlike function having the same degree of multivaluedness as that of the fluid velocity. A classical or single-valued stress-tensor component T_{CC} is obtained by integrating over the multivaluedness parameter(s). The stress tensor is found to play the role of a reaction to the mathematical constraint of single valuedness of velocity; that is, the single valuedness of velocity becomes equivalent to the possiblity of introducing a stress tensor. The resulting equations show how the behavior of the classical velocity component depends on the behavior of the multivalued pulsational component and vice versa.

The new formalism has been applied to a number of fluid problems, including notably the Navier-Stokes equations for a viscous fluid. Though the multivalued-velocity approach also leads to mathematical instabilities in many cases, the introduction of ever higher degrees of multivaluedness or ad hoc higher-order viscosity parameters can force the solutions to become mathematically stable. In both viscous and inviscid cases, the equations can be made to predict a stable regime of oscillations that are both finite and independent of the initial conditions as in the case of real turbulence.

This work was done by Michail A. Zak of Caltech for **NASA's Jet Propulsion Laboratory.** *To obtain a copy of the report, "A Study of Post-instability in Fluids," Circle 58 on the TSP Request Card.*
NPO-16006

Computer Programs

These programs may be obtained at very reasonable cost from COSMIC, a facility sponsored by NASA to make new programs available to the public. For information on program price, size, and availability, circle the reference letter on the COSMIC Request Card in this issue.

System for Structural Synthesis Combines Finite-Element Analysis and Optimization Programs

Two programs are combined to solve a variety of structural optimization problems.

The Programming System for Structural Synthesis, EAL/PROSSS, provides a structural-synthesis capability by combining the EAL and CONMIN computer programs with a set of interface procedures. EAL is a general-purpose finite-element structural-analysis program, and CONMIN is a general-purpose optimization program. The user supplies two smaller problem-dependent programs to define the design variables, constraints, and objective function.

Unlike many other structural optimization programs, the design variables, constraints, and the objective function can be represented in EAL/PROSSS by any choice of quantities, or combination of quantities, that form input and output of structural analysis. This allows one to solve practical optimization problems formulated in many differnt ways.

When the EAL/PROSSS analysis/optimization process is executed, a set of optimum design variables and minimized objective function are produced subject to a set of constraints. The applications include (a) minimum-mass design with cross-sectional areas as variables and stress constraints or (b) the first natural frequency as the objective function with overall shape design variables and stress and buckling constraints.

EAL/PROSSS can be used as follows:

a. as a research tool for the development of optimization techniques that will interface with an efficient analysis program;
b. as a research tool for testing new analysis techniques that will interface with an efficient optimization program; and
c. as an application tool that can be adapted to a wide range of problems.

The analysis and optimization programs are executed repeatedly in a looping manner until the process is stopped by a user-defined termination criterion. This part of the system is referred to as the repeatable part of EAL/PROSSS. Some of the analysis, however, such as model definition, need only be done one time and can be saved for future use. These parts are performed outside of the loop and are referred to as the nonrepeatable part of EAL/PROSSS. Five options are available for organizing optimization procedures by combining nonlinear or piecewise linears programing methods with analytic or finite-difference gradients.

The EAL/PROSSS system is written in FORTRAN IV for batch execution and has been implemented on a CDC 6000-series computer with a central-memory requirement of approximately 100K (octal) of 60-bit words. The EAL/PROSSS user must have access to the CDC version of the commercially-available EAL structural-analysis program. EAL/PROSSS was developed in 1981.

This program was written by James L. Rogers, Jr., of **Langley Research Center.** *For further information, Circle A on the COSMIC Request Card.*
LAR-13046

Minimizing Weight of Structural Designs

Approximation concepts are combined with dual-method algorithms.

The Approximation Concepts Code for Efficient Structural Synthesis (ACCESS3) combines methods to offer the structural system designer a powerful, efficient tool for the synthesis of minimum-weight designs. The approximation concepts convert the general structural synthesis problem into a sequence of explicit problems of separable algebraic form; the dual method exploits this separable form to construct a sequence of explicit dual functions. The dual functions are maximized subject to nonnegativity constraints on the dual variables. This approach is very efficient because the dimensionality of the dual space, where most of the optimization is expended, is relatively low for most structural optimization problems of practical interest.

A general class of structural optimization problems can be concisely stated as a nonlinear programing (NLP) problem involving the minimization of an objective function subject to a set of inequality constraints. For practical structural-design applications, the associated NLP problem is often very complicated due to the large number of design variables, the large set of inequality constraints, and the computational difficulties associated with the constraint functions. The ACCESS3 approach makes such an NLP problem tractable by replacing it with a sequence of relatively-small, explicit mathematical programing problems that approximate the original problem while retaining important problem features. This is accomplished through the coordinated use of design variable linking, constraint deletion techniques, and explicit approximations for retained constraints.

Structures with prescribed configurations and given material properties can be optimized so that their structural weight is minimized. This is achieved by modifying the sizing of the finite elements, in particular their cross-sectional areas or thicknesses. Types of finite elements available in the ACCESS3 program include a truss element, an isotropic constant-strain triangular membrane element, a constant-strain triangular element with arbitrary orthotropic material properties, an isotropic shear panel element, and a thermal shear panel element.

A thermal load analysis capability is included for problems involving load vectors that are dependent on design variables. In addition to the usual Taylor series expansion with respect to the reciprocals of linked design variables, natural frequency constraints may be represented as first- or second-order Taylor series expansions with respect to regular linked variables.

Four distinct optimizer algorithm options are available in the ACCESS3 program. These are the interior point-penalty function method, the second-order primal projection method, the second-order Newton-type dual method, and the first-order gradient projection-type dual method.

Input data for ACCESS3 consists of a finite-element model that exhibits the

topological form, the geometrical configuration, and the structural materials of the structural system to be optimized, along with a set of structural loads and a selection of program options. The output includes a description of the resizing of elements required to achieve minimum weight.

The ACCESS3 program is written in FORTRAN IV for batch execution and has been implemented on an IBM 370-series computer with a central-memory requirement of approximately 800K of 8-bit bytes. ACCESS3 was developed in 1979.

This program was written by Lucien A. Schmit, Jr., and Claude Fleury of the University of California, Los Angeles, for **Langley Research Center.** *For further information, Circle B on the COSMIC Request Card.*
LAR-13107

Free-Vibration Analysis of Structures

Numerical procedure determines natural frequencies and associated modes in structural design.

A unified numerical procedure for the free-vibration analysis of structures has been developed and incorporated into the EIGSOL computer program. Dynamic response analysis is of primary importance in the design of such a wide range of practical structures as spacecraft, buildings, and rotating machineries.

A vital preliminary for such an analysis involves the determination of the natural frequencies and the associated modes. Both spinning and nonspinning structures, with or without viscous and structural damping, as well as the quadratic matrix eigenproblem associated with a finite dynamic discretization, may be analyzed with the EIGSOL program.

For most complex practical structures, such discrete modeling results in a rather large number of simultaneous equations, which are usually of highly banded configuration. The EIGSOL program exploits this inherent matrix sparsity to effect an economical solution of the eigenproblem. The program uses an out-of-core solution strategy so that even large and complex problems may be solved.

The EIGSOL program is written in FORTRAN V for batch execution and has been implemented on a UNIVAC 1100-series computer with a central-memory requirement of approximately 22K of 36-bit words. The EIGSOL program was developed in 1981.

This program was written by Kajal K. Gupta of Caltech for **NASA's Jet Propulsion Laboratory.** *For further information, Circle C on the COSMIC Request Card.*
NPO-15797

Thermal Radiation Analyzer System

System solves radiation-related aspects of thermal-analysis problems.

The Thermal Radiation Analyzer System, TRASYS II, is a computer software system with generalized capability to solve the radiation-related aspects of thermal-analysis problems. When TRASYS II is used in conjunction with a generalized thermal-analysis program, such as the Systems Improved Numerical Differencing Analyzer (SINDA) program, any thermal problem that can be expressed in terms of a lumped-parameter RC thermal network can be solved.

TRASYS II provides for the calculation of internode radiation interchange data and for the calculation of incident and absorbed heat-rate data originating from environmental radiant heat sources. Data of both types are provided by TRASYS II in a format directly usable by such thermal-analyzer programs as SINDA.

TRASYS II consists of two major components: the preprocessor and the processor library. One primary feature of TRASYS II is that it allows users to write their own executive, or driver, programs that organize and direct the library routines toward solving each specific problem in the most expeditious manner.

The preprocessor first reads and converts the user's geometry input data into the form used by the processor library routines. Next, the preprocessor accepts the user's driving logic, written in the TRASYS II-modified FORTRAN language, that directs the user-provided and processor library routines in the solution of the problem.

The processor library consists of FORTRAN routines that perform functions commonly needed to solve thermal-radiation problems. In many cases, the user has a choice of solution techniques to perform the same function. As previously mentioned, users may supply their own routines. In particular, the user may write output routines to provide for an interface between TRASYS II and any thermal-analyzer program using the RC network concept.

Input to the TRASYS II program consists of EDIT/CONTROL data and MODEL data. The EDIT/CONTROL data do not participate in the definition of the thermal-radiation problem but serve as basic program control and offer editing capability. The MODEL data participate in the definition of the mathematical model of the thermal-radiation problem. The MODEL data include surface-geometry, documentation, nodal, block coordinate-system, form-factor, and operations data (the user's driver logic), also user-supplied subroutines.

TRASYS II currently allows problems with as many as 1,000 nodes and time-variable problem geometry. The edit capability allows for the easy modification of complex thermal-radiation problem models.

Output from TRASYS II consists of two basic types of data: internode radiation interchange data and incident- and absorbed-heat rate data. A plot package serves in plotting input geometry, orbit data (for on-station spacecraft problems), the two basic types of data just described, and any other data generated by the user's driver logic. TRASYS II builds a plot data tape that is read by a plotting driver program, which currently displays the plots on a Tektronix 4014 graphics terminal.

The TRASYS II software is written in FORTRAN IV-Plus and has been implemented on a DEC VAX-11/780 computer under VMS 2.0. The DEC VAX implementation of the TRASYS II software was completed in 1981.

This program was written by Joseph Skladany of **Goddard Space Flight Center.** *For further information, Circle D on the COSMIC Request Card.*
GSC-12783

Measuring High Gas Temperatures

Radiation effects are included for more accurate processing of thermocouple data.

A program available from COSMIC provides extrapolation calculations of high gas temperatures based on a theoretical heating curve of pulsed thermocouples.

A pulsed thermocouple is used for measuring gas temperatures above the

(continued on next page)

melting point of common thermocouples. The thermocouple is allowed to heat until it approaches its melting point, and then the thermocouple is cooled by a gas jet. While the gas is off and the thermocouple is heating, the thermocouple output is sampled at a high rate and recorded. The gas temperature is calculated by extrapolation from the initial heating curve.

Previous programs of this type were based on a simple first-order exponential curve fit. This approach is inadequate, mainly because it does not account for radiation effects. This new program is based on a theoretical heating curve that includes the effect of radiation in the extrapolation. The equation that describes the pulsed-thermocouple wire temperature is derived from basic heat-transfer relations. The theoretical heating curve includes heat transfer by radiation from the hot walls of the duct to the wire, from the gas to the wire, and from radiant heat emitted by the wire.

This program uses a curve-fitting procedure called the gradient-expansion method to fit the theory to the thermocouple collected data. The program requires as input the mach number, the wall temperature, and the total pressure in addition to the thermocouple data. Tests indicate that this new program extrapolates reasonably-accurate gas temperatures from pulsed-thermocouple data.

This progam is written in FORTRAN IV for batch execution and has been implemented on an IBM 370-series computer with a central-memory of approximately 66K of 8-bit bytes. This program was developed in 1981.

This program was written by Herbert A. Will of **Lewis Research Center.** *For further information, Circle E on the Cosmic Request Card.*
LEW-13819

Launch-Window Program

Optimum launch windows are selected through parametric scans of input data.

The launch window for an Earth satellite mission defines the dates and the times of day that a satellite can be launched and satisfy the mission constraints. The Parameterized Investigation of Launch Opportunities and Trajectories (PILOT) program was developed to perform mission simulation computations that yield data for use in delimiting optimum launch windows. PILOT performs parametric scans of a user-specified trajectory over launch date and initial right ascension of the ascending node. During each scan, various mission parameters are generated and output to a data file.

The CoPILOT utility program is used to read and format the PILOT-generated data file. The user specifies acceptable limits on the various PILOT-generated parameters. The CoPILOT program checks the data and generates an output table with notations of any constraint violations. When no constraints are violated, an acceptable launch time exists. For each date, the acceptable launch times are printed. A printer plot may also be generated to display visually the launch window.

The PILOT and CoPILOT programs are written in FORTRAN IV for batch execution and have been implemented on an IBM 360-series computer with a central-memory requirement of approximately 338K of 8-bit bytes. PILOT and CoPILOT were developed in 1977.

This program was submitted by Judith A. Erickson of Computer Sciences Corp. for **Goddard Space Flight Center.** *For further information, Circle F on the COSMIC Request Card.*
GSC-12801

Analyzing Flow Fields in Axial-Compressor Rotors and Stators

Three programs calculate three-dimensional, inviscid, rotational flows with shock waves in axial-compressor blade rows.

A computer program, BLADE3D, has been developed for the analysis of inviscid three-dimensional flow fields in a single blade passage of an axial-compressor rotor or stator. The program is applicable to arbitrary axial-compressor hub, tip, and blade geometries, including blades with part-span dampers. The program may also be used for axial turbines but with lowered resolution of flows about blunt leading and trailing edges. The analysis method is valid for subsonic, transonic, and supersonic flows, including choked flows.

A separate program, MESH3D, generates a finite-difference grid from input coordinates of the hub, tip, and blade and computes metric derivations and blade curvatures at the grid points. These data are stored in files used by BLADE3D.

The BLADE3D analysis program uses MacCormack's explicit time-marching finite-difference algorithm in split operator form to solve the unsteady Euler equations. This technique captures shock waves automatically and smears them over several grid points. Input to BLADE3D consists of the blade-row operating conditions. Output quantities are three velocity components, density, and internal energy at each grid point, which may be printed or stored as a solution file.

A third program, GRAPH3D, is used for postprocessing BLADE3D solution files. From these files GRAPH3D calculates total pressures, mach numbers, and streamline locations and produces some printer/plotter output. The calculated data may be stored for use with user-generted graphics routines.

Flows in several transonic compressors have been analyzed and compared with experimental measurements obtained with conventional probes, a gas fluoroscence technique, and laser anemometry. These comparisons have shown that the computed solutions accurately model the measured shock positions and flow fields.

The programs are written in FORTRAN IV. They were developed on a DEC PDP-11/70 and an IBM 3033, but have also been run on a Cray-1, an IBM 360/078, a UNIVAC 110, and a CDC 7600 with little or no modification.

This program was written by William J. Thompkins, Jr., of the Massachusetts Institute of Technology for **Lewis Research Center.** *For further information, Circle G on the COSMIC Request Card.*
LEW-13910

General Maneuver Program

Attitude and orbit maneuvers are modeled for spacecraft.

The General Maneuver Program, GMAN, computes both orbital and spin-axis reorientation maneuver parameters for various spacecraft. Specifically, GMAN computes the detailed maneuver scenarios necessary to achieve desired orbit and attitude maneuvers. The program supports both spinning and inertially-fixed despun spacecraft and includes modeling for either a hydrazine or a Freon propulsion system.

For each modeled maneuver GMAN produces a detailed history of the spacecraft orbital parameters, attitude parameters, mass properties, propulsion-system performance parameters, sensor coverage data, and ground coverage data. Routine maneuver computations and maneuver analysis are also incorporated.

The GMAN consists of a main driver, two subdrivers, and four top-level utilities. The main driver controls program flow as well as main function initialization. Each subdriver performs a main function in the development of a final maneuver computation.

The GMAN currently performs two main functions: orbit propagation and targeting. Associated with the orbit propagation driver is the orbit integrator utility. Associated with the targeting driver are the other three top-level utilities: orbit coarse, attitude coarse, and fine targeting. The coarse targeting employs two-body impulsive assumptions in developing first estimates on ignition time, the length of burn, and necessary spacecraft-control information. The fine targeting employs a detailed spacecraft model and allows testing of the coarse-targeting estimations through modeling of a finite burn.

The GMAN is written in FORTRAN IV and Assembler for batch execution and has been implemented on an IBM 360-series computer with a central-memory requirement of approximately 530K of 8-bit bytes. The program was developed in 1979.

This program was written by Judith A. Erickson of Computer Sciences Corp. for **Goddard Space Flight Center.** *For further information, Circle H on the COSMIC Request Card.*
GSC-12802

The Mission Radius and Maneuverability Characteristics of Fighter Aircraft

Five modules yield accurate performance information while minimizing run time.

A computer program provides detailed analysis of the mission radius and maneuverability characteristics of combat aircraft. It was developed with the assumption that great emphasis would be placed on balanced-radius profiles and that alternate-radius missions would be of interest as tradeoff information. Therefore, the program produces accurate performance results for all mission segments while minimizing the repetitive calculations normally required to balance radii and develop radius trades.

This program has been used at the NASA Langley Research Center to determine critical operational requirements and to determine areas where research programs would be expected to yield the most beneficial results. In turn, the results of research efforts have been evaluated in terms of aircraft performance on selected mission segments and for complete mission profiles.

The program is a combination of five mission modules that represent mission profiles currently of interest. Each mission module is designed to determine the combat radius or range capability for a specific mission with its associated ground rules and profile definitions. Several of these mission profiles contain optional profile segments for use in representing alternate missions. The modules concept permits the addition of new modules, or the modification of existing modules, to represent new or unusual mission-profile specifications. Input to the program includes extensive propulsion data, aerodynamic data, aircraft weight data, and mission requirements. For each requested flight point, an extensive set of aircraft state variables and acceleration rates are output.

This program is written in FORTRAN IV for batch execution and has been implemented on CDC CYBER 175-series computers with a central-memory requirement of approximately 114K (octal) of 60-bit words. This program was developed in 1981.

This program was written by Willard E. Foss, Jr., of **Langley Research Center.** *For further information, Circle J on the COSMIC Request Card.*
LAR-12908

Elliptical Orbit Performance Computer Program

Program simulates space booster performance as a function of payload weight.

The Elliptical Orbit Performance (ELOPE) computer program for analyzing the orbital performance of space boosters uses orbit insertion data obtained from a trajectory simulation to generate parametric data on apogee and perigee altitudes as a function of payload data. These data are then used to generate presentation plots that display the elliptical orbit performance capability of the space booster.

The ELOPE program employs data interpolation and a two-body energy equation to calculate the parametric performance data. The input to the program consists of parametric data on altitude, velocity, and payload weight at orbit insertion. These data are usually obtained from a user-supplied trajectory simulation program.

Trajectory simulations with various values of payload weight and vehicle pitchover rate are used to generate the input data. The ELOPE program interpolates these data at the perigee altitudes of interest for each payload weight. The perigee is assumed to be at the point of insertion, the point at which the booster performance is at its maximum. The resulting interpolated data at each specific perigee are themselves interpolated for the range of payloads of interest.

Values of the perigee velocities are converted to apogee altitudes by solving the two-body energy equation. Thus the parametric orbital performance is calculated and plotted for a specified range of perigee altitudes. In addition, the program can calculate the payload weights that correspond to a circular orbit, an Earth escape orbit, and a user-specified orbit.

The ELOPE program is written in FORTRAN IV for batch execution and has been implemented on a CDC CYBER 170-series computer with a central-memory requirement of approximately 60K (octal) of 60-bit words. The program was developed in 1981.

This program was written by T. R. Myler of Vought Corp. for **Langley Research Center.** *For further information, Circle K on the COSMIC Request Card.*
LAR-13026

Takeoff and Landing of Transport Aircraft

Program assesses aircraft configurations for takeoff and landing performance.

A computer program provides a detailed analysis of the takeoff and landing performance capabilities of transport-category aircraft. Performance is calculated according to the airworthiness standards of the Federal

Aviation Regulations. The aircraft and flight constraints are represented in sufficient detail to permit realistic sensitivity studies in terms of either configuration modifications or changes in operational procedures.

Representation of the aircraft data by the program is extensive and includes realistic limits on engine and aircraft operational boundaries and maximum attainable lift coefficients. The takeoff and climbout flightpath is generated by a stepwise integration of the equations of motion. Special features include options for non-standard-day operation, for balanced field length, for derated throttle to meet a given field length for offloaded aircraft, and for throttle cutback during climbout for community noise alleviation.

The program can also be used to investigate advanced takeoff procedures for noise alleviation, such as programed throttle and control flaps. Approach profiles analyzed by this program may incorporate such advanced procedures as two-segment approaches and decelerating approaches. The landing performance considers the application of wheel brakes, spoilers, and thrust reversers.

The program is not designed to synthesize configurations or to generate aerodynamic, propulsion, or structural characteristics. This type of information is generated externally and is input as a data base for all calculations.

This program is written in FORTRAN IV for batch execution and has been implemented on a CDC CYBER 170-series computer with a central-memory requirement of approximately 105K (octal) of 60-bit words. The program was developed in 1979.

This program was written by Willard E. Foss Jr., of **Langley Research Center.** *For further information, Circle L on the COSMIC Request Card.*
LAR-13086

MiniBriefs describe NASA innovations and reports in an abbreviated format. Readers desiring additional information on these items should request the Technical Support Packages (TSP's), available in most cases, which can be obtained by using the TSP Request Card at the back of this issue.

Accuracy Criterion for Structural Calculations

Completely objective procedures determine the requisite accuracy.

How accurate should an analytical model of structural vibration be? A comparison of real and calculated characteristics such as frequencies and vibration-mode shapes is not enough for determining the requisite model accuracy. Since the errors of the responses and loads are subject to the accuracy requirement, the accuracy of the vibration-forcing functions must also be considered.

A simple but meaningful method of establishing an accuracy criterion is based on comparing the allowable errors and modeling errors. On the basis of this comparison, the amounts of change required to improve the modeling error can be used in the convergence criterion.

This work was done by Jay-Chung Chen of Caltech for **NASA's Jet Propulsion Laboratory.** *For further information, Circle 129 on the TSP Request Card.*
NPO-16008

Thermal and Flow Data From Liquid-Oxygen System

Extensive flow rate, pressure, and temperature data are available for validating computer models of liquid-oxygen transfer systems.

Data describing the actual behavior of the Space Shuttle liquid-oxygen servicing system were collected for the 6-hour period starting at cooldown and ending at launch. Previous modeling of such systems were based on data from small-scale systems; the Space Shuttle system comprises a 3,408-m^3 storage tank and a vacuum-jacketed feedline 500 feet (152 m) long, 6 in. (15 cm) in diameter. The transfer line had a flowmeter located at the pump discharge; sets of transducers were located at the pump suction and pump discharge, the skid inlet and outlet, and the orbiter inlet. Data on "waterhammer" pressure spikes are included.

This work was done by F. N. Lin, W. I. Moore, and S. W. Walker, of **Kennedy Space Center.** *For further information, Circle 130 on the TSP Request Card.*
KSC-11265

Low-Shock Pyrotechnic Actuator

Hatch covers are released with little shock and no contamination.

A miniature 1-ampere, 1-watt pyrotechnic actuator is enclosed in a flexible metal bellows. The bellows confines outgassing products, and pyrotechnic shock reduction is achieved by the action of the bellows, a gas cushion within the device, and minimum use of pyrotechnic material. The actuator is inexpensive, compact, and lightweight. It replaces conventional solenoid and pyrotechnic release mechanisms for hatch covers used aboard spacecraft. Solenoids are heavy and consume considerable power, while conventional pyrotechnic devices can cause damage by shock or chemical contamination.

This work was done by Melvin H. Lucy of **Langley Research Center.** *For further information, Circle 131 on the TSP Request Card.*

Inquiries concerning rights for the commercial use of this invention should be addressed to the Patent Counsel, Langley Research Center [see page A5]. *Refer to LAR-13198.*

Test Frame Simulates Zero Gravity

Counterweighted frame simulates zero gravity in tests of solar-array wing.

Solar-array wings up to 32 meters long extend and retract from satellites under conditions of zero gravity. The extension/retraction and stowage mechanisms are tested on Earth by suspending the flexible array panels from an overhead track. The wing folds and unfolds, drapelike, along the track path. Two counterweights per panel keep the overall center of gravity in the vertical plane of the track, regardless of how far the wing extends. Friction is minimized by roller bearings running on steel tape.

The net effect is a close simulation of the zero-gravity environment in which the wing must function. The frame also facilitates testing and replacement of solar-cell elements and panels.

This work was done by D. T. Chung and D. E. Lindberg of Lockheed Missiles & Space Co., Inc., for **Marshall Space Flight Center.** *For further information, Circle 132 on the TSP Request Card.*
MFS-25518

Simulating a Three-Dimensional Flow in Pipes

Velocity-vector expansion method simulates an unsteady, incompressible flow.

A numerical method simulates in unsteady, incompressible flow in an axisymmetric pipe in three dimensions. The method relies on a velocity-vector expansion technique in which each vector function in the expansion set is divergence-free and satisfies the boundary conditions for viscous flow. In addition, the method applies spectral expansions; i.e., Fourier series in azimuthal and streamwise directions and global polynomials in the radial direction.

Major benefits of the expansion technique are: (a) elimination of the pressure variable from the dynamics, (b) requirement of only two unknowns per "mesh point," (c) implicit treatment of the viscous terms with no extra computation, and (d) no need for fractional time steps. The method was demonstrated successfully with a linear-stability problem for Poiseuille flow.

This work was done by Anthony Leonard and Alan A. Wray of **Ames Research Center.** *For further information, Circle 133 on the TSP Request Card.*

Inquiries concerning rights for the commercial use of this invention should be addressed to the Patent Counsel, Ames Research Center [see page A5]. Refer to ARC-11466.

Microyield Stress in Composite Materials

Multibeam laser interferometer resolves displacements of ±3 μin. (±76 nm).

A new interferometric method for measuring microyield stress — the stress level that causes a permanent strain of 10^{-6} times specimen length — is faster and more accurate than a previous strain-gage method. Multiple laser beams are reflected from corner-cube reflectors arranged in triangular patterns 5 in. (12.7 cm) from each end of a tubular specimen 37 in. (94 cm) long, yielding data sufficient to separate length changes from rigid-body motion and bending.

Stress-versus-strain data are collected throughout each compression-loading cycle. The interferometer tracks displacements as fast as 1 in./s (2.5 cm/s). A thermal shroud maintains sample temperature to a tolerance of 0.25° F (0.14° C).

This work was done by Lyle McMahan and Ray Pond of Boeing Aerospace Co. for **Marshall Space Flight Center.** *For further information, Circle 134 on the TSP Request Card.*
MFS-25709

Inspecting Joints With Grooved Surfaces

The method thoroughly covers the joint at its various depths.

A method of inspecting grooved joints covers the full circumference of the joint at its various depths. The inspection tools include a guide block that holds a fiber-optic scope with a camera attached to its end and that also holds a light pipe with an ultraviolet source attached to its end.

The guide block is placed in the joint and is held at a stationary depth by tetrafluoroethylene tabs that fit into the grooves of the joint. The block is then moved along the circumference of the joint without changing the depth of the scope. After one revolution is completed, the scope is moved to a new depth and examines a different area. Successive steps are repeated until the entire joint is examined.

This work was done by Barry S. Burns of **Marshall Space Flight Center.** *No further documentation is available.*
MFS-25934

Analyzing Vibrations in a Long Mast

Computer model accurately predicts the vibrational modes.

A report describes the mathematical prediction and measurement of vibrations in a lightweight extensible mast of lattice structure 105 ft (32 m) long. With the mast suspended from 10 vertical wires 108 ft (33 m) long, vibrations were excited in the horizontal plane by a motor-driven mechanism or by hand. The vibrations were recorded photographically and with accelerometers.

The vibrational modes were predicted with a computer model using the statically-measured beam stiffness, 40 beam elements for the mast, 4 tension/compression elements for each wire, and rigid mass lumps for the mast-tip fitting, accelerometers, and other attachments. The calculated and measured vibrational modes were in good agreement.

This work was done by B. A. Simpson of Lockheed Missiles & Space Co., Inc., for **Marshall Space Flight Center.** *To obtain a copy of the report, Circle 135 on the TSP Request Card.*
MFS-25746

Tracking Visible Targets Automatically

Automatic instrument-pointing techniques are surveyed.

A report summarizes techniques for the automatic pointing of scientific instruments by reference to visible targets. Although the techniques are intended mainly for experiments aboard spacecraft, applications are also foreseen in industrial robotics.

The proposed tracking-and-positioning system includes gyroscopic stabilization

(continued on next page)

and rotation-rate detection, microprocessor control, various electromechanical actuators, and optical position encoders. A target-body tracker measures the pointing axis relative to the direction to the target. The measurement is done by image analysis based on gradient edge location, image-centroid location, and/or outline matching. To simplify the signal processing, the tracker employs a charge-coupled device as the imaging element.

This work was done by Robert W. Armstrong of Caltech for **NASA's Jet Propulsion Laboratory.** *To obtain a copy of the report, Circle 136 on the TSP Request Card.*

Inquiries concerning rights for the commercial use of this invention should be addressed to the Patent Counsel, NASA Resident Office-JPL [see page A5]. Refer to NPO-15226.

Safe Emergency Evacuation From Tall Structures

A space-age breeches buoy transports people from danger.

An emergency egress system allows people to be evacuated quickly from tall structures. The system was developed to provide a fast and safe way for flight crew, passengers, and ground crew to leave the Space Shuttle in case of danger while the vehicle is still on the launchpad. Conventional exits, such as an elevator or stairs, are too slow and potentially dangerous. The new emergency egress system is applicable to rescues from fires in tall hotels and other buildings.

Essentially, the system consists of a basket on a slide wire. The basket descends by gravity on the sloped slide wire, which is staked to the ground. For the Space Shuttle, the slide wire connects the 195-foot (59-meter) level of the fixed service structure to a ground landing area 1,200 feet (366 meters) away from the launchsite. All personnel can be evacuated within minutes, even in winds as high as 34 knots (17 m/s).

A software package was developed, using finite-element and numerical analysis techniques, to obtain the history and other parameters of a load moving down a catenary.

This work was done by Emile S. Stephan of **Kennedy Space Center.** *For further information, Circle 137 on the TSP Request Card.*
KSC-11225

Mathematical Simulation of Flight Maneuvers

Calculated spacecraft motions are updated with telemetered data.

A mathematical model simulates the response of a spin-stabilized spacecraft to commanded thrustor pulses, using a set of equations based on the known inertial properties of the vehicle and the previously-determined thrustor performance. The model can also be used to generate a sequence of thrustor commands to accomplish a specified maneuver.

The spin rate, attitude, and velocity of the spacecraft must be monitored to calibrate the control algorithm and prevent the accumulation of errors. The spin axis and spin rate are determined from telemetered Sun- and star-sensor data. The component of velocity along the vehicle/ground-station axis is determined from the Doppler shift. The telemetered propellant temperature and pressure are used in the calculation of thrustor behavior.

This work was done by Raymond B. Frauenholz of Caltech for **NASA's Jet Propulsion Laboratory.** *For further information, Circle 138 on the TSP Request Card.*

Inquiries concerning rights for the commercial use of this invention should be addressed to the Patent Counsel, NASA Resident Office-JPL [see page A5]. Refer to NPO-15395.

Trace-Level Solid-Polymer Electrolyte Hygrometer

Water vapor absorbed by a solid polymer electrolyte is detected by measuring the current required to electrolyze the water.

An absolute electrolytic hygrometer for measuring traces of water vapor in vacuum is under development. The electrolytic cell is constructed on a slit glass tube. A gold foil inner electrode surrounds the tube. A strip of solid polymer electrolyte, such as a sulfonated fluorocarbon polymer, is wrapped over the foil. After clamping the tube to compress the slit, an outer electrode of gold-plated nickel wire [0.03 in. (0.8 mm) in diameter] is wound over the polymer. Releasing the clamp lets the tube compress the polymer layer tightly between the electrodes (with guard electrodes). Cell leakage is about 0.1 nA; a current of 1 nA corresponds to electrolyzing 10^{-13} cm^3s^{-1} of water.

This work was done by Eric G. Laue, James B. Stephens, and Mary Mei-Ling Yang of Caltech for **NASA's Jet Propulsion Laboratory.** *For further information, Circle 139 on the TSP Request Card.*

Inquiries concerning rights for the commercial use of this invention should be addressed to the Patent Counsel, NASA Resident Office-JPL [see page A5]. Refer to NPO-15722.

Submicron-Particle Generator

Device operates at high pressure and flow.

A particle generator supplies submicron-size particles to a high-pressure airstream. The generator uses extremely small injection slits. The increase in velocity between the microslit wall (where velocity is zero) and the center of the microslit (where velocity is sonic) provides a shear force large enough to break up already small particles into even smaller ones, about 0.45 micrometer in diameter. The particles serve as light scatterers in a laser velocimeter for ultra-high-speed gas.

A major advantage of the generator is that it produces a cloud of uniform, submicron particles at both high ambient pressures and high flow rates, unlike alternative devices such as smoke generators.

This work was done by E. L. Morrisette and D. M. Bushnell of **Langley Research Center.** *For further information, Circle 140 on the TSP Request Card.*

This invention has been patented by NASA (U.S. Patent No. 4,428,703). Inquiries concerning nonexclusive or exclusive license for its commercial development should be addressed to the

Patent Counsel, Langley Research Center [see page A5]. Refer to LAR-12785.

Partial-Payload Support Structure

A modular, bridgelike structure supports experiments weighing up to 2 tons.

A partial-payload support structure (PPSS) has been developed to mount experiments that occupy a relatively small area or length of the Space Shuttle cargo bay and which must be supported in an elevated position (for view-factor requirements, etc.). The PPSS handles such experiments more economically than the standard Spacelab pallet system.

A (PPSS) module occupies 39.5 in. (100.4 cm) along the cargo bay. Each module is an aluminum-alloy truss adaptable to mounting experiments of various sizes. In orbit, the PPSS maintains experiment alinements to within ±1 degree with respect to the Orbiter Inertial Measurement Unit.

This work was done by R. A. K. Mitchell and Mike Freeman of Brown Engineering for **Marshall Space Flight Center.** *For further information, Circle 141 on the TSP Request Card.*
MFS-25485

Fatigue Testing of Heat-Exchanger Tubes

Thermal stress is simulated mechanically.

Accelerated fatigue-life testing of heat-exchanger tubes is simplified by a technique that substitutes a mechanical side load for thermally-generated axisymmetric stress. The load is applied to a sample tube via two lengthwise clamping bars that are contoured to fit the tube and are placed diametrically opposite each other.

If the tube normally operates colder inside then outside, or vice versa, then the simulated strain will be correct in the loading plane, or at 90° to the loading plane, respectively. Strain gages are attached in the appropriate plane. The load amplitudes are adjusted to produce strains equivalent to those produced by the anticipated thermal stresses.

This work was done by Peter Ackerman of Rockwell International Corp. for **Marshall Space Flight Center.** *For further information, Circle 142 on the TSP Request Card.*
MFS-19599

Portable Fatigue-Testing Machine

Piezoelectric crystal stack adds an oscillatory force to a constant force.

A portable machine has been constructed for the fatigue testing of structural materials or machinery parts that are subjected to fatigue loads. It applies both a constant force and a 2-kHz oscillatory force through a rod to a test sample that is held in a grip. The rod applies a constant force from a ram and an oscillatory force from a piezoelectric crystal stack in the rod. The magnitude of the oscillatory force is controlled by a power regulator. The machine can test a wider variety of objects than can be tested with the usual rotating-beam fatigue test.

This work was done by Jack Lewis and Chuck Daugherty of Rockwell International Corp. for **Marshall Space Flight Center.** *For further information, Circle 143 on the TSP Request Card.*
MFS-19459

Brushless Low-Speed dc Tachometer

A coil moving in a homopolar field generates an emf proportional to shaft angular velocity.

A proposed tachometer would produce voltages proportional to shaft angular velocity and (by differentiation) acceleration. A potentiometer provides a voltage proportional to shaft angular position. Coil leads and a magnetic-field return path limit shaft-rotation angle to a 270° range. Calculated accuracy is 0.1 percent of full-scale maximum absolute error at a shaft speed of 1 radian per second; resolution is 0.005 percent of full scale and bandwidth is better than 50 Hz.

Shielding and low-impedance outputs minimize noise pickup. The design requires high-precision machining and bearings. A ring-shaped high-field rare-earth magnet generates the homopolar field.

This work was done by Mathias B. Handlykken of Caltech for **NASA's Jet Propulsion Laboratory.** *For further information, Circle 144 on the TSP Request Card.*

Inquiries concerning rights for the commercial use of this invention should be addressed to the Patent Counsel, NASA Resident Office-JPL [see page A5]. Refer to NPO-15706.

Optical Turbopump Speed Sensor

An optical tachometer measures shaft rotation from outside the turbopump housing.

A proposed optical tachometer measures turbopump shaft speed from outside the pump housing. A laser-diode beam passes through a quartz lens onto a shaft nut with alternating reflective and nonreflective surfaces. The reflected pulses are collected by the lens and transmitted to a photodetector. The photodetector signal is amplified and processed to give the rpm. A prototype showed low transmission losses and gave clear signals at −150° F (−65° C).

This work was done by David Swain of Rockwell International Corp. for **Marshall Space Flight Center.** *For further information, Circle 145 on the TSP Request Card.*
MFS-19794

Theory for Eccentric and Misalined Annular Seals

Behavior under nonideal operating conditions is examined.

An approximate theory describes the behavior of eccentric and angularly-misalined incompressible-fluid shaft seals. The direct and cross-coupled stiffness and damping coefficients are expressed in terms of the degree of eccentricity and the coefficients of the concentric system. Leakage is estimated for

(continued on next page)

eccentric and misalined seals with laminar or turbulent flow by applying eccentricity and turbulence correction terms to the concentric laminar value.

The theory leads to the following conclusions:

- Leakage is less affected by eccentricity and misalinement in turbulent flow than it is in laminar flow.
- Leakage decreases with misalinement and increases with eccentricity.
- Dynamic coefficients change significantly at high eccentricity or misalinement, especially near minimum clearance.

This work was done by E. D. Jackson and W. C. Chen of Rockwell International Corp. for **Marshall Space Flight Center.** *For further information, Circle 146 on the TSP Request Card.*
MFS-19892

Belleville Spring/Seal

Metallic Belleville seals can be used in liquid nitrogen environments.

A metallic seal for cavity openings in liquid-nitrogen environments uses a Belleville-spring preloaded washer. Due to preloading, Belleville spring/seal washers slide and deflect to accept radial and axial movement between two sealing surfaces while remaining in sealing contact. The spring/seal design also operates as a relief valve. As pressure against the spring overcomes the preload, the spring lifts off one sealing surface, allowing fluid to flow. This design of washers has been tested to 460 psig (3.3 MN/m^2) with no measureable leakage.

This work was done by Douglas P. Bradley of Rockwell International Corp. for **Marshall Space Flight Center.** *For further information, Circle 147 on the TSP Request Card.*
MFS-19596

Leak Test for Pressure-Sealing Zippers

Test jig checks either side of pressure-sealing zippers for leaks.

Pressure-sealing zippers must withstand pressure applied to either side of the rubber sealing lips. Zippers are tested by clamping them between two aluminum unistruts faced with laminated gaskets. A vacuum pump evacuates one side of the jig, and the pressure differential is monitored on a vacuum gage. A flowmeter indicates any air leakage through the zipper. The procedure takes little time, and seal failure may be determined before the zipper is incorporated into a suit.

This work was done by Ellwood Erickson of Kelly Services for **Kennedy Space Center.** *For further information, Circle 148 on the TSP Request Card.*
KSC-11247

Barrier Seals for Hydraulic Actuators

Severe fluid loss is delayed.

A barrier seal slows the loss of pressurized hydraulic fluid due to leakage in a primary seal. The barrier seal, placed downstream of the primary O-ring seal, serves as a secondary obstacle to leakage.

The barrier seal could be a ring (similar to an automotive piston ring) past which the fluid leaks at a rate determined by the fluid pressure and the precise seal dimensions. Alternatively, the barrier seal could consist of a scupper seal, essentially a secondary O-ring seal with volume between the primary and secondary O-rings vented through an orifice. The orifice size would be chosen to allow leakage at a predetermined rate.

This work was done by Richard E. Prout of Rockwell International Corp. and F. G. Miller of Moog, Inc., for **Johnson Space Center.** *No further documentation is available.*
MSC-20390

Supersonic-Nozzle Shock-Wave Analysis

An analytical procedure is used to design nozzles that vibrate less during startup and shutdown.

A new analytical procedure is used to modify the design of high-pressure-ratio nozzles to reduce vibration during startup and shutdown. The vibration is caused by repetitive shock-wave attachment and separation at the nozzle wall. Such nozzles are used in jet engines, laser nozzles and diffusers, wind tunnels, gas turbines, rocket engines, and the like.

The new procedure is used to analyze the progression of the shock-wave structure into and out of the nozzle envelope during operation at pressure ratios below the design value. From the results of this analysis, nozzle design can be brought closer to the design limit, thus reducing nozzle weight and improving reliability.

This work was done by William R. Wagner and Gary H. Ratekin of Rockwell International Corp. for **Marshall Space Flight Center.** *No further documentation is available.*
MFS-19753

Nonseparating High-Area-Ratio Supersonic Nozzles

Nozzles with modified contours throttle to lower pressure ratios without wall-flow separation.

An analytical procedure determines supersonic-nozzle contours that allow higher nozzle-exit wall pressures, thus reducing chamber pressure without causing wall-flow separation as encountered in optimum large-area-ratio nozzle designs. A characteristics mapping method is used that varies the initial throat-exit angle and nozzle-exit angle to provide a high wall pressure with no significant performance loss. Envelopes of thrust performance versus wall-pressure increase are plotted to determine the peak operational point. The procedure applies to chemical-laser nozzles, jet-engine and gas turbines, wind tunnels, rocket nozzles, and the like.

This work was done by William R. Wagner and Rudolf R. Kassner of Rockwell International Corp. for **Marshall Space Flight Center.** *No further documentation is available.*
MFS-19758

Machinery

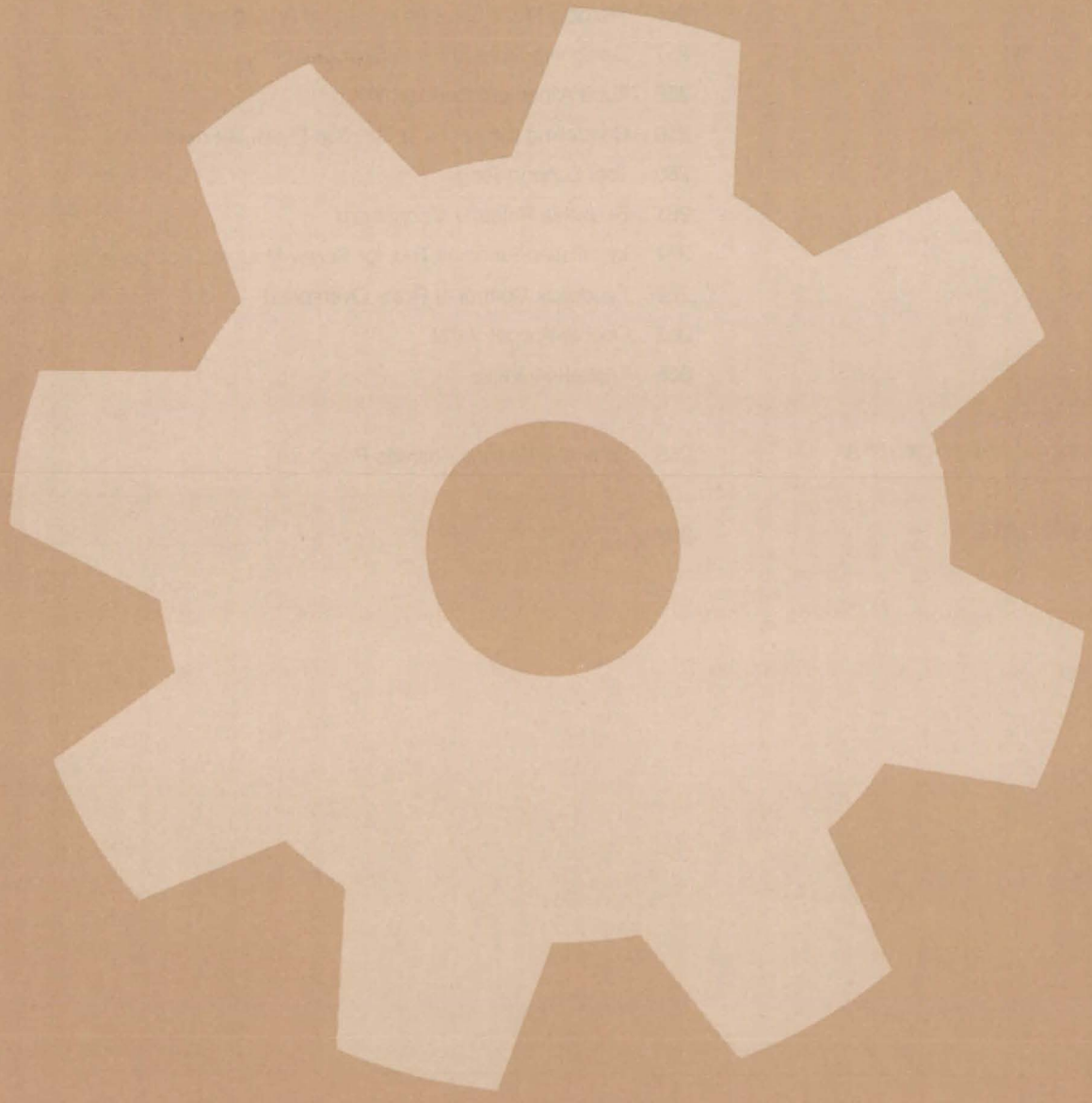

Hardware, Techniques, and Processes

253 Low-Vibration Oscillating Compressor
254 Vertical-Control Subsystem for Automatic Coal Mining
255 Transportable Pumps Could Save Oil Cargoes
256 Memory-Metal Electromechanical Actuators
257 Designing More-Efficient Spur Gears
258 Tube Alinement for Machining
259 Controlling the Focus in Electron-Beam Welders
260 Tool Support Ring
261 Reusable Release Mechanism
261 Installation/Removal Tool for Screw-Mounted Components
262 Feedback Control of Rotor Overspeed
263 Double-Poppet Valve
265 Triple-Seal Valve

Computer Programs

265 Spherical-Bearing Analysis Program

MiniBriefs

266

Low-Vibration Oscillating Compressor

The momenta of opposed pistons cancel.

Goddard Space Flight Center, Greenbelt, Maryland

An oscillating compressor is momentum-compensated so that it produces little vibration in its supporting structure. The compressor requires no lubrication and is virtually free of wear. It can compress working fluids such as helium, nitrogen, or chlorfluorocarbons for Stirling-cycle refrigeration or other purposes.

The proposed compressor includes two mutually opposed ferromagnetic pistons of the same shape and mass (see figure). An electromagnet — the main driving coil — generates a magnetic flux that links both pistons, thus causing a magnetic attraction between them. The symmetrical disposition of the pistons on either side of the coil and the equal piston masses insure that the resulting piston motions are of substantially equal and opposite momenta. Since the net momentum of the machine parts is close to zero, there is very little reaction force and consequently very little vibration.

The magnetizable pistons, in combination with flexible diaphragms, confine the working fluid. The pressure of the working fluid tends to force the pistons apart. However, the magnetic attraction between the pistons draws them together, thereby compressing the working fluid and forcing a portion of it through a vent pipe. Repeated application of current to the main driving coil causes reciprocating movement of the pistons and produces surges of compressed working fluid at the vent.

The masses of the pistons and the compressibility of the working fluid form a naturally-resonant "gas-spring" structure. The compressor can be fine-tuned by adjusting the frequency of excitation of the main driving coil, adjusting mechanical springs on the pistons, or by changing the pressure of additional gas springs acting on the pistons and opposing the working fluid.

In addition to the main driving electromagnet coil, there are four quadrant coils to insure that the two pistons remain in alinement. The quadrant coils are operated in pairs, one pair augmenting the flux produced by the main coil and the other pair partially canceling the main-coil flux. The quadrant coils thus produce controllable torques on the pistons.

The currents in the quadrant coils are regulated in response to the outputs of capacitive radial-displacement sensors in metal or metalized tubes extending from the pistons. The sensors are energized by high-frequency signals from the control circuitry. A pair of axial-displacement sensors operates in a similar manner, and the control circuitry energizes the main coil accordingly.

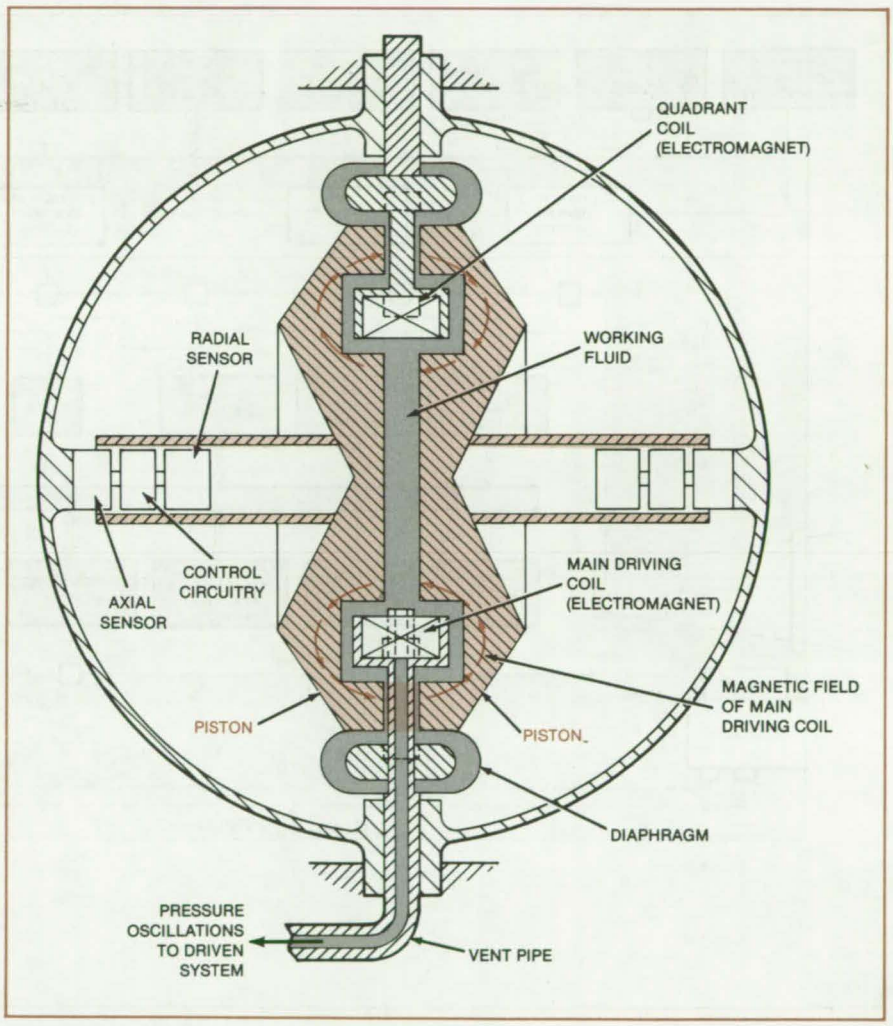

Pulses of Magnetic Flux through enlarged parts of the two pistons pull the pistons together. In the absence of flux, working-fluid pressure forces the pistons apart. A reciprocating movement is thus set up, and the pressure oscillations are coupled out to be used to drive a Stirling-cycle refrigerator or other system.

This work was done by Philip A. Studer of **Goddard Space Flight Center.** *For further information, Circle 59 on the TSP Request Card.*

This invention is owned by NASA, and a patent application has been filed. Inquiries concerning nonexclusive or exclusive license for its commercial development should be addressed to the Patent Counsel, Goddard Space Flight Center [see page A5]. Refer to GSC-12799.

Vertical-Control Subsystem for Automatic Coal Mining

Unit ensures that maximum coal is extracted without digging into ceiling rock.

Marshall Space Flight Center, Alabama

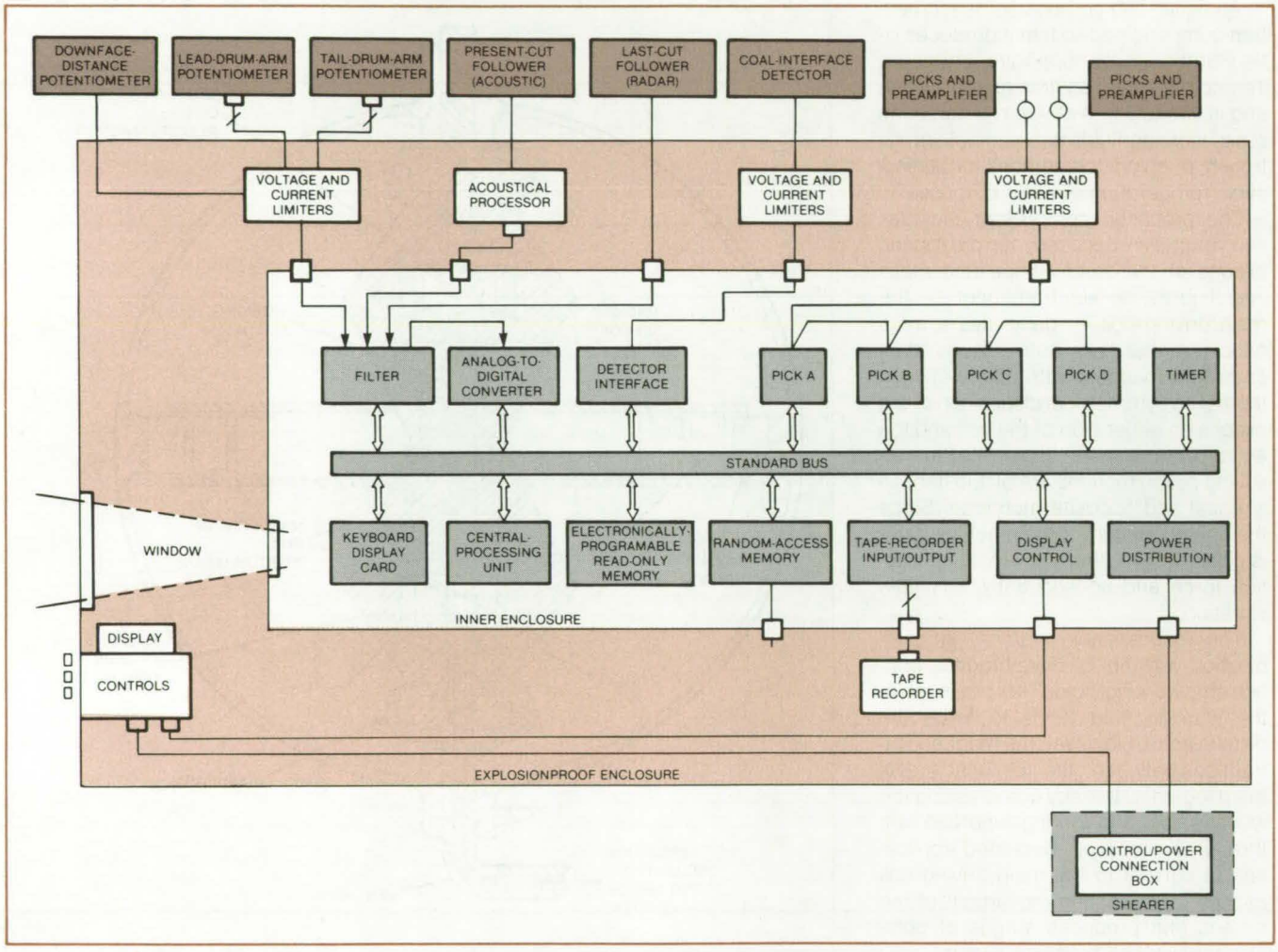

The **Vertical-Control Subsystem** senses the thickness of the coal remaining on the roof and the positions of the two cutting drums. It implements either of two control algorithms to follow the coal/rock interface, removing as much coal as possible without cutting into rock.

A guidance and control system automatically positions the cutting drums of a double-ended longwall shearer so that they follow a coal seam. The system determines the location of the upper interface between coal and shale and continuously adjusts the cutting-drum positions, upward or downward, to track the undulating interface. The objective is to keep the cutting edges as close as practicable to the interface and thus extract as much coal as possible from a seam.

The system employs the following sensors:

- *Downface Distance Sensor* — measures the distance of the shearer from the start of the cut along the face of the longwall.
- *Arm-Position Indicators* — measure the angular position of the shearer arm with respect to its body.
- *Present-Cut Follower* — measures the vertical distance between the trailing-drum centerline and the newly cut roof.
- *Last-Cut Follower* — measures the vertical distance between the centerline of the lead drum and the previously cut roof.
- *Coal-Interface Detector* — a sodium iodide scintillation detector that measures natural gamma-ray emissions from the rock above the coal: the thickness of the coal remaining on the roof is deduced from the attenuation of the gamma rays by the coal.
- *Sensitized Picks — Instrumented With Strain Gages* — measure cutting force to differentiate between cutting coal and cutting rock.

In addition to the sensors, hardware for the subsystem includes a microprocessor, signal-processing elec-

tronics, power supplies, a display, and an interface circuit that converts the control signals to the high-power levels required by the shearer. The complete vertical-control subsystem is shown schematically in the figure.

On the basis of signals from the sensors, the control system follows either of two strategies. If the seam height is fairly consistent from cut to cut, the controller employs strategy 1, in which the system utilizes information about coal thickness left on the roof of the last cut and stored in memory as a function of downface distance. The lead-drum controller maintains the drum at a height that keeps the coal roof thickness as close as possible to a desired value, subject to the constraint that the step size between two consecutive cuts may vary by no more than ± 2 inches (± 5.1 cm) from the preset step size. A signal from one of the sensitized picks will move the lead drum away from the rock, within the allowed step boundaries. The rear drum keeps a constant seam height with reference to the newly cut roof, as directed by the present-cut follower sensor.

Strategy 2 is similar except that the coal thickness is measured in the present cut as close behind the lead drum as possible. The rear drum is controlled as in strategy 1.

The operator can switch from automatic control to manual control by pushing a button either on the machine or on a remote radio-control module. Ordinarily, the operator monitors the shearer from the distance allowed by the radio module. If anything goes wrong, the operator switches to manual control immediately.

This work was done by W. Ronald Griffiths, Martin Smirlock, James Aplin, Roger B. Fish, and David Fish of Foster-Miller Associates, Inc., for **Marshall Space Flight Center.** *Further information may be found in NASA CR-161969 and CR-161970 [N82-18658/NSP and N82-18659/NSP], "Automated Longwall Guidance and Control Vertical Control Subsystem," Volumes I and II [$16 and $31]. Paper copies may be purchased [prepayment required] from the National Technical Information Service, Springfield, Virginia 22161. Copies are also available on microfiche at no charge. To obtain microfiche copies, Circle 60 on the TSP Request Card.*

Inquiries concerning rights for the commercial use of this invention should be addressed to the Patent Counsel, Marshall Space Flight Center *[see page A5].* *Refer to MFS-25811.*

Transportable Pumps Could Save Oil Cargoes

Helicopter-carried pumps for firefighting can serve a dual purpose.

Marshall Space Flight Center, Alabama

Transportable pumps designed for firefighting can also be used to salvage crude oil from tankships that are leaking, burning, or grounded, according to a feasibility study. Such a pump would be incorporated into a self-contained transportable module along with the engine and controls. A module would be carried by a helicopter, a boat, or a van to the site of a fire. It would provide large quantities of water at high pressure in the firefighting mode or would pump the oil into a barge in the salvage mode. The firefighting module is described in "Light, Compact Pumper for Harbor Fires" (MFS-25784), *NASA Tech Briefs* Vol. 7, No. 2 (Winter, 1982), page 199. A picture of the module in action appears on the cover of Vol. 6, No. 3 (Fall/Winter, 1981).

The use of such a pump to unload cargo into a barge (see figure) will allow a vessel to be refloated or allow the trim or hull of a vessel to be corrected. It can prevent large monetary losses for the cargo owner. For example, a damaged vessel may well carry 9.8 million barrels (1.6×10^6 m^3) of crude oil with a market value of $343 million (1982 dollars). It

(continued on next page)

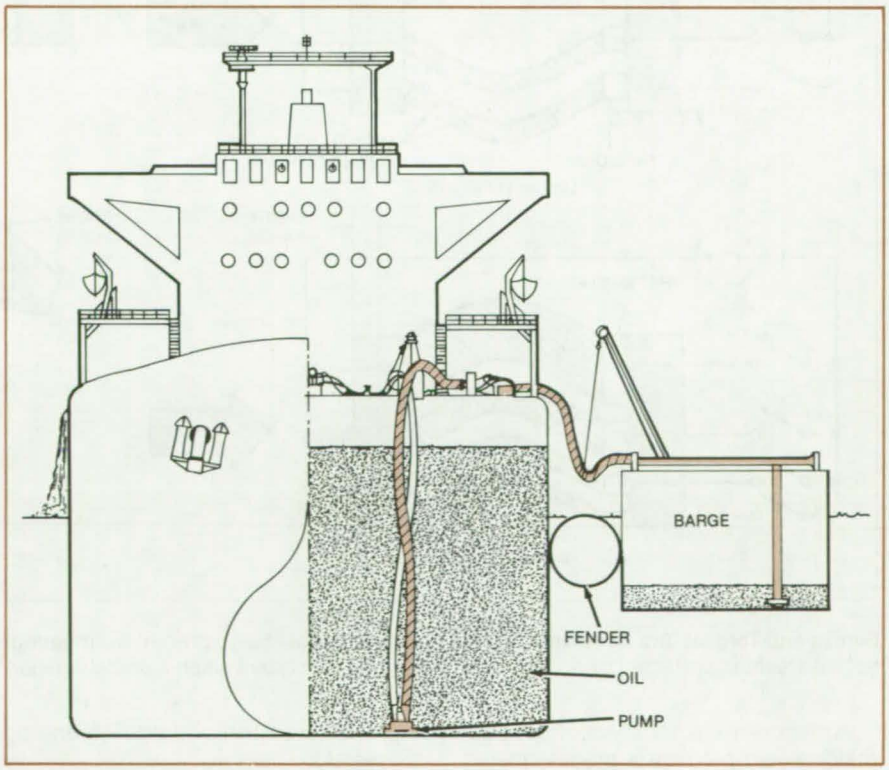

A Turbopump Lowered Into The Tank of a distressed tank vessel would transfer the cargo to a barge.

can also prevent pollution of the environment, a large underwriting loss for the insurer, and the loss of life.

Since the configuration of the turbopump depends largely on the viscosity of the oil cargo to be saved, the range of viscosities for crude oil and petroleum products has been investigated in depth. Tanker-unloading concepts have also been studied, particularly with regard to hose arrangements, human factors, and safety. Dual oil/water pumping units were found to be clearly feasible technically. They are also attractive economically since the dual functions allow a higher utilization, which eventually translates into lower cost.

Two pump configurations have been developed to cover the range of viscosities. Both normal and light crude oils can be unloaded efficiently by a centrifugal pump. For high-viscosity crude oils in winter and for such residual oils as No. 6 fuel oil and Navy heavy oil in winter, a screw-type pump will be required. However, the situations requiring a screw pump are much less likely than those for which a centrifugal pump will suffice.

The centrifugal type of pump appears to offer the best prospects for further development. The screw-type pump requires additional development to reduce its weight and size. Thus, the centrifugal pump should be the primary concept for prototype development and testing.

This work was done by Ralph Burns of IMA Resources, Inc., for **Marshall Space Flight Center.** *For further information, Circle 61 on the TSP Request Card.*
MFS-25881

Memory-Metal Electromechanical Actuators

Memory metals are used to generate fast mechanical response to electrical signals.

NASA's Jet Propulsion Laboratory, Pasadena, California

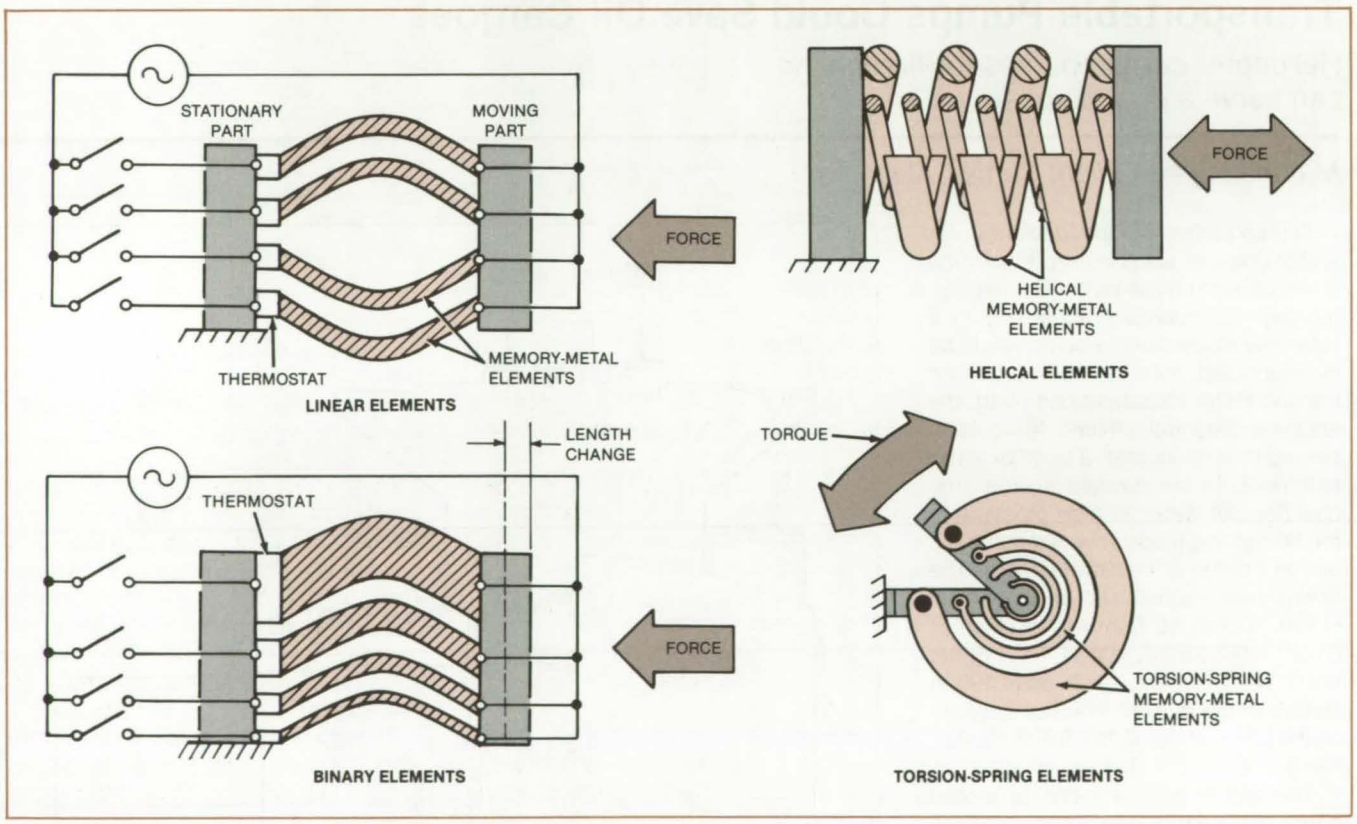

Forces and Torques Are Generated by memory-metal elements. To prevent overheating and consequent loss of the hot-formed shape, each element is protected by a thermostat that turns off current when a predetermined temperature is exceeded.

A proposed electrically controlled actuator would produce a predetermined force, torque, or displacement without motors, solenoids, or gears. Using memory-metal elements, such an actuator would respond to a digital input without electronic digital-to-analog conversion.

Memory metals are alloys that quickly snap from their cold-formed shapes to their stiff hot-formed shapes when a critical temperature is passed. Upon cooling, they return to their compliant cold condition. One memory-metal alloy of nickel and titanium can exert a pressure of 60,000 lb/in.^{2} (400 MPa) in response to a temperature change as small as 18° F (10° C).

In its simplest form, the actuator comprises several identical memory elements in parallel (see figure). Each element is selectively heated by electric current when its series switch is closed. When the temperature of an element rises above the critical temperature, the element reverts to its hot-formed shape. The change is rapid, since its source — heat — arises within the element itself.

As it changes shape or attempts to do so, the actuator applies a force to a load. Actuation may be made even faster by passing a bias current through the elements to keep them just below their critical temperature.

When cool, the memory metal is malleable and exerts little force: It therefore has no tendency to snap back to its cold-formed shape when the current is turned off. If the load exerts a unidirectional force on the actuator (for example, if the load is under the influence of gravity or a spring), the load tends to restore the actuator to its cold shape as it cools. For loads that do not restore the elements to their starting shapes and for faster restoration, a second set of memory-metal actuators can be placed in opposition to the first set.

Another version of the actuator has elements of different thicknesses so that each element has twice the stiffness of its thinner neighbor. With this binary relationship between elements, binary-coded signals may be used directly to control the element switches. The total force exerted by the actuator is then directly proportional to the applied binary signal. This scheme is particularly suited to computer control and eliminates expensive digital-to-analog converters and precise stabilized amplifiers.

The switches may be transistors that connect the elements directly to a supply voltage. Since stiffness is determined by cross-sectional area, it is directly related to resistance. The power drawn by an element is in direct proportion to the heat needed to cause the phase change and is higher for elements of greater stiffness.

A linear actuator having a greater extension range can be constructed from helical elements. The elements may be arranged in a binary stiffness relationship, or they may simply be identical.

A rotary actuator can be formed from memory elements twisted into torsion springs. Again, the elements may be of binary-graded stiffness or of equal stiffness.

This work was done by Carl F. Ruoff of Caltech for **NASA's Jet Propulsion Laboratory.** *For further information, Circle 62 on the TSP Request Card.*

Inquiries concerning rights for the commercial use of this invention should be addressed to the Patent Counsel, NASA Resident Office-JPL [see page A5]. *Refer to NPO-15960.*

Designing More-Efficient Spur Gears

Gear-power losses are used to determine the most efficient design.

Lewis Research Center, Cleveland, Ohio

A relatively simple method to calculate spur-gear system power loss for a wide range of gear geometries and operating conditions has been developed. The method can be used to determine design requirements for an efficient gearset. The effects of spur-gear size, pitch, ratio, pitch-line velocity, and load on efficiency are readily predictable with this method. The analysis uses simple algebraic expressions to determine gear sliding, rolling, and windage losses and also incorporates an approximate ball-bearing power-loss expression. Predicted results have shown good agreement with published data.

A significant source of power loss in many drive systems is due to the gearing. Many methods have been proposed to calculate gear-power loss. Most of these methods utilize only a friction coefficient to calculate the gear-power loss. Few consider the losses associated with forming an elastohydrodynamic film (rolling traction), gear windage, or those associated with the support bearings. These latter power-loss terms contribute significantly to the power loss occurring under part-load operation.

Consideration of these speed-dependent loss terms becomes important in determining the cumulative power consumption of the machines that spend much of their operating lives at less-than-full-power levels. Furthermore, most of these earlier methods do not conveniently account for the effects of gear-mesh geometry, such as diametral pitch, tooth number, width, ratio, and operating conditions on gear-power loss.

This new method considers four major sources of gear-system power losses: sliding, rolling, windage, and support-bearing losses. It is applicable to spur gears of standard tooth proportions in which the gears are jet- or splash-lubricated. No accounting has been made for churning losses of gears running submerged in oil. The analysis considers sliding losses that are the results of friction forces developed as teeth slide across one another. The sliding loss can be found from $\bar{p}_S = C_1 f \bar{W} \bar{V}_S$, where f is the friction coefficient, W the average normal load, and $\bar{V}_S$ the average sliding velocity.

Rolling losses are generated in the formation of an elastohydrodynamic (EHD) film; that is, oil is squeezed between gear teeth and subsequently pressurized. The rolling loss is given by $\bar{P}_R = C_2 \bar{h} \bar{V}_T F CR$, where $\bar{h}$ is the elastohydrodynamic film thickness, $\bar{V}_T$ is the average total rolling velocity, F the face width, and CR the contact ratio (or average number of teeth in contact).

In addition to these losses, the method gives approximate expressions to calculate windage losses of the gears turning in the air/oil gearbox atmosphere and the power loss due to the support bearings. Windage and bearing losses together with the rolling loss often exceed the loss due to sliding alone.

The above method circumvents some of the limitations associated with earlier

(continued on next page)

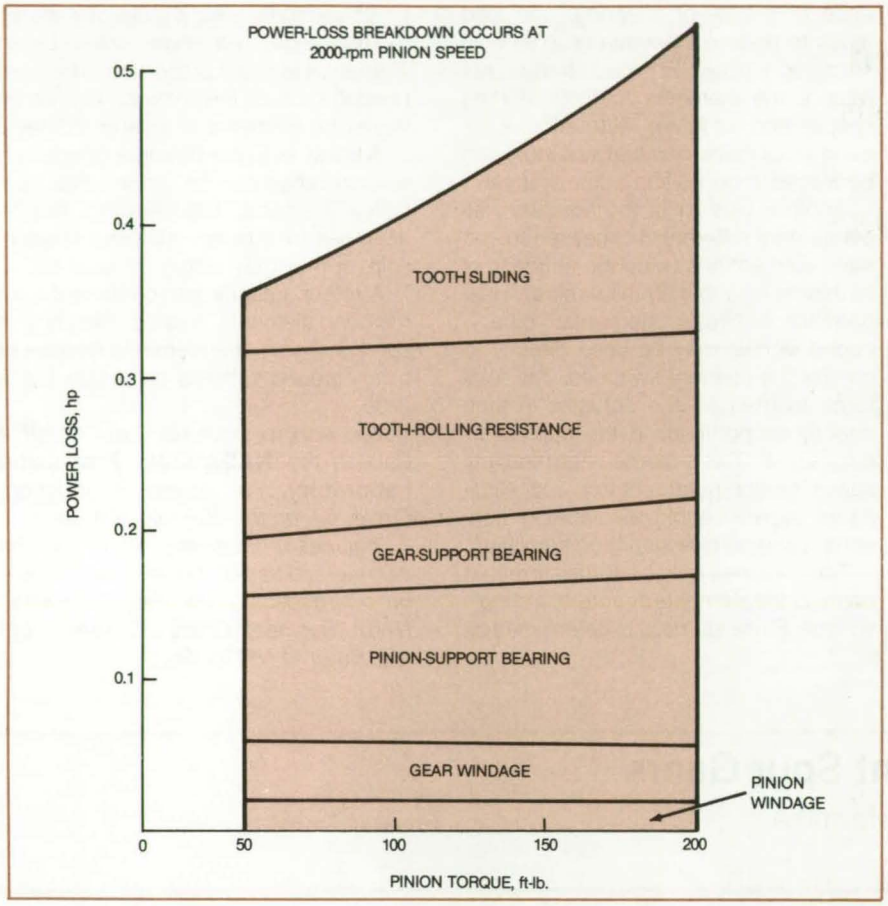

A **Spur-Gear Efficiency Analysis** for a given gear indicates how each of the listed parameters contributes to the gear-power loss. Gear designers can use this information to see which of the parameters are to be controlled to produce the most-efficient gear design.

predictive methods and permits the optimization of gear-tooth geometry for best efficiency consistent with tooth strength and scoring requirements. In general, results from parametric studies using this method suggest that large-diameter, fine-pitched (small-teeth) gears offer best efficiency. Component loss studies indicate that tare (no-load) losses at operating speed can be greater than half of the fully loaded loss, as shown in the figure.

This work was done by Stuart H. Loewenthal of **Lewis Research Center** *and Neil E. Anderson of the U.S. Army Aviation Research and Development Command. Further information may be found in:*

NASA TM-81426 [*N80-18406/NSP*], *"Effect of Geometry and Operating Conditions on Spur Gear System Power Loss"* [*$8.50*], *and*
NASA TM-81625 [*N81-17436/NSP*], *"Design of Spur Gears for Improved Efficiency"* [*$7*].

Copies of these reports may be purchased [prepayment required] from the National Technical Information Service, Springfield, Virginia 22161.
LEW-13921

Tube Alinement for Machining

Tubes are quickly alined with the machine-tool axis.

Marshall Space Flight Center, Alabama

A tool with stepped shoulders alines tubes for machining in preparation for welding. Alinement with the machine tool axis is accurate to within 5 mils (0.13 mm) and is completed much faster than visual setup by the machinist.

As shown in the figure, the tool is held in the chuck, while the tube is loosely clamped to the machine-tool table. The tool centers the tube, which is then tightly clamped on the table. The alinement tool is then removed and replaced with the cutting tool, which machines the tube to a clean cylindrical surface for welding. The stepped shoulders on the tool allow it to be used for tubes of different internal diameters.

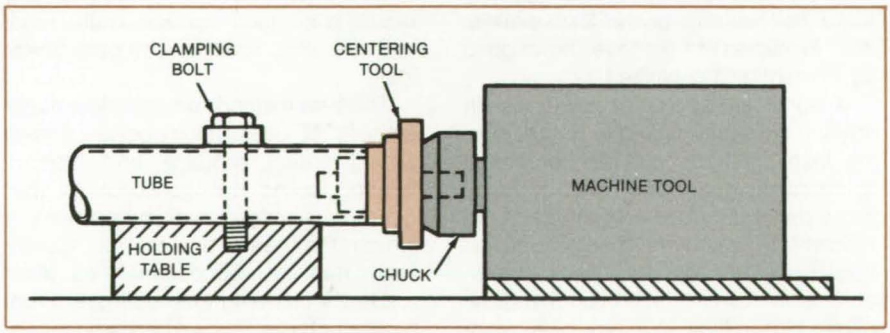

A **Stepped Rod** is held in a machining chuck to aline tubes with the machine tool axis.

This work was done by J. W. Garcia of Rockwell International Corp. for **Marshall Space Flight Center.** *No further documentation is available.*
MFS-19719

Controlling the Focus in Electron-Beam Welders

A set of parallel whirling wires samples the beam to determine its focus.

Marshall Space Flight Center, Alabama

A detector using two whirling wires measures the focus of the beam in an electron-beam welder. Conventional beam-focus detectors employ only a single whirling tungsten wire.

In the single-whirling-wire detector, the potential difference between the wire and ground is sampled, and the time the wire spends in the beam is determined. An oscilloscope displays the beam focus as a variable-width peak, which is monitored as the focus control is adjusted. However, the intense beam at the sharp focus sometimes melts the wire.

In contrast, the multiple-wire beam-sampling method provides for a simple null-meter focus indication that is easily controlled by the operator. The detector not only operates at high beam currents but also eliminates the need for an oscilloscope.

The principle of operation of the beam-focus detector is shown in the figure. Two or more wires, located at two different heights and separated by insulated spacer rings, sample the beam. The whirling wires sample the beam as before; but in this case the outputs from the wires are compared by an electronic circuit, and the resulting signal is fed to a null-meter. The operator merely adjusts the focus control to obtain a null reading on the meter. At that time the beam focus will be centered between the two parallel layers of wires.

This work was done by Douglas I. Macfarlane and Kirk W. Spiegel of Rockwell International Corp. for **Marshall Space Flight Center.** *No further documentation is available.*
MFS-19814

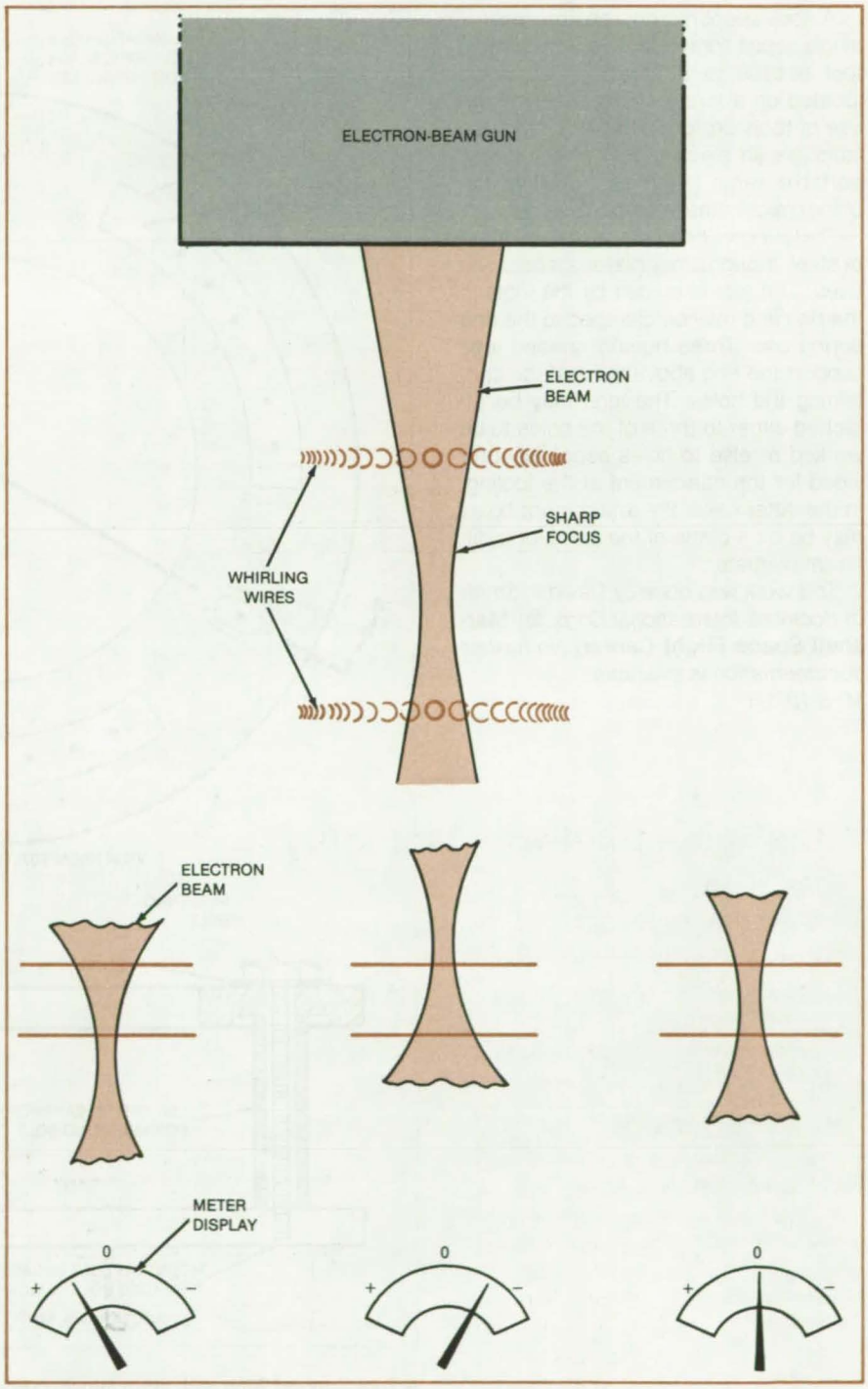

In the **New Electron-Beam Focus Detector,** whirling wires sample the beam at two locations. The new detector can be used at high levels of beam power because the wires are not located at the sharp focus of the beam.

Tool Support Ring

A slotted ring maintains tool alinement over holes on a circle.

Marshall Space Flight Center, Alabama

A tool support ring requires only a single repositioning to give a broaching tool access to a series of 66 holes located on a circle. It could permit the use of tools designed for hand-held use (such as an electric drill) where a less portable setup (such as a milling machine) might otherwise be required.

The support ring (see figure) is made of steel, though other materials could be used. The tool is guided by the slots in the ring and may be clamped to the ring during use. Three equally spaced legs support the ring above the surface containing the holes: The legs may be attached either to three of the holes to be worked or else to holes especially provided for the attachment of the tooling. In the latter case, the attachment holes may be on a circle of the same or a different diameter.

This work was done by David F. Smith of Rockwell International Corp. for **Marshall Space Flight Center.** *No further documentation is available.*
MFS-19765

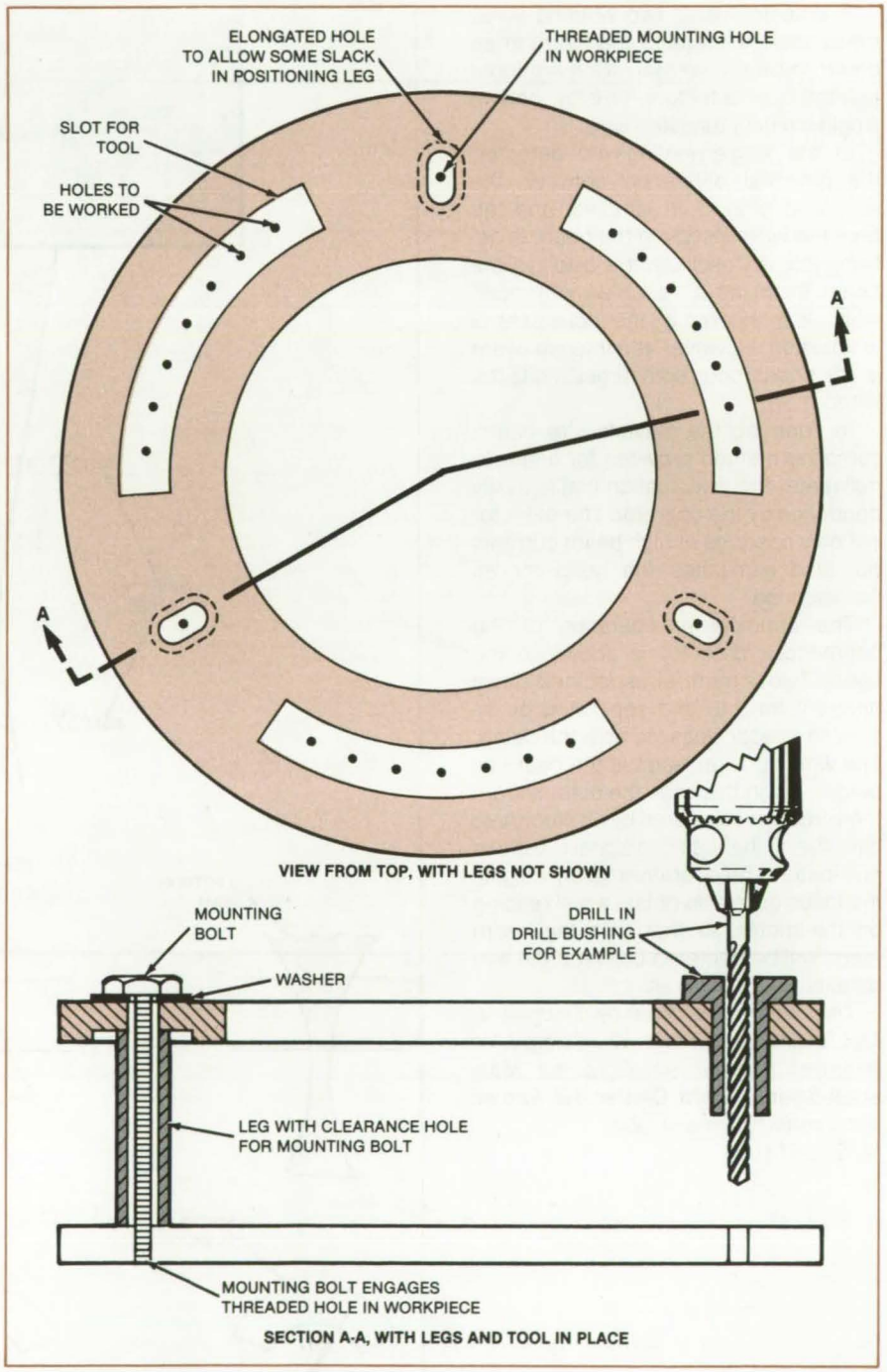

A **Tool Support Ring** with slots allows quick repositioning and reclamping in proper alinment of a tool over a series of holes located on a circle. Although originally devised to speed up use of a broaching tool, the same method would be applicable with such other tools as drills (shown here), reamers, and routers.

Reusable Release Mechanism

Lightweight unit replaces exploding bolts in applications where reuse is an advantage.

Lyndon B. Johnson Space Center, Houston, Texas

Although activated by an explosive charge, a new release mechanism differs from an exploding bolt in a key respect — the new mechanism is reusable, whereas an exploding bolt is not. Only the charge has to be replaced for the new device to be ready for service.

The new mechanism is illustrated in the figure. It is activated by the detonation of a small explosive charge or the rush of a pressurized gas or other fluid into the small chamber above the piston. The force on the piston breaks the shearpin that holds it in place. As the piston moves down, the piston rod pushes a slider downward. When the slider reaches the end of its travel, the rails are completely withdrawn from grooves in the horizontal shank, and the shank is free to move out through a circular hole in the slider. A spring-loaded follower then pushes the shank to the right, out of the sleeve.

Other advantages of the new mechanism include:

- Large areas carry the tensile load.
- The friction load decreases as the pressurized-chamber volume increases.
- The shank is completely relaxed before release.
- There is no appreciable wear or surface work hardening.

Designed to release the external tank from the Space Shuttle, the device has potential industrial applications; for example, in the emergency release of lifting cables from helicopters, cranes, and hoists.

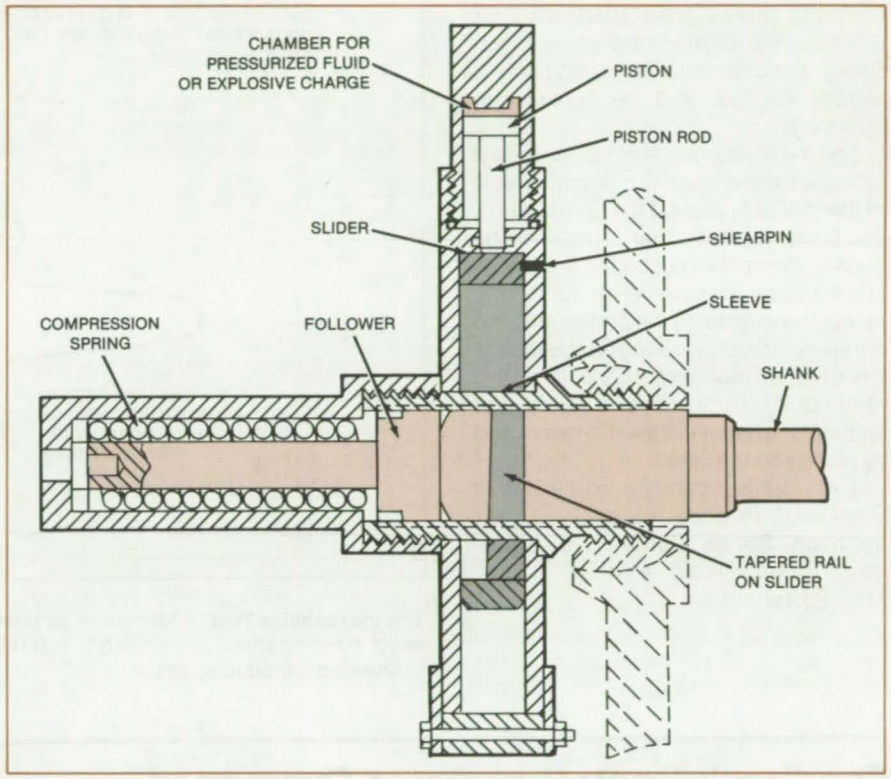

The **Slider Release Mechanism** is reusable. It bears heavy loads while latched, yet gives a smooth release motion. Release is effected by explosively driving the perpendicular slider out of engagement with the load-bearing shank.

This work was done by James W. Bunker and Robert S. Ritchie of TransTechnology Corp. for **Johnson Space Center.** *For further information, Circle 63 on the TSP Request Card.*

This invention is owned by NASA, and a patent application has been filed. Inquiries concerning nonexclusive or exclusive license for its commercial development should be addressed to the Patent Counsel, Johnson Space Center [see page A5]. Refer to MSC-20080.

Installation/Removal Tool for Screw-Mounted Components

Parts are positioned in otherwise-inaccessible places.

Lyndon B. Johnson Space Center, Houston, Texas

A tweezerlike tool simplifies the installation of screws in places that can be reached only through narrow openings. With changes in size and shape, the basic tool concept is applicable to the mounting and dismounting of transformers, sockets, terminal strips, and mechanical parts.

The tool is made from two pieces of steel wire. As shown in the figure, it includes a long, tapered U-shaped member and a short crossmember that bridges and slides along the legs of the "U" to clamp them together. The ends of the longer piece are bent into approximately-circular open-ended loops in the plane perpendicular to that of the "U."

(continued on next page)

Loose-fitting and slightly-open-ended loops on the ends of the shorter member engage the longer member.

For installation of a part, the loops at the end of the "U" are fitted around the mounting screwheads. The crossmember is slid toward the ends of the "U" to clamp the tool onto the screws. The tool is then used to hold the part in position while the screws are started into their mating holes with a long screwdriver. Finally, the crossmember is slid back to release the tool, and the screws are tightened.

For removal, the screws are first loosened just enough to permit the ends of the tool to fit around the screwheads. The crossmember is then slid toward the ends to clamp the tool on the screws as in installation. The screws are turned the rest of the way out of their holes, and the part is removed by pulling on the tool. In the case of multiwire connectors, this method of removal eliminates the damage that would otherwise be caused by pulling on the wires.

This work was done by John P. Ash of Rockwell International Corp. for **Johnson Space Center.** *No further documentation is available.*
MSC-20606

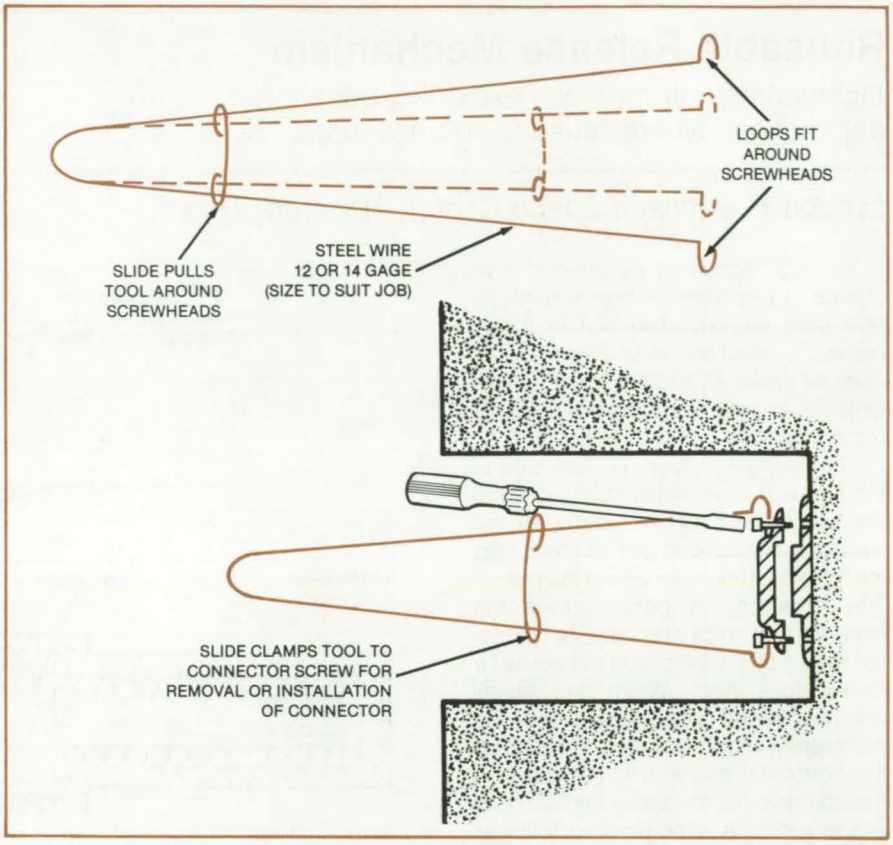

The **Inexpensive Tool** is fabricated as needed by bending two pieces of steel wire. The exact size and shape are slected to suit the part to be manipulated and the nature of the inaccessible mounting space.

Feedback Control of Rotor Overspeed

Developed for helicopter rotors, a servo alleviates the pilot's concern about overspeed.

Ames Research Center, Moffett Field, California

A proposed feedback system for automatically governing helicopter rotor speed promises to lessen the pilot's workload, enhance maneuverability, and protect the airframe. With suitable modifications, the concept could also be applied to control the speed of electrical generators, automotive engines, and other machinery.

An overspeeding helicopter rotor can shake the aircraft apart; yet the times when overspeed is most likely to occur — during abrupt change-of-direction maneuvers or rapid deceleration — are precisely the times when a pilot's attention is diverted. Thus the usual way of preventing overspeed by manual control of collective pitch can easily be neglected. The proposed system would control the rotor speed even when it is necessary to dissipate power and the engine cannot act as a brake. It will eliminate the problems of gear-train resonance at excessive speeds. It will also eliminate the drive-train-torque impact and the sudden increase in power demand upon the engine that occur when the overrunning clutch is reengaged to a previously overspeeding rotor.

With the new speed-control concept, a servomechanism, installed as a series servo in the collective control system (see figure), regulates rotor speed when it exceeds a predetermined limit. The rotor speed is continuously compared with the limit. When the speed is below the limit, a diode in the servomechanism circuit blocks the comparison signal. When the speed exceeds the limit, the servomechanism becomes active.

The servo progressively increases the collective pitch of the rotor blades. The rotor thus dissipates overspeed energy through dynamic braking. The airframe

and pilot are protected from extreme pitch excursions by limiting the maximum total pitch change to a small value: 3° are representative, although the precise value depends on the helicopter type.

Both instantaneous-proportional and time-integral gain functions are included in the servo circuit so that the frequency response and damping ratio can be adjusted for the particular aircraft. The input to the integrator also provides positive system recovery after overspeed has been brought under control.

This work was done by Gary B. Churchill of **Ames Research Center.** *No further documentation is available.*

Inquiries concerning rights for the commercial use of this invention should be addressed to the Patent Counsel, Ames Research Center [see page A5]. Refer to ARC-11404.

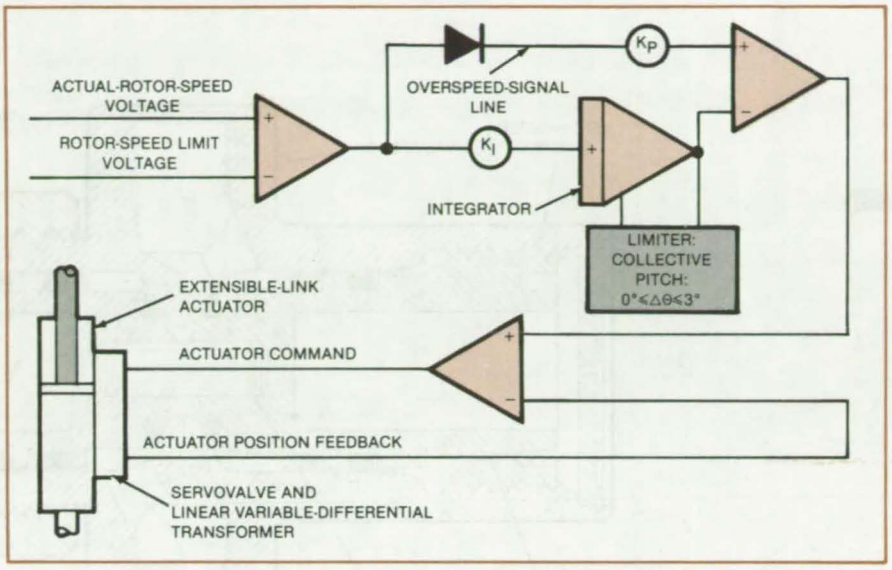

The **Rotor Collective-Pitch Increment** is set in response to instantaneous and time-integrated overspeed signals. A limit is set electrically to prevent the integral gain from overdriving the system. The pitch limit must correlate with the travel available from the extensible-link actuator. K_p represents the feedback-system proportional gain (degrees collective pitch/overspeed), and K_I represents the feedback-system integral gain (degrees collector pitch/time integral of overspeed).

Double-Poppet Valve

Two coactuated poppets seal redundantly.

Lyndon B. Johnson Space Center, Houston, Texas

A new valve design includes two poppet/seat combinations that are actuated simultaneously. If one fails, the other continues to seal against fluid flow. As with the triple-seal valve described in the following article, the valve is primarily useful for handling dangerous fluids and is lighter and more compact than comparable redundant-valve systems used at present.

The new valve contains two opposing poppets with conical sealing surfaces and an O-ring groove in each such surface. Each poppet seals against one of the two conical surfaces of an annular seating projection that is part of the valve body.

In the non-rotating-poppet version (Figure 1), the poppets engage a common axial shaft: one via right-hand threads and the other via left-hand threads. A knob is attached to the shaft at one end. Keys fixed to the valve body

(continued on next page)

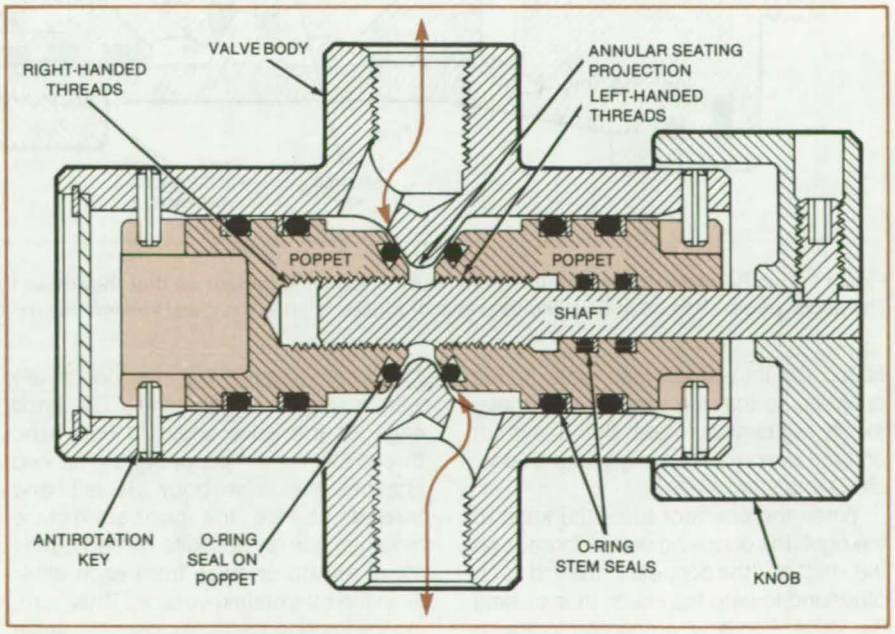

Figure 1. **Two Nonrotating Poppets** are moved toward or away from each other and their seats by turning a shaft with opposing threads.

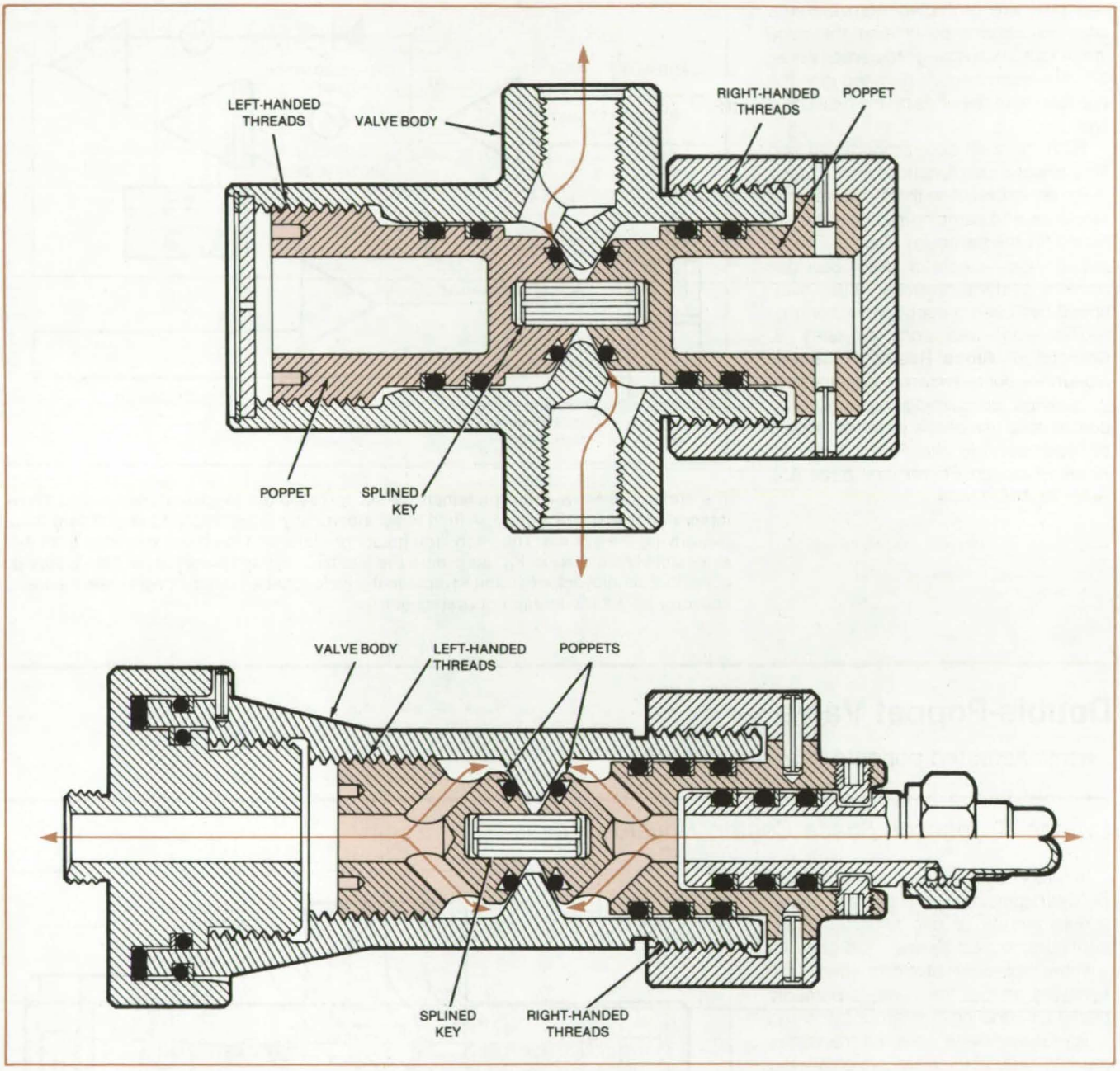

Figure 2. **Two Rotating Poppets** turn together but on opposing threads so that they move toward or away from each other and their seats. The upper version has crossflow like the valve of Figure 1, while the lower version has axial flow.

fit loosely into lengthwise slots in the poppets, so that the poppets can move axially but cannot rotate. Both the shaft and the poppets are equipped with double O-ring stem seals.

When the operator turns the knob to the right, the opposing sets of threads on the shaft pull the poppets in toward each other and toward the seats, thus closing the valve. Similarly, a counterclockwise knob motion opens the valve.

In the rotating-poppet versions (Figure 2), there is no shaft, and the knob is fixed to one of the poppets. That poppet is keyed to the other in such a way that they rotate together but can slide axially with respect to each other. The knob engages the valve body via right-hand threads, while the poppet at the far end engages the valve body via left-hand threads. Since the poppets rotate together but on opposite threads, they move toward or away from each other as in the nonrotating version. Thus, turning the knob to the right closes the valve by seating both poppets, while rotating to the left opens the valve by unseating them.

One characteristic of the new design that should be noted is that the stem seals on the upstream side are subjected to high pressure even when the valve is closed. This feature may increase the susceptibility to leakage to the environment, thus precluding use in some hazardous-fluid systems.

This work was done by William C. Huber of **Johnson Space Center.** *No further documentation is available.*

Inquiries concerning rights for the commercial use of this invention should be addressed to the Patent Counsel, Johnson Space Center [see page A5]. *Refer to MSC-20627*

Triple-Seal Valve

All flow paths include three barriers to leakage.

Lyndon B. Johnson Space Center, Houston, Texas

The handling of poisonous, flammable, or corrosive fluids should be made safer by a new triple-seal valve concept. Three valves would be assembled in series, with the stem mechanism for one valve serving as the body of the next valve. The new design is lighter and more compact than the conventional three-series-valve combinations used with hazardous fluids.

According to the new design, the three valves would be stacked along a common cylindrical axis (see figure). Each valve has three stem seals, with each seal at a different diameter so that a scratch on one cylinder wall is unlikely to cause a leak in all three.

Each stem body has an axial flow passage. The passage diverges into two or more passages at the small end to circumvent a hardened ball that serves as the poppet. In the closed position, the ball seats at the edge of the hole in the adjacent body, thus blocking the flow from and to the passage in the adjacent body.

Each valve is opened or closed by turning its actuator collar. The collar for one stem body is engaged by threads to the adjacent body. When a collar is rotated clockwise, it pushes against a Belleville spring that pushes against a retaining ring on the stem body, thereby pushing the stem body into the seated (closed) position. The loading of the Belleville spring helps to prevent the loosening of the actuator collar during vibration.

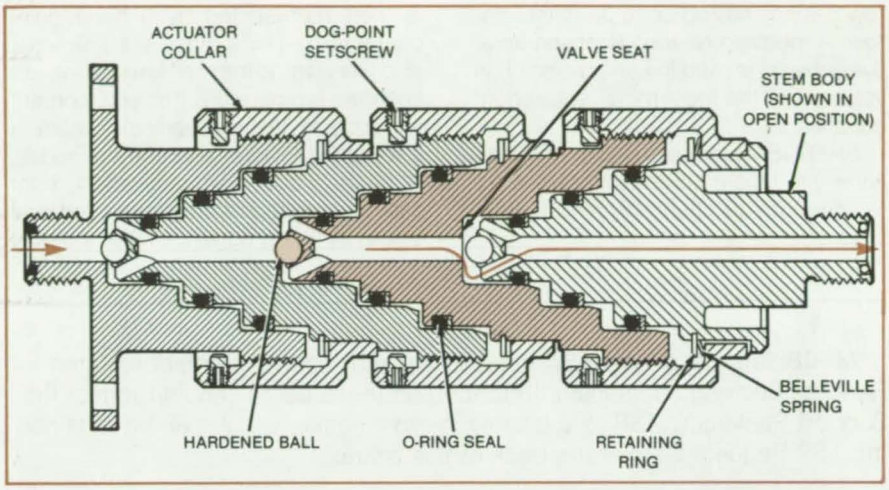

The **Triple-Seal Valve Assembly** for dangerous fluids consists of three in-line valves, each equipped with three stem seals for extra protection against leaks. The left and middle valves are depicted in closed position, while the right valve is shown open.

A valve is opened by turning its collar counterclockwise. A dog-point setscrew prevents the collar from being accidentally unscrewed from the threaded body.

This work was done by William C. Huber of **Johnson Space Center.** *No further documentation is available.*

Inquiries concerning rights for the commercial use of this invention should be addressed to the Patent Counsel, Johnson Space Center *[see page A5].* *Refer to MSC-20628.*

Computer Programs

These programs may be obtained at very reasonable cost from COSMIC, a facility sponsored by NASA to make new programs available to the public. For information on program price, size, and availability, circle the reference letter on the COSMIC Request Card in this issue.

Spherical-Bearing Analysis Program

Program predicts thermomechanical performance of spherical roller bearings.

Computer program SPHERBEAN, has been developed to predict the thermomechanical performance characteristics of double-row spherical roller bearings over a wide range of operating conditions. The analysis allows six degrees of freedom for each roller and three for each half of an optionally split cage. Program capabilities provide sufficient generality to allow the detailed simulation of both high-speed (i.e., 1.0×10^6/DN) and conventional bearing operation. Emphasis has been placed on detailing the effects of roller skew, roller end-to-flange contact, and changes in clearance as functions of speed, mounting fits, and temperature.

The complete range of EHD (elastohydrodynamic) contact considerations has been treated in the computation of raceway and flange contact detail. A flexible outer-ring option is made available for the simulation of planet bearing performance, where the outer ring of the bearing is integral with the planet gear. The program will also compute the effects of carrier motion on bearing performance

(continued on next page)

by the consideration of centrifugal forces generated by the kinematics of planetary motion.

SPHERBEAN has the capability to address quasi-dynamic equilibrium with the consideration of EHD and hydrodynamic forces at the raceway and flange, cage skew control, heat generation, and centrifugal loads for single- or double-row designs having up to 30 rollers per row. A modified Newton-Raphson iterative scheme is used to compute solution values for the governing equilibrium equation set.

SHERBEAN may be used to compute either the time-transient or steady-state temperature distribution within a system defined by the bearing and its environment. The temperature portion is designed to produce temperature maps for an axisymmetric mechanical system of any geometrical shape. The physical system is first approximated by an equivalent "nodal network," which consists of a number of elements having simple geometric shapes. Each element is then represented by a node point characterized by a mass, surface area, and having either a known or an unknown temperature. The environment surrounding the mechanical system is also represented by one or more nodes. With the node points selected, heat balance equations are formulated and solved by the program for the nodes of unknown temperature. These equations become nonlinear when there is radiation between two or more of the node points considered.

The SPHERBEAN program is written in FORTRAN IV for use on a UNIVAC 1100 computer. The program requires preparation of input data that, in general, describe the bearing geometry, properties of the materials used, and specify the imposed operating conditions.

This program was written by Robert J. Kleckner of SKF Industries for **Lewis Research Center.** *For further information, Circle M on the COSMIC Request Card.*

LEW-13626

MiniBriefs describe NASA innovations and reports in an abbreviated format. Readers desiring additional information on these items should request the Technical Support Packages (TSP's), available in most cases, which can be obtained by using the TSP Request Card at the back of this issue.

Depth Gage for Threaded Holes

Tool gives a direct reading of depth, eliminating estimates and calculations.

A tool for measuring the threaded depth of tapped holes is accurate and easy to use. The depth is read from a graduated scale on the tool.

The threaded end of the tool is screwed into the hole to be measured. A measuring sleeve is pushed up the shaft of the tool by the surface surrounding the tapped hole as the tool is screwed into the hole. Finally, the tool bottoms out in the hole as the thread ends. At this point, the top edge of the sleeve indicates the hole depth on the scale. When the tool is removed from the hole, the spring-loaded sleeve returns to zero.

This work was done by Michael A. Kahn of Rockwell International Corp. for **Marshall Space Flight Center.** *For further information, Circle 151 on the TSP Request Card.*

Inquiries concerning rights for the commercial use of this invention should be addressed to the Patent Counsel, Marshall Space Flight Center [see page A5]. Refer to MFS-19884.

Stalled-Flow and Head-Loss Model for Diffuser Pumps

The inlet transition zone is modeled as a two-dimensional cascade.

A modeling procedure approximates the inlet transition zone (blade leading edge to blade throat) of a diffuser pump as a two-dimensional cascade, the properties of which are well known. (The stall phenomenon starts in the transition region when the pump operates far enough below design flow.) The model can be applied to stators as well as rotors. The procedure is much faster than previous methods.

The stall-flow and head-loss properties predicted by this procedure agree well with the experimental data available for three pumps, the Space Shuttle main-engine preburner pump, high-pressure fuel pump, and low-pressure oxidizer inducer.

This work was done by Sen Y. Meng of Rockwell International Corp. for **Marshall Space Flight Center.** *For further information, Circle 152 on the TSP Request Card.*

MFS-19748

Retention Mechanism for Spinning Objects

The mechanism holds securely but allows release of a rotating body or shaft.

A mechanism enables the controlled release of two rotating objects. Designed to retain a spin-stabilized satellite during launch and spinup in orbit and eject it into space at high velocity, the mechanism may be applicable to some kinds of motor starters, drive shafts, or other drive systems that must be released while rotating.

The mechanism consists of three lugs on the driven object that reach through the spin table and engage three spring-loaded pins pressing outwardly against a stationary retaining cylinder. The lugs, spin table, and pins are rotated by an electric motor. For ejection, the spin table is pushed outward (along the spin axis) by a pneumatic piston rod. When the three pins clear the retaining cylinder, they move radially outward and disengage from the lugs. The driven object separates from the mechanism along the spin axis.

This work was done by Richard A. Cloyd of **Marshall Space Flight**

Center. *For further information, Circle 153 on the TSP Request Card.*

Inquiries concerning rights for the commercial use of this invention should be addressed to the Patent Counsel, Marshall Space Flight Center [see page A5]. Refer to MFS-25957.

Miniature Rotator

It provides precise rotation in tight spaces.

A device for making a small, precise rotation of objects in cramped spaces consists of a V-groove machined in a block of aluminum (or nylon) and a flat, slotted bar clamped across the groove. A cylindrical object to be rotated rests in the groove, with the slotted bar bearing on its surface. Using a drivescrew, the bar is moved horizontally, causing the cylinder to rotate because of friction between the bar and the cylinder. The device has been used to rotate lenses until they are in precise alinement with the optical axis of an injection laser.

Each lens was 0.3 in. (7.6 mm) in diameter and lay in the V-groove with about 0.025 in. (0.64 mm) above the block surface. The bar was moved less than 0.5 in. (12.7 mm) to rotate a lens the few degrees needed for alinement.

This work was done by Clyde Carl Neil of RCA Corp. for **Langley Research Center.** *No further documentation is available.*
LAR-12765

Preventing Motor Damage Due to Rapid Reversal

A reversal switch that took more time to operate allowed gentler deceleration before reversal.

A dc motor on a rotating table could be switched from forward to reverse by the flick of a switch. However, the motor shaft (which operated at up to 1,750 rpm) was damaged repeatedly because it was not designed to withstand the stresses. Replacing the switch with one that required both a twisting and a pulling motion solved the problem by slowing down the reversal procedure, giving the motor time to decelerate gradually.

This work was done by Robert Fetters of Rockwell International Corp. for **Marshall Space Flight Center.** *No further documentation is available.*
MFS-19702

A One-Hand Nut and Bolt Assembly Tool

C-clamp-shaped box- and socket-wrench assembly holds nut on blind side in alinement to receive bolt from open side.

A special wrench speeds nut and bolt assembly when there is insufficient room to hold the nut behind the bolthole with a standard tool. A C-shaped part with a box-wrench head (located in the same position as the anvil in a C-clamp) holds the nut behind the bolthole. A shaft with a socket-wrench head to hold the bolt passes through a close-fitting hole in the near end of the C-shaped part (like the screw in a C-clamp). As the shaft is turned, it advances the bolt through the bolthole into the nut.

This work was done by James M. Spencer of Rockwell International Corp. for **Marshall Space Flight Center.** *For further information, Circle 154 on the TSP Request Card.*
MFS-19691

Portable Power Broach

Openings can be cut at remote or confined places.

Small holes or grooves are broached by a portable tool that runs on hydraulic or pneumatic power. The tool is designed for use on parts that previously had to be brought to a stationary broaching machine.

The tool is a hand-held version of the larger stationary broaching machines. It is equipped with fittings and hoses to connect to a power source and is small enough to be carried in the field or used in confined spaces.

This work was done by Alan J. Appleton of Rockwell International Corp. for **Marshall Space Flight Center.** *For further information, Circle 155 on the TSP Request Card.*
MFS-19679

Pressure-Driven Waterflow Cleaning Device

High-pressure gas mixed with water is an effective cleaner.

When a gas at high pressure is mixed with water, the expanding gas bubbles in the jet give more vigor to the liquid. This fluid agitation can be effectively used to clean a small, normally inaccessible cavity or passage. Internal contamination can be removed by flowing and backflushing with the high-pressure water jet. Because pressures in excess of 100 psi (700 kN/m^2) are commonly used, extreme safety precautions must be followed to prevent damage to the internal components of the object cleaned.

This work was done by R. Rhea and M. Gants of Rockwell International Corp. for **Marshall Space Flight Center.** *No further documentation is available.*
MFS-19638

Temporary Sealing of Cavities for Leak Testing

Wax seals cavity openings to permit helium leak test of cavity welds.

The testing of repaired pinhole leaks with helium in the Space Shuttle main-engine combustion chamber necessitated a way to seal off passages leading to a manifold that was not yet installed. A wax, such as Rigidax or equivalent, proved to be effective in sealing the passage.

This technique facilitates leak testing of cavities in components of larger systems that cannot be otherwise sealed off at the time the leak testing should be done. Testing separate components also avoids the potentially higher costs of delaying the test until after final assembly.

This work was done by J. Little of Rockwell International Corp. for **Marshall Space Flight Center.** *No further documentation is available.*
MFS-19646

Transformer and Meter Tester

The components that determine and indicate home position on a numerically-controlled machine tool are tested.

A numerically-controlled 5-axis machine tool (Sunstrand OM-3, or equivalent) uses a transformer and a meter to determine and indicate whether the tool is in home position, but lacks a built-in test mode to check them. The tester makes it possible to test and, if need be, repair these components at the machine rather than replace them when their operation seems suspect. This reduces

(continued on next page)

the number of new units used and reduces the number of units required for backup. The tester operates on 120 Vac and contains a meter, a transformer, two potentiometers, and a power switch.

This work was done by Russell M. Stoms of Rockwell International Corp. for **Marshall Space Flight Center.** *For further information, Circle 156 on the TSP Request Card.*
MFS-19708

Hydraulic Tube Expander

Versatile tool is useful in hard-to-reach locations.

A portable hydraulic tube expander expands small, thick-walled tubes in hard-to-reach locations. The tool is particularly useful in situations where a mechanical expander is too fragile to produce the desired expansion; for example, in the small tubular elements of preburner injectors.

The tool consists of a long, thin tube attached to a firing mechanism for discharging a 22-caliber (6-mm) cartridge. The thin tube, inserted into a tube designated for expansion, has four small outlets located at its end. These outlets release the pressure from the fired cartridge, causing the desired expansion.

This work was done by Richard K. Burley of Rockwell International Corp. for **Marshall Space Flight Center.** *For further information, Circle 157 on the TSP Request Card.*
MFS-19731

Burner-Injector-Post Tip

Bimetallic tips attached to injector posts improve burner performance and reliability.

Copper- or nickel-tipped inserts attached to preburner and main-burner injector posts prevent local ignition spots. The bimetallic tip attached by plating, welding, or threading to the tip of the steel posts allows excess heat generated at the tip to be dissipated circumferentially and axially through thermal conduction. Allowable injector performance and reliability are increased, and jet-burning symmetry is improved.

This work was done by William R. Wagner and Robert Saxelby of Rockwell International Corp. for **Marshall Space Flight Center.** *For further information, Circle 158 on the TSP Request Card.*
MFS-19827

Attaching Chuck Keys to Machine Tools

Chuck keys are attached to portable machine tools by retracting lanyards.

Each machine tool must have its chuck key available for use at all times. If it is attached to the tool by a dangling cord, both convenience and safety are compromised. At NASA's Kennedy Space Center, one end of the grasping pin is welded to a lanyard and the other fits into a hole drilled in the base of the tool. The lanyard is held taut by a recoil caddy attached to the tool base. The chuck key is thus available for use when needed and is safely secured during operation of the tool.

This work was done by V. H. Richardson of Boeing Services International for **Kennedy Space Center.** *For further information, Circle 159 on the TSP Request Card.*
KSC-11249

Retrofitting Vibration Dampers

Force-fit tubes eliminate fatigue problem.

A simple method of installing support tubes allows retrofitting of vibration-reducing elements. The method was developed for preburners on the Space Shuttle main engine. A preburner contains a cylindrical central oxidizer post surrounded by a fuel sleeve, with varying clearance between the post and the sleeve. The cantilevered post tended to vibrate as high-pressure fuel impinged on it and was thus prone to failure.

The problem was solved by three small tubes inserted in the clearance between the post and the sleeve at equally spaced intervals around the circumference of the post and parallel to the post axis. The tubes deform elastically as they are inserted and expand partially as the gap becomes wider. The tubes are still slightly deformed in their final location in a force fit and are thus retained there. They provide the support necessary to dampen the vibrations of the post.

This work was done by Theodore C. Adams and Premysl Jencek of Rockwell International Corp. for **Marshall Space Flight Center.** *For further information, Circle 160 on the TSP Request Card.*
MFS-19790

Wire Electrical-Discharge Machining Aid

Rerouting cutting wire by adding idler rollers permits some cuts that would otherwise be blocked.

The wire in a standard wire electrical-discharge machine (WEDM) goes in a straight line from one wire spool to the other. Accordingly, only simple straight-through cuts are possible. By adding two idler rollers, which put two right-angle bends in the wire path, the WEDM can be temporarily modified to permit some types of cuts that would otherwise be blocked by projections on the part being machined, such as an overhanging lip or flange.

This work was done by T. E. Gollihugh of Rockwell International Corp. for **Marshall Space Flight Center.** *For further information, Circle 161 on the TSP Request Card.*
MFS-19643

Motorized Cryogenic Valve

An electronic controller operates a modified cryogenic angle valve.

A remotely-controlled cryogenic valve operates over a temperature range from room temperature to 2 K. The valve can be used in helium dilution refrigerators, cryostats, and adiabatic-demagnetization refrigerators.

A standard cryogenic angle valve, the major component, is machined to reduce its weight. The valve seat is made of copper. The valve is operated by a miniature dc motor and an integral gearset that is coupled to a power transmission.

To prevent sticking, an electronic controller varies the current, which is limited to 1.2 A to prevent overheating and damage during operation. In opening the valve, the controller allows a high initial current, which quickly falls off. Operation in closing the valve is similar, except that the motor is allowed to stall as the valve seats. The stall current is maintained for about 3 seconds to ensure seating.

This work was done by L. J. Salerno, J. Vorreiter, Y. Matsumoto, and W. B. Van Ark, of **Ames Research Center** *and A. L. Spivak of Transbay Electronics, Inc. For further information, Circle 162 on the TSP Request Card.*
ARC-11452

Fabrication Technology

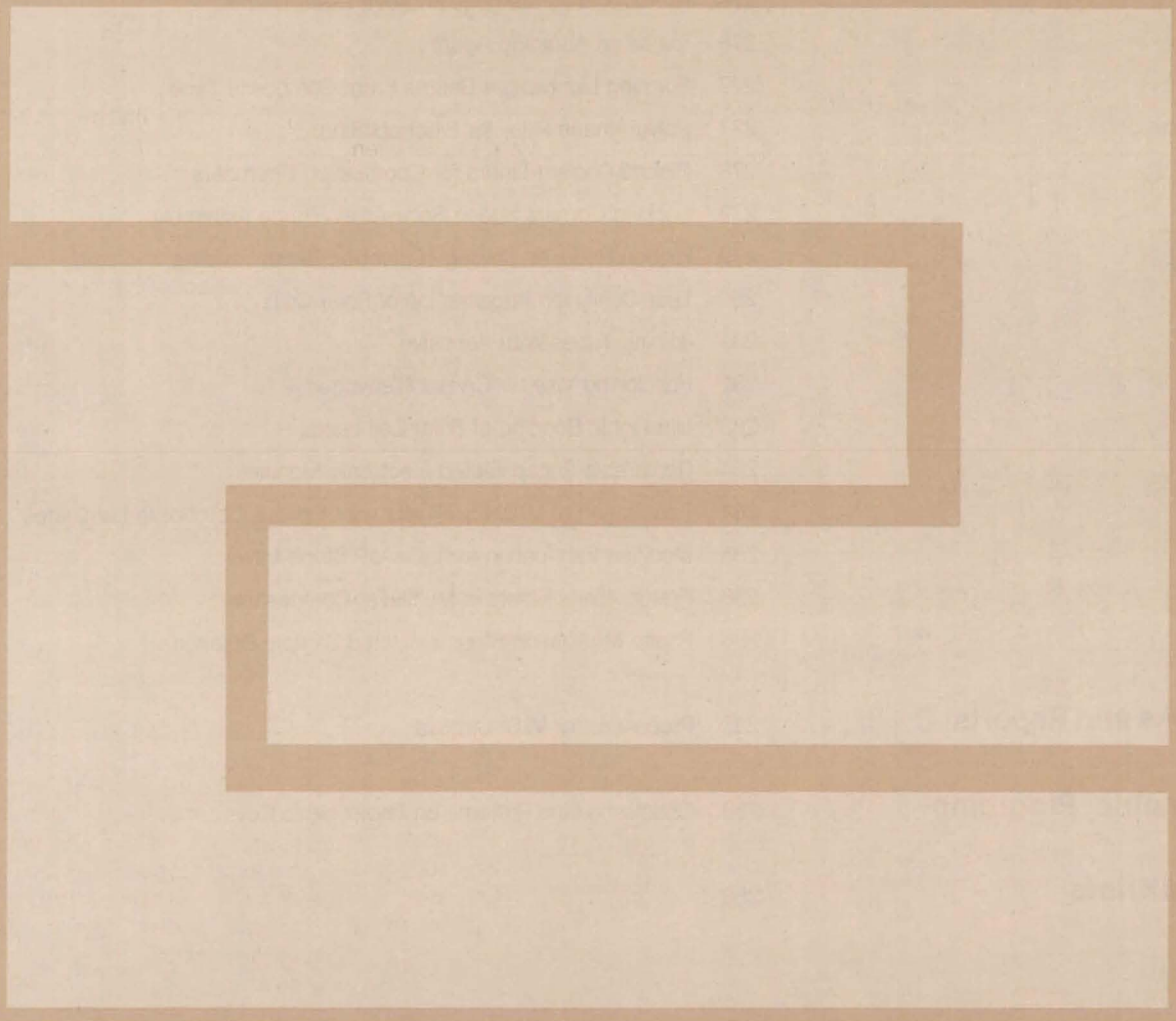

Hardware, Techniques, and Processes

271 Bonded Lockstitch for Insulating Blankets
272 Repairing Hidden Cracks in Coolant Tubes
273 Automatic Guidance System for Welding Torches
274 Fitting Flexible Coverings to Contoured Surfaces
275 IC Fabrication Methods Improve Laser Diodes
276 Ice as an Abrading Agent
277 Forming Lightweight Beams From Composite Tape
277 Polyurethane Filler for Electroplating
278 Ribbed Coolant Liners for Combustion Chambers
279 Locking Corners Speed Solar-Array Frame Assembly
279 Ribbon Reduces Spiking in Electron-Beam Welding
280 Less-Costly Ion Implantation of Solar Cells
281 Joining Tubes With Adhesive
282 Positioning Vise for Crystal Cleavage
283 Ultrasonic Bonding of Solar-Cell Leads
284 Repairable Encapsulated Electronic Modules
284 Fabrication of Multi-Ply Birefringent Fibrous Composite Laminates
285 Modified Fabrication for InGaAsP Stripe Laser
286 Frame Alines Fibers in Multilayer Composites
286 Phase Modulation Stops Levitated Sample Rotation

Books and Reports

287 Processes for VLSI Circuits

Computer Programs

288 Optimizing Grid Patterns on Photovoltaic Cells

MiniBriefs

288

Bonded Lockstitch for Insulating Blankets

An adhesive prevents unraveling at high temperatures.

Lyndon B. Johnson Space Center, Houston, Texas

An improved sewing technique for high-temperature [750°-to-1,200° F (400°-to-650° C)] insulating blankets prevents stitch failure in hot, turbulent environments. In the new technique, the standard lockstitch is modified to isolate single-stitch failures.

The insulating blanket consists of a fibrous batting sandwiched between a quartz-fabric outer facing and a glass-fabric inner facing, with nominal total thickness ranging from 0.45 to 0.95 in. (1.1 to 2.4 cm). The inner and outer facings are stitched with an outer (needle) thread of polytetrafluoroethylene-coated quartz and an inner (bobbin) thread of glass, with a stitch density of 4 ± 1 per in. (1.6 ± 0.4 per cm).

In conventional lockstitching (shown in the middle part of figure), a loop of the needle thread is passed through the two facings and caught by the bobbin thread. The needle thread is then pulled back until the interlacing of both threads is midway between the facings. If the thread fails at one stitch, the thread can loosen along its entire length, thus unraveling an entire row of stitches.

In the improved technique (lower part of figure), the bobbin thread is kept at the blanket surface. A silicone adhesive is applied to all the bobbin/needle intersections, so that a failure at one point will not propagate along the thread.

The improved blanket has been tested in experiments and is scheduled for use on the Space Shuttle. It is suitable for use in aerodynamic and other applications where there is turbulence. Fabrication is simple, since the modified lockstitch can be produced by a simple adjustment of thread tension and sewing-machine timing.

This work was done by Jonathan M. Rivin, Charles A. Morant, and Richard M. Ehret of Rockwell International Corp. for **Johnson Space Center.** *For further information, Circle 64 on the TSP Request Card.*
MSC-20283

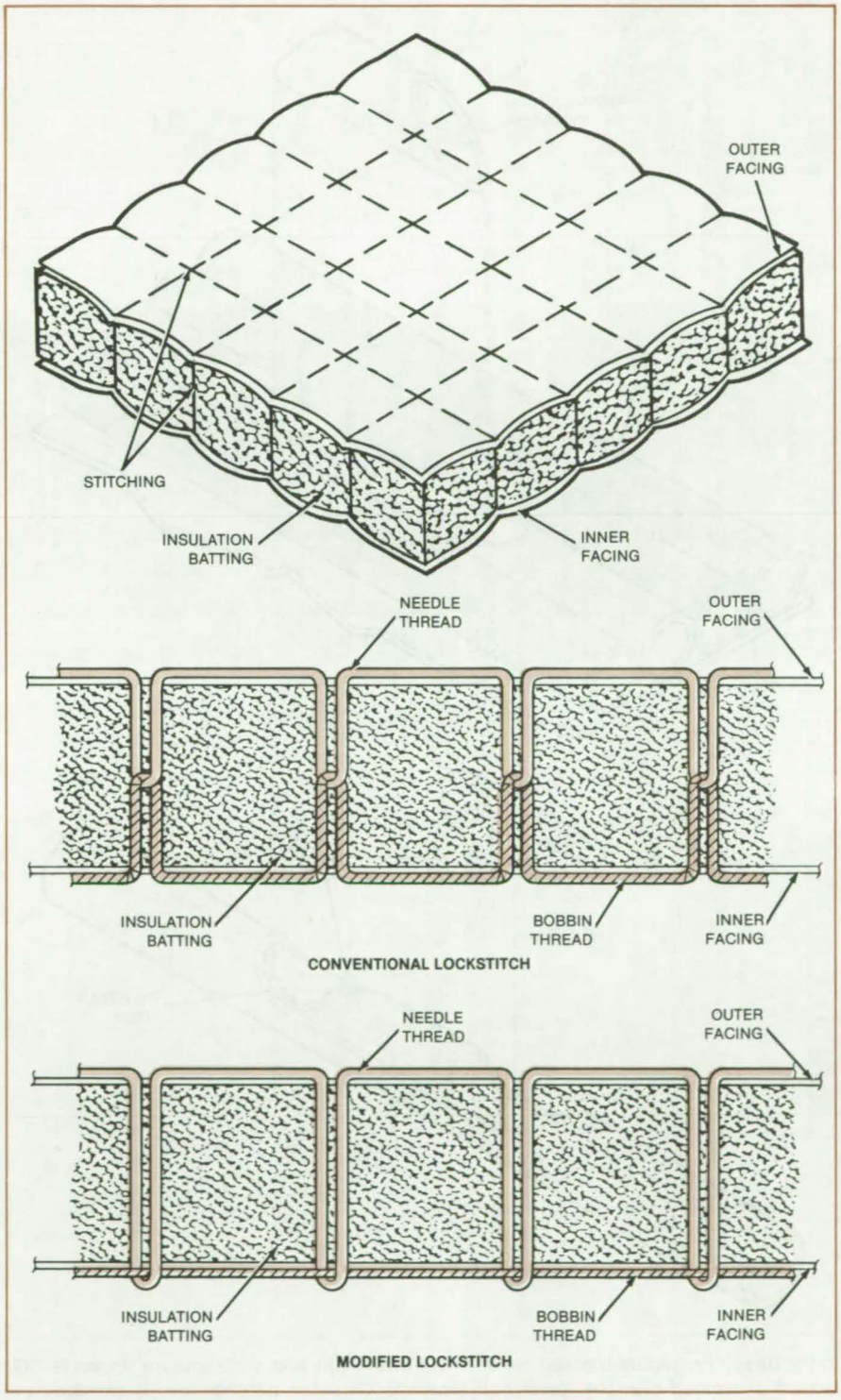

An Insulating Blanket (top) is sewn with conventional (middle) or modified (bottom) lockstitches. The threads are cemented together at their intersections in the modified stitching method to prevent unraveling.

Repairing Hidden Cracks in Coolant Tubes

"Fishmouth" inserts stop leaks in hidden walls of tubes.

Marshall Space Flight Center, Alabama

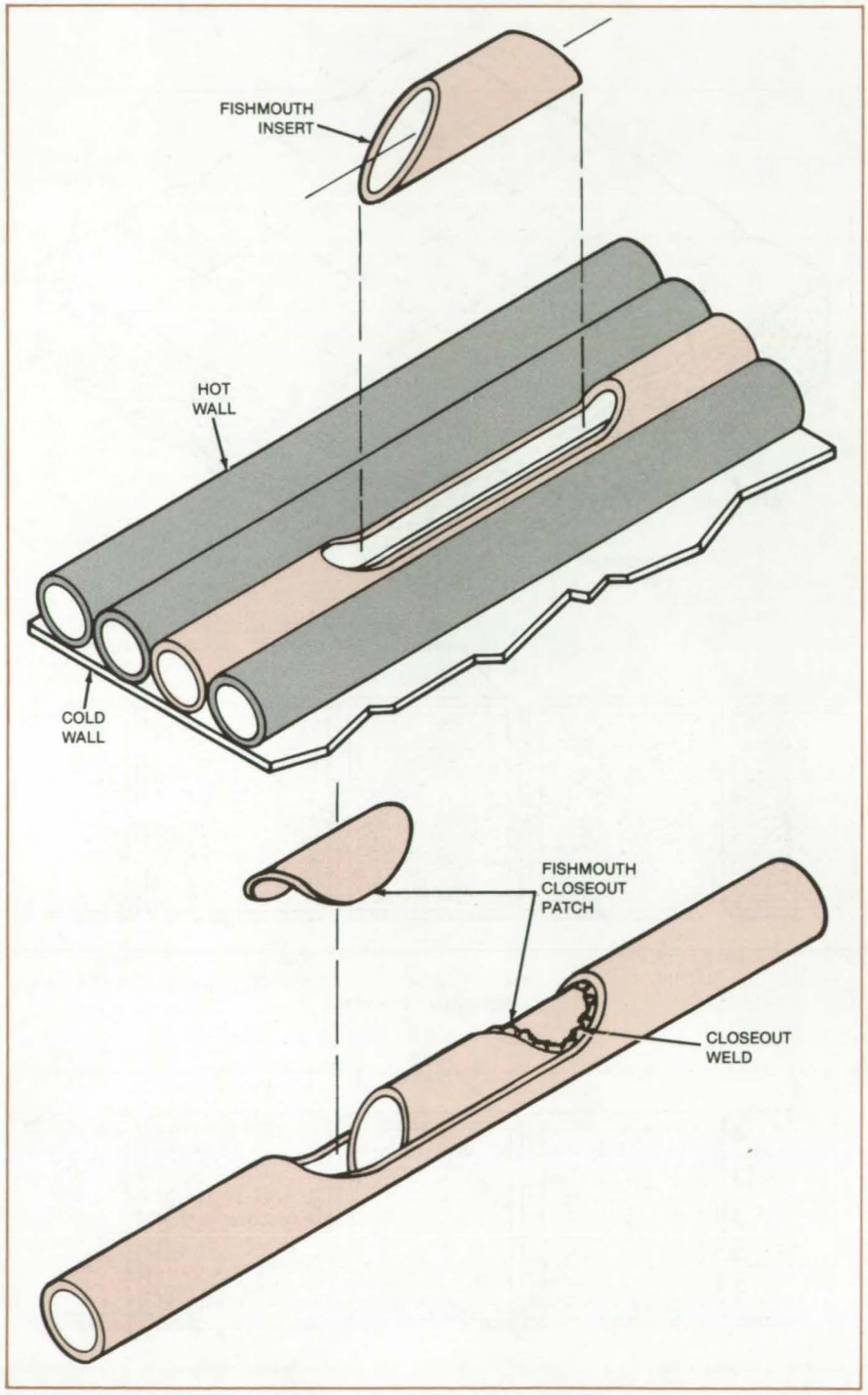

In the **Repair Procedure** the wall crown is cut away (top), and a "fishmouth" insert is TIG brazed or welded over the lower half (bottom). Closeout patches are then brazed or welded to close up the "fishmouth" openings at both ends.

A repair technique closes leaks in tubes or conduits where access is limited to the wall opposite the crack. Although originally developed to repair fatigue cracks and leaks in the Space Shuttle Main Engine (SSME) nozzle-coolant tubes, the technique is applicable to any tubular assembly where tubes are bundled together or bonded to a supporting shell, such as in heat exchangers.

As shown in the figure, access to the defect is gained by cutting away the hot-wall crown. A "fishmouth" insert is then installed to isolate the defect and is tungsten-inert-gas (TIG) brazed or welded over the lower half. This effectively isolates the failed section of tubing and restores structural integrity.

Once the insert is installed, patches are brazed or welded to close up the "fishmouth" openings at each end. Longitudinal attaching welds between the fishmouth insert and the original tube wall may also be necessary depending upon structural requirements. The length of the fishmouth insert and the use of the sidewall attaching welds are dictated by local structural requirements and thermal environment.

The repair procedure provides structural support to the area that has failed and uninterrupted flow without significantly altering the heat-transfer profile. The technique has restored many SSME nozzles to service that would have been otherwise rejected.

This work was done by R. C. Mills, Sr., and Joseph Duesberg of Rockwell International Corp. for **Marshall Space Flight Center.** *No further documentation is available.*

Inquiries concerning rights for the commercial use of this invention should be addressed to the Patent Counsel, Marshall Space Flight Center [see page A5]. *Refer to MFS-19796.*

Automatic Guidance System for Welding Torches

Sensing and control are fully digital.

Marshall Space Flight Center, Alabama

A digital system under development automatically guides a welding torch to produce square-butt, V-groove, and lap-joint weldments within a tracking accuracy of +0.2 millimeter. The guidance system employs a digital television camera and a microprocessor. It compensates for thermal expansion and intense heat at the joint. In addition, the system uses algorithms that minimize the effects of stray light reflection, changes in light level, erroneous signals, momentary loss of signal, and scratches on the workpiece.

The television camera views the joint to be welded, at a point near the welding torch. The camera and torch are mounted on the cross-seam actuator and move together over the joint (see figure). The camera contains a charge-injection device with 60,512 light-sensing elements. It scans each element sequentially, digitizes the light-level signal from each, and transmits the signals as 8-bit words to a buffer memory. The memory is updated once every 33 milliseconds.

The microprocessor analyzes the light-level signals, determining what levels correspond to the surrounding metal (bright area) and to the joint (dark line). The tracking error is computed as the distance (in picture elements) between the joint and the reference picture element. The microprocessor sends a correction signal to the controller for the cross-seam drive motor, ordering the necessary change in the welding-torch position.

The motor is a digital stepping unit. Each pulse from the controller makes the motor shaft rotate 1.8°. With the particular gearing used, this moves the cross-seam actuator and the torch 0.0079 millimeter.

The field of view is illuminated through a cable of optical fibers. The fibers make the lighting relatively uniform and occupy little space.

For prealinement, it is necessary only to position the camera so that the weld-joint image appears on the monitor screen. Part of the system program automatically alines the torch with the

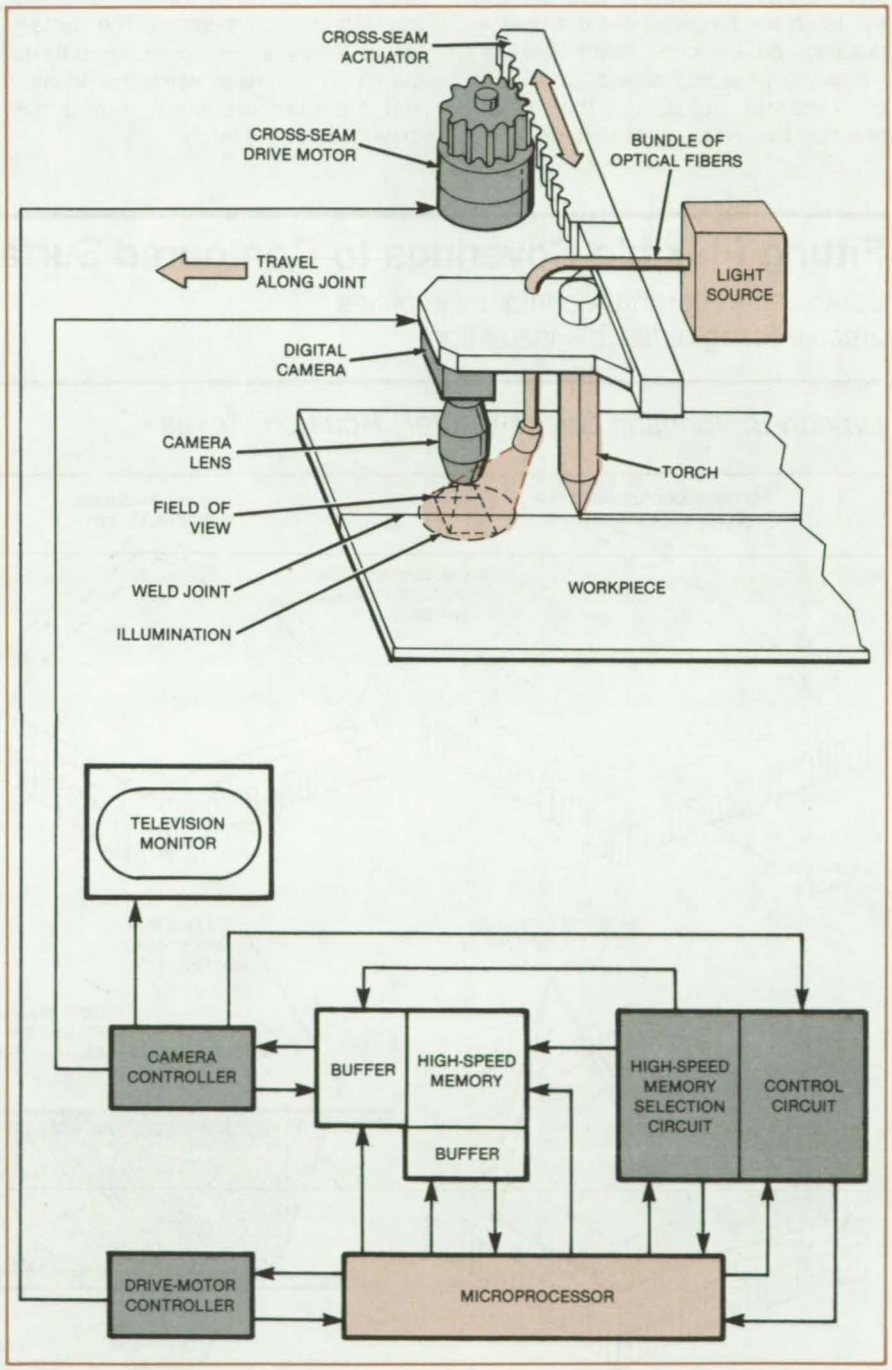

A **Television Camera Observes and Traverses** a weld joint, carrying the welding torch behind it. The image of the joint is digitized, and the resulting data are used to derive control signals that enable the torch to track the joint.

joint on command: The system searches the entire viewing area and selects the widest dark area as the joint. The system then starts tracking the joint automatically, welding the joint as it does so.

In its present form, the automatic guidance system can guide a torch only along a straight or nearly straight joint. This is in part because the sensor and the torch are mounted in fixed relative positions on the cross-seam actuator. However, if the sensor and torch were on separate actuators, the microprocessor could control the torch along nonuniform, curved joints by using delayed data feedback.

Delayed feedback would also improve tracking if the camera and torch must be mounted an appreciable distance apart; for example, where a welding-wire feed mechanism has to be placed between them. In that case, the system would store travel speed and tracking data in memory. The system would then present correction data to the motor controller when it estimates that the area previously viewed has moved under the torch.

This work was done by H. E. Smith, W. A. Wall, and M. R. Burns, Jr., of **Marshall Space Flight Center.** *For further information, Circle 65 on the TSP Request Card.*

This invention is owned by NASA, and a patent application has been filed. Inquiries concerning nonexclusive or exclusive license for its commercial development should be addressed to the Patent Counsel, Marshall Space Flight Center [see page A5]. *Refer to MFS-25807.*

Fitting Flexible Coverings to Contoured Surfaces

Contour-transferring technique simplifies precise fitting of flexible insulation.

Lyndon B. Johnson Space Center, Houston, Texas

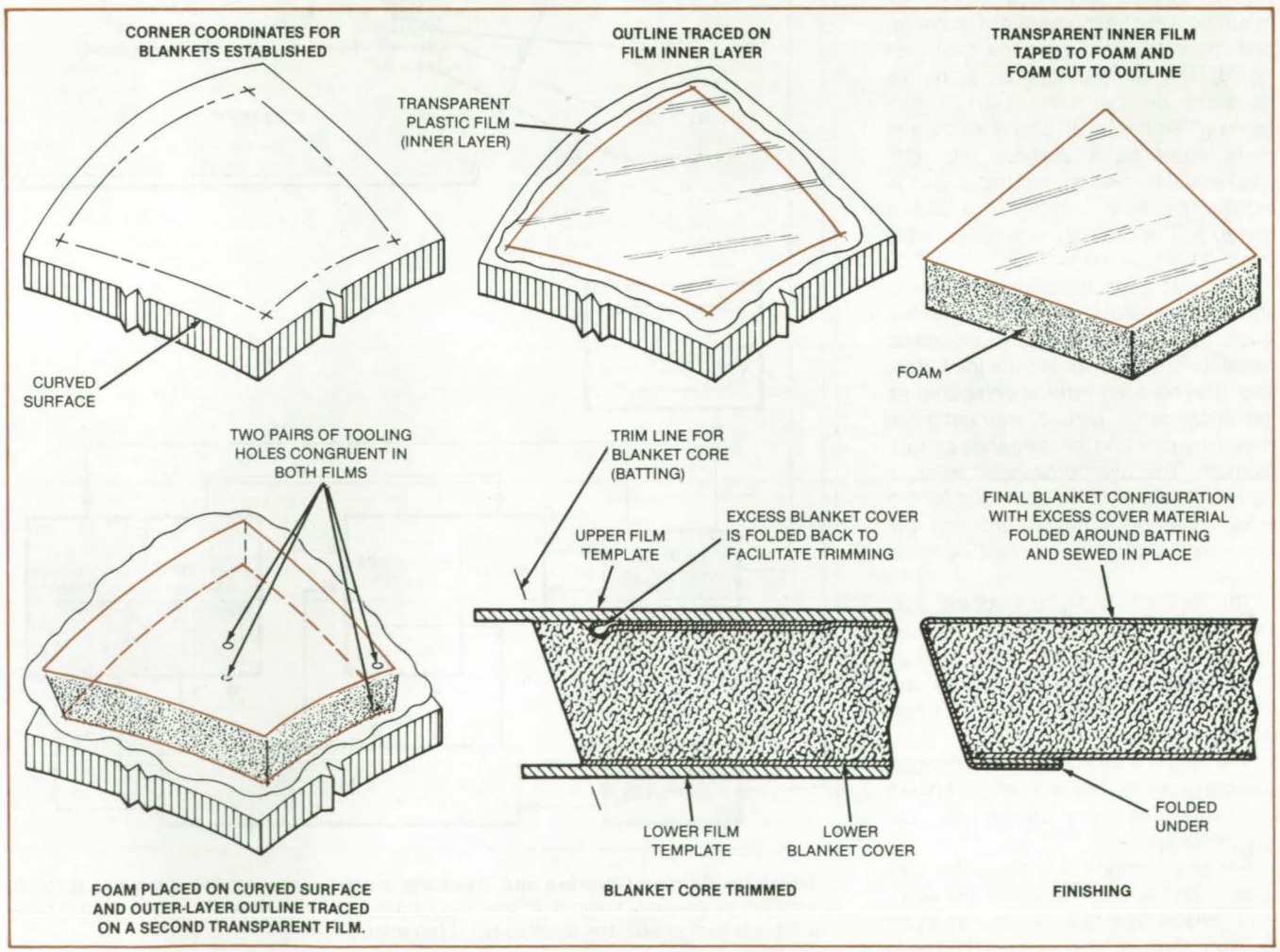

Figure 1. **Steps in the Contour-Transferring Procedure** are straightforward. With the procedure, many pieces of blanket insulation can be cut so that they fit snugly together on a contoured surface.

A method using two transparent plastic sheets and a polyethylene foam spacer produces flat templates from contoured surfaces. Once prepared, the templates are laid flat, and insulation inserted between the two templates is cut to shape to fit the contoured surface. The method was developed for fitting flexible insulation blankets over contoured surfaces aboard the Space Shuttle.

Figure 1 shows how the templates are prepared. The contoured surface is marked with corner coordinates where the actual insulation will be placed. A transparent plastic film is laid over the surface, and the outline is traced on the film layer. Polyethylene foam of the same thickness as the insulation is next taped on the outlined film and cut along the outline. This completes one template that defines the inner mold line.

The shaped foam and film are placed again on the marked surface, film down. Another sheet of film is placed on the foam, and the outline of the outer surface of the foam is traced on it. Alinement holes are punched in both films, and the upper film is trimmed along the foam perimeter. The second template is complete and defines the outer mold line.

The assembly is removed and the foam spacer detached. Insulation of the same thickness as the spacer is inserted between the two alined templates and trimmed along the template perimeters. When this insulation is installed, it will conform to the contoured surface.

The procedure can also be used for tailoring protective covers or for the installation of vibration-absorbing material over contoured surfaces. Figure 2 shows a contoured surface with insulation sections in place.

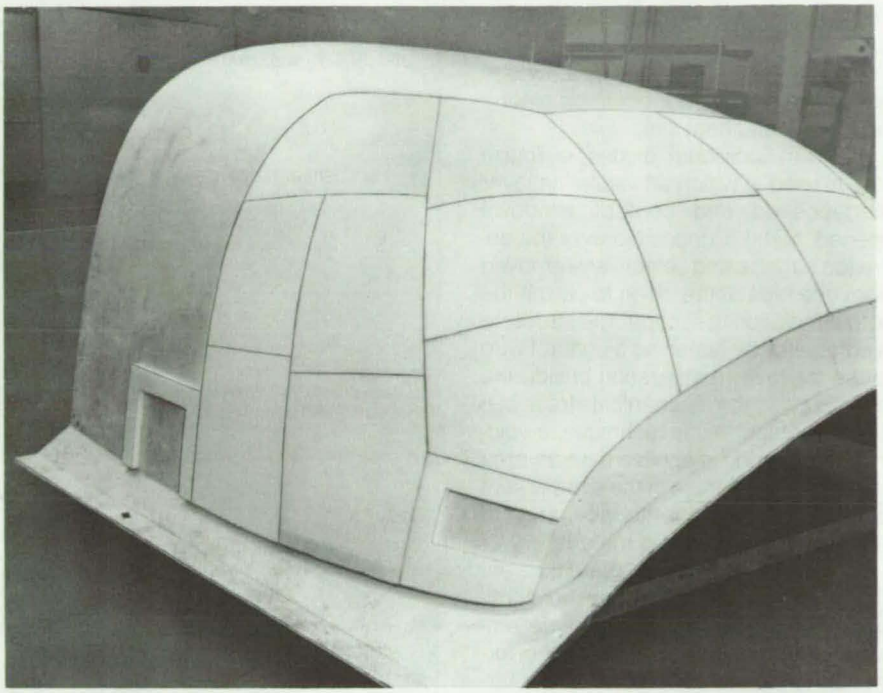

Figure 2. **Sections of Insulation** prepared by the contour-transferring technique fit the contoured surface precisely.

This work was done by Donald D. Helman, Stanley Y. Yoshino, and David S. Wang of Rockwell International Corp. for **Johnson Space Center.** *No further documentation is available.*
MSC-20503

IC Fabrication Methods Improve Laser Diodes

These high-performance diodes withstand longer thermal cycling and shelf life.

Langley Research Center, Hampton, Virginia

A family of high-performance, tunable diode lasers has been developed for use as local oscillators in a passive laser heterodyne spectrometer. The diodes, based on lead/tin telluride, operate in the 8- to 15-μm wavelength region, with specific target wavelengths of 893.37 cm^{-1} (11.2 μm) and 1,081.1 cm^{-1} (9.25 μm).

The fabrication method that has made this possible uses multiple-source molecular-beam epitaxy (MBE) to grow precisely-controlled multilayer structures of (Pb/Sn)Te on BaF_2 substrates. The diodes are fabricated using standard IC processes that include photolithography, selective etching, and vacuum deposition of metals and insulators. Packaging refinements have improved the thermal-cycling characteristics of the diodes and increased their room-temperature shelf life.

Lasers were fabricated that operate from 10 to 14 μm. CW operation was attained at heat-sink temperatures from 12 to 60 K. The maximum multimode diode CW-output power is 10 to 20 μW. These laser diodes have survived 1-month storage at 40° C and 1-year storage at room temperature; they have also survived repetitive thermal cycling without degradation.

Multiple-source MBE offers better flexibility and control than other crystal-growth techniques. Substrate selection, however, is critical. The laser-diode fabrication starts with MBE film growth on a BaF_2 substrate and ends with a bonded, electrically contacted laser (see figure). A multilayer vertical structure is grown (by MBE) on the substrate.

To achieve adequate heat sinking to permit CW operation above 12 K, the film is removed from the BaF_2 and bonded to a thermal-expansion-matched substrate through back-surface metalization and a low-temperature soldering to an oxygen-free, high-conductivity copper block. The BaF_2 is dissolved with a continuous directed stream of warm deionized water. At that point, individual Fabry-Perot

(continued on next page)

cavities are formed photolithographically. The (Pb/Sn)Te mesas are isolated from each other electrically by a reverse pn junction but have a common electrical ground and heat sink.

To form individual diodes, a fourth step is used in which an insulating layer is deposited and contact windows opened. Metal is deposited over the entire top surface and selectively removed from one face of the diode to permit the output radiation to escape. The structure is completed by fastening a contact wire to the top-layer metalization beside the laser to avoid the mechanical stress of a direct contact. In this technique, a void-free solder bond is applied over an area of 8 by 10 mm. Stress in the bond is kept low enough to permit the fabrication of lasers from the soldered material.

Although the laser diodes are conventionally fabricated from cleaved semiconductor material, the technique employs wet-chemical etching for the formation of the laser cavities. As an alternative to forming Fabry-Perot cavities, ion milling also has been used, permitting improved geometric definition as compared to the wet-chemical etching. The finished diode has the top contact adjacent to the mesa, rather than on top of it. This structure offers considerably less strain than the conventional sandwich structure and is expected to be more reliable during thermal cycling.

This work was done by M. D. Miller and V. Y. Pickhardt of Perkin-Elmer Corp. for **Langley Research Center.**

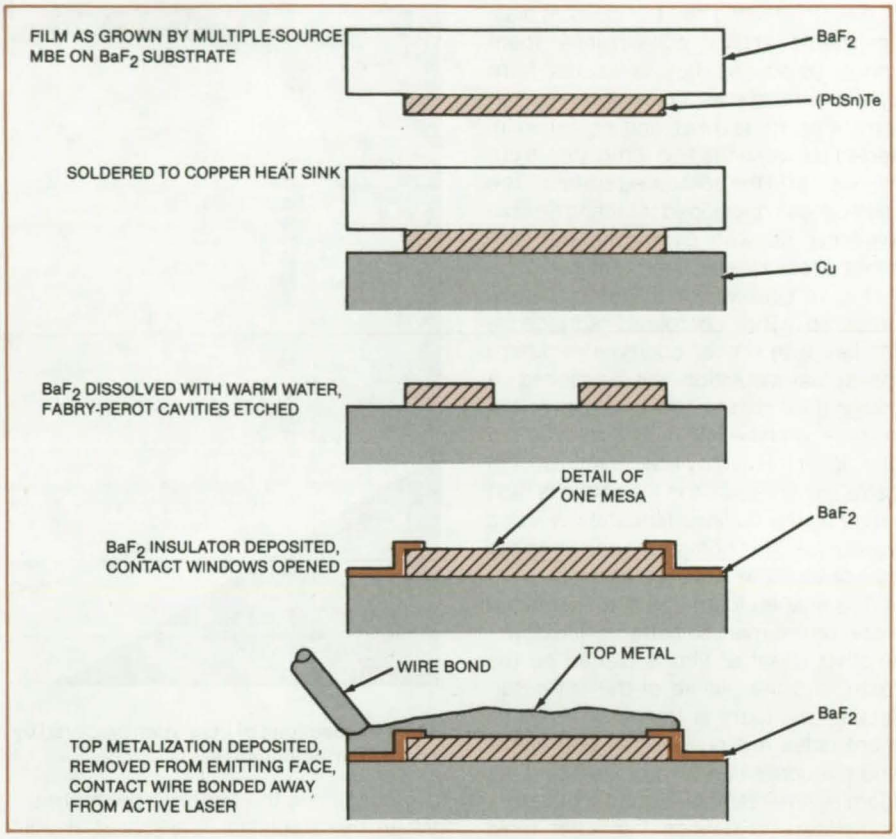

These **Five Processing Steps** outline the laser-diode fabrication.

Further information may be found in NASA CR-165683 [N82-11453/NSP], "Development of MBE Grown Pb-Salt Semiconductor Lasers for the 8.0 to 15.0 Micrometer Spectral Region" [$11.50]. A copy may be purchased [prepayment required] from the National Technical Information Service, Springfield, Virginia 22161.
LAR-13059

Ice as an Abrading Agent

Solvent-induced corrosion is avoided by grit-blasting with frozen pellets.

Marshall Space Flight Center, Alabama

A proposed grit-blasting method may make it unnecessary to disassemble equipment for cleaning. There is no reactive solvent to become entrapped in the recesses in the equipment and cause corrosion.

A stream of small, frozen pellets is directed at the assembly to be cleaned. The pellets could consist of deionized-water ice, carbon dioxide ice, or another substance that does not react chemically with the parts to be cleaned and leaves no residue. The pellets abrade away dirt and contaminants. Stubborn stains and flaking are removed readily.

Of course, the pellet material must be removed after the cleaning operation, or else some might remain behind to cause contamination. Therefore, after grit blasting, the assembly is placed in a vacuum, then purged with hot air or nitrogen to remove the traces of pellet material.

The method is well suited to cleaning titanium and parts that touch liquid oxygen. Standard halogenated solvents are incompatible with titanium because they cause rapid corrosion.

This work was done by Raymond K. Blow of Rockwell International Corp. for **Marshall Space Flight Center.** *No further documentation is available.*
MFS-19837

Forming Lightweight Beams From Composite Tape

Durable structural members could be rapidly formed in a continuous process.

Marshall Space Flight Center, Alabama

Hollow beams for assembling trusses and other structures would be produced from graphite/polysulfone tape in a manufacturng process originally proposed for Earth orbit. The process would result in structures that are strong, light, and durable. It could be used to mass produce other lightweight parts besides beams.

Polysulfone was selected as the matrix material because it does not outgas excessively in the vacuum of space. In contrast, thermosetting materials, such as liquid matrices and preimpregnating resins, present serious outgassing problems in such an environment.

The tape would consist of three layers having graphite fiber orientations of 0°, 45°, and 0°, respectively. The process (see figure) would begin with the tape feeding through a series of stations in which it is first heated along the fold lines for the triangular cross section and then folded into an equilateral triangle with a lap seam along one corner. An array of heat pipes would allow localized application of heat from a single heat source. This source could be a metal block containing the ends of the heat pipes and heated by radio-frequency induction.

The tape would then run through a short heating die to compress and weld the seam and to consolidate the entire laminate. The short heating die would be followed by a chilling die to cool the laminate. The triangular section would be pulled through the system by three elastomeric wheels pressing against the outer surface of the rib. Rollers inside the beam at the exit end of the chill die would support the section against the puller wheels.

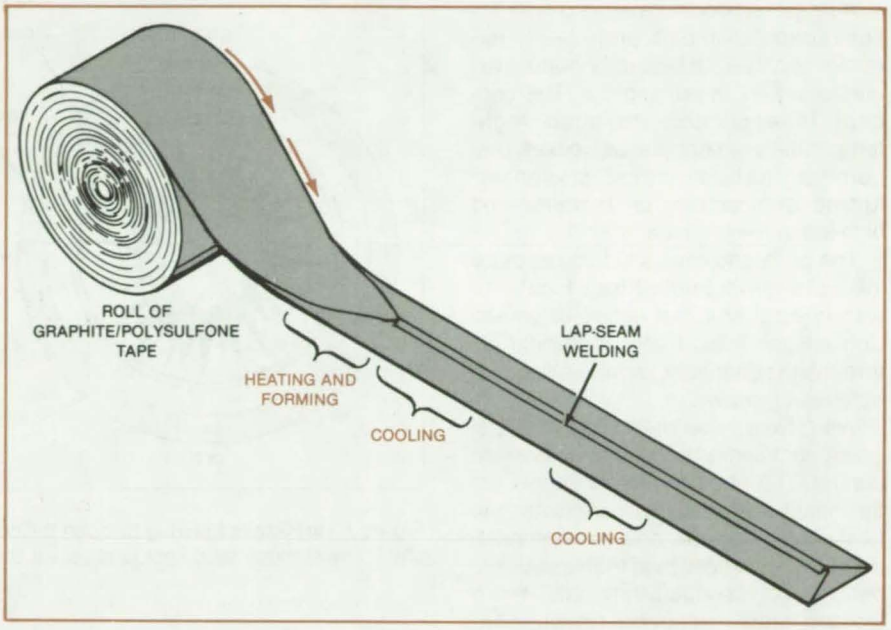

The **Steps of the Forming Process** are shown in simplified form to illustrate the transformation of flat tape to a strong, lightweight structural member.

This work was done by Goldsworthy Engineering, Inc., for **Marshall Space Flight Center.** *No further documentaion is available.*
MFS-25880

Polyurethane Filler for Electroplating

Bath contamination is lower than with wax.

Marshall Space Flight Center, Alabama

Polyurethane foam has proved suitable as a filler for slots in parts to be electroplated with copper or nickel. The polyurethane causes less contamination of the plating bath and of the cleaning and filtering tanks than do the wax fillers used previously. The direct cost of maintenance and the indirect cost of reduced operating time during tank cleaning are therefore reduced.

A polyurethane-foam filler is easily prepared by mixing an isocyanate with a polyol. It is also easily removed with methyl chloride.

Since the foam filler is less dense than wax, foam-filled parts are lighter in weight than wax-filled parts. The use of polyurethane foam also speeds the preparation of parts to be plated: Considerable time must otherwise be spent waiting for the wax to cool after pouring into the slots before masking can be done.

This work was done by John L. Beasley of Rockwell International Corp. for **Marshall Space Flight Center.** *No further documentation is available.*
MFS-19851

Ribbed Coolant Liners for Combustion Chambers

Coolant channels and fins remove heat efficiently.

Marshall Space Flight Center, Alabama

A proposed coolant-carrying liner for combustion chambers promises to run cooler and tolerate high-temperature excursions without burning out. The concept is applicable to such high-temperature chambers as rocket preburners, turbojet cans, stationary-turbine combustors, oil burners, and high-pressure chemical reactors.

The proposed liner is a rigid structure joined to the outershell (see Figure 1), with internal ribs that define channels. Coolant gas flows freely and uniformly through the channels, providing dependable heat removal.

With fixed, predetermined channel cross sections, coolant flow is easy to control. The ribs between channels act as heat-transfer fins, increasing the heat-exchange area and accommodating bursts of excess heat from the chamber. The high-conductivity metals used in the new liner — copper or nickel — further improve heat-transfer capacity.

The fabrication of such a liner begins with the electroforming of a layer of copper or nickel on the shell (Figure 2). Channels are milled in this layer. The channels are filled with a wax or other temporary material, and a final layer of metal is electroformed over the channels. Since this fabrication process takes place at or slightly above room temperature, the heat-treated metal shell is not weakened.

A conventional liner consists of a sheet-steel cylinder inside the structural shell, separated from the shell by a narrow gap. Cooling fluid flowing along the cylinders in the gap removes heat from the liner. This type of liner can be weakened and its shape distorted by brazing or welding in fabrication or by thermal expansion in service, so that it does not conform to the internal shape of the shell. The gap may become constricted as a result; gas flow is thus reduced at the constriction, and a hotspot results. The liner may also be installed off center, in which case the airgap — and coolant gas flow — will not be uniform around the liner periphery.

A conventional liner is also subject to burnout from a sudden increase in temperature in the chamber. Such an increase can result from an inadvertent change in the fuel-oxidizer ratio, for example.

This work was done by William R. Wagner of Rockwell International Corp. for **Marshall Space Flight Center.** *No further documentation is available.*
MFS-19829

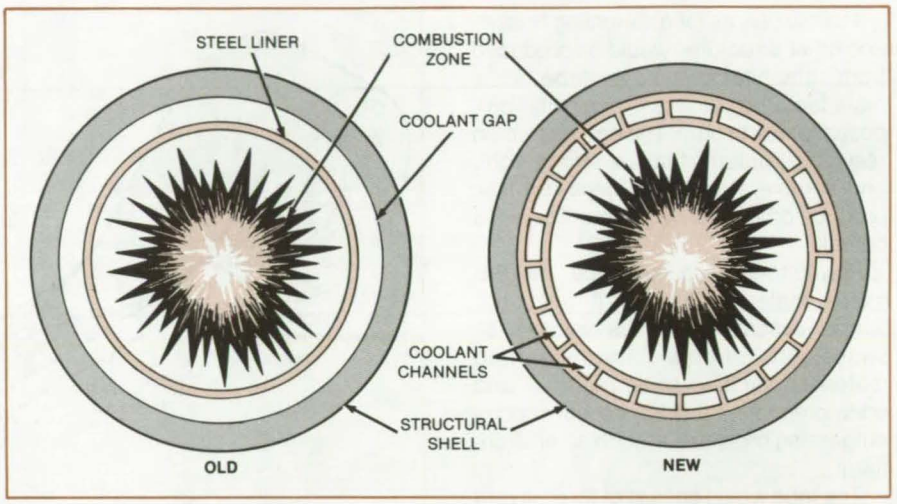

Figure 1. **Hot Gases Flowing** through the core are prevented by a liner from damaging the shell. The conventional liner is simply a thin steel cylinder.

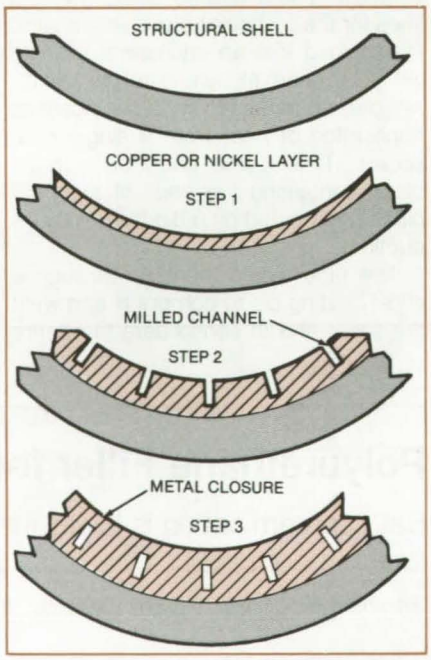

Figure 2. A **New Liner Is Built Up** in the structural shell in three steps: the deposition of metal, the milling of channels, and the deposition of a closure layer of metal.

Locking Corners Speed Solar-Array Frame Assembly

Interlocking parts are simply pushed together.

NASA's Jet Propulsion Laboratory, Pasadena, California

The mitered corners of solar-array frames are joined together by a single angle brace and two springs. Previously the frames were held together by welds, rivets, or screws, all of which required special tools for installation. The new fastening system could also possibly be used to assemble window screens and picture frames.

The corner brace and springs are inserted into channels in the ends of the two frames to be joined (see figure). The springs compress as they are inserted and slide into the channel. If an attempt is made to reverse the motion, the spring expands and digs into the soft aluminum frame, locking it in place. After the brace and spring are installed into the first of two mating frames, the second frame is pushed over the end of the brace-and-spring assembly. This makes a secure 90° joint. The procedure is repeated until all four members are joined into a rectangular frame.

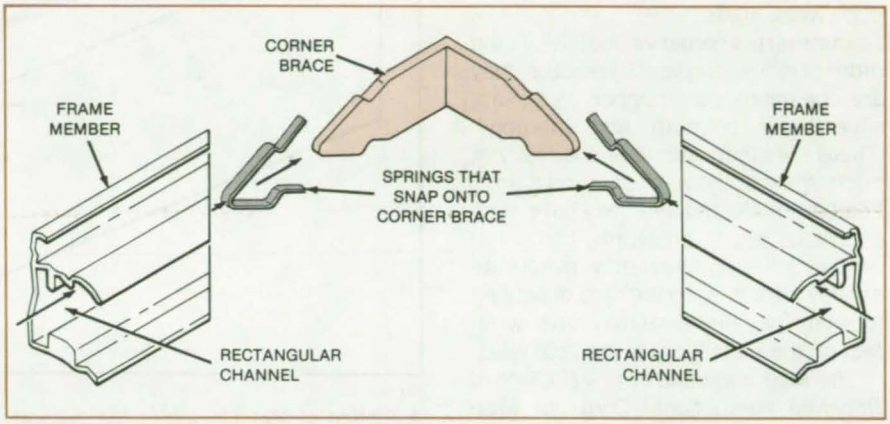

Locking Corner Braces and Mating Frame Members for solar-cell frames are pushed together by hand or assembled automatically.

This work was done by Stephen Olah and William J. Sampson of Applied Solar Energy Corp. for **NASA's Jet Propulsion Laboratory.** *For further information, Circle 66 on the TSP Request Card.*

NPO-15750

Ribbon Reduces Spiking in Electron-Beam Welding

Finer welds are made by increasing the vapor pressure.

Marshall Space Flight Center, Alabama

Spiking in electron-beam welding is reduced by placing a high-vapor-pressure substance along the path of the electron beam. The technique has been used successfully on nickel alloys and aluminum alloys and may be effective on steel and titanium.

Spiking — uneven penetration of the weld in the metal — occurs when the forces of vaporization and surface tension become unbalanced. When an electron beam delivers energy to a workpiece, it vaporizes a conical hole in the metal and melts the metal adjacent to the hole. In the desired operating mode, the pressure of the metal vapor prevents the surface tension of the molten metal from closing up the hole.

If the beam energy is strongly concentrated at the apex of the hole, then the temperature difference between the hotter bottom (apex) of the hole and the cooler top becomes considerable. Since the vapor pressure increases while the surface tension decreases with increasing temperature, the surface tension at the top of the hole sometimes wins out over the vapor pressure. When this happens, the top closes, and the rim intercepts the beam. Less energy is delivered to the bottom, and penetration is temporarily decreased. Then suddenly the surface vaporizes, the rim recoils, the surface cools, and the cycle begins again. The result is a weld the depth of which varies somewhat irregularly along the length of the weld. Frequently, such a weld contains voids along its bottom surface.

In the new technique, a strip of metal having a vapor pressure higher than that of the base metal at the same temperature is placed in a slot machined along the weld line (see figure). The strip vaporizes as the beam strikes it, and its vapor pressure keeps surface tension from closing off the top of the channel.

Aluminum alloy 5083 (94 percent aluminum, 5 percent magnesium, and 1 percent manganese) was selected for the first test of the new technique. Slots 0.032 by 0.120 inch (0.81 by 3 mm) were milled in blocks of the alloy, and pieces of mangnesium ribbon ranging in size from 9.8 to 39.2 mg per cm were laid in a part of each slot. A sharply-focused electron beam was moved along the slots. The resulting welds were sectioned, and a reduction of spiking was evident in the portions of the slots that had contained magnesium ribbons.

(continued on next page)

Tests of manganese ribbon in a slot in a nickel alloy were also made. Spiking was eliminated almost entirely. More investigation is needed to determine how much manganese is needed. Moreover, the metallurgical effects of adding manganese are yet to be determined. Manganese is a brittle metal; and if it does not mix well in the alloy, it may produce weak areas.

There are alternative metals: In the order of increasing vapor pressure, they are chromium, gold, copper, aluminum, silver, lead, bismuth, and antimony. (There are others, but their chemistry or price makes them poor candidates.) Lead, bismuth, and antimony have such enormous vapor pressures compared with nickel that they may evaporate entirely after they do their job of fighting tension. They therefore may have no effect on the metallurgy of the final weld.

This work was done by Roy E. Olson of Rockwell International Corp. for **Marshall Space Flight Center.** *No further documentation is available.*

Inquiries concerning rights for the commercial use of this invention should be addressed to the Patent Counsel, Marshall Space Flight Center [see page A5]. *Refer to MFS-19701.*

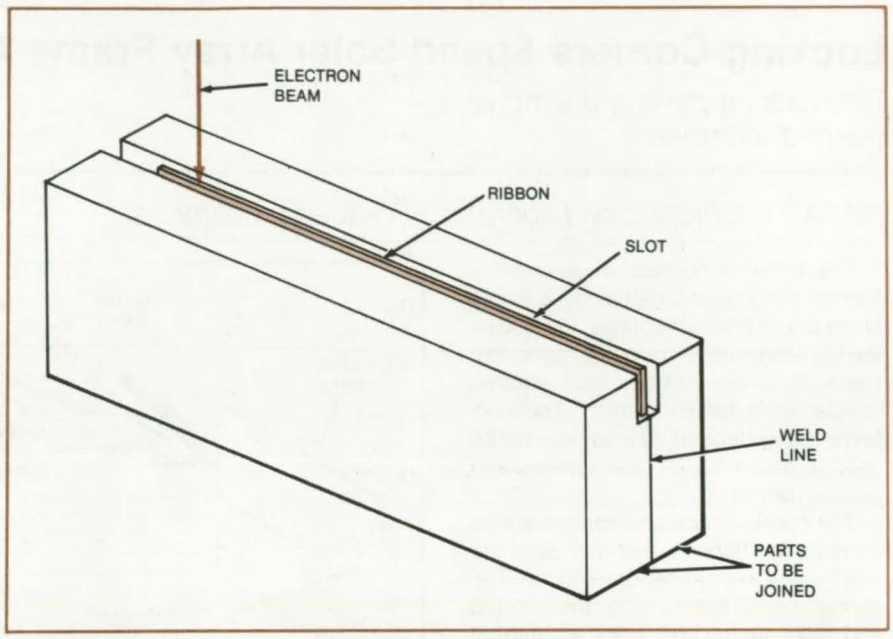

A Ribbon of Metal in a slot can alleviate spiking in electron-beam welds. The ribbon should have a higher vapor pressure than that of the base metal at the same temperature and should not adversely affect the metallurgy of the final weld.

Less-Costly Ion Implantation of Solar Cells

Broad-beam phosphorus could be used instead of a single mass-analyzed ionic species.

NASA's Jet Propulsion Laboratory, Pasadena, California

Experiments at NASA's Jet Propulsion Laboratory point the way toward more relaxed controls over ion-implantation dosage and uniformity in solar-cell fabrication. If the preliminary results hold up when the methods are scaled up to production runs, the complexity and cost of cell fabrication would be lowered, and production rates would be increased.

These results were obtained for phosphorus-doped silicon solar cells. Previously, it was thought necessary to filter the ion beam from a red-phosphorus source before it strikes the silicon substrate. Filtering through a mass spectrometer isolates one phosphorus species; for example, P_4^+ or P^+. However, the new data indicate that cell performance, measured by output current density at a fixed voltage, is virtually the same whether the implant is a particular ion species or a broad-beam mixture of

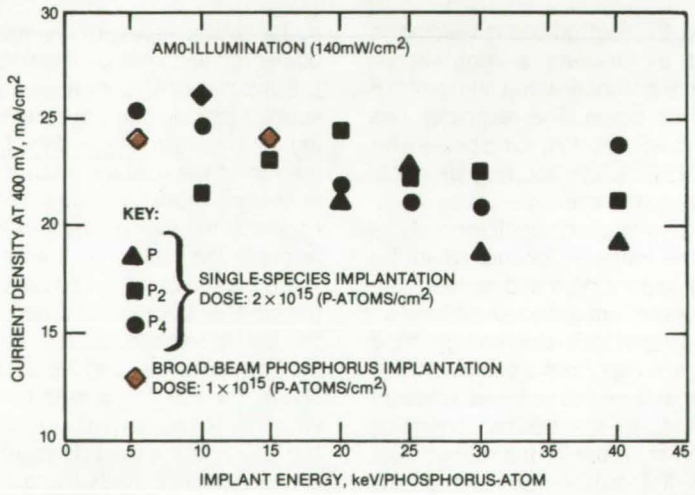

Solar-Cell Output changes very little whether broad-beam phosphorus or single species are used. The maximum power point is assumed to be at 400 mV so that the current density at this voltage is used as the figure of merit for cell performance.

several species. The data also show that the cell performance is relatively insensitive to dosage above about 2×10^{15} atoms/cm^2. Thus, strict control over dosage may be unnecessary, and — possibly more importantly — a broader less uniform beam can be used, thereby increasing throughput.

The three principal constituents of the phosphorus ion beam, P_2^+, P^+, and P_4^+, were implanted separately into silicon samples. The figure shows the output current density of solar cells fabricated with these constituents. For simplicity, it was assumed that the maximum power point was at about 400 millivolts; therefore, the current density at 400 mV was used as a figure of merit for cell performance.

The samples were ion-implanted at a dose of 2×10^{15} atoms/cm^2 over a range in energy from 5 to 40 keV/atom. Note that a P_4^+ ion implanted at 80 keV is equivalent to four phosphorus atoms implanted at 20 keV, therefore, the actual dose is four times larger than the "apparent" dose measured by integrating the sample current and the energy per atom is four times less than the ion accelerating potential.

Only a few samples were implanted for each point in the figure. However, it is apparent that there is no clear-cut distinction in performance between the molecular phosphorus and the atomic phosphorous ions. Other data (not shown) appear to display a general trend toward improved performance as the implant energy is decreased.

The effect of the implant dose on the power output was evaluated using the P_2^+ molecular ion. These data show a definite decrease in performance as the dose is decreased below about 1×10^{15} atoms/cm^2. The data also show that the performance is substantially constant at higher dosages.

This work was done by Dennis J. Fitzgerald of Caltech for **NASA's Jet Propulsion Laboratory.** *For further information, Circle 67 on the TSP Request Card.*
NPO-15511

Joining Tubes With Adhesive

Tapered ends and spacing wires ensure strong joints.

Marshall Space Flight Center, Alabama

Cylindrical tubes can be joined together, end to end, by a method employing an adhesive, tapered ends, and spacing wires. The method was developed for assembling structural elements made of composite materials.

As shown in the figure, thin wires are clipped on the tapered end of a tubular element. A liquid adhesive is then applied to the tapered section. The tapered section is inserted in a tapered countersunk hole in a tube of slightly larger diameter. The adhesive is allowed to cure, and a strong joint is formed.

The spacing wires prevent the adhesive from being scraped away when the tubes are pushed together. A uniform layer is thus maintained over the bonding surfaces, and bond strength is thereby improved. The tapered section allows the bonding surfaces to be wedged together so that they provide pressure while the adhesive cures. The joining method does not obstruct the hollow centers of the tubes.

This work was done by William A. Bateman of Rockwell International Corp. for **Marshall Space Flight Center.** *No further documentation is available.*
MFS-25958

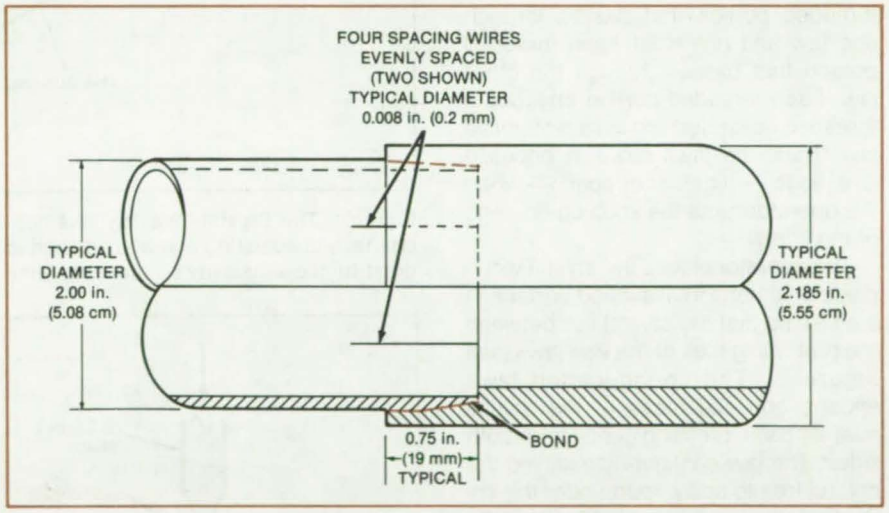

A **Tapered Joint Between Tubular Structural Elements** provides pressure between the bonding surfaces during adhesive curing. The spacing wires prevent the adhesive from being scraped away when one element is inserted in the other.

Positioning Vise for Crystal Cleavage

Smoothly moving parts ensure correct orientation of crystals.

Goddard Space Flight Center, Greenbelt, Maryland

A vise manipulates brittle crystals, such as lithium fluoride, so that they are in the proper position for cleaving. The vise allows crystals as thin as 2 millimeters or less to be positioned so that they can be cleaved without breakage. Previously, the crystal had to be carefully measured, clamped in a jig, and painstakingly centered under a cleaving blade by an operator.

In the new vise (see Figure 1) the jaws are fitted with ball bushings that ride on guide rods. The guide rods support the jaws and maintain their alinement, thereby maintaining the crystal or other workpiece in alinement. The bushings reduce both starting friction and sliding friction so that the operator always has a good tactile sense of the forces on the jaws.

The adjusting screw has a right-hand threaded portion that passes through one jaw and has a left-hand threaded portion that passes through the other jaw. Each threaded portion engages a threaded collar bushing in its respective jaw. Thus, the jaws move in opposite directions — together or apart — when the operator turns the knob on one end of the screw.

The operator places the crystal workpiece on a horizontal support surface in the vise so that the crystal lies between the protruding toes of the vise jaws (see Figure 2). The spring-loaded jaws engage opposite faces of the crystal near its base, pressing gently from both sides. The jaw configuration leaves the crystal free to splay apart under the impact of the cleaving blade with little horizontal restraint and minimal damping of the impact shock wave.

The workpiece is centered under the blade when both toes engage it. Thus, the blade strikes the crystal at its midpoint so that shock wave is equally distributed on both sides of the midpoint and cannot shatter the crystal. When inserting the workpiece in the vise, the operator turns a knurled knob to drive the jaws toward each other. When the rigid jaws make contact, the workpiece is centered. The cleaving blade is then lowered to contact the workpiece, keeping it centered while the vise is backed off so that only the spring-loaded jaws make contact. The operator then releases the hammer that strikes the blade and cleaves the workpiece or crystal.

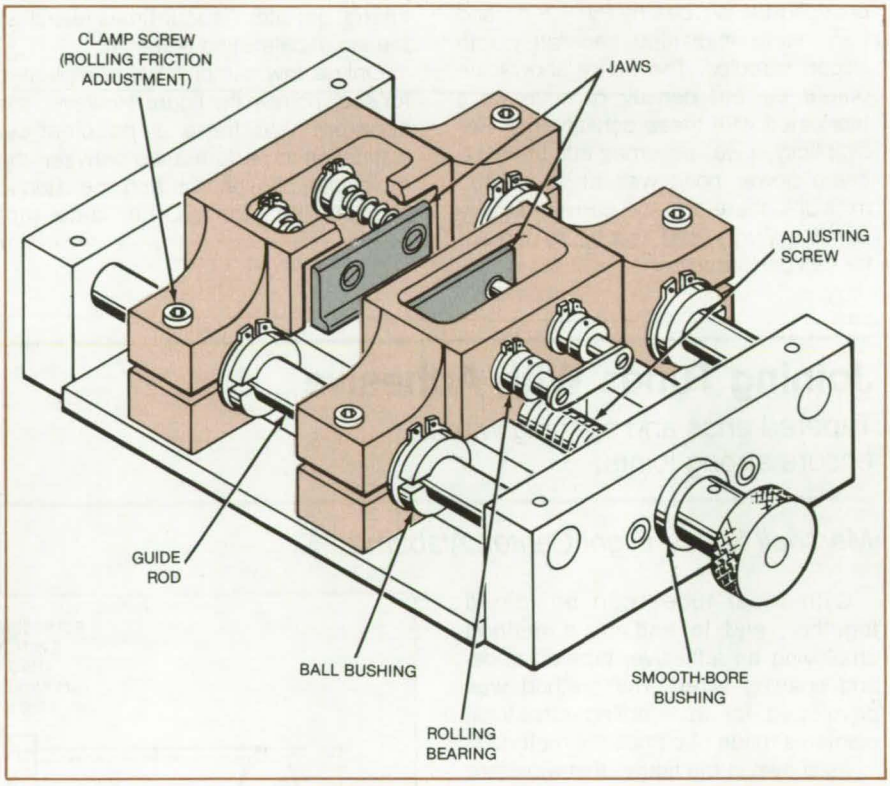

Figure 1. The **Crystal-Cleaving Vise** holds a workpiece firmly but gently. Its bushings, shafts, and adjusting screw are designed to move the jaws smoothly and uniformly with great tactile sensitivity so that they aline the crystal and hold it for a clean cut.

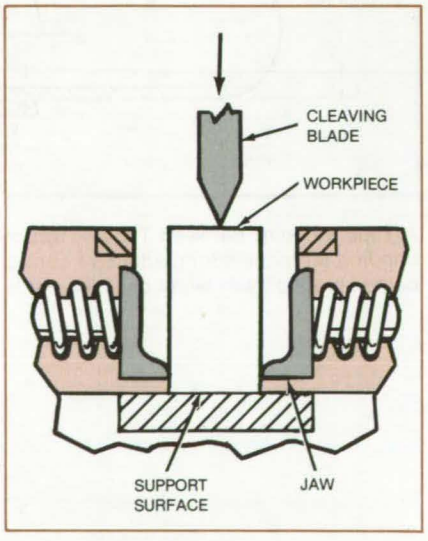

Figure 2. A **Crystal Is Held Gently** between the toes of the jaws while it rests on the support surface.

This work was done by Frederick C. Hallberg and Clyde J. Morgan of **Goddard Space Flight Center.** *For further information, Circle 68 on the TSP Request Card.*

This invention is owned by NASA, and a patent application has been filed. Inquiries concerning nonexclusive or exclusive license for its commercial development should be addressed to the Patent Counsel, Goddard Space Flight Center [see page A5]. Refer to GSC-12762.

Ultrasonic Bonding of Solar-Cell Leads

A rolling ultrasonic tool spot-bonds flat solar-cell leads faster than a seam welder.

NASA's Jet Propulsion Laboratory, Pasadena, California

A new rolling ultrasonic spot-bonding method successfully joins aluminum interconnect fingers to silicon solar cells with copper metalization. The technique, which combines the best features of ultrasonic rotary seam welding and ultrasonic spot bonding, allows for fast bond cycles and high indexing speeds without the use of solder or flux. It achieves reliable bonds at production rates without damage to the solar cells.

The new ultrasonic bonding tool shown in the figure employs a carbide wedge that is inserted into the horn of the ultrasonic transducer. The tool engages only the area to be bonded. Initially, the wedge descends on the workpiece at an angle so that only a portion of the tool contacts the aluminum interconnect ribbon. As ultrasonic power is applied, the tool rolls through a small angle, progressively bonding the entire area, similar to the action of a rotary seam welder.

The rolling ultrasonic system bonds the cells several times faster than the rotary seam welder. It subjects the cells to less localized stress, resulting in less or no damage to the cells. In addition, the lower mass of the new bonding head permits the use of two parallel heads in the same bonding station. The new bonding system should be of interest for all solar-cell assemblies and other assemblies using flat leads (rather than round wires).

This work was done by Walter Frasch of Kulicke and Soffa Industries, Inc., for **NASA's Jet Propulsion Laboratory.** *For further information, Circle 69 on the TSP Request Card.*
NPO-16140

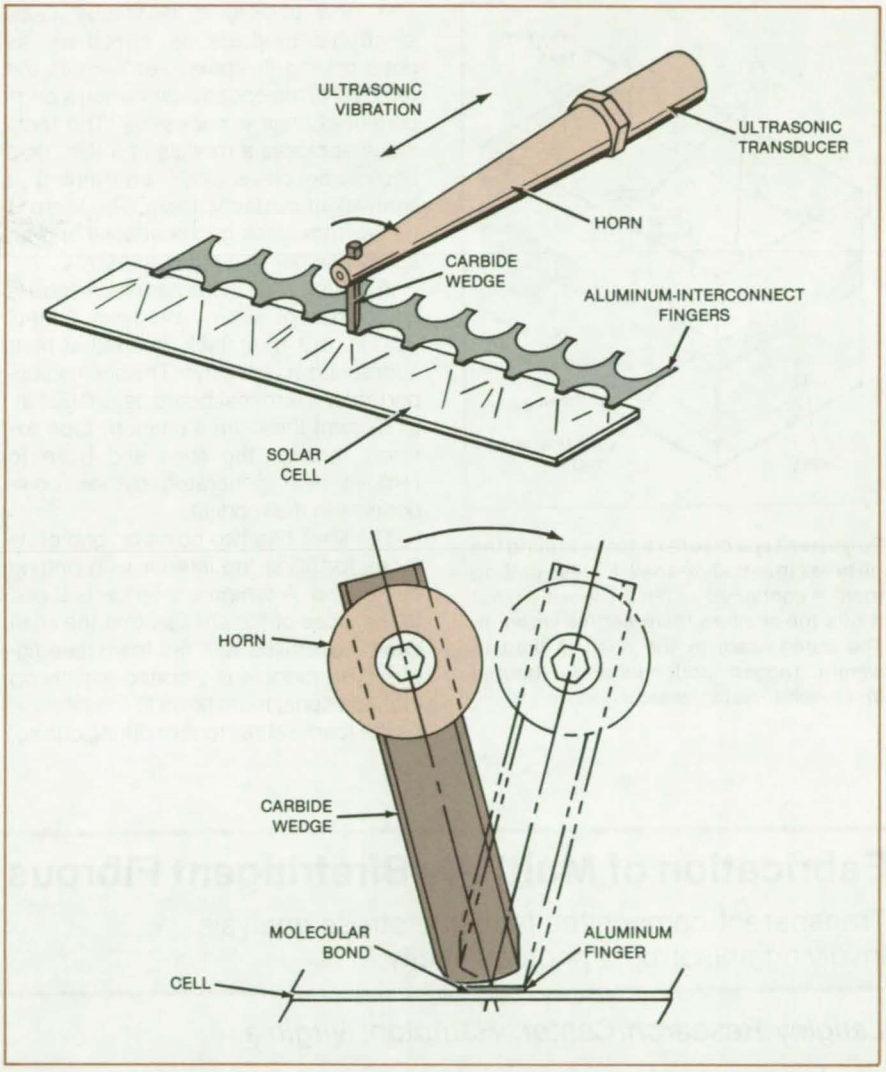

The Rolling Ultrasonic Spot-Bonding Tool employs a carbide wedge that may be replaced easily. Initially, only a portion of the tool contacts the bond area; as the power is applied, the tool rolls through a small angle, progressively bonding the entire area.

Reusable Release Mechanism

A release mechanism is activated by a small explosive charge or the rush of gas or other fluid into the small chamber above a piston. Only the charge has to be replaced for the new device to be ready for service. The mechanism bears heavy loads while latched, yet gives a smooth release. The lightweight unit replaces explosive bolts in applications where reuse is an advantage.
(See page 261.)

Low-Thermal-Resistance Baseplate Mounting

A mounting technique improves the thermal contact between a heat-producing device and a heat sink. The baseplate of the hot device is preloaded to force it to assume a slightly convex shape. When it is bolted to the flat heat-sink, the two surfaces flex slightly, coming into intimate contact over the entire surface.
(See page 236.)

Liquid-Droplet Radiative Cooler

A large-area radiative cooler may be applicable to industrial processes requiring noncontact cooling of process fluids. Oil low vapor pressure would be sprayed as fine droplets toward a collector. The disk-shaped collector would rotate, its periphery acting as a centrifugal pump to recirculate the oil.
(See page 225.)

Repairable Encapsulated Electronic Modules

Syntactic foam protects modules but is easy to remove and replace.

NASA's Jet Propulsion Laboratory, Pasadena, California

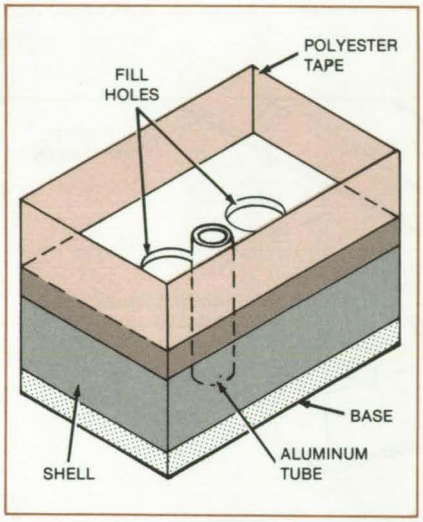

Polyester Tape creates a fence around the fill holes in a module shell. Excess potting foam is contained within the fence so that it fills the shell as foam settles within it. The cured foam in the shell is light in weight, rugged, and minimizes thermal and mechanical stresses.

A new packaging technique seals electronic modules as effectively as does potting in epoxy, yet permits the removal of the encapsulant when a component change is necessary. The technique encloses a module in a thin, rigid epoxy/fiberglass shell containing a lightweight syntactic foam. The foam is made from glass microballoons and an epoxy powder that cures at 100° C.

A potting shell in the new technique is composed of epoxy/fiberglass sheets 0.20 in. (5.1 mm) thick, bonded at their edges with an adhesive. The shell is supported by a terminal-board base 0.031 in. (0.79 mm) thick. An aluminum tube extends through the shell and base to remove heat generated by the components in the module.

The shell has two holes on one of its faces for filling the interior with potting compound. A temporary fence is taped to the sides of the shell so that the shell can be overfilled with the foam (see figure). The module is vibrated initially so that additional foam flows to the interior. As the foam settles further during curing, additional material flows into the shell from the overfill volume.

The resulting encapsulant is a rigid, low-density material with the consistency of sandstone. Excess material is cut away after the cure, and the exposed foam in the fill holes is sealed with polyurethane.

When the module has to be reopened, the shell is cut away with a temperature-controlled electric hot knife. The foam around the component to be reworked is then removed by blasting with ground walnut shells. Residual foam particles are blown away with a dry nitrogen jet.

After the component has been removed and replaced, the sides of the shell are replaced and rebonded. A new fence is erected around the face with fill holes (positioned over the new component), and the foam-potting procedure is repeated.

This work was done by Paul C. Dozois and Robert C. Mayne of Caltech for **NASA's Jet Propulsion Laboratory.** *For further information, Circle 70 on the TSP Request Card.*
NPO-15079

Fabrication of Multi-Ply Birefringent Fibrous Composite Laminates

Transparent composites facilitate stress analysis involving anisotropic photoelasticity.

Langley Research Center, Hampton, Virginia

A fabrication method produces unidirectional, multi-ply, transparent birefringent fibrous composite laminates for use in macromechanical stress analysis conducted by means of anisotropic photoelasticity. Before this development, the material for anisotropic photoelastic studies has not been readily available. Existing fabrication techniques produced materials with limitations in mechanical and optical properties.

The new laminates are glass-fiber-reinforced plastics for which the matrix and fibers have the same index of refraction. Such transparent fibrous composites can be made to simulate the anisotropy of opaque fibrous composites, such as boron/epoxy, graphite/epoxy, and others. The transparent composites can be treated as homogeneous materials with anisotropic elastic and optical properties.

The matrix resin used to produce the orthotropic birefringent laminates has a pot life of several hours and cures at room temperature with a minimum amount of shrinkage, producing a water-clear casting. Type 1062 glass roving is used as reinforcement. The glass roving is dry-wound over various metal frames in a filament-winding machine.

Eight-ply unidirectional plates are prepared as well as angle-ply $(+45_2/-45_2)$ plates and quasi-isotropic plates. A measured quantity of the epoxy resin and hardener is mixed, and half is poured on one side of the winding and spread as uniformly as possible. The wet layup is then covered with a release sheet, the plate turned over, the remaining half of the resin poured on it and spread, and the plate covered with another release sheet.

The frame with the wet layup between the release sheets is mounted over a plywood plate with a square cutout and

placed in an autoclave press between two steel plates. The assembly is covered with glass cloth to provide vacuum passage and with a rubber blanket. Full vacuum is drawn and a mechanical pressure of 655 kPa (95 psi) applied. The vacuum is cut off after 30 minutes and the plate cured under pressure at room temperature in approximately 18 hours.

The same procedures are used in the fabrication of thicker laminates. Sixteen-ply laminates of the following layups were fabricated: (0_{16}), $(+45_2/-45_2)_{2s}$, and $(0_2/+45_2/-45_2/90_2)_s$. Twice as many windings and twice as much resin are used compared with the eight-ply laminates, and the plates are cured under similar conditions. The birefringence response of the laminates remains linear up to at least a fringe order of 4 corresponding to a uniaxial tensile stress of 310 MPa (45,000 psi).

The availability of transparent composite laminates of various layups makes it possible to conduct macromechanical stress anslyses by means of anisotropic photoelasticity. Stress distributions around such stress raisers as holes, cracks, and other defects can be studied experimentally; thickness effects can be studied using the thicker laminates. The properties of transparency and birefringence can be utilized in studying failure modes in notched and unnotched laminates, failure initiation, and failure propagation. The use of stereoscopic photography can be investigated as a means of determining the location of flaws and failures through the thickness.

The study of failure initiation in the form of microcracks between fibers in various plies during cyclic fatigue is of great importance and could be greatly facilitated with transparent composites. The ability to see and locate flaws easily should help in studying the influence and failure growth of the flaws during service loading. Furthermore, the ability to detect and characterize flaws optically can serve to set standards for the calibration of conventional nondestructive evaluation instruments. The method of anisotropic photoelasticity can be further utilized in structural applications of composites, such as in bonded or bolted joints.

This work was done by I. M. Daniel and T. Niiro of ITT Research Institute for **Langley Research Center.** *Further information may be found in NASA CR-165709 [N81-26183/NSP], "Development of Orthotropic Birefringent Materials for Photoelastic Stress Analysis" [$10.50]. A copy may be purchased [prepayment required] from the National Technical Information Service, Springfield, Virgina 22161.*

LAR-12960

Modified Fabrication for InGaAsP Stripe Laser

Replacement of the oxide stripe with an n-type layer increases laser efficiency and reduces laser spot size.

Langley Research Center, Hampton, Virginia

An improved fabrication of InGaAsP stripe lasers involves the replacement of the oxide stripe in a quaternary laser by an n-type layer of InP grown on top of a quaternary cap layer (see figure). This process allows the use of a stop etch that selectively removes InP and does not etch InGaAsP, making the fabrication especially convenient. Such a stop etch may consist of HCl or HCl + H_2O combinations.

The application of the InP n-type layer on top of the p-type quaternary InGaAsP layer offers such advantages as very high laser efficiency in the spontaneous mode with a very-small laser spot size and well-confined current. Such improvements are important in fiber-optic coupling applications. Laser life is expected to increase because of reduced stress, since no lattice mismatch exists between the stripe and the material. Thus lasers with better modal control than that available with standard oxide-stripe lasers can be produced with this process modification.

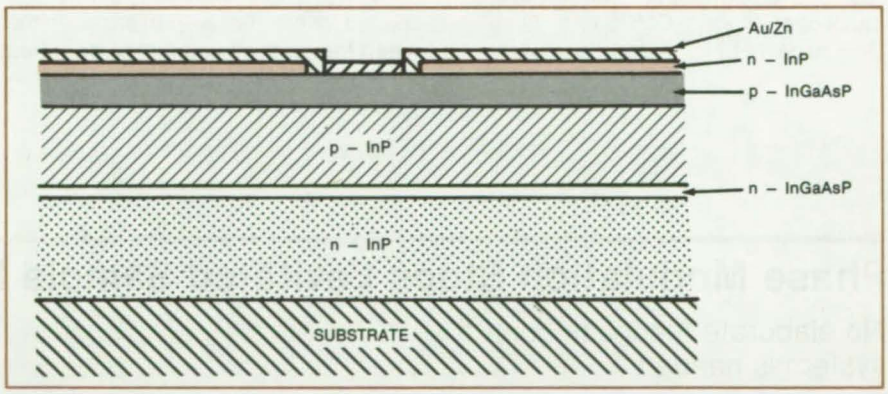

An **n-Type Layer of InP** on top of a p-type quaternary layer replaces the oxide stripe, offering improved laser performance.

This work was done by Ivan Ladany and Theodore R. Furman of RCA Corp. for **Langley Research Center.** *No further documentation is available.*

LAR-12986

Frame Alines Fibers in Multilayer Composites

Laminae are stacked in oriented rectangular holes.

Marshall Space Flight Center, Alabama

A jig ensures that the layers of fiber-reinforced preimpregnated tape are correctly oriented in the assembly of composite panels. The jig enables the fast and reproducible alinement of fibers in multiaxis layups.

For example, a jig (see figure) can be fabricated from wood to form a 0°, ±45°, 90° layup. Concentric square holes with 12-in. (30.5-cm) sides are cut from a wood panel at 45° intervals, producing a star-shaped hole in the panel. Squares of prepeg tape are placed in the holes at the various required orientations until the final thickness of the composite laminated panel is built up. On completion of the layup, the composite panel is ready for curing.

This work was done by J. M. Clemons, F. E. Ledbetter III, B. G. Penn, W. T. White and J. G. Daniels of **Marshall Space Flight Center.** *No further documentation is available.*
MFS-25959

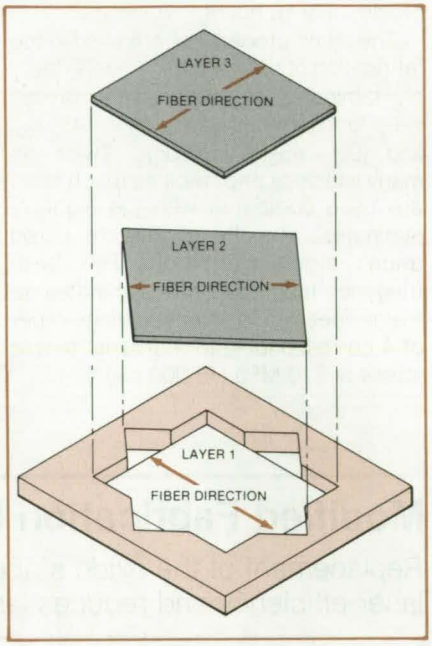

The **Axes of the Square Cutouts** are spaced 45° apart in this jig for assembling layers of prepeg tape in a 0°, ±45°, 90° orientation. A 12-point star would be used for assembling a 0°, ±60° composite. Constructed to accommodate 12-inch squares of tape for laboratory tests, the jig can readily be constructed for larger panel sizes.

Finding Open Faults in CMOS Circuits

In complementary metal-oxide-semiconductor (CMOS) integrated circuits, a stuck-open fault introduces spurious memory into the affected circuit element, so that the output depends on past as well as on present inputs. An algorithm specifies a sequence of input test signals and the interpretation of the resulting output signals for identifying stuck-open faults in CMOS circuits.
(See page 171.)

Neutron Probe of Building-Wall Composition

Neutron radiography aids the preservation and restoration of historic buildings by showing the presence of contaminants and chemical changes in a wall. A neutron source position on the rear wall surface and alined with a gamma-ray detector on the front wall surface yield a map of the composition of a wall. The sampling points are spaced for minimal overlap based on the mean free path of gamma rays emitted from the wall materials.
(See page 193.)

Phase Modulation Stops Levitated Sample Rotation

No elaborate feedback-control system is needed.

NASA's Jet Propulsion Laboratory, Pasadena, California

Rotation of the sample in an acoustic levitator is prevented by a relatively-simple phase-modulation scheme. The new technique differs from older methods in that no feedback control or observation of the sample is required nor is it necessary to carefully tune or detune two oscillators to precise frequency differences from resonance.

In a levitator with equal-frequency acoustic excitation along two perpendicular axes, the local acoustic torque about the third axis varies with the size

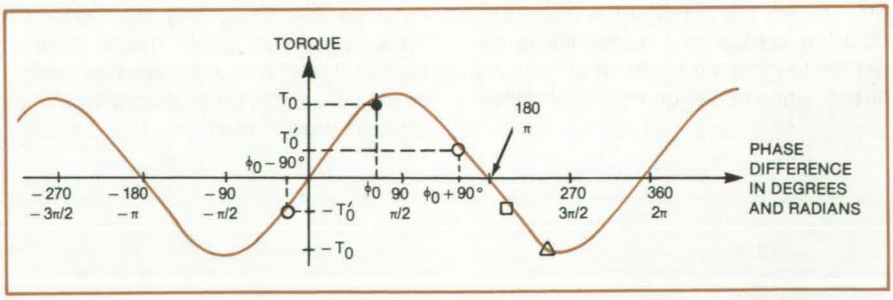

Figure 1. The **Local Acoustic Torque** varies sinusoidally with the local phase difference between two perpendicular acoustic excitations at the same frequency.

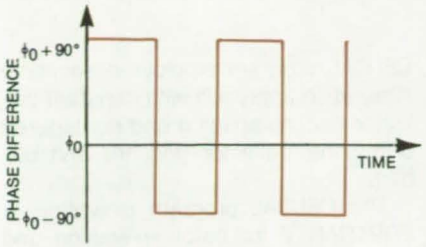

Figure 2. The **Phase of One Acoustic Driver** is modulated with a phase amplitude of 90° so that the phase difference between the two perpendicular excitations alternates between two values 180° apart. The acoustic torque therefore alternates between equal-magnitude positive and negative values and has zero time-average value.

and shape of the sample and is proportional to the sine of the local phase difference between the two excitations (see Figure 1). Rather than attempt the difficult and often impractical task of measuring and controlling the local phase difference, it is simpler to modulate the phase of the excitation in one axis in such a way that zero time-average torque is produced.

The phase-modulation period must be short enough so that the sample does not have enough time at either torque extreme to spin up to an appreciable rotational speed. The phase-modulation amplitudes must be such as to result in a phase difference of an odd multiple of π radians between the modulation peaks. If the local unmodulated phase difference is ϕ_0, the phase modulation for one of the acoustic drivers would be

$$\alpha + (2n - 1)\frac{\pi}{2}$$

on the positive half cycle and

$$\alpha - (2n - 1)\frac{\pi}{2}$$

on the negative half cycle, where α is any real number and n is an integer. The average torque would then be proportional to

$$\sin\left[\phi_0 + \alpha + (2n - 1)\frac{\pi}{2}\right] + \sin\left[\phi_0 + \alpha - (2n - 1)\frac{\pi}{2}\right] = 0 \text{ for any } \phi_0 \text{ or } \alpha$$

The simplest scheme that gives this result is the symmetrical modulation $\alpha = 0, n = 1 (\phi_0 \pm 90°)$, as shown in Figure 2. A modulation frequency of 20 Hz was found to be effective in experiments.

This work was done by Martin B. Barmatz and H. Jordan Brown of Caltech for **NASA's Jet Propulsion Laboratory.** *For further information, Circle 71 on the TSP Request Card.*
NPO-16002

Books and Reports

These reports, studies, and handbooks are available from NASA as Technical Support Packages (TSP's) when a Request Card number is cited; otherwise they are available from the National Technical Information Service.

Processes for VLSI Circuits

Advanced fabrication methods are described and evaluated.

A four-volume document reviews key technologies for interconnections in very-large-scale integrated (VLSI) circuits. The document also discusses current and proposed research into novel fabrication techniques for interconnections.

Part I covers lift-off processes for forming dense interconnection patterns. It surveys lift-off techniques in commercial use and discusses experimental lift-off methods that have been investigated by the author.

A lift-off process includes the deposition of a photoresist on a silicon wafer and patterning the photoresist layer (by etching, for example) so that it forms a stencil for the interconnection material. A conductive layer is then deposited on the wafer and stencil. Unwanted conductive areas are lifted off by removing the underlying stencil, so that the required interconnections remain.

Part II covers multilevel metal interconnections for VSLI circuits, with polyimide as the interlayer dielectric material. It characterizes polyimide materials and discusses experiments with a double-level test pattern. It also presents a novel double-exposure polyimide patterning process. This process offers the advantages of low-temperature fabrication, decreased capacitive coupling between metal layers, greater packing density for both layers, an absence of oversized pads for via holes between layers, and suitability for either wet-chemical or dry-plasma production techniques.

Part III covers dry-plasma processes, including plasma etching, reactive ion etching, reactive ion milling, and plasma deposition processes. It provides a characterization of the processes and surveys equipment available for them. Part III also examines trends in microelectronic fabrication methods, including patterning technology, lithography, material deposition, and packaging.

Part IV presents results of a study aimed at finding the material or combination of materials that will exploit the full potential of the double-layer metal process. The study emphasized polyimide dielectrics because of their favorable electrical, chemical, thermal, and mechanical properties as well as their ease of processing and acceptance in the semiconductor industry. In addition to such single-material dielectrics as polyimides, silicon dioxide, and quartz, the study evaluated such combinations as polyimide and silicon dioxide, polyimide and quartz, and polyimide and silicon nitride.

This work was done by Thomas E. Wade of Mississippi State University for **Marshall Space Flight Center.** *For further information, Circle 72 on the TSP Request Card.*
MFS-25857

Computer Programs

These programs may be obtained at very reasonable cost from COSMIC, a facility sponsored by NASA to make new programs available to the public. For information on program price, size, and availability, circle the reference letter on the COSMIC Request Card in this issue.

Optimizing Grid Patterns on Photovoltaic Cells

Grid patterns are optimized for different cell geometries and metalization processes.

The CELCAL computer program helps in optimizing the grid patterns for different photovoltaic cell geometries and metalization processes. Five different power-loss phenomena are associated with the front-surface metal grid pattern on photovoltaic cells. These phenomena of sheet resistance, contact resistance, collector gridline resistance, bus-bar losses, and shadowing are accounted for by the CELCAL program.

CELCAL calculates each of these losses and their total for any given choice of design input variables. Stepwise variation of inputs by the designer allows grid pattern optimization for the chosen cell geometry (circular or rectangular), the number of horizontal bus bars (1, 2, or 3), and the metalization process (defined by input variables). The CELCAL program employs a sectional integration approach with constant collector gridline spacing and nontapered orthogonal collector gridlines and bus bars.

The CELCAL program is written in FORTRAN V for batch execution and has been implemented on a UNIVAC 1100-series computer with a central-memory requirement of approximately 8K of 36-bit words. The CELCAL program was developed in 1981.

This program was written by Dale R. Burger of Caltech for **NASA's Jet Propulsion Laboratory.** *For further information, Circle N on the COSMIC Request Card.*
NPO-15841

MiniBriefs describe NASA innovations and reports in an abbreviated format. Readers desiring additional information on these items should request the Technical Support Packages (TSP's), available in most cases, which can be obtained by using the TSP Request Card at the back of this issue.

Oxidation Protection for Thermocouples

A thin platinum film covers the thermocouple sheath.

A thin platinum film on a thermocouple sheath protects non-noble-metal thermocouples from deterioration in oxygen-rich atmospheres. The coating should work on nickel-alloy sheathed thermocouples that would otherwise be destroyed by corrosion in pure oxygen at 1,000° C. Thermocouples with the platinum coating can be used in blast furnaces, glass furnaces, and high-temperature oxygen-producing solid-electrolyte cells.

To coat the sheath, a thin film of thick platinum paste is painted on it. The coated thermocouple then is fired at 1,000° C for 10 minutes before exposing it to an oxygen-rich atmosphere.

This work was done by Robert Richter of Caltech for **NASA's Jet Propulsion Laboratory.** *For further information, Circle 163 on the TSP Request Card.*

Inquiries concerning rights for the commercial use of this invention should be addressed to the Patent Counsel. NASA Resident Office-JPL [see page A5]. Refer to NPO-15605.

Toroidal Ellipsoid Float-Zone Heater

The heated zone is visible for process control or experimentation.

An experimental furnace heats and melts a circumferential ring of material (the "float zone") on a round bar. In float-zone processing, the bar is pulled through the furnace so that the zone travels along the bar.

Heating wires lie at the near focuses of two toroidal reflectors that are coaxial with the rod. The far focuses of the reflectors coincide at the heated ring. Since there is a space between the reflectors, the float zone is visible from all azimuthal angles from a range of viewing angles ($\pm 20°$ in the particular design) on either side of the plane of the float zone.

This work was done by Roderick B. Davidson of Technology Development Corp. for **Marshall Space Flight Center.** *For further information, Circle 164 on the TSP Request Card.*
MFS-25771

Repairing Thermal Tiles

Method reduces cure time and temperature requirements.

Small chips and depressions in the surfaces of surface insulation tiles can be repaired using Ludox® (or equivalent) colloidal silica solution and silica powder. Loose material is brushed from the damaged area. The silica solution is then brushed over the damaged area and allowed to dry. A slurry of 2 parts solution to 1 part silica powder is prepared and the damaged area is filled flush to the surface. After the surface is air-dried, the silica solution mixed with 5 percent by weight of SiB_4 (silicide tetraboron) is applied to restore the emissivity. The surface is air-dried again.

No waiting time is necessary between mixing the filler and using it. The patch cures quickly without heat being applied.

® Ludox is a registered trademark of E. I. du Pont de Nemours & Co., Inc.

This work was done by Charles R. McCain, Jr., and Charles W. Feiler of Rockwell International Corp. for **Johnson Space Center.** *No further documentation is available.*
MSC-20336

Bellows With Longitudinal Seams

Bellows constructed with longitudinal side seams ease assembly and repair.

Bellows assembled using two longitudinal side seams will allow seam joints to be placed in axial directions of bellows. Bellows segments may be joined by welding, folding, crimping, or adhesives. This design is of particular importance in difficult situations where frequent assembly or repair is required or in limited-access areas where it is not desirable to disassemble the total unit to replace a one-piece bellows.

This work was done by W. L. Garvin of Rockwell International Corp. for **Marshall Space Flight Center.** *For further information, Circle 165 on the TSP Request Card.*
MFS-19633

Strain Analysis of Graphite/Epoxy Pressure Vessels

In some situations, a lightweight composite could be substituted for steel.

A NASA Technical Paper discusses the stiffness parameters of filament-wound graphite/epoxy pressure vessels. Although the study is motivated by the problem of replacing a rocket-motor case with a lighter case of adequate rigidity, some of the subject matter is transferable to pressure vessels in general. The study takes account of the filament-wound-case configuration, including its mass and mass distribution compared to those of a steel case. Design-stiffness criteria, the stiffness-degrading effects of manufacturing processes and vessel operation, nonisotropic stress/strain analysis, testing with scale models, and case dynamics are all considered.

This work was done by V. Verderaime and M. Rheinfurth of **Marshall Space Flight Center.** *Further information may be found in NASA Technical Paper 2117 [N83-16400/NSP], "Identification and Management of Filament-Wound Case Stiffness Parameters" [$7]. A paper copy may be purchased [prepayment required] from the National Technical Information Service, Springfield, Virginia 22161. A copy is also available on microfiche at no charge. To obtain a microfiche copy, Circle 166 on the TSP Request Card.*
MFS-27018

Electroformed Electrodes for Electrical-Discharge Machining

Copper electrodes are easier and cheaper to make.

Copper electrodes may replace graphite electrodes in many instances of the electrical-discharge machining (EDM) of complex shapes. One of the advantages is that the same electroforming mandrel can be used repeatedly to make a number of electrodes. The complicated shape, therefore, has to be machined only once in making the mandrel, and the electrodes nearly duplicate the machining precision.

Copper electrodes wear longer and cause less contamination of the EDM dielectric fluid than do graphite electrodes. Graphite is relatively expensive, and the worn electrodes must be discarded. In contrast, worn copper electrodes can be redissolved and used to electroform new ones.

This work was done by A. R. Werner and M. L. Cassidenti of Rockwell International Corp. for **Marshall Space Flight Center.** *For further information, Circle 167 on the TSP Request Card.*
MFS-19651

Securing Identification Sleeving

Two layers of heat-shrunk tubing are used.

Identification sleeving that slides or bunches during handling or vibration can be held in place by shrinkage tubing. In a NASA application, the part number and the serial number of an accelerometer cable were stamped on a section of yellow heat-shrink tubing. The tubing was then slid over one end of the cable and shrunk with a hand-held hot-air gun. A shorter length of tubing was slid over the yellow tubing and also heat-shrunk, fixing the identification permanently.

This work was done by Elton P. Seiggum of Rockwell International Corp. for **Marshall Space Flight Center.** *No further documentation is available.*
MFS-19685

Cryogenic Separation of a Ceramic From Its Mandrel

The technique takes advantage of the difference in expansion coefficients.

A thermally sprayed ceramic can be released from its mandrel by immersing the ceramic part and mandrel in a cryogenic liquid, such as liquid nitrogen. The technique takes advantage of the relative difference in expansion between the mandrel and the ceramic; for example, a brass mandrel shrinks considerably compared to the ceramic material.

This work was done by Edward W. Covington III of **Langley Research Center.** *No further documentation is available.*
LAR-12904

Pressure/Vacuum Bonding for Low-Curvature Mirrors

Reflecting surfaces are attached to nonreflecting substrates.

A pressure/vacuum bonding technique facilitates the assembly of large solar-concentrator mirrors. Reflectors with radii of curvature of approximately 600 in. (15 m) are made by bonding glass or metallized-plastic reflecting material about 0.060 in. (1.5 mm) thick to rigid substrates of the desired surface figure.

The mirror sheet is held, by vacuum, on a diaphragm, then coated with adhesive. The diaphragm is inflated from underneath until it and the mirror sheet have a curvature greater than that of the substrate. The substrate is placed on top of the adhesive-coated mirror sheet, making contact first at the center. The substrate is then weighted down to make the contact spread out to the edge, pushing the air bubbles out of the adhesive as it goes.

This work was done by Peter O. Frickland of Caltech for **NASA's Jet Propulsion Laboratory.** *For further information, Circle 168 on the TSP Request Card.*
NPO-15613

Flame-Test Chamber

It simulates atmospheric flame propagation.

An experimental chamber 14 ft (4.27 m) long and 96 in. (2.44 m) in diameter provides a controlled environment for the observation and measurement of flames propagating in an expanding plume of flammable air/fuel mixture under atmospheric conditions. The chamber consists of galvanized-steel walls and thin polyethylene endpieces. The plastic ends blow out when the mixture is ignited. Pressure sensors, flame sensors, thermocouples, and high-speed motion-picture cameras are mounted at observation posts on the walls and ceiling. The chamber has been designed to evaluate the quenching capability of screen-type flame arresters in atmospheric vents of fuel cargo tanks aboard marine cargo vessels.

This work was done by Roy A. Bjorklund of Caltech for **NASA's Jet Propulsion Laboratory.** *For further information, Circle 169 on the TSP Request Card.*
NPO-15407

Airlock Entry

A proposed airlock for inflated domes would be easy to assemble.

A proposed airlock could be retrofitted to air-inflated polymeric domes to accommodate large vehicles. The airlock would be inexpensive, simple to assemble, adaptable to any terrain and any size required, and require no external power.

The airlock passageway is a polymer-film tube, sealed at one end, that is supported by an aluminum frame. After people and equipment are in the passageway, the tube is attached to the dome with a polymeric zipper. A vent in the dome door is then opened to pressurize the passageway so that the door can be opened. Exiting the dome is a straightforward procedure: the door and its vent are closed and the tube is unzipped.

This work was done by Peter O. Frickland and Edward L. Cleland of Caltech for **NASA's Jet Propulsion Laboratory.** *For further information, Circle 172 on the TSP Request Card.*
NPO-15415

Adjusting the Contour of Reflector Panels

The contour can be adjusted manually.

Postfabrication adjustment of the contour of panels for a reflector, such as a parabolic reflector for radio antennas, is possible with a simple mechanism consisting of a threaded stud, two nuts, and a flexure. A structural framework behind a reflector panel is attached at several locations by threaded studs. Each stud is supported by a flexure to minimize the effect of temperature difference between the framework and the panel. Contour adjustment is made with the two nuts.

This work was done by William B. Palmer and Martin M. Giebler of TRW, Inc., for **NASA's Jet Propulsion Laboratory.** *For further information, Circle 171 on the TSP Request Card.*
NPO-15319

Automated Variable-Polarity Plasma-Arc Welding

Plasma-arc method produces better welds at lower cost.

The variable-polarity plasma-arc method produces better welds at lower cost than gas-shielded tungsten-arc welding in the assembly of the Space Shuttle external fuel tank. The plasma jet allows 'open-keyhole' welding, where contaminants escape to the far side of the aluminum alloy workpiece. Weld porosity is very low and costs of joint preparation, depeaking, inspection, and weld repair are minimized. Thick workpieces may be welded in one pass instead of the multiple passes required by the tungsten-arc process.

Electrical polarity is reversed for 4 ms out of 23 ms, subjecting the workpiece to cathodic cleaning. Arc-voltage control circuitry holds the straight-polarity voltage constant by moving the torch towards or away from the workpiece. Parameters for tapered welds are controlled by a microcomputer.

This work was done by A. C. Numes, Jr., E. O. Bayless, Jr., S. C. Jones III, P. M. Munafo, A. P. Munafo, A. P. Biddle, and W. A. Wilson of **Marshall Space Flight Center.** *For further information, Circle 170 on the TSP Request Card.*
MFS-27042

Welding Tubes in Place

Welding apparatus is small but effective.

Special welding equipment joins metal tubes that will carry pressurized cryogenic fluids. The equipment is small enough to be used in the confined spaces in which such tubes are often mounted.

A hand-operated flanging tool prepares the tube ends. Two flanged ends are butted together, tack-welded, then clamped in the welding head. Inside the head, a motor-driven tungsten arc-welding electrode moves along the joint. The flanges serve as filler material. To prevent oxidation, the tube and head are purged with argon before welding.

The joints are reliable, as shown by radiographic, helium-leak, and mechanical-strength tests. The welded joints are lighter in weight and more leak-proof than joints made with mechanical fittings.

This work was done by R. Meredith of North American Aviation, Inc., for **Marshall Space Flight Center.** *For further information, Circle 173 on the TSP Request Card.*
MFS-25714

Hot Forming With Electron-Beam Welder

Thin flanges are brought within tolerance.

Hot forming to restore the size and shape of thin metal parts can be done with an electron-beam welder. The workpiece is heated in a scanning defocused electron beam rather than in a conventional heat-treating furnace.

The technique has proved successful in straightening some thin flanges of nickel alloy and titanium. First, a flange is clamped tightly between straightening jaws. The flange and jaws are both placed in the welding vacuum chamber and the electron beam is adjusted to give a bright red color at a temperature up to 1,600° F (870° C). The beam is moved along the flange at about 8 in./min (3.4 mm/s). After cooling, the clamp is removed, and the flange is ready for further processing.

This work was done by Robert K. Dobson and Edwin L. Whiffen of Rockwell International Corp. for **Johnson Space Center.** *No further documentation is available.*
MSC-20413

Microfissuring in Alloys During Welding

Concentrated strain on grain boundaries results in intergranular brittleness.

It is possible to evaluate the cause of intergranular cracking (microfissuring) in high-temperature alloys during welding by measuring the number of microcracks as a function of temperature and plastic strain. Two mechanisms of microfissuring in the heat-affected zone are suggested: One is based on the separation of intergranular liquid; the other involves tearing of solid ligaments separating pools of liquid on the grain boundaries. Both mechanisms concentrate strain on the grain boundaries, resulting in low-strain intergranular brittleness.

This work was done by the College of Engineering of Clemson University for **Marshall Space Flight Center.** *For further information, Circle 174 on the TSP Request Card.*
MFS-25604

Acoustic-Levitation Chamber

A sealed chamber eliminates contamination in ultrapure-material processing.

Uncontaminated environments for highly-pure material processing can be provided within a completely sealed levitation chamber that suspends particles by acoustic excitation. The chamber is designed for processing semiconductor and integrated-circuit materials at high temperatures in an environment where even minute contamination and nucleation are unacceptable. This technique is ideally suited for material processing in the low gravity environment of space.

The entire acoustic chamber is vibrated to excite its levitation modes. With the proper chamber geometry, only one acoustic transducer, producing longitudinal, transverse, or a combination of the two oscillations, is required to suspend the particles.

This work was done by Martin B. Barmatz, Dan Granett, and Mark C. Lee of Caltech for **NASA's Jet Propulsion Laboratory.** *For further information, Circle 175 on the TSP Request Card.*

Inquiries concerning rights for the commercial use of this invention should be addressed to the Patent Counsel, NASA Resident Office-JPL [see page A5]. Refer to NPO-16142.

Monitoring Acoustically Levitated Samples

A sample is viewed through a sapphire window.

The physical behavior of a sample acoustically levitated in a high-temperature oven is optically monitored by a system developed at NASA's Jet Propulsion Laboratory. The optical system allows visible and infrared monitoring of an acoustically levitated sample. Optical sources and detectors provide silhouette, surface feature, and radiometric images of the levitated object.

This work was done by Thomas A. Glavich, Daniel J. Kerrisk, John M. McLauchlan, Jaroslav K. Langmaier, and Fred R. Chamberlain III of Caltech for **NASA's Jet Propulsion Laboratory.** *For further information, Circle 176 on the TSP Request Card.*
NPO-15193

Solar-Cell-Manufacturing System

A low-cost manufacturing technique improves solar-cell assemblies.

The cost of manufacturing solar arrays can be minimized by using polyimide-ribbed substrates together with silver-plated coils of low-expansion nickel/iron ribbon welded on solar cells. The ribbon can be easily silver-plated or silver-clad without burrs. Because the thermal-expansion coefficient of the ribbon is well-matched to that of silicon, the spot welds will not load one another under thermal stress. The cell can be glassed without cleaning.

The polyimide taped to the ribbon protects the cell from abrasion or from sticking to other tooling. The system is so tolerant of cracked cells that most cracked cells need not be scrapped and replaced.

This work was done by Franklin G. Kelly of TRW, Inc., for **Marshall Space Flight Center.** *For further information, Circle 177 on the TSP Request Card.*
MFS-25483

Automated Assembly of Solar Panels

A robot places photoelectric cells in a lamination chamber and then removes the cured panel.

An array of vacuum cups mounted on a robot arm places an interconnected string of photoelectric cells on a sheet substrate. Another sheet is placed over the cells and cut to size. After an hour of thermal-curing under vacuum, the robot arm removes the laminated panel from the chamber. This automated process is expected to lower the cost of solar-panel fabrication.

This work was done by John J. Hagerty of MB Associates for **NASA's Jet Propulsion Laboratory.** *For further information, Circle 178 on the TSP Request Card.*
NPO-16206, 7, 8, 9

Purifying Silicon During Crystal Growth

Current causes impurities to electromigrate from growing crystal.

Direct current applied to molten silicon during crystallization causes impurities to migrate away from the interface of the growing crystal. This method improves the purity of the crystal without interfering with the growth process or requiring additional operator attention. Since the power expended for electromigration results in ohmic heating of the melt, the process is energy efficient. The electrodes for the process can be either the crucible and the crystal or the die halves of the EFG (edge-defined film-fed growth) silicon-ribbon process; in the latter case, the impurities are sequestered on one side of the ribbon.

This work was done by Paul J. Shlichta of Caltech for **NASA's Jet Propulsion Laboratory.** *For further information, Circle 179 on the TSP Request Card.*

This invention has been patented by NASA (U.S. Patent No. 4,330,359). Inquiries concerning nonexclusive or exclusive license for its commercial development should be addressed to the Patent Counsel, NASA Resident Office-JPL [see page A5]. Refer to NPO-14831.

Silicon-Film Growth by Continuous Edge-Supported Melt Skimming

A proposed technique would grow thin sheets of silicon at high speeds with minimal contamination.

Silicon films can be grown in a novel and continuous manner without the presence of a substrate. Two rails or filaments of wetting or nonwetting nature are kept at a fixed distance apart and drawn across the surface of a silicon melt. A thin film of liquid silicon forms between the two filaments and solidifies away from the melt surface. The film is replenished at the melt surface by capillary action — this provides for a continuous formation of silicon sheet.

Current methods of producing thin silicon sheets directly from molten silicon are all subject to one or more of the following limitations: excessive contamination from foreign substrates or dies, highly sensitive temperature controls, highly stressed surfaces, inaccessible film surface for solar-cell back contacts, slow speed of growth, highly irregular surface morphology, and poor dimensional control. This method does not have any of these limitations.

This work was done by Guenter H. Schwuttke and James K. Liu of Caltech for **NASA's Jet Propulsion Laboratory.** *For further information, Circle 180 on the TSP Request Card.*

Inquiries concerning rights for the commercial use of this invention should be addressed to the Patent Counsel, NASA Resident Office-JPL [see page A5]. Refer to NPO-15532.

Alining Solder Pads on a Solar Cell

The back-surface location is marked while the front pad is screened.

A mechanism consisting of a stylus and hand-operated lever can be incorporated into a screening machine to precisely register the front and back solder pads during solar-cell assembly. An operator moves the lever as the front panel is being screened. The stylus, under spring pressure, contacts the back surface and marks it at the location of the solder pad. Although not directly applicable to automated solar-cell assembly, the technique may interest those assembling solar cells manually for research or prototype work.

This work was done by Angelo Gino Lazzery of RCA Corp. for **NASA's Jet Propulsion Laboratory.** *For further information, Circle 181 on the TSP Request Card.*
NPO-15298

Terminal System for Photovoltaic Arrays

A dual-ended plug fits into recessed sockets in adjacent arrays.

A quick-connect terminal system provides both electrical contact and physical alinement between adjacent photovoltaic modules. Dual-ended plugs connect adjacent modules; single-ended plugs connect bus cables. No tools are required to insert the plugs and no live terminals are exposed before, during, or after connection.

The terminal housings are injection-molded from high-temperature-tolerant, carbon-black-filled, UV-stable, nonconducting, thermoplastic polyester. The absence of exposed metal parts eliminates the need for grounding devices, conduits, and the like. The terminals inside the sockets and plugs are spring-loaded, rhodium-plated, leaded copper with an expected minimum life of 20 years.

This work was done by Timothy J. Maloney of AIA Research Corp. for **NASA's Jet Propulsion Laboratory.** *For further information, Circle 182 on the TSP Request Card.*
NPO-15739

Mathematics and Information Sciences

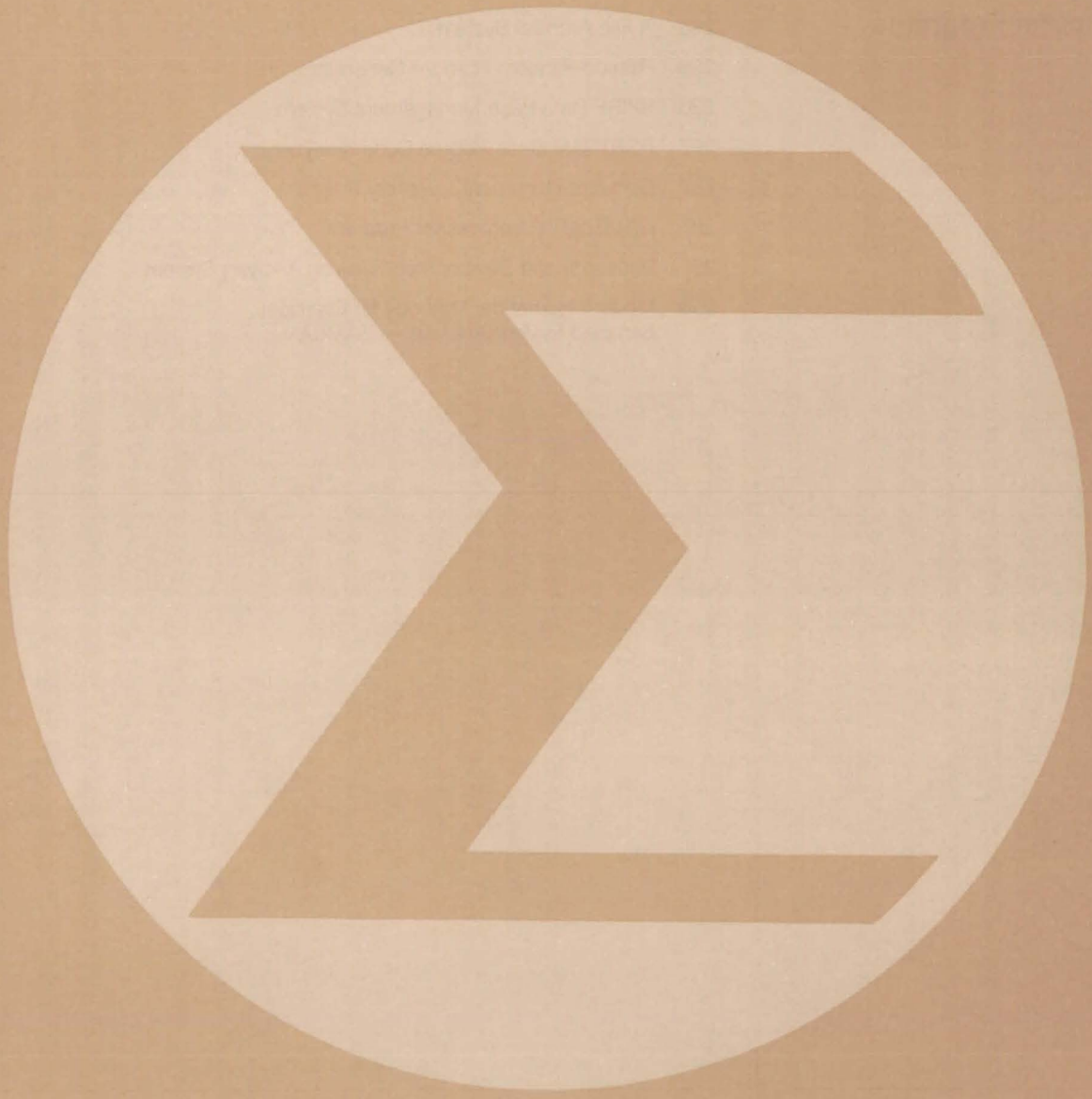

Hardware, Techniques, and Processes

295 Efficient Coding for Optical Communication

Computer Programs

295 A File Archival System

296 Pseudo-Random Number Generators

296 SPIRE Data-Base Management System

297 FORTRAN Static Source Code Analyzer

297 Software Document Inventory Program

297 NAMELIST Preprocessor Program

297 Research and Development Mission Analysis System

298 Modern Numerical Methods for Classical Sampled System Analysis — SAMSAN

Efficient Coding for Optical Communication

Photon counting yields a higher capacity than conventional linear amplification.

NASA's Jet Propulsion Laboratory, Pasadena, California

The possibility of using photon counting, rather than conventional linear amplification, for optical communications is raised by the results of a recent study at NASA's Jet Propulsion Laboratory. The study suggests that a combination of pulse-position modulation and Reed-Solomon coding would give a signaling efficiency of 3 or 4 bits/photon. Although this is less than the theoretical maximum, it is substantially more than the 1.44 bits/photon capacity of linear-amplification methods.

In pulse-position modulation (PPM) the transmission interval is divided into consecutive blocks of q slots each. In each such block, a laser is pulsed in one (and only one) of the slots at a fixed intensity. Each of the resulting q signal patterns is considered to be a character in the sender's alphabet.

At the receiver is a device that detects the presence or absence of photons in each timeslot. For example, if q = 4, the possible characters are represented by 0001, 0010, 0100, 1000, and the "erasure" symbol 0000, which is reported if the transmitted photons are not detected.

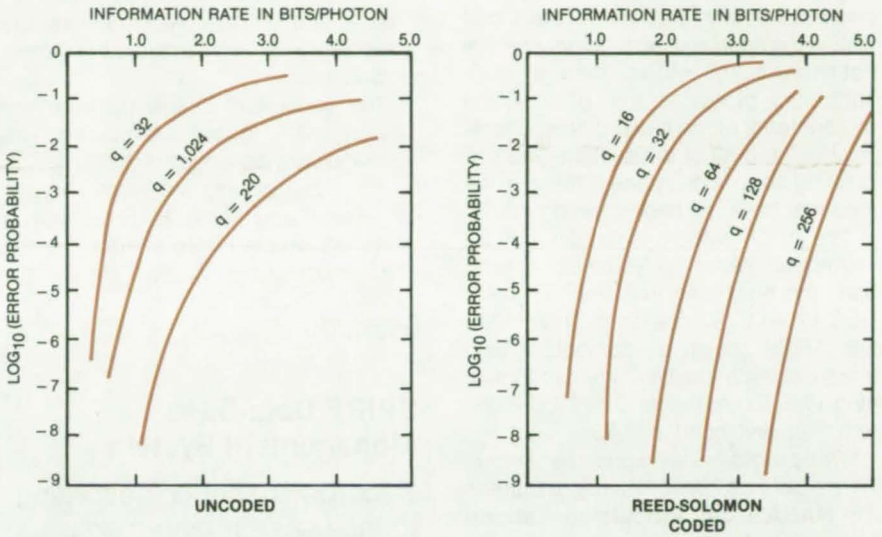

The Performances of Uncoded and Coded PPM are compared in terms of error probability and information rate.

Reed-Solomon error-correcting codes can be used to "fill in" most of the erasures that occur in this way. The figure gives a comparison of error probabilities and information rates with uncoded and RS-coded PPM. For a decoding-error probability of 10^{-6}, the curves show that coded PPM with q = 32 works as well as uncoded PPM with $q = 2^{20} = 1{,}048{,}576$.

This work was done by Robert J. McEliece of Caltech for **NASA's Jet Propulsion Laboratory.** *For further information, Circle 73 on the TSP Request Card.*
NPO-15856

Computer Programs

These programs may be obtained at very reasonable cost from COSMIC, a facility sponsored by NASA to make new programs available to the public. For information on program price, size, and availability, circle the reference letter on the COSMIC Request Card in this issue.

A File Archival System

System for the DEC VAX simplifies offline storage and retrieval of arbitrary files.

ARCH, a file archival system for the DEC VAX, provides for the easy offline storage and retrieval of arbitrary files on a DEC VAX system. The system was designed to eliminate situations that can tie up disk space and lead to confusion when different programers develop different versions of the same programs and their associated files.

ARCH can handle any of the three types of Files-11 file formats (indexed, sequential, and relative), with a given type of file being allowed to have any arbitrary contents. The files are initially stored on disk with eventual movement to tape storage. A complete history is maintained by means of a directory file containing a list of the entire contents of each backup tape. Each tape also contains enough information to effect a system recovery.

During archiving, ARCH copies a file into a special disk directory and makes an extensive entry for the file in the internal catalogs. The file is changed to internal format, and two classes of user-supplied comments may be added: a (short) summary description and a (long) detailed description. Groups of files from this special disk directory can be moved onto tape. The system can always be restored to the state it had at the time of the latest backup-tape generation, should a catastrophic disk failure occur.

Several features aid the user in searching for a particular file among the archived files to eliminate the unnecessary "dearchiving" of files. When a file is retrieved (dearchived), the new user file duplicates the original file with the option of adding the user-supplied archive

(continued on next page)

comments. An internal help facility provides assistance in all phases of the ARCH system.

Privileged management functions provided by ARCH include commands that allow initialization or restoration of the special disk directory, commands that allow recalculation (realphabetization) of the index of files resident on disk, and a command that will locate those files in the special disk directory that are not known to the system. There are also subsidiary programs that allow listing the contents of the catalog files, checking the integrity of the system, and calculating how much space is taken up by files that have not been moved to tape.

The ARCH system is written in FORTRAN and VAX-11 MACRO-32, Assembler and has been implemented on a DEC VAX-11/780 operating under VMS 3.2. ARCH should be compatible with any machine of the DEC VAX family running VMS 3.0 or higher. The ARCH system was developed in 1983.

This program was written by John L. Fanselow and John L. Vavrus of Caltech for **NASA's Jet Propulsion Laboratory.** *For further information, Circle P on the COSMIC Request Card.*
NPO-16274

Pseudo-Random Number Generators

Package features a comprehensive selection of probabilistic distributions.

High-speed computers make it possible to use probabilistic simulation techniques. These Monte Carlo simulations are resorted to whenever the systems being studied are not amenable to deterministic analyses or when direct experimentation is not feasible. Random numbers having a certain specified distribution characteristic are an integral part of these simulations. This package consists of a collection of "pseudo-random" number generators for use in Monte Carlo simulations. They are called "pseudo-random" because they are generated by numerical algorithms.

The basic element in all Monte Carlo simulations is the uniform random-number generator. All other distributions can be obtained either by the probability integral transformation or by applying some known relationship between the desired distribution and the uniform distribution.

The uniform random-number generator in this package is based on the central-limit method. The package also supplies the following continuous distributions: normal, lognormal, Weibull, gamma, exponential, chi-square, F, and beta. Also included are random-number generators for the following discrete distributions: binomial, poisson, Meyman type A, and Thomas. All the generators are constructed with emphasis on speed and accuracy.

The generators in this package are written in APL for batch execution. This package was developed in 1982.

This program was written by Leonard W. Howell and Mario H. Rheinfurth of **Marshall Space Flight Center.** *For further information, Circle R on the COSMIC Request Card.*
MFS-27017

SPIRE Data-Base Management System

Records are set up according to the user's requirements.

The Spacelab Payload Integration and Rocket Experiment (SPIRE) data-base management system (DBMS) is based on a relational model of data bases. The data bases are typically used for engineering and mission analysis tasks and, unlike most commercially available systems, allow data items and data structures to be stored in forms suitable for direct analytical computation. The SPIRE DBMS is designed to support data requests from interactive users as well as from applications programs. The following description is related to interactive use of the DBMS via a "Relational Calculus" known as Query-by-Example (QBE).

User interaction with the SPIRE DBMS via a CRT or hard-copy terminal provides for the easy and timely access to the user's data while still allowing a full range of retrieval and manipulative capabilities. The SPIRE DBMS readily accommodates both the new user who knows very little about data-base management and the more sophisticated user who can operate at a lower level in the system. SPIRE includes a supervisor that employs a password security procedure to limit user access to the system, to data files, and to various commands.

The QBE provides a "user-specific view" of how a set of data ought to be related in a user-friendly environment along with data retrieval and manipulative capabilities. Through the QBE language, the user interacts with the SPIRE DBMS as though examining and manipulating a set of tables. This is achieved by allowing each user to develop a template for a set of data in terms of the user "view."

The important characteristic of the template, as far as the user is concerned, is that it is in a record layout form. The QBE allows each and every user to have a different "view" of a common set of data. Further, the user may "view" a data base as containing records that are made up of parts of explicit data-base records or transformations of explicit data-base records, such as a subset of the existing range of values in a given field. In the simplest case, a user "view" may be nothing more than renaming the existing field and record names in a given data base.

Almost every user interaction with a relational data-base system results in more data-base components (i.e., relations). Results of a request remain in the system, look like part of the workspace file, and are available to the user as data-base components.

The QBE language includes the Boolean operators OR, AND, and NOT and the arithmetic operators LESS THAN, LESS THAN OR EQUAL, EQUAL, GREATER THAN, and GREATER THAN OR EQUAL for aiding the user in making a request. The JOIN operator allows the user to create new data from existing data.

The QBE also includes two functions: One sums the contents of a numeric field for "data records" satisfying selection criteria, and the other counts the number of "data records" that satisfy selection criteria. Thus, with QBE the user can readily request; for example, "the number and the sum of checks of amounts greater than $100 written to XYZ, Inc., in the month of June." Although the QBE language is not a true English-like language, its query-by-example nature is readily picked up by the first-time user.

The SPIRE data-base management system is written in FORTRAN IV and MACRO Assembler for interactive execution and has been implemented on a DEC VAX-11/780 under VMS 2.0. The SPIRE data-base management system was developed in 1980.

This program development was managed by Charles F. Fuechsel of **Goddard Space Flight Center.** *For further information, Circle S on the COSMIC Request Card.*
GSC-12684

FORTRAN Static Source Code Analyzer

FORTRAN code is assigned a figure of complexity.

The FORTRAN Static Source Code Analyzer program, SAP (DEC VAX version), automatically gathers statistics on the occurrences of statements and structures within a FORTRAN program and provides reports of those statistics. Provisions have been made for weighting each statistic and to provide an overall figure of complexity.

The statistics, as well as figures of complexity, are gathered on a module-by-module basis; overall summed statistics are also accumulated for the complete input source file. SAP accepts as input syntactically-correct FORTRAN source code written for the DEC FORTRAN IV-Plus compiler or the IBM S/360 FORTRAN IV, Level H, compiler.

SAP utilizes two external files in its analysis procedure. A keyword file allows flexibility in classifying statements and in marking a statement as either executable or nonexecutable. A statistical weight file allows the user to assign weights to all output statistics, thus allowing the user flexibility in defining the figure of complexity.

The program is written in FORTRAN IV for batch execution and has been implemented on a DEC VAX series computer with a central-memory requirement of approximately 94K of 8-bit bytes. SAP was developed in 1978.

This program was written by Phillip Merwarth of **Goddard Space Flight Center.** *For further information, Circle T on the COSMIC Request Card.*
GSC-12724

Software Document Inventory Program

Program offers ways to file and locate sources of reference.

An information-storage and report-generation tool, DOCLIB, supports the document inventory at the Godddard Space Flight Center Software Engineering Library. The DOCLIB system consists of two parts to serve the needs of two types of users: the general user and the librarian. The general-user part enables the user to examine the contents of the inventory data base to locate or validate documents currently maintained in the inventory. The librarian part of the DOCLIB system enables the data-base librarian to add, delete, or modify information in the data base concerning the document inventory.

The DOCLIB system provides the user with an interactive, menu-driven document inventory capability. Each document in the inventory is described by information that includes the following: reference number, title, author(s), publication date, sponsoring organization, the number of pages, subject(s), document type, and organization document number.

The general user can browse through the document inventory data base by displaying a particular document description, displaying document arrivals after a specified date, or by performing a document search. The user can search for documents by author, reference number, title fragment, originating organization, and category. Results of a document search may be displayed during the user session and may be routed for hard-copy printing.

The DOCLIB system is written in FORTRAN IV-Plus and MACRO Assembler for interactive execution and has been implemented on a DEC PDP-11/70 computer under RSX-11M with a central-memory requirement of approximately 50K of 16-bit words. The DOCLIB system was developed in 1981.

This program was written by Phillip D. Merwarth of **Goddard Space Flight Center.** *For further information, Circle U on the COSMIC Request Card.*
GSC-12803

NAMELIST Preprocessor Program

Input data can be reviewed without elaborate formatting.

The NAMELIST Preprocessor Program, NPP, provides the DEC VAX with capabilities identical to the IBM FORTRAN IV NAMELIST feature. The preprocessor modifies FORTRAN code containing NAMELIST statements acceptable to the IBM FORTRAN IV compiler, to generate equivalent code that is acceptable to the VAX FORTRAN IV compiler.

The NAMELIST feature provides the FORTRAN programer with additional, flexible input and output capabilities. This feature is particularly useful in the area of data input because NAMELIST data are input in the form of the variable symbolic name being set equal to a constant value, similar to a standard FORTRAN statement. This allows the user to review input data readily and relieves the user from having to place data in certain columns and formats as required in formatted READ statements.

NPP software consists of two parts: the NAMELIST preprocessor and the NAMELIST library routines. The preprocessor modifies FORTRAN code containing NAMELIST statements into FORTRAN code acceptable to the VAX FORTRAN IV compiler. The NAMELIST library routines, which must be included in task builds containing NAMELIST preprocessor code, are the run-time routines called by the inserted preprocessor code. The FORTRAN programer should find it easy and efficient to incorporate the NAMELIST feature into many applications.

NPP software is written in FORTRAN IV and Assembler code for batch execution and has been implemented on a DEC VAX series computer with a central-memory requirement of approximately 74K of 8-bit bytes. The NPP software system was developed in 1978.

This program was written by Phillip D. Merwarth of **Goddard Space Flight Center.** *For further information, Circle V on the COSMIC Request Card.*
GSC-12711

Research and Development Mission Analysis System

Program forms a basis for solving complex mission-analysis problems.

The Research and Development Mission Analysis System, RADMAS, facilitates the solution of mission-analysis problems in a research and development environment. RADMAS provides a flexible data-management and control structure from which existing mission-analysis programs can be invoked and new R. & D. models can be developed and executed. The system centers on an executive structure that controls function selection and execution.

The main driver for any RADMAS solution is an automatic sequence. This sequence is written in the Mission Analysis Language (MAL), a FORTRAN-based high-level language that contains special constructs. RADMAS drivers and

(continued on next page)

handlers control solution execution through automatic sequences that invoke independent tasks to perform the desired function. Problem solution is controlled interactively through menu and parameter displays that enable the user to redirect execution of the task based on run-time information.

The built-in RADMAS handlers and drivers include such a wide variety of system capabilities as intertask communication, data editing and parameter modification, resource and process management, automatic system error-interception and recovery, dynamically allocated arrays, and multiple graphics device capability. The system can incorporate new capabilities without necessitating major changes to RADMAS itself. The user may also supply other functions that are required for a particular problem.

Foremost among the built-in RADMAS functions is the orbit propagation information that produces the vehicle state for other functions. Included in this function are a parametric calculation module, which supplies various output parameters, and a comprehensive selection of stopping conditions on which to terminate propagation. Targeting and optimization procedures are included to aid the mission analyst in determining constraints. Error analysis based on a Monte Carlo procedure gives the R. & D. user a tool for statistical analysis of a mission.

RADMAS is written in FORTRAN 77 and Assembler for batch or interactive execution. The system has been implemented on a DEC VAX-11/780 operating under VMS with a central-memory requirement of approximately 820K of 8-bit bytes. For graphics output the system supports the following devices: Tektronix, I2S, VT100, CALCOMP, and various user terminals. RADMAS was developed in 1982.

This program was written by Wayne A. Taylor of Computer Science Corp. for **Goddard Space Flight Center.** *For further information, Circle W on the COSMIC Request Card.*
GSC-12847

Modern Numerical Methods for Classical Sampled System Analysis — SAMSAN

Program provides a set of algorithms that can be readily integrated for solving control-system problems.

SAMSAN aids the control-system analyst by providing a self-consistent set of computer algorithms that support large-order control-system design and evaluation studies, with an emphasis placed on sampled system analysis. Control-system analysts have access to a vast array of published algorithms to solve an equally large spectrum of controls-related computational problems. The analyst usually spends considerable time and effort bringing these published algorithms to an integrated operational status only to find them less general than desired.

SAMSAN reduces the burden on the analyst by providing a set of algorithms that have been well tested and documented and that can be readily integrated for solving control-system problems. Algorithm selection for SAMSAN has been biased toward numerical accuracy for large-order systems with computational speed and portability being considered important but not paramount.

In addition to containing relevant subroutines from EISPACK for eigenanalysis and from LINPACK for the solution of linear systems and related problems, SAMSAN contains the following seven not so generally available capabilities:

1. Reduction of a real nonsymmetric matrix to block diagonal form via a real similarity transformation matrix, which is well conditioned with respect to inversion;
2. Solution of the generalized eigenvalue problem with balancing and grading;
3. Computation of all zeros of the determinant of a matrix of polynomials;
4. Matrix exponentiation and the evaluation of integrals involving the matrix exponential, with option to block-diagonalize first;
5. Root locus and frequency response for single variable transfer functions in the S-, Z-, and W-domains;
6. Several methods of computing zeros for linear systems; and
7. The ability to generate documentation "on demand."

All matrix operations in the SAMSAN algorithms assume nonsymmetric matrices with real double-precision elements. There is no fixed size limit on any matrix in any SAMSAN algorithm; however, it is generally agreed by experienced users, and in the numerical error-analysis literature, that computation with nonsymmetric matrices of order greater than about 200 should be avoided or treated with extreme care. SAMSAN attempts to support the needs of application-oriented analysis by providing the following:

a. A methodology with unlimited growth potential;
b. A methodology to insure that associated documentation is current and available "on demand";
c. A foundation of basic computational algorithms upon which most controls-analysis procedures are based;
d. A set of checkout and evaluation programs that demonstrate usage of the algorithms on a series of problems that are structured to expose the limits of applicability of each algorithm; and
e. Capabilities that support both a priori and a posteriori error analysis for the computational algorithms provided.

The SAMSAN algorithms are coded in FORTRAN IV for batch or interactive execution and have been implemented on a DEC VAX-11/780 computer under VMS 2.0. An effort was made to assure that the FORTRAN source code was portable, and thus SAMSAN may be adaptable to other machine environments. The SAMSAN package was developed in 1982.

This program was written by Harold P. Frisch of **Goddard Space Flight Center.** *For further information, Circle X on the COSMIC Request Card.*
GSC-12827

SUBJECT INDEX

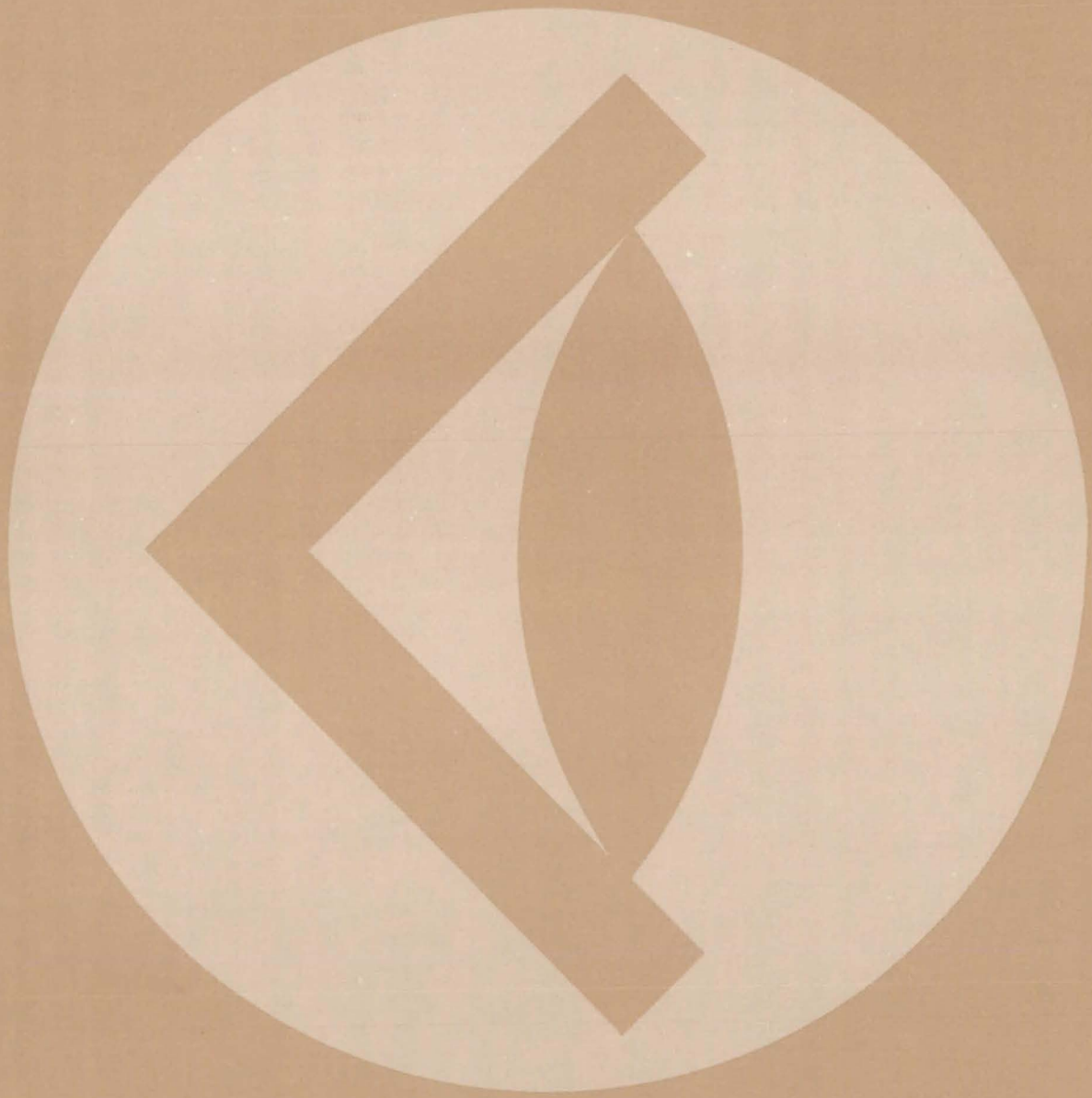

ABRASIVES
Ice as an abrading agent
page 276 MFS-19837

ACCESS CONTROL
A file archival system
page 295 NPO-16274

ACCURACY
Power-measurement errors due to instrument lag
page 176 NPO-15029

Accuracy criterion for structural calculations
page 246 NPO-16008

ACOUSTIC LEVITATION
Phase modulation stops levitated sample rotation
page 286 NPO-16002

Monitoring acoustically levitated samples
page 291 NPO-15193

Acoustic-levitation chamber
page 291 NPO-16142

ACOUSTIC MEASUREMENT
Acoustic imaging of combustion noise
page 198 NPO-15698

ACTUATORS
Low-shock pyrotechnic actuator
page 246 LAR-13198

ADDITIVES
Less-costly ion implantation of solar cells
page 280 NPO-15511

ADHESIVES
Heater ensures strain-gage bond reliability
page 240 MFS-19859

Bonded lockstitch for insulating blankets
page 271 MSC-20283

Joining tubes with adhesive
page 281 MFS-25958

ADJUSTING
Servo lead compensation
page 175 MFS-19614

AEROSOLS
Silane pyrolysis with silicon-seed aerosol
page 217 NPO-16054

AIR CONDITIONING
Air conditioning for electric vehicles
page 199 NPO-15183

AIRCRAFT NOISE
Acoustic imaging of combustion noise
page 198 NPO-15698

Predicting noise in complex aircraft structures
page 238 LAR-13032

AIRCRAFT PERFORMANCE
Takeoff and landing of transport aircraft
page 245 LAR-13086

The mission radius and maneuverability characteristics of fighter aircraft
page 245 LAR-12908

AIRFLOW
Miniature airflow sensor
page 226 LAR-13065

In situ measurement of ground-surface flow resistivity
page 229 LAR-13053

Identifying boundary-layer transitions on aircraft skin
page 232 LAR-13089

AIRLOCK MODULES
Airlock entry
page 290 NPO-15415

ALGORITHMS
Modern numerical methods for classical sampled system analysis
page 298 GSC-12827

ALIGNMENT
Visual alinement technique for infrared LIDAR
page 196 NPO-15826

Positioning vise for crystal cleavage
page 282 GSC-12762

ALLOCATIONS
Deallocating defective space on Winchester disks
page 188 KSC-11287

ALUMINA
Packed alumina absorbs hypergolic vapors
page 206 KSC-11278

AMORPHOUS MATERIALS
Containerless solidification of amorphous metals
page 207 NPO-15776

AMPLIFIERS
High-common-mode-rejection differential amplifier
page 176 MFS-25868

AMPLITUDE MODULATION
Demodulator for AM and SSB-SC signals
page 174 LAR-12716

ANECHOIC CHAMBERS
Acoustic-levitation chamber
page 291 NPO-16142

ANTENNAS
Stripline antenna beam-forming network
page 171 NPO-15743

Sideband-aided receiver arrays
page 180 NPO-15873

Detecting deformations in phased-array antennas
page 181 NPO-15390

Automatic phasing for active antenna elements
page 182 NPO-15920

ARTERIOSCLEROSIS
Speculation on ultrasonic disintegration of arterial deposits
page 222 MFS-25161

ASSEMBLING
A one-hand nut and bolt assembly tool
page 267 MFS-19691

ATTITUDE CONTROL
General maneuver program
page 244 GSC-12802

AUTOMATIC TEST EQUIPMENT
Finding open faults in CMOS circuits
page 171 NPO-15838

BAND STRUCTURE OF SOLIDS
Multiple-band-gap solar-cell concept
page 176 MFS-25724

BARRIER LAYERS
Schottky-barrier photocell with intermediate metal layer
page 169 GSC-12816

BARRIERS
Barrier seals for hydraulic actuators
page 250 MSC-20390

BATTERY SEPARATORS
In situ cross-linking of polyvinyl alcohol films
page 213 LEW-13135

BEAM INJECTION
Ion accelerator merges several beams
page 192 NPO-15547

BEAM SPLITTERS
Imaging fluid flow
page 195 MFS-25897

Laser beam separator
page 201 NPO-15723

BEARINGS
Spherical-bearing analysis program
page 265 LEW-13626

BELLOWS
Bellows with longitudinal seams
page 289 MFS-19633

BIMETALS
Burner-injector-post tip
page 268 MFS-19827

BIOMASS
Solvent extraction of furfural from biomass
page 222 NPO-15987

BONDING
Ultrasonic bonding of solar-cell leads
page 283 NPO-16140

Pressure/vacuum bonding for low-curvature mirrors
page 289 NPO-15613

BOOLEAN ALGEBRA
Self-checking memory interface
page 179 NPO-15889

BRIDGES (STRUCTURES)
Partial-payload support structure
page 249 MFS-25485

BUOYS
Safe emergency evacuation from tall structures
page 248 KSC-11225

BURNERS
Burner-injector-post tip
page 268 MFS-19827

CARBON FIBERS
Binder for carbon-fiber coating
page 214 NPO-14988

CASTING
High-temperature, low-gravity casting furnace
page 217 MFS-25605

CATALYSTS
Catalytic coal liquefaction with iron sulfate
page 216 NPO-15727

Removing sulfur dioxide from flue gases
page 217 NPO-15758

CATHODES
Improved hollow cathode
page 200 NPO-15560

CERAMIC COATINGS
Cryogenic separation of a ceramic from its mandrel
page 289 LAR-12904

CHARGE COUPLED DEVICES
Eliminating "hotspots" in digital image processing
page 185 NPO-15684

CHARRING
Charring, nonmelting epoxy foams
page 208 MFS-25911

CHEMICAL COMPOSITION
Neutron probe of building-wall composition
page 193 GSC-12808

CLEAVAGE
Positioning vise for crystal cleavage
page 282 GSC-12762

CLOCKS
Estimating flicker noise in clock signals
page 188 NPO-15525

CMOS
Finding open faults in CMOS circuits
page 171 NPO-15838

COAL
Vertical-control subsystem for automatic coal mining
page 254 MFS-25811

COAL LIQUEFACTION
Catalytic coal liquefaction with iron sulfate
page 216 NPO-15727

COATINGS
Two-layer glass thermal-control coating
page 209 ARC-11164

Conductive plasma-sprayed coatings
page 217 NPO-15927

COMBUSTION CHAMBERS
Ribbed coolant liners for combustion chambers
page 278 MFS-19829

COMMUTATION
Simplified high-power inverter
page 167 NPO-15961

COMPARATORS
Digital control of analog detector
page 175 MFS-19608

COMPOSITE MATERIALS
Microyield stress in composite materials
page 247 MFS-25709

Forming lightweight beams from composite tape
page 277 MFS-25880

Frame alines fibers in multilayer composites
page 286 MFS-25959

COMPRESSORS
Analyzing flow fields in axial-compressor rotors and stators
page 244 LEW-13910

Low-vibration oscillating compressor
page 253 GSC-12799

COMPUTER COMPONENTS
Self-checking memory interface
page 179 NPO-15889

COMPUTERIZED DESIGN
Minimizing weight of structural designs
page 242 LAR-13107

CONDUCTIVE HEAT TRANSFER
Low-thermal-resistance baseplate mounting
page 236 MFS-25908

CONSTRUCTION INDUSTRY
Waterproof raised floor makes utility lines accessible
page 228 ARC-11363

CONTAINERLESS MELTS
Containerless solidification of amorphous metals
page 207 NPO-15776

Containerless processing of advanced glasses
page 214 MFS-27002

CONTAMINANTS
Dye indicators for acidic or basic surface contamination
page 214 MFS-19387

CONTINUITY
Continuity/isolation checker
page 176 NPO-15632

CONTROL EQUIPMENT
Displaying force and torque of a manipulator
page 186 NPO-15942

CONTROL SYSTEMS
Phase modulation stops levitated sample rotation
page 286 NPO-16002

Modern numerical methods for classical sampled system analysis
page 298 GSC-12827

CONTROL UNITS (COMPUTERS)
Digital control of analog detector
page 175 MFS-19608

COOLING
Liquid-droplet radiative cooler
page 225 MFS-25890

Cooldown strategy for cryogenic wind tunnels
page 238 LAR-13012

COPPER
Electroformed electrodes for electrical-discharge machining
page 289 MFS-19651

CORRELATION FUNCTIONS
Autocovariance computer
page 237 LAR-12968

CORROSION RESISTANCE
Etchants for some corrosion-resistant metals
page 216 MFS-25467

Oxidation protection for thermocouples
page 288 NPO-15605

COVERINGS
Fitting flexible coverings to contoured surfaces
page 274 MSC-20503

CRACK FORMATION
Microfissuring in alloys during welding
page 291 MFS-25604

CRACKING (FRACTURING)
Hot microfissuring in nickel alloy
page 216 MFS-25763

Additional heat treatment for silica-fiber insulation
page 216 MSC-20600

CROSSLINKING
In situ cross-linking of polyvinyl alcohol films
page 213 LEW-13135

CRYOGENIC EQUIPMENT
Motorized cryogenic valve
page 268 ARC-11452

Cryogenic separation of a ceramic from its mandrel
page 289 LAR-12904

Continuous-reading cryogen level sensor
page 234 MFS-25873

CRYOGENIC WIND TUNNELS
Cooldown strategy for cryogenic wind tunnels
page 238 LAR-13012

CRYSTAL GROWTH
Purifying silicon during crystal growth
page 291 NPO-14831

Silicon-film growth by continuous edge-supported melt skimming
page 292 NPO-15532

CRYSTAL OSCILLATORS
Central control of local oscillator frequencies
page 187 GSC-12804

CUMULATIVE DAMAGE
Estimating lifetime of nickel/cadmium cells
page 212 NPO-15145

CURVED PANELS
Adjusting the contour of reflector panels
page 290 NPO-15319

CURVED SURFACES
Fitting flexible coverings to contoured surfaces
page 274 MSC-20503

DATA BASE MANAGEMENT SYSTEMS
SPIRE data-base management system
page 296 GSC-12684

Software document inventory program
page 297 GSC-12803

DATA MANAGEMENT
Research and development mission analysis system
page 297 GSC-12847

DATA SYSTEMS
NAMELIST preprocessor program
page 297 GSC-12711

DECELERATION
Preventing motor damage due to rapid reversal
page 267 MFS-19702

DEFORMATION
Detecting deformations in phased-array antennas
page 181 NPO-15390

DEGASSING
Packed alumina absorbs hypergolic vapors
page 206 KSC-11278

DEMODULATORS
Demodulator for AM and SSB-SC signals
page 174 LAR-12716

DEPTH MEASUREMENT
Depth gage for threaded holes
page 266 MFS-19884

DESALINIZATION
High-flow asymmetric reverse-osmosis membranes
page 221 ARC-11359

DESIGN ANALYSIS
Radiation-hardness data for semiconductor devices
page 174 NPO-15787

Optimizing grid patterns on photovoltaic cells
page 288 NPO-15841

DETECTION
Detection of floating inputs in logic circuits
page 185 LAR-13073

DEVIATION
Predicting solar deficits
page 201 NPO-15667

DIFFERENTIAL AMPLIFIERS
High-common-mode-rejection differential amplifier
page 176 MFS-25868

DIFFRACTION GRATINGS
Optical measurement of particle size and velocity
page 200 MFS-27036

Efficiency reflection gratings
page 202 NPO-15852

DIFFUSION PUMPS
Stalled-flow and head-loss model for diffuser pumps
page 266 MFS-19748

DIGITAL COMMUNICATION
Digital-image enhancement
page 187 MFS-25679

DIGITAL FILTERS
Interstitial digital-image-point generator
page 183 MFS-25871

DIGITAL TO ANALOG CONVERTERS
Digital control of analog detector
page 175 MFS-19608

DILATOMETERS
Automated mercury dilatometer
page 227 NPO-14884

DIODES
Low-noise submillimeter-wave diode
page 166 NPO-15935

DISPLAY DEVICES
Displaying force and torque of a manipulator
page 186 NPO-15942

DOCUMENT STORAGE
A file archival system
page 295 NPO-16274

Software document inventory program
page 297 GSC-12803

DYES
Dye indicators for acidic or basic surface contamination
page 214 MFS-19387

DYNAMIC STRUCTURAL ANALYSIS
Accuracy criterion for structural calculations
page 246 NPO-16008

ECCENTRICITY
Theory for eccentric and misalined annular seals
page 249 MFS-19892

ECONOMIC DEVELOPMENT
Solar-cell-manufacturing system
page 291 MFS-25483

EDDY CURRENTS
Paint-thickness checker
page 176 KSC-11270

EGRESS
Safe emergency evacuation from tall structures
page 248 KSC-11225

EJECTORS
Retention mechanism for spinning objects
page 266 MFS-25957

ELASTODYNAMICS
Mathematical instability criteria for elastic structures
page 240 NPO-15090

ELASTOHYDRODYNAMICS
Designing more-efficient spur gears
page 257 LEW-13921

ELECTRIC CONNECTORS
Shielding electric connectors from lightning
page 175 NPO-15688

Installation/removal tool for screw-mounted components
page 261 MSC-20606

ELECTRIC EQUIPMENT TESTS
Transformer and meter tester
page 267 MFS-19708

ELECTRIC MOTOR VEHICLES
Air conditioning for electric vehicles
page 199 NPO-15183

ELECTRIC MOTORS
Controlling an inverter-driven three-phase motor
page 175 MFS-25215

ELECTRIC TERMINALS
Terminal system for photovoltaic arrays
page 292 NPO-15739

ELECTRICAL FAULTS
Finding open faults in CMOS circuits
page 171 NPO-15838

ELECTRICAL RESISTIVITY
Continuity/isolation checker
page 176 NPO-15632

Making $Si_xN_yC_z$ fibers by pyrolysis
page 215 MFS-25621

ELECTRODES
Electroformed electrodes for electrical-discharge machining
page 289 MFS-19651

ELECTROLYTIC CELLS
Trace-level solid-electrolyte hygrometer
page 248 NPO-15722

ELECTRON BEAM WELDING
Controlling the focus in electron-beam welders
page 259 MFS-19814

Ribbon reduces spiking in electron-beam welding
page 279 MFS-19701

Hot forming with electron-beam welder
page 290 MSC-20413

ELECTRON BEAMS
Sampling of silicon powder for impurity analysis
page 216 NPO-15840

ELECTRONIC EQUIPMENT TESTS
Detection of floating inputs in logic circuits
page 185 LAR-13073

ELECTRONIC MODULES
Repairable encapsulated electronic modules
page 284 NPO-15079

ELECTROPLATING
Polyurethane filler for electroplating
page 277 MFS-19851

ELLIPTICAL ORBITS
Elliptical orbit performance computer program
page 245 LAR-13026

EMBOLISMS
Speculation on ultrasonic disintegration of arterial deposit
page 222 MFS-25161

ENERGY CONSUMPTION
Energy-saving inverter
page 168 NPO-15291

ENERGY CONVERSION
Instrumentation and control for fossil-energy processes
page 187 NPO-15581

ENERGY CONVERSION EFFICIENCY
Multiple-band-gap solar-cell concept
page 176 MFS-25724

Improved heat-engine solar-energy system
page 201 NPO-15762

ENERGY TECHNOLOGY
Parabolic solar collectors
page 202 NPO-15674

ENERGY TRANSFER
Long heat pipe transports 2.6 kW
page 231 NPO-16017

ENGINE CONTROL
Feedback control of rotor overspeed
page 262 ARC-11404

ENTRANCES
Airlock entry
page 290 NPO-15415

ERROR ANALYSIS
Power-measurement errors due to instrument lag
page 176 NPO-15029

ETCHANTS
Etchants for some corrosion-resistant metals
page 216 MFS-25467

ETCHING
Modified fabrication for InGaAsP stripe laser
page 285 LAR-12986

EVACUATING (TRANSPORTATION)
Safe emergency evacuation from tall structures
page 248 KSC-11225

EXPANSION
Hydraulic tube expander
page 268 MFS-19731

EXPLOSIVE DEVICES
Low-shock pyrotechnic actuator
page 246 LAR-13198

Reusable release mechanism
page 261 MSC-20080

EXTINGUISHING
Flame-test chamber
page 290 NPO-15407

EXTRUDING
Fire-resistant TFE extrusions
page 212 MFS-25917

FAILURE ANALYSIS
Hardware fault simulator generates test vectors for complex IC's
page 188 NPO-15362

FATIGUE (MATERIALS)
Repairing hidden cracks in coolant tubes
page 272 MFS-19796

FATIGUE TESTS
Portable fatigue-testing machine
page 249 MFS-19459

Fatigue testing of heat-exchanger tubes
page 249 MFS-19599

FAULT TOLERANCE
Continuity/isolation checker
page 176 NPO-15632

Self-checking memory interface
page 179 NPO-15889

FEEDBACK CONTROL
Feedback control of rotor overspeed
page 262 ARC-11404

FIBER COMPOSITES
Making $Si_xN_yC_z$ fibers by pyrolysis
page 215 MFS-25621

Fabrication of multi-ply birefringent fibrous composite laminates
page 284 LAR-12960

FIELD EFFECT TRANSISTORS
Energy-saving inverter
page 168 NPO-15291

FILLERS
Polyurethane filler for electroplating
page 277 MFS-19851

FILM THICKNESS
Paint-thickness checker
page 176 KSC-11270

FINITE ELEMENT METHOD
System for structural synthesis using EAL and CONMIN
page 242 LAR-13046

FIRE PREVENTION
Fire-resistant TFE extrusions
page 212 MFS-25917

FITTINGS
Tube alinement for machining
page 258 MFS-19719

FIXTURES
Tool support ring
page 260 MFS-19765

FLAME PROPAGATION
Flame-test chamber
page 290 NPO-15407

FLAME TEMPERATURE
Radially-graduated turbine-temperature profile
page 231 MFS-19831

FLANGES
Hot forming with electron-beam welder
page 290 MSC-20413

FLEXING
Adjusting the contour of reflector panels
page 290 NPO-15319

FLIGHT MECHANICS
General maneuver program
page 244 GSC-12802

FLIGHT SIMULATION
Mathematical simulation of flight maneuvers
page 248 NPO-15395

FLIP-FLOPS
Flip-flop digital modulator
page 172 MSC-20334

FLOORS
Waterproof raised floor makes utility lines accessible
page 228 ARC-11363

FLOW CHARACTERISTICS
Stalled-flow and head-loss model for diffuser pumps
page 266 MFS-19748

FLOW DISTRIBUTION
Autocovariance computer
page 237 LAR-12968

Analyzing flow fields in axial-compressor rotors and stators
page 244 LEW-13910

FLOW RESISTANCE
In situ measurement of ground-surface flow resistivity
page 229 LAR-13053

FLOW THEORY
Advances in multivalued-velocity theory of turbulence
page 241 NPO-16006

FLOW VISUALIZATION
Simulating a three-dimensional flow in pipes
page 247 ARC-11466

FLOWMETERS
Miniature airflow sensor
page 226 LAR-13065

FLUE GASES
Removing sulfur dioxide from flue gases
page 217 NPO-15758

FLUID FLOW
Imaging fluid flow
page 195 MFS-25897
Simulating a three-dimensional flow in pipes
page 247 ARC-11466
FOAMING
Low-density high-strength foamed materials
page 211 NPO-15411
FOAMS
Charring, nonmelting epoxy foams
page 208 MFS-25911
Repairable encapsulated electronic modules
page 284 NPO-15079
FOOD CHAIN
Yeasts with increased glycogen levels
page 222 NPO-15571
FORMING TECHNIQUES
Fitting flexible coverings to contoured surfaces
page 274 MSC-20503
FORTRAN
FORTRAN static source code analyzer
page 297 GSC-12724
NAMELIST preprocessor program
page 297 GSC-12711
FOSSIL FUELS
Instrumentation and control for fossil-energy processes
page 187 NPO-15581
FOUNDATIONS
Alining solder pads on a solar cell
page 292 NPO-15298
FRAMES
Test frame simulates zero gravity
page 247 MFS-25518
Locking corners speed solar-array frame assembly
page 279 NPO-15750
FREQUENCY CONTROL
Central control of local oscillator frequencies
page 187 GSC-12804
FREQUENCY MODULATION
Flip-flop digital modulator
page 172 MSC-20334
FUEL PRODUCTION
Destroying toxic wastes
page 215 NPO-15655
FURFURYL ALCOHOL
Solvent extraction of furfural from biomass
page 222 NPO-15987
FURNACES
High-temperature, low-gravity casting furnace
page 217 MFS-25605
Furnace for rapid heating and cooling
page 218 MFS-25707
FUSIBILITY
Automated variable polarity plasma arc welding
page 290 MFS-27042

GALLIUM ARSENIDE LASERS
Modified fabrication for InGaAsP stripe laser
page 285 LAR-12986
GAS TEMPERATURE
Measuring high gas temperatures
page 243 LEW-13819
GAS TURBINES
Radially-graduated turbine-temperature profile
page 231 MFS-19831
GEARS
Designing more-efficient spur gears
page 257 LEW-13921
GEOMETRY
Optimizing grid patterns on photovoltaic cells
page 288 NPO-15841
GLASS
Containerless processing of advanced glasses
page 214 MFS-27002
Hollow spheres of metallic glass
page 215 NPO-15991
GLASS COATINGS
Two-layer glass thermal-control coating
page 209 ARC-11164
GLASS FIBERS
Collecting light from point images
page 194 NPO-15887
GLYCOGENS
Yeasts with increased glycogen levels
page 222 NPO-15571
GRAIN BOUNDARIES
Microfissuring in alloys during welding
page 291 MFS-25604
GRAPHITE EPOXY COMPOSITES
Strain analysis of graphite/epoxy pressure vessels
page 289 MFS-27018
GRATINGS (SPECTRA)
Efficiency reflection gratings
page 202 NPO-15852
GROUND TESTS
In situ measurem nt of ground-surface flow resistivity
page 229 LAR-13053
GUIDANCE (MOTION)
Automatic guidance system for welding torches
page 273 MFS-25807
GUIDANCE SENSORS
Sun tracker operates a year between calibrations
page 197 NPO-15810

HARDENING (MATERIALS)
High-temperature, low-gravity casting furnace
page 217 MFS-25605
HEAT EXCHANGERS
Airflow assists solar receiver
page 196 NPO-15784
Improved heat-engine solar-energy system
page 201 NPO-15762
Repairing hidden cracks in coolant tubes
page 272 MFS-19796
HEAT MEASUREMENT
Temperature-averaging thermal probe
page 236 GSC-12795
HEAT PIPES
Long heat pipe transports 2.6 kW
page 231 NPO-16017
HEAT STORAGE
Saltless solar ponds
page 202 NPO-15808
HEAT TRANSMISSION
Low-thermal-resistance baseplate mounting
page 236 MFS-25908
HEAT TREATMENT
Additional heat treatment for silica-fiber insulation
page 216 MSC-20600
Heater ensures strain-gage bond reliability
page 240 MFS-19859
Securing identification sleeving
page 289 MFS-19685
HEATING
Furnace for rapid heating and cooling
page 218 MFS-25707
HEATING EQUIPMENT
Toroidal ellipsoid float-zone heater
page 288 MFS-25771
HISTOGRAMS
Digital-image enhancement
page 187 MFS-25679
HOLLOW CATHODES
Improved hollow cathode
page 200 NPO-15560
HOLOGRAPHY
Efficiency reflection gratings
page 202 NPO-15852
HOMOPOLAR GENERATORS
Brushless low-speed dc tachometer
page 249 NPO-15706
HONEYCOMB STRUCTURES
Saltless solar ponds
page 202 NPO-15808
HOT WORKING
Hot microfissuring in nickel alloy
page 216 MFS-25763
Hot forming with electron-beam welder
page 290 MSC-20413
HYDRAULIC EQUIPMENT
Hydraulic tube expander
page 268 MFS-19731
HYGROMETERS
Trace-level solid-electrolyte hygrometer
page 248 NPO-15722

ICOSAHEDRONS
General-purpose icosahedral structure
page 235 GSC-12854
IDLERS
Wire electrical-discharge machining aid
page 268 MFS-19643
IMAGE ENHANCEMENT
Interstitial digital-image-point generator
page 183 MFS-25871
Digital-image enhancement
page 187 MFS-25679
IMAGE PROCESSING
Eliminating "hotspots" in digital image processing
page 185 NPO-15684
Collecting light from point images
page 194 NPO-15887
IMAGE RESOLUTION
Interstitial digital-image-point generator
page 183 MFS-25871
Improved gamma- and X-ray pinhole camera
page 191 GSC-12851
High-resolution X-ray telescope
page 200 NPO-15971
IMAGING TECHNIQUES
Acoustic imaging of combustion noise
page 198 NPO-15698
Lensless image scanner
page 200 NPO-16004
IMPURITIES
Sampling of silicon powder for impurity analysis
page 216 NPO 15840
INELASTIC STRESS
Mathematical instability criteria for elastic structures
page 240 NPO-15090
INFRARED SCANNERS
Improved infrared multispectral scanner
page 200 NPO-16143
INPUT/OUTPUT ROUTINES
NAMELIST preprocessor program
page 297 GSC-12711
INSERTS
Feedthrough seal for high-pressure vessel
page 170 MSC-20625
Burner-injector-post tip
page 268 MFS-19827
INSPECTION
Inspecting joints with grooved surfaces
page 247 MFS-25934
INSTRUMENT COMPENSATION
Sun tracker operates a year between calibrations
page 197 NPO-15810

INSTRUMENT ERRORS
Power-measurement errors due to instrument lag
page 176 NPO-15029

INSTRUMENTAL ANALYSIS
Automated mercury dilatometer
page 227 NPO-14884

INSULATION
Plasma-sprayed copper tie-in for nic el plating
page 215 MFS-19481

Bonded lockstitch for insulating blankets
page 271 MSC-20283

INTEGRAL TRANSFORMATIONS
Pseudo-random-number generators
page 296 MFS-27017

INTEGRATED CIRCUITS
Infrared-responsive monolithic MOS circuit
page 165 GSC-12782

Optical testing of integrated circuits
page 174 MFS-25498

Miniature temperature-control circuit
page 175 LAR-12900

Hardware fault simulator generates test vectors for complex IC's
page 188 NPO-15362

Processes for VLSI circuits
page 287 MFS-25857

INTEGRATORS
Servo lead compensation
page 175 MFS-19614

INTEGRITY
Deallocating defective space on Winchester disks
page 188 KSC-11287

INTERFEROMETRY
Microyield stress in composite materials
page 247 MFS-25709

INTERGRANULAR CORROSION
Etchants for some corrosion-resistant metals
page 216 MFS-25467

INTERLOCKING
Locking corners speed solar-array frame assembly
page 279 NPO-15750

INVENTORY MANAGEMENT
Software document inventory program
page 297 GSC-12803

INVERTERS
Simplified high-power inverter
page 167 NPO-15961

Energy-saving inverter
page 168 NPO-15291

Controlling an inverter-driven three-phase motor
page 175 MFS-25215

ION ENGINES
Ion engine with solid-electrolyte ion generator
page 199 NPO-15809

ION IMPLANTATION
Ion accelerator merges several beams
page 192 NPO-15547

Less-costly ion implantation of solar cells
page 280 NPO-15511

ION SOURCES
Improved hollow cathode
page 200 NPO-15560

IRISES (MECHANICAL APERTURES)
Controlling TV-camera f-stop remotely
page 200 KSC-11269

ISOLATORS
Predicting noise in complex aircraft structures
page 238 LAR-13032

JOINTS (JUNCTIONS)
Inspecting joints with grooved surfaces
page 247 MFS-25934

Joining tubes with adhesive
page 281 MFS-25958

Welding tubes in place
page 290 MFS-25714

LABELING (MARKING)
Securing identification sleeving
page 289 MFS-19685

LAMINATES
Fabrication of multi-ply birefringent fibrous composite laminates
page 284 LAR-12960

LARGE SCALE INTEGRATION
Integrated tactile sensor for robots
page 233 NPO-15094

Processes for VLSI circuits
page 287 MFS-25857

LASERS
Visual alinement technique for infrared LIDAR
page 196 NPO-15826

Optical measurement of particle size and velocity
page 200 MFS-27036

Measuring delay in lasers
page 201 NPO-15242

Laser beam separator
page 201 NPO-15723

Autocovariance computer
page 237 LAR-12968

IC fabrication methods improve laser diodes
page 275 LAR-13059

Modified fabrication for InGaAsP stripe laser
page 285 LAR-12986

LATTICE VIBRATIONS
Analyzing vibrations in a long mast
page 247 MFS-25746

LAUNCH WINDOWS
Launch-window program
page 244 GSC-12801

LAY-UP
Frame alines fibers in multilayer composites
page 286 MFS-25959

LEAKAGE
Theory for eccentric and misalined annular seals
page 249 MFS-19892

LIFETIME (DURABILITY)
Estimating lifetime of nickel/cadmium cells
page 212 NPO-15145

LIGHT AMPLIFIERS
Concentrator-enhanced solar array
page 202 NPO-15628

LIGHT SCATTERING
Submicron-particle generator
page 248 LAR-12785

LINE SPECTRA
Catalog of spectral lines
page 201 NPO-15181

LININGS
Ribbed coolant liners for combustion chambers
page 278 MFS-19829

LIQUEFACTION
Catalytic coal liquefaction with iron sulfate
page 216 NPO-15727

LIQUID COOLING
Furnace for rapid heating and cooling
page 218 MFS-25707

Liquid-droplet radiative cooler
page 225 MFS-25890

LIQUID LEVELS
Continuous-reading cryogen level sensor
page 234 MFS-25873

LIQUID NITROGEN
Cooldown strategy for cryogenic wind tunnels
page 238 LAR-13012

LIQUID OXYGEN
Thermal and flow data from liquid-oxygen system
page 246 KSC-11265

LOADS (FORCES)
Improvements in vibration-analysis technique
page 241 MFS-25919

LOGIC CIRCUITS
Detection of floating inputs in logic circuits
page 185 LAR-13073

LOW DENSITY MATERIALS
Low-density high-strength foamed materials
page 211 NPO-15411

LOW NOISE
Low-noise submillimeter-wave diode
page 166 NPO-15935

MACHINE TOOLS
Tube alinement for machining
page 258 MFS-19719

Transformer and meter tester
page 267 MFS-19708

Attaching chuck keys to machine tools
page 268 KSC-11249

MAGNETIC PERMEABILITY
Automated magnetic-susceptibility analysis
page 217 MFS-25935

MANAGEMENT SYSTEMS
A file archival system
page 295 NPO-16274

MANEUVERABILITY
The mission radius and maneuverability characteristics of fighter aircraft
page 245 LAR-12908

MANEUVERS
Mathematical simulation of flight maneuvers
page 248 NPO-15395

MANIPULATORS
Displaying force and torque of a manipulator
page 186 NPO-15942

MATERIAL REMOVAL (MACHINING)
Tube alinement for machining
page 258 MFS-19719

MATERIALS HANDLING
Thermal and flow data from liquid-oxygen system
page 246 KSC-11265

MATERIALS RECOVERY
Recovering zinc from discarded tires
page 205 NPO-16046

Cryogenic separation of a ceramic from its mandrel
page 289 LAR-12904

MEASURING INSTRUMENTS
Automated magnetic-susceptibility analysis
page 217 MFS-25935

MECHANICAL DEVICES
Miniature rotator
page 267 LAR-12765

Alining solder pads on a solar cell
page 292 NPO-15298

MECHANICAL MEASUREMENT
Depth gage for threaded holes
page 266 MFS-19884

MEMBRANE STRUCTURES
High-flow asymmetric reverse-osmosis membranes
page 221 ARC-11359

METAL COATINGS
Binder for carbon-fiber coating
page 214 NPO-14988

Oxidation protection for thermocouples
page 288 NPO-15605

METAL CUTTING
Wire electrical-discharge machining aid
page 268 MFS-19643

METAL FOAMS
Low-density high-strength foamed materials
page 211 NPO-15411

METAL FORMING
Containerless solidification of amorphous metals
page 207 NPO-15776

METAL OXIDE SEMICONDUCTORS
Infrared-responsive monolithic MOS circuit
page 165 GSC-12782

METAL SHELLS
Shielding electric connectors from lightning
page 175 NPO-15688

METALLIC GLASSES
Hollow spheres of metallic glass
page 215 NPO-15991

METALS
Memory-metal electromechanical actuators
page 256 NPO-15960

MICROPARTICLES
Submicron-particle generator
page 248 LAR-12785

MICROSTRIP TRANSMISSION LINES
Stripline antenna beam-forming network
page 171 NPO-15743

MICROWAVE RADIOMETERS
Determining the nonlinearity of microwave receivers
page 188 NPO-15355

MICROWAVE SWITCHING
Automatic phasing for active antenna elements
page 182 NPO-15920

MICROYIELD STRENGTH
Microyield stress in composite materials
page 247 MFS-25709

MINERAL EXPLORATION
Unmanned instrument platform for undersea exploration
page 184 NPO-15878

MINIATURE ELECTRONIC EQUIPMENT
Miniature temperature-control circuit
page 175 LAR-12900

Miniature airflow sensor
page 226 LAR-13065

MINING
Display for mining-machine operators
page 188 MFS-25955

MIRRORS
Concentrator-enhanced solar array
page 202 NPO-15628

Pressure/vacuum bonding for low-curvature mirrors
page 289 NPO-15613

MISSION PLANNING
Launch-window program
page 244 GSC-12801

The mission radius and maneuverability characteristics of fighter aircraft
page 245 LAR-12908

Research and development mission analysis system
page 297 GSC-12847

MIXING
Continuous monitoring of melt composition
page 210 NPO-15896

MODULATORS
Flip-flop digital modulator
page 172 MSC-20334

MOLECULAR BEAM EPITAXY
IC fabrication methods improve laser diodes
page 275 LAR-13059

MONITORS
Status panel for video cassette recorders
page 187 KSC-11254

MONTE CARLO METHOD
Pseudo-random-number generators
page 296 MFS-27017

MOUNTING
Low-thermal-resistance baseplate mounting
page 236 MFS-25908

Internally mounting strain gages
page 239 GSC-12824

Installation/removal tool for screw-mounted components
page 261 MSC-20606

MULTISPECTRAL BAND SCANNERS
Improved infrared multispectral scanner
page 200 NPO-16143

NEUTRON ACTIVATION ANALYSIS
Neutron probe of building-wall composition
page 193 GSC-12808

NICKEL ALLOYS
Hot microfissuring in nickel alloy
page 216 MFS-25763

NICKEL CADMIUM BATTERIES
Estimating lifetime of nickel/cadmium cells
page 212 NPO-15145

NICKEL PLATE
Plasma-sprayed copper tie-in for nickel plating
page 215 MFS-19481

NIOBIUM ALLOYS
X-ray-diffraction analysis of Nb/Ge alloys
page 217 MFS-27038

NOISE PREDICTION
Estimating flicker noise in clock signals
page 188 NPO-15525

NOISE REDUCTION
Predicting noise in complex aircraft structures
page 238 LAR-13032

Takeoff and landing of transport aircraft
page 245 LAR-13086

NONDESTRUCTIVE TESTS
Optical testing of integrated circuits
page 174 MFS-25498

Paint-thickness checker
page 176 KSC-11270

NONLINEARITY
Determining the nonlinearity of microwave receivers
page 188 NPO-15355

NOZZLE DESIGN
Supersonic-nozzle shock-wave analysis
page 250 MFS-19753

Nonseparating high-area-ratio supersonic nozzles
page 250 MFS-19758

O RING SEALS
Barrier seals for hydraulic actuators
page 250 MSC-20390

Double-poppet valve
page 263 MSC-20627

OIL RECOVERY
Transportable pumps could save oil cargoes
page 255 MFS-25881

OPERATIONS RESEARCH
Thermal and flow data from liquid-oxygen system
page 246 KSC-11265

OPTICAL COMMUNICATION
Efficient coding for optical communication
page 295 NPO-15856

OPTICAL EQUIPMENT
Laser beam separator
page 201 NPO-15723

OPTICAL MEASURING INSTRUMENTS
Optical turbopump speed sensor
page 249 MFS-19794

OPTICAL PROPERTIES
Containerless processing of advanced glasses
page 214 MFS-27002

OPTICAL RADAR
Visual alinement technique for infrared LIDAR
page 196 NPO-15826

OPTICAL SCANNERS
Optical testing of integrated circuits
page 174 MFS-25498

OPTIMIZATION
System for structural synthesis using EAL and CONMIN
page 242 LAR-13046

ORBITS
Elliptical orbit performance computer program
page 245 LAR-13026

OXIDATION RESISTANCE
Oxidation-resistant slurry coating for carbon-based materials
page 208 LEW-13951

PANELS
General-purpose icosahedral structure
page 235 GSC-12854

PARABOLIC REFLECTORS
Parabolic solar collectors
page 202 NPO-15674

PARTICLE PRODUCTION
Submicron-particle generator
page 248 LAR-12785

PARTICLE SIZE DISTRIBUTION
Optical measurement of particle size and velocity
page 200 MFS-27036

PELLETS
Ice as an abrading agent
page 276 MFS-19837

PERFORMANCE PREDICTION
Modeling of solar concentrators
page 201 NPO-15034

PH
Dye indicators for acidic or basic surface contamination
page 214 MFS-19387

PHASE CONTROL
Automatic phasing for active antenna elements
page 182 NPO-15920

PHASE MODULATION
Phase modulation stops levitated sample rotation
page 286 NPO-16002

PHASED ARRAYS
Detecting deformations in phased-array antennas
page 181 NPO-15390

PHOTOCONDUCTORS
Infrared-responsive monolithic MOS circuit
page 165 GSC-12782

PHOTOELECTRIC CELLS
Schottky-barrier photocell with intermediate metal layer
page 169 GSC-12816

Automated assembly of solar panels
page 291 NPO-16206

PHOTOLITHOGRAPHY
IC fabrication methods improve laser diodes
page 275 LAR-13059

PHOTOMASKS
Processes for VLSI circuits
page 287 MFS-25857

PHOTOVOLTAIC CELLS
Modeling of solar concentrators
page 201 NPO-15034

Optimizing grid patterns on photovoltaic cells
page 288 NPO-15841

Terminal system for photovoltaic arrays
page 292 NPO-15739

PIERCING
Portable power broach
page 267 MFS-19679

PIEZOELECTRIC CRYSTALS
Portable fatigue-testing machine
page 249 MFS-19459

PINHOLE CAMERAS
Improved gamma- and X-ray pinhole camera
page 191 GSC-12851

PLANETARY MAPPING
High-resolution X-ray telescope
page 200 NPO-15971

PLASMA ARC WELDING
Automated variable polarity plasma arc welding
page 290 MFS-27042

PLASMA PROPULSION
Plasma-sprayed copper tie-in for nickel plating
page 215 MFS-19481

PLASMA SPRAYING
Conductive plasma-sprayed coatings
page 217 NPO-15927

PLUGS
Terminal system for photovoltaic arrays
page 292 NPO-15739

POINTING CONTROL SYSTEMS
Tracking visible targets automatically
page 247 NPO-15226

POISONS
Destroying toxic wastes
page 215 NPO-15655

POLYACRYLATES
Binder for carbon-fiber coating
page 214 NPO-14988

POLYMERIC FILMS
Airlock entry
page 290 NPO-15415

POLYTETRAFLUOROETHYLENE
Fire-resistant TFE extrusions
page 212 MFS-25917

POLYURETHANE FOAM
Polyurethane filler for electroplating
page 277 MFS-19851

POLYVINYL ALCOHOL
In situ cross-linking of polyvinyl alcohol films
page 213 LEW-13135

PORTABLE EQUIPMENT
Portable fatigue-testing machine
page 249 MFS-19459

Transportable pumps could save oil cargoes
page 255 MFS-25881

Portable power broach
page 267 MFS-19679

POSITION INDICATORS
Display for mining-machine operators
page 188 MFS-25955

POSITIONING
Tool support ring
page 260 MFS-19765

Miniature rotator
page 267 LAR-12765

Frame alines fibers in multilayer composites
page 286 MFS-25959

Positioning vise for crystal cleavage
page 282 GSC-12762

POTTING COMPOUNDS
Repairable encapsulated electronic modules
page 284 NPO-15079

PREBURNERS
Ribbed coolant liners for combustion chambers
page 278 MFS-19829

PRESSURE DISTRIBUTION
Internally mounting strain gages
page 239 GSC-12824

PRESSURE EFFECTS
Pressure-driven waterflow cleaning device
page 267 MFS-19638

PRESSURE SENSORS
Continuous-reading cryogen level sensor
page 234 MFS-25873

PRESSURE SUITS
Leak test for pressure-sealing zippers
page 250 KSC-11247

PRESSURE VESSELS
Feedthrough seal for high-pressure vessel
page 170 MSC-20625

Strain analysis of graphite/epoxy pressure vessels
page 289 MFS-27018

PROCESS CONTROL (INDUSTRY)
Toroidal ellipsoid float-zone heater
page 288 MFS-25771

PRODUCTION MANAGEMENT
Continuous monitoring of melt composition
page 210 NPO-15896

PROGRAMMING LANGUAGES
SPIRE data-base management system
page 296 GSC-12684

PROPULSION SYSTEM PERFORMANCE
Elliptical orbit performance computer program
page 245 LAR-13026

PSEUDORANDOM SEQUENCES
Pseudo-random-number generators
page 296 MFS-27017

PULSE POSITION MODULATION
Efficient coding for optical communication
page 295 NPO-15856

PUMPS
Transportable pumps could save oil cargoes
page 255 MFS-25881

PURIFICATION
Purifying silicon during crystal growth
page 291 NPO-14831

PYROLYSIS
Making $Si_xN_yC_z$ fibers by pyrolysis
page 215 MFS-25621

Silane pyrolysis with silicon-seed aerosol
page 217 NPO-16054

PYROTECHNICS
Low-shock pyrotechnic actuator
page 246 LAR-13198

QUALITY CONTROL
Hardware fault simulator generates test vectors for complex IC's
page 188 NPO-15362

RADIATION EFFECTS
Measuring high gas temperatures
page 243 LEW-13819

RADIATION LAWS
Thermal radiation analyzer system
page 243 GSC-12783

RADIATION TOLERANCE
Radiation-hardness data for semiconductor devices
page 174 NPO-15787

RADIO ASTRONOMY
Catalog of spectral lines
page 201 NPO-15181

RADIO FREQUENCY HEATING
Forming lightweight beams from composite tape
page 277 MFS-25880

RADIO RECEIVERS
Sideband-aided receiver arrays
page 180 NPO-15873

RADIO TRANSMITTERS
Remotely-operated traffic control light
page 175 ARC-11406

RADIOGRAPHY
Neutron probe of building-wall composition
page 193 GSC-12808

RC NETWORKS
Thermal radiation analyzer system
page 243 GSC-12783

REACTION TIME
Preventing motor damage due to rapid reversal
page 267 MFS-19702

RECEIVERS
Determining the nonlinearity of microwave receivers
page 188 NPO-15355

RECEPTION DIVERSITY
Sideband-aided receiver arrays
page 180 NPO-15873

RECORDING INSTRUMENTS
Status panel for video cassette recorders
page 187 KSC-11254

REFLECTORS
Adjusting the contour of reflector panels
page 290 NPO-15319

REFRIGERATORS
Motorized cryogenic valve
page 268 ARC-11452

RELEASING
Reusable release mechanism
page 261 MSC-20080

Retention mechanism for spinning objects
page 266 MFS-25957

RELIABILITY ANALYSIS
Screening plastic-encapsulated solid-state devices
page 173 MFS-25802

RELIEF VALVES
Belleville spring/seal
page 250 MFS-19596

REPORT GENERATORS
Launch-window program
page 244 GSC-12801

RESEARCH AND DEVELOPMENT
Research and development mission analysis system
page 297 GSC-12847

RETROFITTING
Retrofitting vibration dampers
page 268 MFS-19790

REUSE
Reusable release mechanism
page 261 MSC-20080

REVERSE OSMOSIS
High-flow asymmetric reverse-osmosis membranes
page 221 ARC-11359

RIBBONS
Solar-cell-manufacturing system
page 291 MFS-25483

RING STRUCTURES
Tool support ring
page 260 MFS-19765

ROBOTS
Integrated tactile sensor for robots
page 233 NPO-15094

Automated assembly of solar panels
page 291 NPO-16206

ROLLER BEARINGS
Spherical-bearing analysis program
page 265 LEW-13626

ROTATING BODIES
Free-vibration analysis of structures
page 243 NPO-15797

Retention mechanism for spinning objects
page 266 MFS-25957

ROTATING VEHICLES
Miniature rotator
page 267 LAR-12765

ROTOR SPEED
Feedback control of rotor overspeed
page 262 ARC-11404

SAFETY DEVICES
Triple-seal valve
page 265 MSC-20628

Attaching chuck keys to machine tools
page 268 KSC-11249

SAMPLED DATA SYSTEMS
Modern numerical methods for classical sampled system analysis
page 298 GSC-12827

SAMPLES
Controlling the focus in electron-beam welders
page 259 MFS-19814

SCANNERS
Improved infrared multispectral scanner
page 200 NPO-16143

Lensless image scanner
page 200 NPO-16004

SCHLIEREN PHOTOGRAPHY
Imaging fluid flow
page 195 MFS-25897

SCHOTTKY DIODES
Schottky-barrier photocell with intermediate metal layer
page 169 GSC-12816

SEALING
Double-poppet valve
page 263 MSC-20627

Triple-seal valve
page 265 MSC-20628

SEALS (STOPPERS)
Feedthrough seal for high-pressure vessel
page 170 MSC-20625

Theory for eccentric and misalined annular seals
page 249 MFS-19892

Bellville spring/seal
page 250 MFS-19596

Barrier seals for hydraulic actuators
page 250 MSC-20390

SEAMS (JOINTS)
Bellows with longitudinal seams
page 289 MFS-19633

SEMICONDUCTOR DEVICES
Screening plastic-encapsulated solid-state devices
page 173 MFS-25802

Radiation-hardness data for semiconductor devices
page 174 NPO-15787

SEPARATED FLOW
Nonseparating high-area-ratio supersonic nozzles
page 250 MFS-19758

SERVICE LIFE
Transformer and meter tester
page 267 MFS-19708

SERVOCONTROL
Servo lead compensation
page 175 MFS-19614

SEWING
Bonded lockstitch for insulating blankets
page 271 MSC-20283

SHEARING
Display for mining-machine operators
page 188 MFS-25955

Vertical-control subsystem for automatic coal mining
page 254 MFS-25811

SHIELDING
Shielding electric connectors from lightning
page 175 NPO-15688

SHOCKWAVE PROPAGATION
Supersonic-nozzle shock-wave analysis
page 250 MFS-19753

SIGNAL DISTORTION
Estimating flicker noise in clock signals
page 188 NPO-15525

SIGNAL ENCODING
Efficient coding for optical communication
page 295 NPO-15856

SIGNAL TO NOISE RATIOS
High-common-mode-rejection differential amplifier
page 176 MFS-25868

SILICON
Sampling of silicon powder for impurity analysis
page 216 NPO-15840

Silane pyrolysis with silicon-seed aerosol
page 217 NPO-16054

Purifying silicon during crystal growth
page 291 NPO-14831

Silicon-film growth by continuous edge-supported melt skimming
page 292 NPO-15532

SINGLE SIDEBAND TRANSMISSION
Demodulator for AM and SSB-SC signals
page 174 LAR-12716

SLEEVES
Securing identification sleeving
page 289 MFS-19685

SLIDING
Designing more-efficient spur gears
page 257 LEW-13921

SLURRIES
Oxidation-resistant slurry coating for carbon-based materials
page 208 LEW-13951

SOLAR ARRAYS
Concentrator-enhanced solar array
page 202 NPO-15628

Locking corners speed solar-array frame assembly
page 279 NPO-15750

Automated assembly of solar panels
page 291 NPO-16206

SOLAR CELLS
Multiple-band-gap solar-cell concept
page 176 MFS-25724

Modeling of solar concentrators
page 201 NPO-15034

Less-costly ion implantation of solar cells
page 280 NPO-15511

Ultrasonic bonding of solar-cell leads
page 283 NPO-16140

Solar-cell-manufacturing system
page 291 MFS-25483

Alining solder pads on a solar cell
page 292 NPO-15298

SOLAR COLLECTORS
Predicting solar deficits
page 201 NPO-15667

Parabolic solar collectors
page 202 NPO-15674

Pressure/vacuum bonding for low-curvature mirrors
page 289 NPO-15613

SOLAR ENERGY
Improved heat-engine solar-energy system
page 201 NPO-15762

SOLAR HEATING
Airflow assists solar receiver
page 196 NPO-15784

Air conditioning for electric vehicles
page 199 NPO-15183

Saltless solar ponds
page 202 NPO-15808

SOLAR RADIATION
Predicting solar deficits
page 201 NPO-15667

SOLAR REFLECTORS
High-temperature helical-tube solar receiver
page 202 NPO-15768

SOLID ELECTROLYTES
Ion engine with solid-electrolyte ion generator
page 199 NPO-15809

SOLID STATE DEVICES
Screening plastic-encapsulated solid-state devices
page 173 MFS-25802

SOLVENT EXTRACTION
Recovering zinc from discarded tires
page 205 NPO-16046

Solvent extraction of furfural from biomass
page 222 NPO-15987

SONAR
Unmanned instrument platform for undersea exploration
page 184 NPO-15878

SOURCE PROGRAMS
FORTRAN static source code analyzer
page 297 GSC-12724

SPARK MACHINING
Wire electrical-discharge machining aid
page 268 MFS-19643

Electroformed electrodes for electrical-discharge machining
page 289 MFS-19651

SPECTROSCOPY
Collecting light from point images
page 194 NPO-15887

Continuous monitoring of melt composition
page 210 NPO-15896

SPEED CONTROL
Controlling an inverter-driven three-phase motor
page 175 MFS-25215

SPEED INDICATORS
Optical turbopump speed sensor
page 249 MFS-19794

Brushless low-speed dc tachometer
page 249 NPO-15706

SPHERICAL SHELLS
Hollow spheres of metallic glass
page 215 NPO-15991

SPIKING
Ribbon reduces spiking in electron-beam welding
page 279 MFS-19701

SPRAYED COATINGS
Oxidation-resistant slurry coating for carbon-based materials
page 208 LEW-13951

Conductive plasma-sprayed coatings
page 217 NPO-15927

STANDARDS
Catalog of spectral lines
page 201 NPO-15181

STAR TRACKERS
Sun tracker operates a year between calibrations
page 197 NPO-15810

STATISTICAL ANALYSIS
FORTRAN static source code analyzer
page 297 GSC-12724

STIFFNESS
Analyzing vibrations in a long mast
page 247 MFS-25746

STIRLING CYCLE
Low-vibration oscillating compressor
page 253 GSC-12799

STRAIN GAGES
Internally mounting strain gages
page 239 GSC-12824

Heater ensures strain-gage bond reliability
page 240 MFS-19859

STRESS ANALYSIS
Strain analysis of graphite/epoxy pressure vessels
page 289 MFS-27018

STRIP TRANSMISSION LINES
Stripline antenna beam-forming network
page 171 NPO-15743

STRUCTURAL ANALYSIS
Mathematical instability criteria for elastic structures
page 240 NPO-15090

System for structural synthesis using EAL and CONMIN
page 242 LAR-13046

Free-vibration analysis of structures
page 243 NPO-15797

STRUCTURAL ENGINEERING
General-purpose icosahedral structure
page 235 GSC-12854

STRUCTURAL MEMBERS
Joining tubes with adhesive
page 281 MFS-25958

STRUCTURAL STRAIN
Retrofitting vibration dampers
page 268 MFS-19790

STRUCTURAL VIBRATION
Accuracy criterion for structural calculations
page 246 NPO-16008

STRUCTURE DESIGN
Minimizing weight of structural designs
page 242 LAR-13107

SUBLIMATION
Identifying boundary-layer transitions on aircraft skin
page 232 LAR-13089

SUBMILLIMETER WAVES
Low-noise submillimeter-wave diode
page 166 NPO-15935

SULFUR DIOXIDES
Removing sulfur dioxide from flue gases
page 217 NPO-15758

SUPERCONDUCTIVITY
X-ray-diffraction analysis of Nb/Ge alloys
page 217 MFS-27038

SUPERSONIC FLOW
Supersonic-nozzle shock-wave analysis
page 250 MFS-19753

SUPERSONIC NOZZLES
Nonseparating high-area-ratio supersonic nozzles
page 250 MFS-19758

SUPPORTS
Partial-payload support structure
page 249 MFS-25485

SURFACE DEFECTS
Deallocating defective space on Winchester disks
page 188 KSC-11287

SURFACE TREATMENT
Repairing thermal tiles
page 288 MSC-20336

SWITCHES
Preventing motor damage due to rapid reversal
page 267 MFS-19702

TACHOMETERS
Brushless low-speed dc tachometer
page 249 NPO-15706

TACTILE DISCRIMINATION
Integrated tactile sensor for robots
page 233 NPO-15094

TECHNOLOGY ASSESSMENT
Instrumentation and control for fossil-energy processes
page 187 NPO-15581

TELESCOPES
Eliminating "hotspots" in digital image processing
page 185 NPO-15684

TELEVISION CAMERAS
Controlling TV-camera f-stop remotely
page 200 KSC-11269

TEMPERATURE CONTROL
Miniature temperature-control circuit
page 175 LAR-12900

Airflow assists solar receiver
page 196 NPO-15784

Liquid-droplet radiative cooler
page 225 MFS-25890

TEMPERATURE DEPENDENCE
Automated magnetic-susceptibility analysis
page 217 MFS-25935

TEMPERATURE DISTRIBUTION
Radially-graduated turbine-temperature profile
page 231 MFS-19831

TEMPERATURE PROBES
Temperature-averaging thermal probe
page 236 GSC-12795

TEST CHAMBERS
Flame-test chamber
page 290 NPO-15407

TEST STANDS
Test frame simulates zero gravity
page 247 MFS-25518

Partial-payload support structure
page 249 MFS-25485

THERMAL CONTROL COATINGS
Two-layer glass thermal-control coating
page 209 ARC-11164

THERMAL ENERGY
Long heat pipe transports 2.6 kW
page 231 NPO-16017

THERMAL INSULATION
Additional heat treatment for silica-fiber insulation
page 216 MSC-20600

Repairing thermal tiles
page 288 MSC-20336

THERMAL MAPPING
Temperature-averaging thermal probe
page 236 GSC-12795

THERMAL RADIATION
Thermal radiation analyzer system
page 243 GSC-12783

THERMAL STRESSES
Fatigue testing of heat-exchanger tubes
page 249 MFS-19599

THERMOCOUPLES
Measuring high gas temperatures
page 243 LEW-13819

Oxidation protection for thermocouples
page 288 NPO-15605

THERMOMECHANICS
Spherical-bearing analysis program
page 265 LEW-13626

THREE DIMENSIONAL FLOW
Analyzing flow fields in axial-compressor rotors and stators
page 244 LEW-13910

Simulating a three-dimensional flow in pipes
page 247 ARC-11466

THRUST CONTROL
Mathematical simulation of flight maneuvers
page 248 NPO-15395

THYRISTORS
Simplified high-power inverter
page 167 NPO-15961

TILES
Repairing thermal tiles
page 288 MSC-20336

TIME LAG
Measuring delay in lasers
page 201 NPO-15242

TIRES
Recovering zinc from discarded tires
page 205 NPO-16046

TOKAMAK DEVICES
Ion accelerator merges several beams
page 192 NPO-15547

TOOLS
Inspecting joints with grooved surfaces
page 247 MFS-25934

Installation/removal tool for screw-mounted components
page 261 MSC-20606

Depth gage for threaded holes
page 266 MFS-19884

Portable power broach
page 267 MFS-19679

A one-hand nut and bolt assembly tool
page 267 MFS-19691

Hydraulic tube expander
page 268 MFS-19731

Attaching chuck keys to machine tools
page 268 KSC-11249

TORCHES
Automatic guidance system for welding torches
page 273 MFS-25807

TRACKING (POSITION)
Tracking visible targets automatically
page 247 NPO-15226

Vertical-control subsystem for automatic coal mining
page 254 MFS-25811

TRAFFIC CONTROL
Remotely-operated traffic control light
page 175 ARC-11406

TRANSMITTERS
Central control of local oscillator frequencies
page 187 GSC-12804

TRANSPORT AIRCRAFT
Takeoff and landing of transport aircraft
page 245 LAR-13086

TRUSSES
Forming lightweight beams from composite tape
page 277 MFS-25880

TUBE HEAT EXCHANGERS
High-temperature helical-tube solar receiver
page 202 NPO-15768

Fatigue testing of heat-exchanger tubes
page 249 MFS-19599

TUBES
Repairing hidden cracks in coolant tubes
page 272 MFS-19796

TURBINE PUMPS
Optical turbopump speed sensor
page 249 MFS-19794

TURBULANT BOUNDARY LAYER
Identifying boundary-layer transitions on aircraft skin
page 232 LAR-13089

TURBULENCE
Advances in multivalued-velocity theory of turbulence
page 241 NPO-16006

TWO DIMENSIONAL FLOW
Stalled-flow and head-loss model for diffuser pumps
page 266 MFS-19748

ULTRASONIC WELDING
Ultrasonic bonding of solar-cell leads
page 283 NPO-16140

ULTRASONICS
Speculation on ultrasonic disintegration of arterial deposits
page 222 MFS-25161

UNDERWATER TESTS
Unmanned instrument platform for undersea exploration
page 184 NPO-15878

VACUUM TESTS
Leak test for pressure-sealing zippers
page 250 KSC-11247

VALVES
Double-poppet valve
page 263 MSC-20627

Triple-seal valve
page 265 MSC-20628

Motorized cryogenic valve
page 268 ARC-11452

VANADIUM COMPOUNDS
Charring, nonmelting epoxy foams
page 208 MFS-25911

VAPOR TRAPS
Packed alumina absorbs hypergolic vapors
page 206 KSC-11278

VELOCITY DISTRIBUTION
Advances in multivalued-velocity theory of turbulence
page 241 NPO-16006

VIBRATION
Improvements in vibration-analysis technique
page 241 MFS-25919

Free-vibration analysis of structures
page 243 NPO-15797

VIBRATION DAMPING
Low-vibration oscillating compressor
page 253 GSC-12799

VIBRATION ISOLATORS
Retrofitting vibration dampers
page 268 MFS-19790

VIBRATION MODE
Analyzing vibrations in a long mast
page 247 MFS-25746

VIDEO EQUIPMENT
Status panel for video cassette recorders
page 187 KSC-11254

VIEWING
Monitoring acoustically levitated samples
page 291 NPO-15193

VISUAL CONTROL
Controlling TV-camera f-stop remotely
page 200 KSC-11269

VISUAL PERCEPTION
Tracking visible targets automatically
page 247 NPO-15226

VOLUMETRIC ANALYSIS
Automated mercury dilatometer
page 227 NPO-14884

WARNING SYSTEMS
Remotely-operated traffic control light
page 175 ARC-11406

WASHERS (SPACERS)
Belleville spring/seal
page 250 MFS-19596

WASHING
Pressure-driven waterflow cleaning device
page 267 MFS-19638

WASTE DISPOSAL
Destroying toxic wastes
page 215 NPO-15655

WATER FLOW
Pressure-driven waterflow cleaning device
page 267 MFS-19638

WATER VAPOR
Trace-level solid-electrolyte hygrometer
page 248 NPO-15722

WATERPROOFING
Waterproof raised floor makes utility lines accessible
page 228 ARC-11363

WEBS (SUPPORTS)
Silicon-film growth by continuous edge-supported melt skimming
page 292 NPO-15532

WEIGHT REDUCTION
Minimizing weight of structural designs
page 242 LAR-13107

WEIGHTLESSNESS SIMULATION
Test frame simulates zero gravity
page 247 MFS-25518

WELDED JOINTS
Welding tubes in place
page 290 MFS-25714

WELDING
Controlling the focus in electron-beam welders
page 259 MFS-19814

Automatic guidance system for welding torches
page 273 MFS-25807

Ribbon reduces spiking in electron-beam welding
page 279 MFS-19701

Automated variable polarity plasma arc welding
page 290 MFS-27042

Microfissuring in alloys during welding
page 291 MFS-25604

WELDING MACHINES
Welding tubes in place
page 290 MFS-25714

WINDOWS (APERTURES)
Monitoring acoustically levitated samples
page 291 NPO-15193

WRENCHES
A one-hand nut and bolt assembly tool
page 267 MFS-19691

X RAY DIFFRACTION
X-ray-diffraction analysis of Nb/Ge alloys
page 217 MFS-27038

X RAY IMAGER
Improved gamma- and X-ray pinhole camera
page 191 GSC-12851

Lensless image scanner
page 200 NPO-16004

X RAY TELESCOPES
High-resolution X-ray telescope
page 200 NPO-15971

YEAST
Yeasts with increased glycogen levels
page 222 NPO-15571

ZINC SULFIDES
Recovering zinc from discarded tires
page 205 NPO-16046

ZIPPERS
Leak test for pressure-sealing zippers
page 250 KSC-11247

ZONE MELTING
Toroidal ellipsoid float-zone heater
page 288 MFS-25771

National Aeronautics and
Space Administration

Washington, D.C.
20546

Official Business
Penalty for Private Use $300

THIRD-CLASS BULK

THIRD-CLASS BULK RATE
POSTAGE & FEES PAID
NASA
WASHINGTON, D.C.
PERMIT No. G27

NASA

An automated electrophoresis system described previously in NASA Tech Briefs is now a commercial product with applications in biochemistry, medicine, and law enforcement. The researcher shown here is using the system to study proteins. *[See the bottom of page A1.]*